A Study of the Imaging of Contrast Agents for use in Computerised Tomography.

A thesis for the degree of

PHILOSOPHIAE DOCTOR

Presented to

DUBLIN CITY UNIVERSITY

By

Neil John O'Hare B.Sc.
The School of Physical Sciences
Dublin City University

Research Supervisor
Joseph Fryar B.Sc. Ph.D

August 1991

This thesis is dedicated to all my friends who, in one form or another, enabled me to finally finish school. Of these, four deserve special mention. Firstly my parents, John and Lucy, who , through times good and bad, offered continued support and encouragement. Secondly Jonie, the woman in my life, thanks for listening. Finally Joe Fryar, my supervisor. His enthusiasm for the subject made me start and his guidance enabled me to finish. No more could I ask for. Domo Arigato.

He who knows others is wise
He who knows himself is enlightened
He who conquers others is strong
He who conquers himself is mighty
He who knows contentment is rich
He who keeps on his course with energy has will
He who does not deviate from his proper place will long endure
He who may die but not perish has longevity

Tao Te Ching

Declaration

This thesis is based on my own work.

Table of Contents.

Chapter IV
Determination of the Sensitivity of CT to contrast agents in cylinders.

Chapter V
**Experimental results on the sensitivity of CT to contrast
agents in cylinders.**

Chapter VI
Conclusion and future work.   185

Acknowledgments.

List of appendices.

Appendices.

Table of Figures.

Abstract

A computed tomography (CT) scanner is a device which is capable of mapping the variation in linear attenuation coefficient in a slice through an object. This is achieved by the multiple measurement of the attenuation of an X-ray beam at various positions and angles through the body. In medical diagnostic imaging using CT, contrast agents are administered to patients resulting in increased attenuation of the beam in the areas where the contrast agent resides. The increased contrast results in the easier and more accurate visualisation of abnormalities.

In contrast-enhanced CT, iodine is almost universally used as the contrast agent when imaging the heart and associated arteries / veins. This is due to its low toxicity and high enhancement. It has been used extensively in traditional diagnostic radiology prior to the introduction of CT. A study was performed to determine whether iodine was the optimum element, in terms of the minimum concentration needed for visualisation, to use in contrast-enhanced CT scanning of the myocardium / heart wall. The results of this study show that gadolinium, and not iodine, is the optimum element to use as a CT contrast agent. Gadolinium, chelated to DTPA, is presently used as a contrast agent in MRI.

The above study concentrated only on the particular case of imaging the myocardium. A theoretical study was undertaken to determine the minimum concentration of any element when scanned using two different imaging methods. The situation studied was that of administering the contrast agent / analyte to a cylinder, which is itself contained inside another cylinder, the space between filled with some matrix. By varying the size of the inner cylinder, administration of a contrast agent to various organs or arteries can be simulated. By varying the size of the outer cylinder, various object / patient sizes can be studied.

In the first imaging method, two scans are performed at any energy, one with and one without the analyte present. These scans are subtracted to yield an image of the analyte alone. In the second method two scans are performed; one on the high side and one on the low side of the K absorption edge of the analyte. Again these are subtracted to yield an image of the analyte since the variation in the attenuation of the matrix across the K-edge is minor compared to that of the analyte.

The equations were verified by both computer simulations and experimental scans. Two important results were obtained. As the relative size of the inner cylinder decreases, firstly the optimum element shifts towards higher atomic number transition elements and secondly, the ratio of the minimum concentration of the optimum elements to the minimum concentration of iodine needed decreases making the case for using the transition elements as contrast agents stronger when imaging low relative size objects.

Chapter I
Introduction to Computerised Tomography and its applications.

1.1   Introduction:

The discovery of X-rays in 1895 by Roentgen heralded a new age in the area of medical diagnosis; visualisation of the interior of a patient without the need for painful or life-threatening surgery. X-rays formed the basis for a new area of medicine which became known as radiology. Since then, there have been four major developments in the area of diagnostic imaging. These are the Anger or Gamma - camera, the computerised axial tomography (CAT) scanner, the nuclear magnetic resonance (NMR) scanner and the ultrasound imager. Of these, the CAT scanner has had the most impact on the effectiveness of diagnostic imaging because it offers ease of use and excellent image quality in a short time period.

The CAT scanner was originally developed by a British scientist Godfrey Hounsfield in 1973 and since then has gone through a "trail-blazing" stage of development culminating in the development of the fourth generation scanner in the early 1980's. The development of computerised tomography (CT) since the early 1980's until the present time is in what is referred to as the "nitty-gritty" stage of development with refinements to the theoretical understanding and potential applications of this modality.

The work presented in this thesis covers two main areas. The first is an investigation into which element, when used as a contrast enhancing agent in CT imaging of the myocardium / heart wall, requires the lowest concentration for a particular visibility. Iodine is universally used for this purpose, however the results presented here show that this is not the optimum element

1

to use as a contrast agent. In the second section, an investigation is carried out into the minimum concentration of a contrast agent that is necessary for visualisation when contained in the inner cylinder of two concentric cylinders, both being of any absolute or relative size and containing some matrix material. Two cases are studied: the first when the contrast agent or analyte can be added to the object after an initial scan without any analyte; the second when the analyte is already present and two scans are performed at energies which straddle the K-absorption edge of the analyte. This investigation is aimed at helping the determination of the amount of contrast agent necessary for visualisation in different sized organs, ie. liver, heart, blood vessels.

1.2   Principles and History of Computed Tomography.

The name tomography comes from a combination of two Greek words- *tome:* a cutting, and *graphien:* to write - and tomography, or body-section radiography, can be defined as the imaging of structures lying in a determined plane of tissue. In conventional radiography the X-ray image is obscured by the images cast by anatomical features above and below the structures of interest. All tomographic techniques try to overcome this difficulty. Until the early 70's all varieties of tomography used photographic techniques to blur the images from the unwanted structures and keep the desired structures in focus. The principle of tomography can be demonstrated by means of the optical principle of parallax: if an object such as a pencil is held up and one's head is moved from side to side, only objects in the plane parallel to the direction of movement and at the same distance as the pencil do not show any relative movement. This approach, which became known as *focal-plane tomography,* was introduced in the early 1920's by a French surgeon Bocage [1]. Figure 1.01 shows this technique. Here the source and film are moved in opposite directions along parallel lines. Because of this movement, structures within the plane of interest form an image on the plate that moves at the same rate as the film and
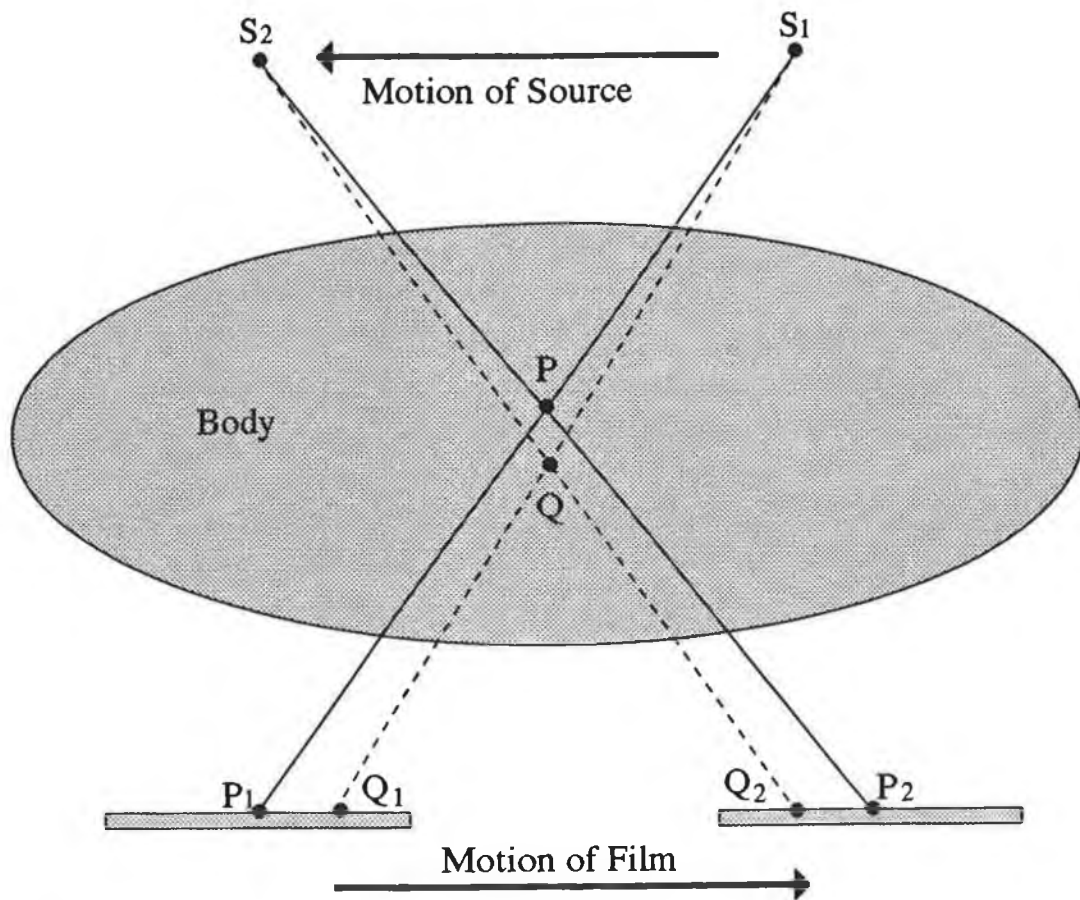
Figure 1.01
Diagram showing the effect of focal plane tomography. As the source-film combination move, only plane P remains in focus on the film.

therefore produces a sharp image. Images formed from planes above or below the plane of interest move faster or slower than the film and therefore get blurred during exposure.

Computed tomography improved on this conventional technique in three areas. 1) Although conventional tomography resolves the problem of underlying / overlying structures to some degree, structures above and below the tomographic section may remain visible in the image if they differ considerably in their X-ray attenuation properties from structures within the section. 2) Conventional detectors (ie. film and intensifying screens) are not able to resolve small differences (1-2%) in the intensity of the incident radiation [2]. 3) The large-area X-ray beams used in conventional X-ray imaging

3

produce considerable scattered radiation that interferes with the imaging of small contrast difference subjects. Focusing grids can partially alleviate this problem.

The image reconstruction techniques used in computed tomography were developed for use by Bracewell in radio astronomy [3], and by DeRosier et al. [4] and Gordon et al. [5] in electron microscopy. In 1963 Kuhl and Edwards [6] determined the distribution of a ^{241}Am source using a technique similar to conventional tomography. In spite of these early efforts, computed tomography remained unexploited for clinical use until the development by Godfrey Hounsfield in 1973 [7] of a practical X-ray imaging computed tomography (CT) scanner. This development was carried out while Hounsfield was working at EMI Ltd. in England and the scanner became known as the EMI head scanner. Hounsfield received the Nobel Prize in Medicine in 1979 for his invention. The prize was shared with Cormack, who years earlier developed a mathematical method to deal with the problems of reconstruction that arise in CT scanning. In 1974, Ohio Nuclear Inc. also developed a whole body CT scanner and by 1977, 16 or so commercial companies were marketing more than 30 models of transmission CT scanners [8].

Basic Concepts: The basic idea of CT scanning is illustrated in figure 1.02. An X-Ray tube emitting a pencil like beam is coupled to a radiation detector. The two are moved together on a carriage so that a plane in the head is scanned by a series of parallel rays as the translation takes place. For each ray the fraction of the radiation transmitted is measured and stored in a computer. In Hounsfield's original scanner 160 transmission measurements were made during one translation. The source – detector combination was then rotated through one degree and the procedure repeated. To see how this data can be used to create a CT image consider figure 1.03. Here is shown a cylindrical object superimposed on a coarse rectangular grid. The problem is to determine the attenuation coefficient for each pixel in the image from the transmission measurement made during the scan.

4
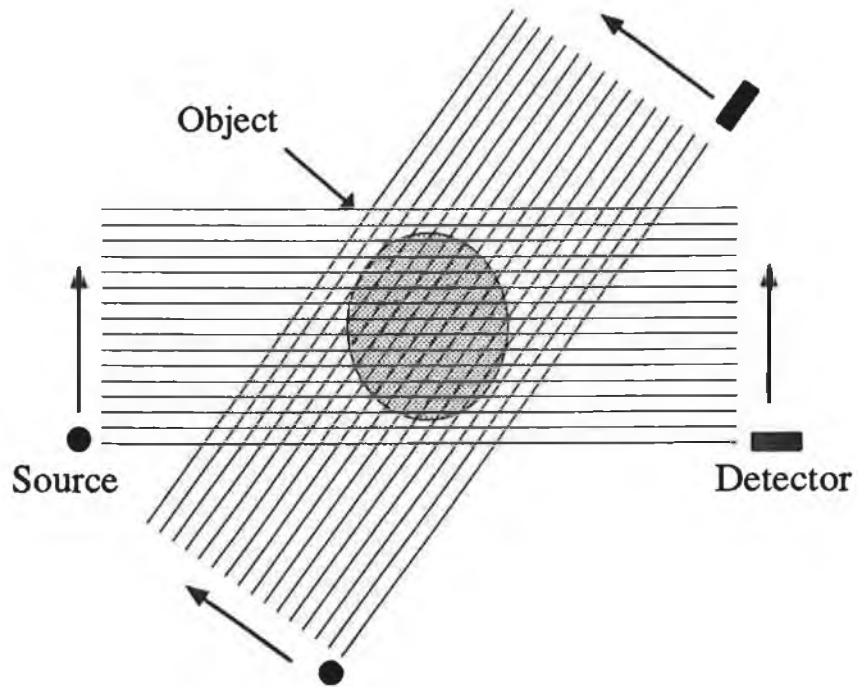
Figure 1.02
**First generation scanner with one source and one detector.
The above diagram shows two rotations and multiple steps.**
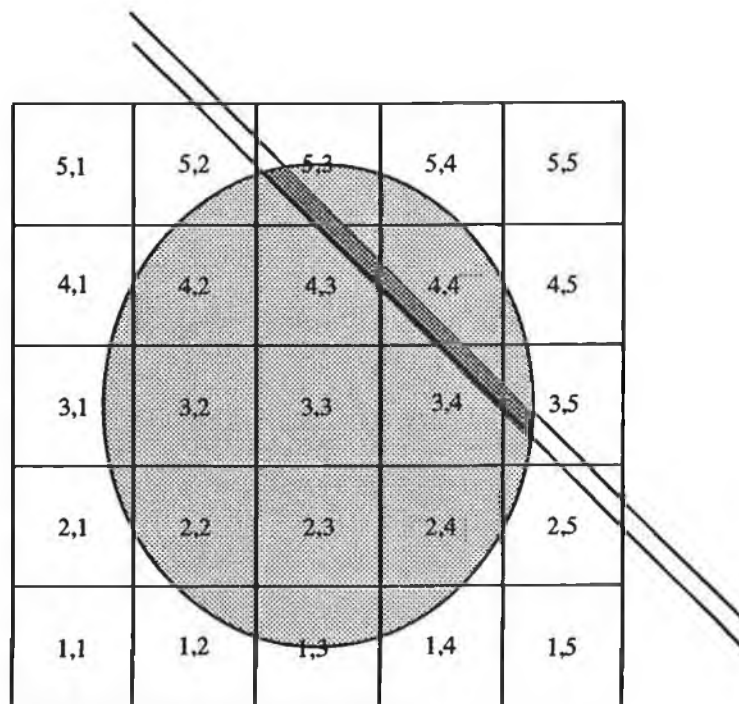
Figure 1.03
**Schematic diagram of pixels with a cross section
of an object superimposed. A typical beam through
the object is shown with the path lengths through
the pixels shaded.**

Let $U(x,y)$ be the average linear attenuation coefficient of the tissues in the pixel (x,y) for the radiation emitted by the X-ray source. The number of photons transmitted, N_t, is related to the incident radiation N_0 by:

$$N_t = N_0 \exp\left(-\sum U(x,y) \, \Delta l(x,y) \right)$$

where $\Delta l(x,y)$ is the path length through the pixel (x,y) and the summation is carried out along the source-detector path length. If we take the natural log of both sides and rearrange we get;

$$\ln(N_0/N_t) = \sum U(x,y) \, \Delta l(x,y)$$

The elements of length $\Delta l(x,y)$, are determined by the geometry of the system and hence can be stored in memory. N_0 and N_t are measured during the scan for each position. Knowing these, the reconstruction process creates an image that is a map of the X-ray attenuation ($U(x,y)$) coefficients of the tissue in the plane under examination. The image is viewed on a TV screen either as shades of grey or in colour. There are three main methods of reconstructing the image from the projection data. These are *Fourier Transform Reconstruction*, *Convoluted Backprojection* and *Iterative Methods*. These reconstruction techniques will be discussed in more detail in chapter 2.

Attenuation coefficients for soft tissue in the human body approximate those of water. Bone has an attenuation coefficient nearly double that of water while air has such a low attenuation coefficient that it is almost negligible in comparison. A universal scale, based on the linear attenuation coefficients, was established in 1972. The unit in this scale was named the Hounsfield Unit (HU) after the inventor of CT and is defined as follows;

$$\text{CT values (HU)} = 1000 \times \frac{U_x - U_w}{U_w}$$

where U_w and U_x are the linear attenuation coefficients of water and the tissue in question respectively. On this scale air has a value of approximately -1000 while dense bone has a value of about +1000. Most tissues lie in the range -100 to +100 with fat slightly negative and muscle slightly positive.

1.3 Commercial Scanner Developments.

In Fig. 1.02 a simple method of data acquisition in CT scanning is illustrated. Here a single source and detector are synchronously scanned to provide the required projection data. This system is also equivalent to moving the object and leaving the source-detector stationary. This system, because of chronology, is known as a 'first-generation' scanner. It is identified by a two-motion translate-rotate scan using a single detector. The principal difficulty with this instrument is its relatively long scan time. Only a small portion of the total X-ray output of the tube is utilized, requiring relatively long scanning times to achieve adequate statistics. These scanners continue to achieve relatively wide use because of their low cost.
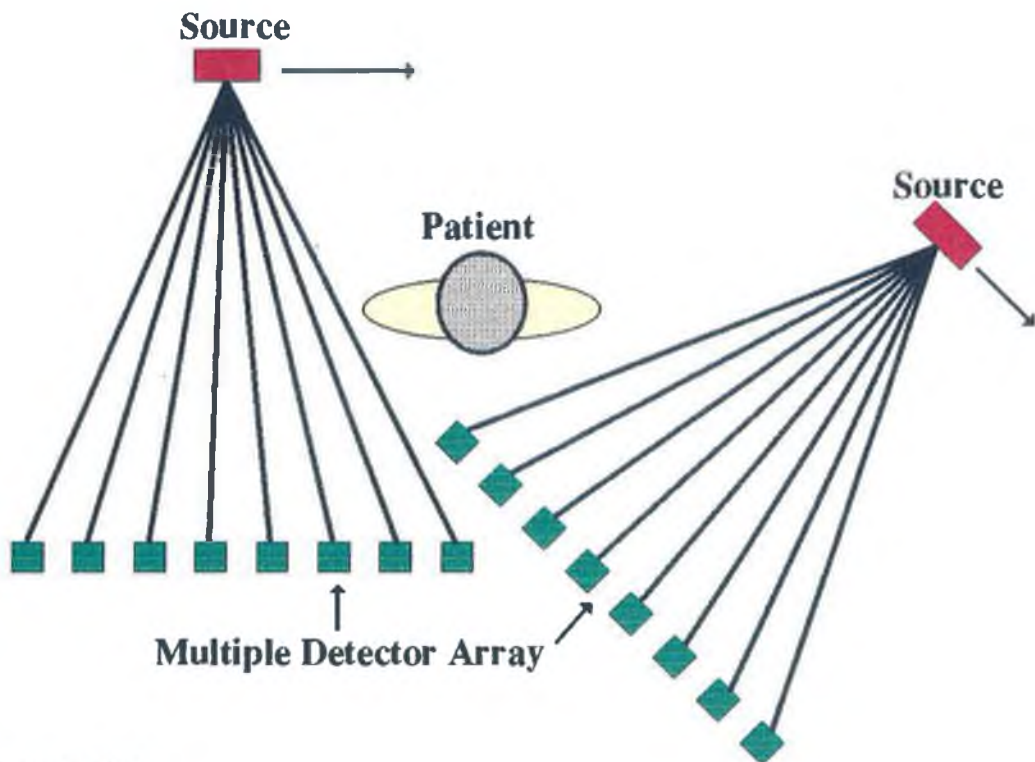
Figure 1.04
Second-generation scanner, using multiple detector translate-rotate system.

Figure 1.04 is an illustration of a second generation scanner at two intervals of the scan. Here the same

7

translate-rotate motions are used with a multiple-detector system. In this way several projections are acquired during each traverse. For example, if there are 10 detectors, each 1° apart, a single translation acquires all 10 projections. During the subsequent rotation the gantry is indexed 10° rather than 1°, resulting in a 10:1 time reduction.

One important feature of both the first and second generation scanners is self-calibration. Either preceding or following each traverse, each X-ray beam impinges on the detector with no intervening material. This provides a reference measurement of N_o, the intensity in the absence of any attenuating medium. This value is required to calculate the line integral. Although it is theoretically constant, drifts in both source and detector often require frequent measurements.
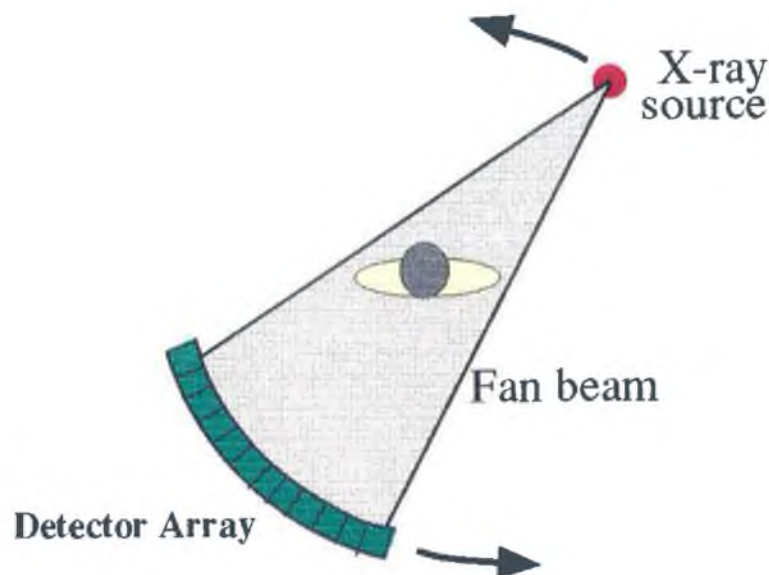
Figure 1.05
Third-generation fan-beam scanner, using a rotating source and detector array.

The third generation scanner involves rotation only of a fan beam, as illustrated in figure 1.05. Both the source and the detector are rotated about a common centre within the patient. The main advantage of this approach is the mechanical simplicity and ability to provide very high speeds, with scan times as low as 1 sec. One disadvantage

of this system is the lack of self-calibration. The system cannot be calibrated after the object has entered the beam path. In the earlier days of these instruments 'ring artifacts' were prevalent due to errors in individual detectors which were uncalibrated. These have since been minimized through improved detectors and software corrections.

The fourth generation scanner is characterized by a rotating fan beam impinging on a 360° stationary detector array as illustrated in figure 1.06. A source, generating a fan-beam, is rotated about the object. The transmitted rays are collected by the stationary detector array. This simple mechanical motion of the source only allows for a rapid scan time. In addition, the system is self-calibrating since, at different portions of the scan, each detector is irradiated by the source without any intervening material. Also the system is relatively immune to ring artifacts since detector errors are distributed throughout the image, rather than representing a specific radius.
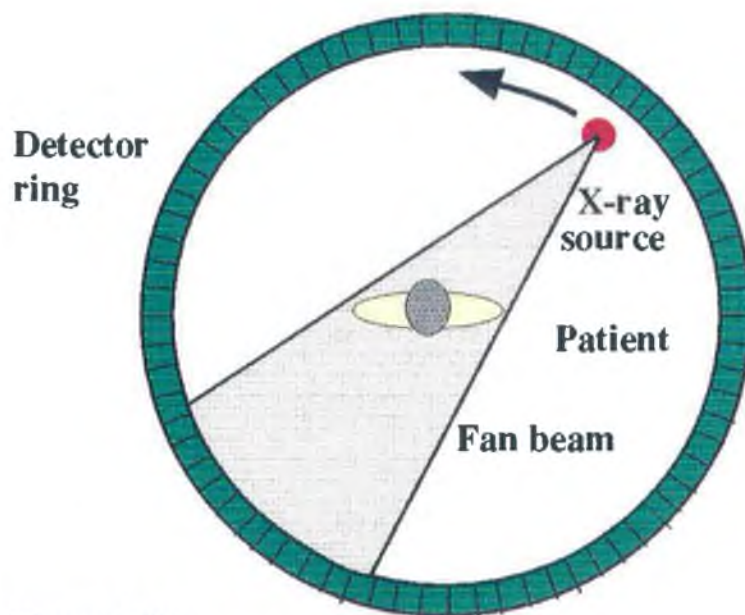
Figure 1.06

Fourth-generation scanner, using a rotating fan-beam and a stationary ring detector.

One difficulty with the scanner is the varying angle at which the rays strike the detectors. In the third

9

generation scanner the detectors can be aligned along the rays since the entire structure rotated. Here, however, at different source positions the rays strike a given detector at different angles. This meant that the detectors should be relatively shallow to avoid the rays entering adjacent detectors.

The third and fourth generation scanners derive their measurements using fan-beam rather than parallel-beam projections. These require somewhat modified approaches to the reconstruction problem. One approach is known as re-binning, where the various fan-beam rays from different projections are reassembled as parallel beam projections. The original reconstruction algorithms can then be used. An alternative approach is to use a modified reconstruction algorithm which accounts for fan-beam data.

1.4   *Computerised Tomography Applications.*

1.4.1   Medical:

The CT scanner, as originally devised by Hounsfield, was developed for use only in medicine. Subsequently other uses and forms of CT were developed, mainly for use in industry. Medically, the first application of this new imaging modality was in interior density visualisation of the head. At present this is still the most common CT scan performed, eg. to check for suspected cranial haemorrhaging / clotting of road traffic accident victims, etc. However, today's scanners perform a much wider choice of scans than the original EMI "Head Scanner", with scans being routinely performed of any part of the body. Plate 1.1 shows a series of CT scans of a patient's foot with a conventional X-ray image showing the position of each scan included.

Two of the many scans performed still pose difficulties for present day scanners due to motion artifacts. These are scans of the heart and scans of the lower abdomen. In the heart, its beating causes blurring of the final image and in the lower abdomen, movement of gas bubbles cause streak artifacts to occur. These effects can be significantly reduced by decreasing the scan time. This area is covered in more detail in chapter 3.

CT is now also used extensively in the areas of radiation therapy and surgical planning. Bloch and Udupa use three dimensional reconstruction of CT data to both plan a course of radiation therapy for a cancer patient and plan a surgical reconstruction [9]. Traditional radiation therapy requires planning the delivery of radiation that results in a uniform dose to the cancerous tissue while maintaining a minimum dose to the surrounding healthy tissue. This can be greatly aided by the attenuation coefficients supplied by a CT image data. In surgical planning, the object is to plan a manipulation of the organ / bone in order to achieve the desired results. An excellent example of this is given by Trux and Tsiaras [10].

EXAM CODE   :
EXAM NAME   :
DATE/TIME   : 02/05/91 11:28-13:30
HOSPITAL NAME : HOSPITAL
COMMENT   :

IMAGE DATA   : TOTAL SCANO NORM CE

HEATH HOSPITAL DUBLIN
HEATH HOSPITAL DUBLIN
HEATH HOSPITAL DUBLIN
HEATH HOSPITAL DUBLIN
HEATH HOSPITAL DUBLIN

1.4.2   Industrial:

CT was originally developed as a medical diagnostic for providing medical information about the interior details of patients. In medical applications, the range of X-ray energies is relatively small (typically 30 - 140 keV), the dose limitation is severe, and the time available for acquiring the data is small. In industrial applications these restrictions may not exist. A machine designed for medical CT is rarely used for other NDT work. For industrial applications, the first design decision involves the X-ray energy required. The number of mean free paths through the object should lie between 1 and 5 [11], any thinner and most of the photons do not contribute to the absorption signal, any thicker and the detectable counts may be too small thus incurring large statistical noise. The next decision involves the system configuration, ie. do the source / detector rotate or does the object. Mechanical tolerances for both of these configurations are limited by the spatial resolution needed in the final image. Detector design considerations are formed by the energy of the X-rays, the source flux, the spatial resolution and the generation of the scanner.

Industrial CT scanners have been developed for imaging various objects including large solid-fuel rockets with an X-ray energy of 15 MeV [11], soil attenuation coefficients for various areas [12], the measurement of annual rings on a live tree [13] and Elliot et al. imaged a 600μm diameter freshwater snail with a pixel size of 12 x 12 μm [14]. These are just some of the vast range of X-ray CT industrial applications.

1.5 *Other Forms of Computerised Tomography*

1.5.1 Gamma-Ray CT:

X-ray CT machines have been used on non-medical objects with high quality images being obtained for objects whose size, density and composition do not differ greatly from that of the human body. However, the energies normally available on a medical scanner are too soft for the majority of higher density, higher atomic number materials encountered in many industrial objects and thus poor images result.

Gamma-ray sources provide a cheap and easy to use alternative to X-ray sources. They have the advantage of providing higher energies than are readily available with commercial X-ray sources and the beam is quasi - monochromatic. Sources are also available which provide several quasi - monochromatic energies useful for elemental imaging. However, they have two major disadvantages. The source strengths commercially available are far lower than those obtained from X-ray tubes. Due to self-absorption, gamma sources can only be easily manufactured with strengths of up to a few tens of Curies; X-ray tubes possess photon fluences equivalent to a radioactive source strength in the region of 1000 Curies. The second disadvantage is that gamma sources cannot be "turned off" and thus require extensive shielding. Any adjustments to the collimators, shielding, etc. requires extensive safety procedures.

Sweeney was probably the first to seriously evaluate the potential of gamma-ray tomography at the Lawrence Livermore Lab in 1974 [15]. Here a collimated 40 Ci source of ^{192}Ir, emitting photons in the range 296 - 613 KeV, was used to study small objects such as a hand lamp and lens assembly.

Using a multi-energy source with an energy dispersive detector, tomograms can be recorded simultaneously over a wide range of energies. For example a ^{152}Eu source has been used at Surrey [16] and this provides 9 quasi - monoenergetic gamma-ray peaks over the range 40 KeV to

1.4MeV. McCuaig et al. used gamma CT to image fluidized beds to assist in the understanding of the fluid mechanics for the oil industry [17]. SMS of Texas have developed a gamma CT scanner for examining wooden power line support poles and concrete structures. They use a high intensity 100 Ci Ir source and achieved a spatial resolution of 1 mm [18,19,20].

1.5.2   Neutron CT:

The first requirement for an imaging system is its ability to penetrate the object or material under test. X-rays and gamma-rays perform this task and interact with the electron cloud in the process. The extent of this interaction can be expected to generally increase with atomic number, since the electron cloud density increases. Neutrons have a much higher penetrating power than equivalent energy X- or gamma-rays and interact with the nuclei to an extent which depends on the existence of stable configurations of neutrons and protons in the nuclei of the object. For a few types of nuclei the addition of a neutron forms a particularly stable configuration so that the probability of an interaction for these materials is particularly high. These materials include hydrogen, boron, lithium, cadmium and gadolinium [21].

Neutrons have been used extensively in the areas of neutron radiography and radiotherapy (see the review article by Spowart [21]). They have also been utilised in the formation of CT images. At the University of Missouri's 10MW research reactor, a well-collimated, neutron beam was used to image a fuel assembly in a steel casing [22]. However, it took 15 days to collect the data for this single slice. Overley obtained CT images of the concentration of several light elements with a precision of several percent using neutron transmission techniques [23].

1.5.3   Electrical Impedance CT:

There has been a significant amount of research carried out concerning the use of measurements of the electrical impedance from one point to another on a patient's skin for diagnostic purposes (see for example [24]). These are non-imaging techniques. Henderson and Webster [25] reported the development of an impedance camera which formed a low-resolution image of the impedance through the thorax in a process similar to ordinary X-ray projection images.

The basic idea in impedance CT is to apply small potential difference between various points on the patient's body and measure the resulting small currents (the resulting current densities in the patient are of the order of 1 mA/cm^2). This technique has been developed by Price [26] who suggests that this method would have the following advantages over conventional CT; 1) reduced biological hazard, 2) less expensive hardware, 3) easily extended to three-dimensional, 4) very high data collection rates and 5) the ability to make unique physiological measurements.

1.6   Summary

In this chapter the basic ideas governing CT are discussed showing the progress from projection radiography, through planer tomography, which is still in clinical use, to computer assisted tomography which is the subject of this thesis. The various generations of scanners are explained along with medical and non-medical applications of X-ray CT. Other forms of CT that have been developed are also discussed by way of a background.

In the following the topics more intrinsic to this work are discussed, eg. reconstruction algorithms, differential absorptiometry.

16

References.

[1] E.M. Bocage
Patent No. 536,464, Paris France.
(Quoted in History of Tomography, J. Mossiot, Medica
Mundi, Vol. 19, pp.106-115, 1974).

[2] Tsoulfanidis, N.,
"Measurement and Detection of Radiation."
McGraw-Hill series in Nuclear Engineering, New York, 1983.

[3] Bracewell, R.,
"Strip Integration in Radio Astronomy.",
Aust. Jour. Phys., Vol. 9, No. 2, pp.198-217, 1956

[4] DeRosier, D., Klux, A.,
"Reconstruction of Three Dimensional Structures from
Electron Micrographs."
Nature, Vol 217, pp.130-134, 1968.

[5] Gordon, R., Bender, R., Herman, T.,
"Algebraic Reconstruction Techniques for three dimensional
electron microscopy and X-ray photography."
Jour. Theor. Biol., Vol. 29, pp.471-481, 1970

[6] Kuhl, D., Edwards, R.,
"Image separation radioisotope scanning."
Radiology, Vol. 80, No. 4, pp.653-662, 1963.

[7] Hounsfield, G.,
"Computerised Transverse Axial Scanning (tomography): Part
1, description of the system."
Br. Jour. Radiology, Vol. 46, pp.1016-1022, 1973.

[8] Waggener, R., Kereiakes, J.G., Shalek, R.J.,
"Handbook of Medical Physics: Volume II."
CRC Press Inc., Florida, 1984.

[9] Bloch, P, Udupa, J.,
"Application of Computerised Tomography to Radiation
Therapy and Surgical Planning."
Proc. IEEE., Vol. 71, No.3, pp.351-355, 1983.

[10] Trux, J., Tsiaras, A.,
"The Healing Image",
The Sunday Times Magazine, Mar 19, pp.22 - 30, 1989.

[11] Burstein, P., Bjorkholm, P.J., Chase, R.C., Seguin, F.
"The Largest and Smallest X-Ray Computed Tomography
Systems."
Nucl. Inst. & Meth., Vol 221, pp.207-212, 1984.

[12] Cesareo, R.,
"Using a Computed Tomography Scanner for Nonmedical
Applications."
Nucl. Inst. & Meths., Vol. A275, pp.420-429, 1989.

[13] Onoe, M., Tsao, J.W., Yamada, H., Nakamura, H., et. al.
"Computed Tomography for Measuring the Annual Rings of a Live Tree."
Nucl. Inst. & Meths., Vol. 221, pp.213-220, 1984.

[14] Elliot, J.C., Dover, S.D.,
"X-Ray Microscopy using Computerised Axial Tomography."
Jour. Microscopy., Vol. 138, Pt.3, pp.329-331, 1985.

[15] Sweeney, D.W.,
"Radiation gage imaging for nondustructive testing applications."
LLL, Univ. California, Report No. UCRL-51641, Sep 1974.

[16] Gilboy, W.B. Foster, J, Folkard, M.,
"A Tomographic gamma-ray scanner for industrial applications."
Nucl. Inst. & Meths., Vol. 193, pp.209-214, 1982

[17] MacCuaig, N., Seville, P.K., Gilboy, W.B., et. al.
"Application of gamma-ray tomography to gas fluidized beds."
Applied Optics, Vol.24, No.23, pp.4083-4085, 1985.

[18] Ellinger, H.D., Hopkins, F.F., Morgan, I.L., et. al.
"Tomographic analysis of structural materials."
SPIE Proc, Vol. 182, pp.179-186, 1979.

[19] Hopkins, F.F., Morgan, I.L., Ellinger, H.D., et. al.
"Industrial tomography applications."
IEEE Trans. Nucl. Sci., Vol. NS-28, pp.1717-1720, 1982.

[20] Hopkins, F.F., Morgan, I.L., Ellinger, H.D., et. al.
"Tomographic image analysis."
Mater Eval., Vol.40, pp.1226-1228, 1982.

[21] Spowart, A.R.,
"Neutron Radiography"
Jour. Phys. E, Vol.5, pp.497-510, 1972.

[22] Schlapper, G.A., Brugger, R.M., Koeppe, R.A., et.al.,
"A demonstration of filtered neutron beam computed tomography: evaluation of a pin fuel assembly phantom."
Mater. Eval., Vol.39, pp.1121-1125, 1981.

[23] Overley, J.C.,
"Element-Sensitive Computed Tomography with Fast Neutrons."
Nucl. Inst. & Meths., Vol. B24/25, pp.1058-1062, 1987.

[24] Geddes, L.A., Baker, L.E.,
Principles of Applied Biomedical Instrumentation.
Chapt. 10, New York, Wiley & Sons.

[25] Henderson, R.P., Webster, J.G.,
"An impedance camera for spatially specific measurements in the thorax."
IEEE Trans. Biomed. Eng., Vol.BME-25, No.3, pp.250-254, 1978.

[26] Price, L.R.,
"Electrical Impedance Computed Tomography (ICT): A new CT imaging technique."
IEEE Trans. Nucl. Sci., Vol. NS-26, No.2, pp.2736-2739, 1979.

Chapter II
Basic X-ray physics, Differential Absorptiometry and Reconstruction Algorithms.

2.1.1 Production of X-Rays.

During the 1890's, a large number of physicists were studying the conduction of electricity in gases at low pressure. Many of these workers were able to promptly confirm and extend the results reported by Roentgen [01] in his paper of December, 1895 on the discovery of X-rays. Interest in the new *X-rays* was immediate and intense. In a few months, the first cases of injury due to radiation exposure were observed, with neither the causes or cures known.

For many years X-rays were generated by an electrical discharge between cold-metal electrodes in a partially evacuated tube. Huge spark-coils were used to generate a few tens of kilovolts to maintain the discharge. Some residual gas was needed to sustain the current flow. As the tube was used, some of the gas was adsorbed on the walls and the discharge became hard to start.

In 1913, W.D. Coolidge introduced the basic design features of the tubes in use today, see figure 2.01. These X-ray tubes operate in a very high vacuum. Electrons are supplied by a hot cathode or filament, usually contained in an electrode shaped to provide some focusing action for the electron beam as it is directed onto the anode. Anode-cathode voltages of up to 150 kVp are common on modern diagnostic X-ray tubes.

Another form of the X-ray tube that has been utilised is that of the *field-emission tubes* in which the electrons are extracted from a cold cathode by the intense electric field that exists near an electrode with a small radius of curvature. In these tubes, a high potential is suddenly

applied across a needle like cathode and the anode. A current of many amps will flow for about 10^{-6} sec. to produce a short pulse of high-intensity X-rays.

When an X-ray beam is studied with a spectrometer, in general, two components can be identified in the spectrum.

1) A *continuous spectrum* which has a definite lower wavelength limit, decreasing slowly in intensity towards the longer wavelengths.
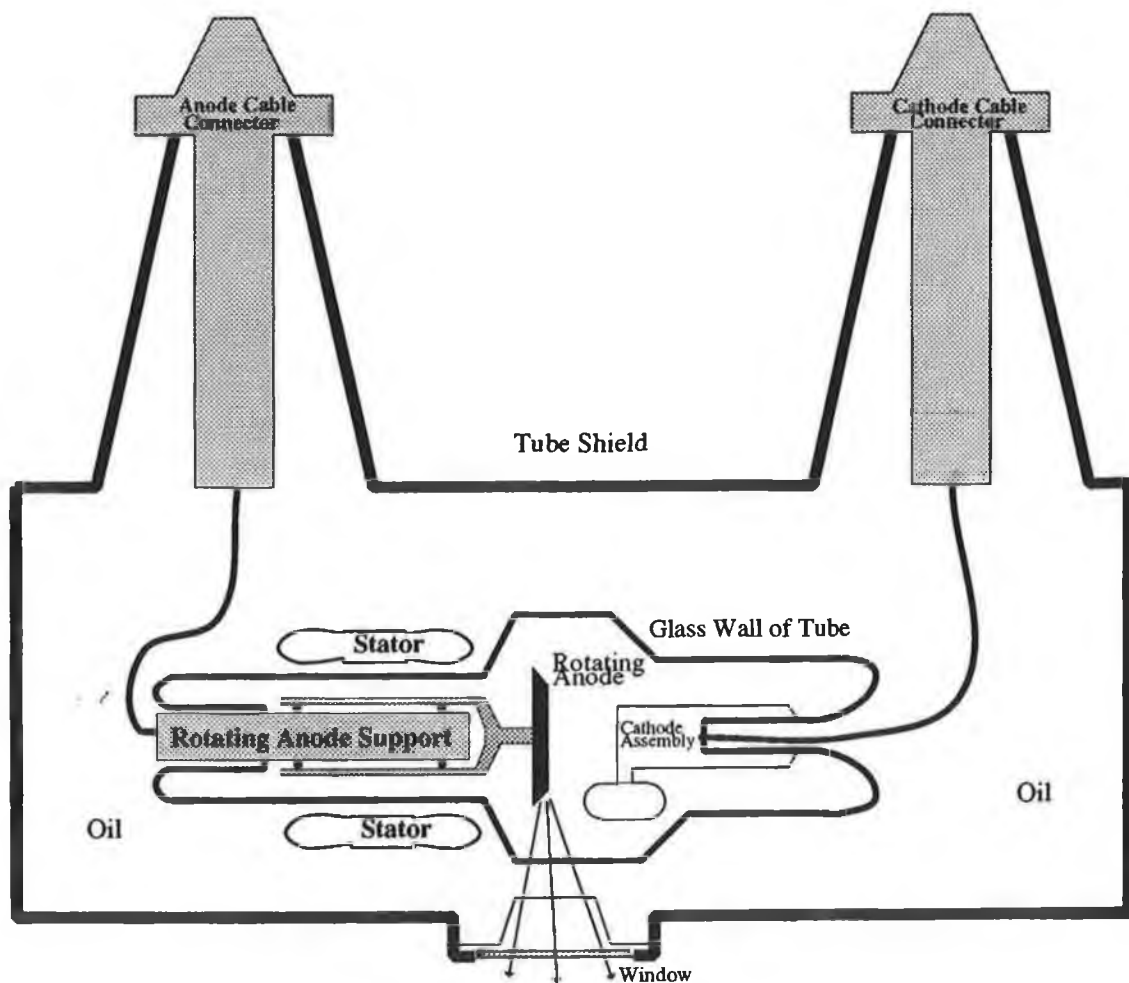
Figure 2.01
The rotating anode X-ray tube assembly.

2) A *characteristic or line spectrum* which appears as sharp peaks, the X-rays of which are characteristic of the element used as the target.

The continuous X-ray emission is known as *bremsstrahlung* and is produced whenever moving charges undergo a series of random accelerations. This happens when an electron is incident on a target, with the most drastic acceleration possible occurring when an electron gives up its entire energy in a single encounter, giving a photon of energy

$$E = Ve \qquad (2.01)$$

where V is the accelerating voltage. Encounters as described are rare, with the electron more probably dissipating its energy over a series of interactions, to produce the continuous energy distribution that is characteristic of a bremsstrahlung spectrum. Kramers has derived an expression for the distribution of intensity in this type of spectrum [02];

$$I_\lambda = \frac{KiZ}{\lambda^2}\left(\frac{1}{\lambda_o} - \frac{1}{\lambda}\right) \qquad (2.02)$$

where I_λ is the intensity at any wavelength , K is a constant, i is the tube current, Z is the atomic number of the target and λ_o is the limiting wavelength given by equation 2.01. The above equation predicts a wavelength of maximum intensity emission, as can be seen by setting $dI_\lambda/d\lambda = 0$ giving $\lambda_{max} = 3\lambda_o/2$.

X-rays produced by atomic de-excitation result in a line-spectrum, the lines of which are uniquely characteristic of the element involved. They are known as *characteristic x-rays* and form the basis of a number of analytical techniques such as X-ray fluorescence. Strong lines appear in groups or 'series' the wavelengths of which shift regularly with the atomic number of the emitting element. The group of lines with the shortest wavelength is known as the K-series, followed by the L, M, N, etc. Individual lines in each series are denoted by α, β, etc. as in K_α, K_β. Moseley [03] showed in 1913, that the wavenumber of any particular series line is given by

22

$$\nu = \frac{1}{\lambda} = R.(Z-S)^2\left(\frac{1}{n_1^2} - \frac{1}{n_2^2}\right) \qquad (2.03)$$

where Z is the atomic number and n_1 and n_2 are the principal quantum numbers of the particular lines. S is a screening factor which is needed because orbital electrons in the outer shells will be partially shielded from the nuclear charge by the negative charges in the inner shells.

Later work has shown that each of the lines reported by Moseley has a fine structure, being made up of several lines closely spaced in energy, therefore the K_α becomes $K_{\alpha 1}$, $K_{\alpha 2}$, etc. Figure 2.02 shows some of these atomic energy levels and figure 3.25 shows a 120 kVp continuous X-ray spectrum along with the superimposed characteristic lines of the tungsten target.
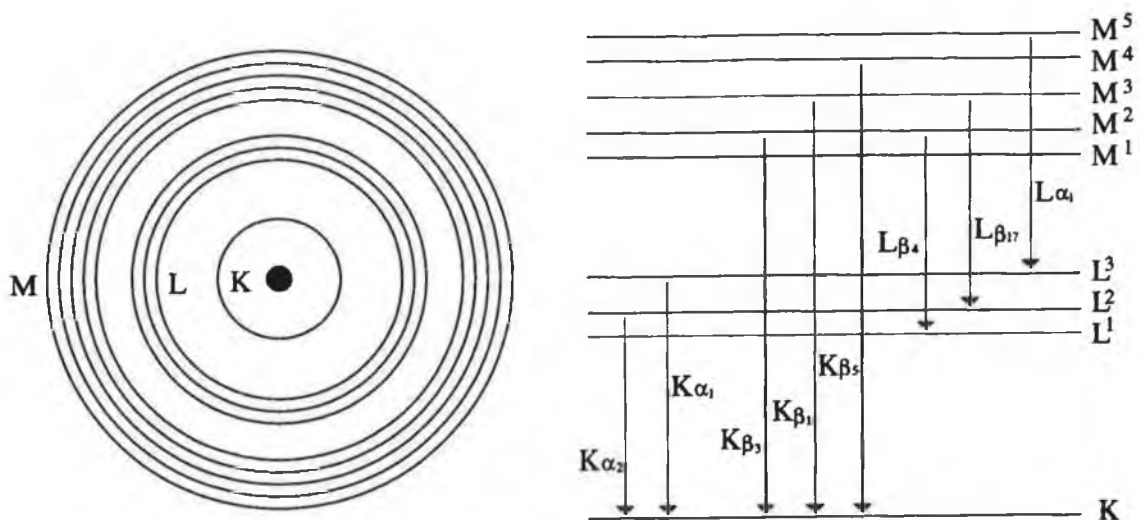
Figure 2.02
Electron transitions producing the characteristic line X-ray spectrum.

Other processes that tend to involve the K-shell electrons, such that subsequent de-excitation provides characteristic X-rays, involve the use of radionuclides. Radionuclides which decay by the emission of gamma radiation may, as an alternative, de-excite by the process of *Internal Conversion* in which an atomic electron receives the gamma energy and is ejected from the atom. Another nuclear process in which atomic electrons are

23

involved is the form of beta decay known as *Electron Capture* in which an electron is absorbed directly into the nucleus. In addition, sources of energetic beta particles usually produce some bremsstrahlung via interactions between the betas and other material present in the source.

2.1.2 Interaction of X-Rays with Matter.

When a beam of X-rays pass through matter, it is attenuated and the intensity falls to a value given by

$$I = I_o.exp(-U.x) \qquad (2.04)$$

where U is the linear attenuation coefficient and is characteristic of the material and X-ray energy and x is the distance traversed by the beam. The attenuation of the beam occurs from a number of interaction processes.

There are four main interaction processes which can occur when a beam of X-rays is incident on matter. If conditions are correct, all of these processes can occur simultaneously, however for the energy range covered in this work, only two of these will be significant. The four processes are as follows:

1) Classical or Thomson scattering, also known as unmodified scattering.

2) Photoelectric Effect.

3) Compton or modified scattering.

4) Pair-Production.

Classical or Thomson scattering occurs as a result of an interaction between an incoming photon and an electron, the binding energy of which is significantly greater than that of the incoming photon. The incident radiation is assumed to set the electron into forced resonant oscillation such that the electron re-emits radiation of the same frequency but in all directions. While this phenomenon is of little clinical importance in the work presented here, never contributing more than 10% to the overall attenuation for a low range of energies <5keV [4], it has great significance in the area of X-ray crystallography. It will not be dealt with further.

The photoelectric effect is an interaction between a

24

photon and a bound atomic electron. As a result of this interaction, the photon is absorbed and the electron is ejected from the atom. If the photon has energy $h\nu$, then the kinetic energy of the electron is given by

$$T = h\nu - W \qquad\qquad (2.05)$$

where W is the binding energy of the electron. This process is shown in figure 2.03. The photoelectric contribution to the mass absorption coefficient is proportional to $\lambda^3 Z^4$ where λ is the incident photon wavelength and Z is the atomic number [04]. This proportionality to Z^4 explains the remarkable results which can be achieved with contrast media based upon materials of high atomic numbers compared to the normal constituents of the human body.
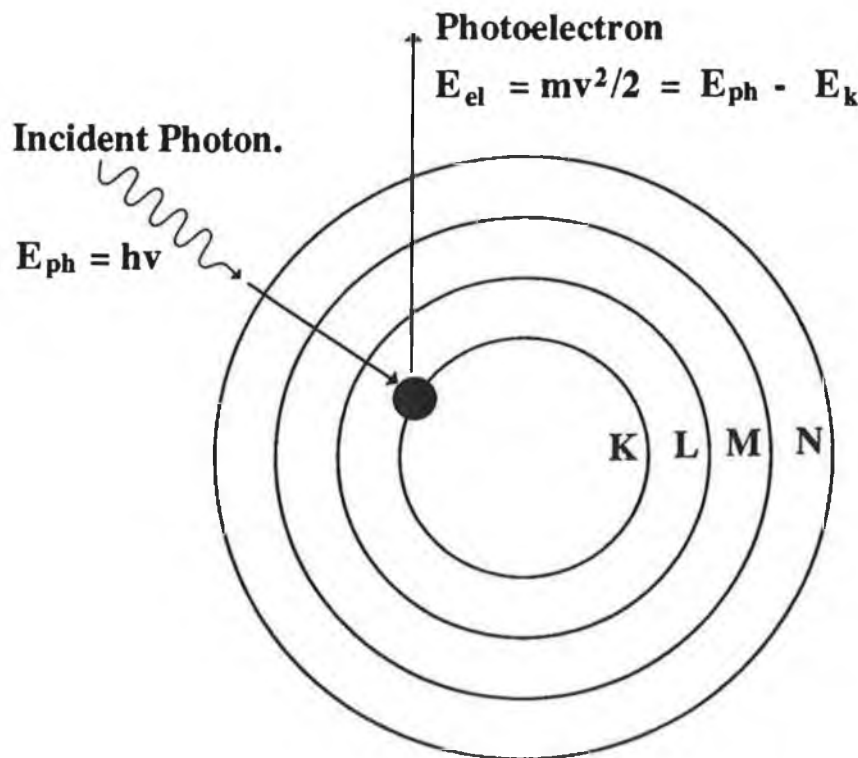
Figure 2.03
The Photoelectric Effect showing the incident photon and the ejected electron.

The Compton effect is a collision between a photon and a free electron. Normally all the electrons in a medium are not 'free' but bound. However, if the energy of the photon is of the order of keV or more, and the binding energy of the electron is of the order of 1eV, then the

25

electron may be considered free. The photon does not disappear after being Compton scattered, unlike the photoelectric / pair-production effects; only its direction and energy change, see figure 2.04.
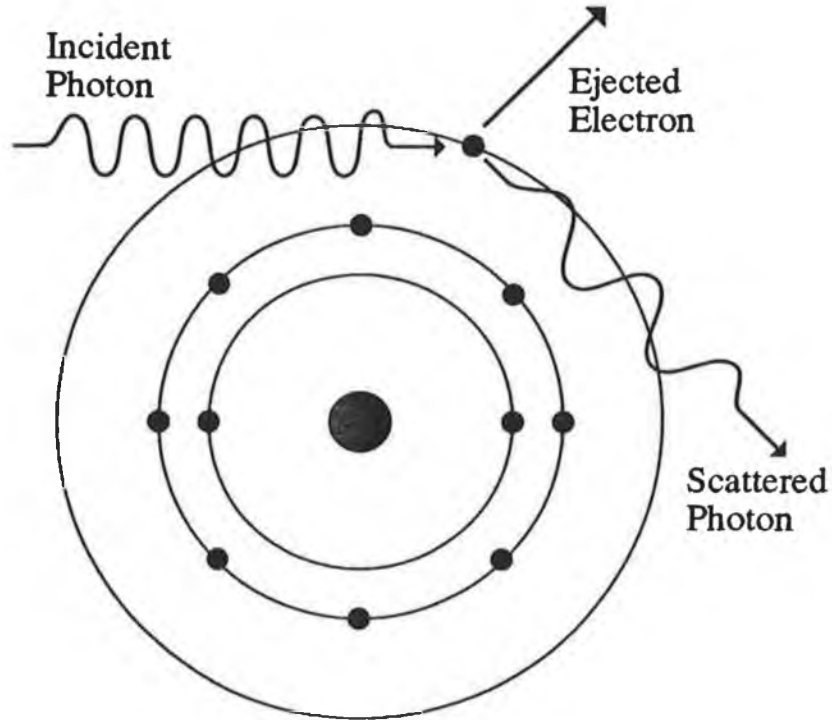
Figure 2.04
Diagram showing the effect of compton scattering. The photon looses energy to the electron and is thus scattered at a longer wavelength.

Assuming the electron to be initially at rest, then the conservation of energy gives the kinetic energy of the electron after the collision as

$$T = E_\gamma - E_\gamma' \qquad (2.06)$$

where E_γ is the initial photon energy and E_γ' is the photon energy after the interaction. The energy of the scattered photon, as a function of scattering angle (θ) is given by

$$E_\gamma' = \frac{E_\gamma}{1+(1-\cos\theta)E_\gamma//mc^2} \qquad (2.07)$$

and the kinetic energy of the electron is

$$T = \frac{(1-\cos\theta)E_\gamma//mc^2}{1+(1-\cos\theta)E_\gamma//mc^2} E_\gamma \qquad (2.08)$$

The minimum energy of the scattered photon is obtained

26

when $\theta = 180°$

$$\Rightarrow E_{\gamma min} = \frac{E_\gamma}{1 + 2E_\gamma//mc^2} \qquad (2.09)$$

This is a non-zero value, therefore in Compton scattering, it is impossible for all the energy of the incident photon to be given to the electron.

In the intense electric field close to a charged particle, usually the nucleus, the energetic X-ray photon may be converted into a positron-electron pair. This is pair-production and the two particles share the available energy. Since the energy equivalent of the mass of an electron is 0.51 MeV, the creation of an electron-positron pair requires 1.02 MeV. Consequently, photons with energy less than this value do not interact by pair-production. This is the case in the work presented here.
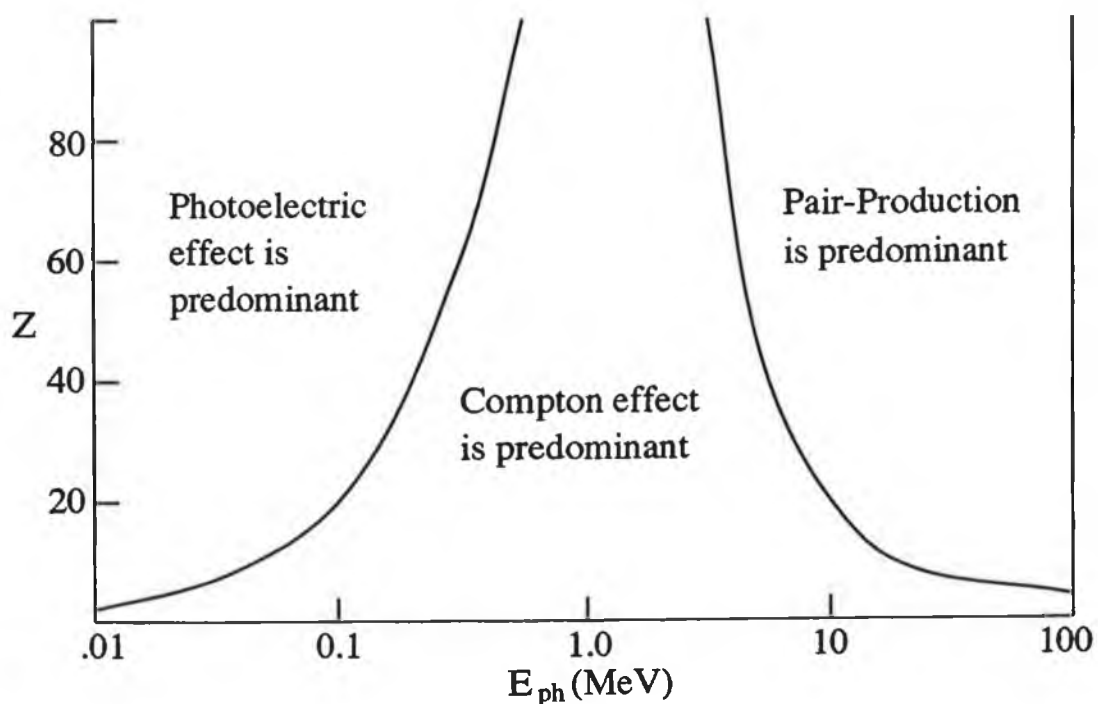
Figure 2.05
The relative importance of the three major X-ray photon interactions. Z is the atomic number and E_{ph} the photon energy.
("The Atomic Nucleus", R. Evans, McGraw-Hill, 1972)

When a photon travels through matter, it may interact through any of the processes described above depending on its energy. Figure 2.05 shows the relative importance of

the photoelectric, Compton and pair-production effects.
For example, a 0.1 MeV photon travelling through carbon
(Z=6) interacts mainly by the Compton effect. However, the
same photon travelling through Iodine (Z=53) interacts
mainly by the photoelectric effect. The total mass
attenuation coefficient is a combination of the absorption
coefficients for these four major processes. However, in
the energy range associated with this thesis only the
photoelectric and Compton absorption coefficients are
significant.

2.1.3 Detection of X-rays.

Generally, the various X-ray detectors used are based
on the indirect effect of the X-ray photon on the
electronic structure of matter. At energies less than 50
keV, this interaction is usually photoelectric absorption,
with each photon producing an electron with a certain
kinetic energy. These electrons expend their energy in
various ways, depending on their environment. In
photographic emulsions they make grains of silver halide
sensitive to the developer. In *fluorescent screens* and
scintillation phosphors, they excite atomic electrons to
high atomic energy levels, which de-excite with the
emission of a visible or ultraviolet photon. In *gas-filled*
detectors, they ionise gas atoms, producing an
ion-electron pair and in *semiconductor detectors* they
excite valence band electrons into the conduction band,
creating electron-hole pairs. The latter two electronic
detectors can be operated in either of two modes; 1)
continuous-current detectors where the output current is
proportional to the incident X-ray intensity and 2) photon
counters which produce a discrete pulse for each incident
photon. The semiconductor detector was used extensively in
the experimental work presented in chapter 5 and will
thus be explained now in greater detail. The gas-filled
and scintillation detectors are described in greater
detail in appendix 6.

Semiconductor Detectors: These detectors are solid -
state devices that operate essentially like ionisation

chambers. However, the charge carriers are electron-hole pairs and not electron-ion pairs. At present, the most successful semiconductor detectors are made of silicon and germanium. Other materials have been tried with some success, eg. CdTe and HgI_2 [05]. The most important advantage of the semiconductor detectors, compared to other radiation detectors, is their superior energy resolution. Other advantages include high efficiency, fast pulse rise times and linear response over a wide energy range [06]. The operation of a semiconductor is based essentially on the properties of a p-n junction in reverse bias. Radiation incident on the junction produces electron - hole pairs; for example, a 5 MeV alpha particle will create approximately one million e-h pairs if it deposits all its energy. The junction region is of the order of a few millimeters wide and the charge carriers can traverse this region in times of the order of 10^{-7}sec. The several types of semiconductor detectors that exist differ from one another because of the material used in their construction or the method by which the material is treated. These include surface-barrier detectors, diffused-junction detectors, lithium-drifted silicon, lithium-drifted germanium and hyperpure germanium detectors [06].

2.1.4 Biological Effects of Radiation.

The interaction of ionising radiation in the human body leads to biological effects which may show up later as medical symptoms. The effects can be divided into two classes: *somatic* effects, which affect only the person irradiated and *hereditary* effects, which occur in the children of the irradiated person.

When ionising radiation is incident on a cell, it most commonly causes ionisation of a water molecule, of which cells are largely composed. This ionisation can lead to chemical changes which manifest themselves as clinical symptoms such as radiation sickness, cataracts or cancers. This process of radiation damage is usually split into four stages [07].

1) *Initial Physical Stage:* Here, the radiation energy is deposited causing ionisation; eg.

$$H_2O \xrightarrow{\text{Radiation}} H_2O^+ + e^-$$
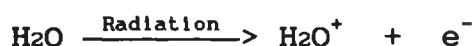
2) *Physico-Chemical Stage:* Now, the ions interact with other water molecules resulting in a number of new products;

$$H_2O^+ \longrightarrow H^+ + OH$$

$$H_2O + e^- \longrightarrow H_2O^- \longrightarrow H + OH^-$$
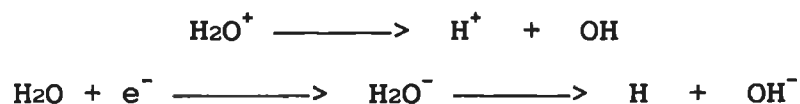
Two of the products, H and OH , are called free radicals and are highly chemically reactive.

3) *Chemical Stage:* These free radicals may attack the complex molecules which form the chromosomes or break links in these long chain molecules.

4) *Biological Stage:* These chemical changes can cause a) an early death of the cell, b) the prevention / delay of the cell division or c) a permanent modification which is passed on to the daughter cells.

As well as somatic and hereditary effects, another two terms have been introduced by the ICRP (International Commission on Radiation Protection). They are *stochastic* and *non-stochastic* effects. The former relates to probability of occurrence of radiation effects depending on the dose received and the latter relates to the severity of the effects depending on the dose.

2.1.5 Radiation Units:

Until quite recently the unit of radioactivity was the *curie* (Ci). It was originally related to the activity of one gram of radium but the definition was later standardized as 3.7×10^{10} nuclear disintegrations per second, which is almost the same. The SI unit of activity is the *Becquerel* (Bq) which is defined as 1 nuclear disintegration per second.

The ionization of a gas provides a means of detecting radiation and the first widely used radiation unit, the *roentgen,* was based on the ionizing effect on air of X- and γ-radiation. The unit has several limitations and so two further units, the *rad* and the *rem,* were introduced.

More recently, these latter two units have been replaced in the SI system by the *gray* and the *sievert*, respectively. These units will now be defined.

Exposure is a quantity expressing the amount of ionization caused in air by X- and γ-radiation. The special unit is the *roentgen* (R) which corresponds to the production of ions carrying a charge of 2.58×10^{-4} coulombs per kilogram of air. This corresponds to 0.00869 J/Kg of air. This unit is inadequate as a radiation unit since it applies only to X- and γ-radiation and their effect on air. The concept of radiation absorbed dose was introduced to overcome these difficulties.

Absorbed dose is a measure of energy deposition in any medium by all types of ionizing radiation. The original unit was the *rad* and was defined as an energy deposition of 0.01 J/Kg. In the SI system the unit of absorbed dose is the *gray (Gy)* and is defined as an energy deposition of 1 J/Kg. Thus 1 Gy = 100 rad.

Although the quantity of absorbed dose is a very useful physical concept, it is found that in a biological system the same degree of damage is not necessarily produced by the same absorbed dose of different types of radiation. For example, 0.01 Gy of fast neutrons can do as much damage as 0.1 Gy of gamma radiation. This difference must be taken into account if we wish to add doses of different radiations to obtain the total effective dose. To do this we must multiply the absorbed dose of each type of radiation by its *Quality Factor (Q)* which is a measure of the ability of a particular radiation to cause damage. The quantity obtained when the absorbed dose is multiplied by the quality factor is known as the *dose equivalent* the unit of which was originally the *rem.* In the SI system the unit of dose equivalent is the *Sievert* (SV) which is given by the following:

dose equivalent (Sv) = absorbed dose (Gy) x Q x **N**

where **N** is a further modifying factor which might take into account such factors as absorbed dose rate and fractionation. (Radiation treatment is usually fractionated, that is, given in a series of daily doses spread over a number of weeks. There are four factors that

may influence the effect of such fractionated treatment, these are the *repair* of sublethal damage, *repopulation* by surviving cells in the irradiated tissues, *redistribution* of cells and *reoxygenation* of hypoxic cells.)

The following table gives the values of Q for different forms of radiation.

Type of Radiation	Q
X-Rays, γ-rays & electrons	1
Thermal Neutrons	2.3
Fast Neutrons & Protons	10
α-particles	20

For non-uniform irradiation of the whole body, weighting factors have been assigned to the various individual organs, relative to the whole body as 1.0, reflecting the harm attributable to irradiation of each organ. These weighting factors are shown in the following table [07].

Tissue	W_r
Gonads	0.25
Breast	0.15
Red Bone Marrow	0.12
Lung	0.12
Thyroid	0.03
Bone Surfaces	0.03
Remainder	0.30

2.2 *Differential X-Ray Absorptiometry.*

2.2.1 Introduction to Differential X-Ray Absorptiometry.

After the discovery of X-rays by Roentgen in 1895 [01], one of the first properties discovered about their interaction with matter was the presence of jumps in the absorption coefficient by Barkla [08] in 1909. These jumps are now known to be due to the photoelectric effect described previously. The energy at which this transition in the absorption coefficient occurs was found to be characteristic of the element under investigation. Differential X-ray absorptiometry (or X-ray absorption edge spectrometry), first applied by Glocker and Frohnmayer [09] in 1925, is based on this phenomenon. One or more energies on each side of the elemental absorption edge are passed through a sample and the analyte concentration is calculated using the measured intensities of these energies.

Engstrom et al. [10] used an X-ray source with a secondary target to supply two fluorescent lines above and below the K-edge to achieve chemical analysis of a sample. The method was developed later by Jacobson and Heedman [11] for the determination of iodine uptake in the thyroid. Atkins et al. [12] improved the technique with the addition of a semiconductor detector enabling them to look at several fluorescent lines thereby allowing limited multielement concentration determination to be performed. Mistretta et al. [13] altered the experimental technique by filtering the primary beam allowing high intensities to be achievable. This technique of differential X-ray absorptiometry has been used by several authors in the area of Differential Tomography, see chapter 3.

Differential X-ray absorptiometry (or the similar technique of monochromatic X-ray absorptiometry) is used in this thesis to determine the minimum concentration visible when an object is scanned using the technique of computerised tomography. The process and theory of this method will now be explained by way of an introduction to

its subsequent application.

2.2.2 Theory of Differential X-Ray Absorptiometry.

For a monochromatic X-ray pencil beam passing through a specimen containing an analyte (a) within a matrix (m), the detected flux after passing through the specimen is given by

$$N = N_o e^{-\mu t} \tag{2.10}$$

where μ is the mass attenuation coefficient of the specimen and t is the equivalent thickness given by $t = \rho x$ where ρ is the density and x is the thickness. The total mass attenuation coefficient μ is a combination of the analyte and matrix mass attenuation coefficients;

$$\mu = W_a \mu_a + W_m \mu_m \tag{2.11}$$

where W_a and W_m are the weight fractions of the analyte and matrix respectively. Substituting this into equation 2.10 gives

$$N = N_o \exp\left\{ - \left(W_a \mu_a + W_m \mu_m \right) t \right\} \tag{2.12}$$

If the beam consists of two energies, one with an energy just to the low side and the other just to the high side of the K-absorption edge of the analyte, then the following are the detected number of photons at these energies;

$$N_l = N_{ol} \exp\left\{ - \left(W_a \mu_{al} + W_m \mu_{ml} \right) t \right\} \tag{2.13}$$

$$N_h = N_{oh} \exp\left\{ - \left(W_a \mu_{ah} + W_m \mu_{mh} \right) t \right\} \tag{2.14}$$

Dividing these equations gives

$$\frac{N_l}{N_h} = \left\{ \frac{N_{ol}}{N_{oh}} \right\} \cdot \exp\left\{ W_a \left(\mu_{ah} - \mu_{al} \right) t \right\} \cdot \exp\left\{ W_m \left(\mu_{mh} - \mu_{ml} \right) t \right\} \tag{2.15}$$

Rearranging this equation gives

$$W_a t = \ln\left\{ \frac{N_l N_{oh}}{N_h N_{ol}} \right\} \cdot \left(\mu_{ah} - \mu_{al} \right)^{-1} - W_m t \cdot \left\{ \frac{\mu_{mh} - \mu_{ml}}{\mu_{ah} - \mu_{al}} \right\} \tag{2.16}$$

With reference to figure 2.06, it can be seen that when $E_l \cong E_h$ that the mass attenuation coefficient of the matrix changes very little resulting in $\mu_{mh} - \mu_{ml} \cong 0$. Therefore the equivalent thickness of the analyte is given by

34

Mass Attenuation Coefficient.
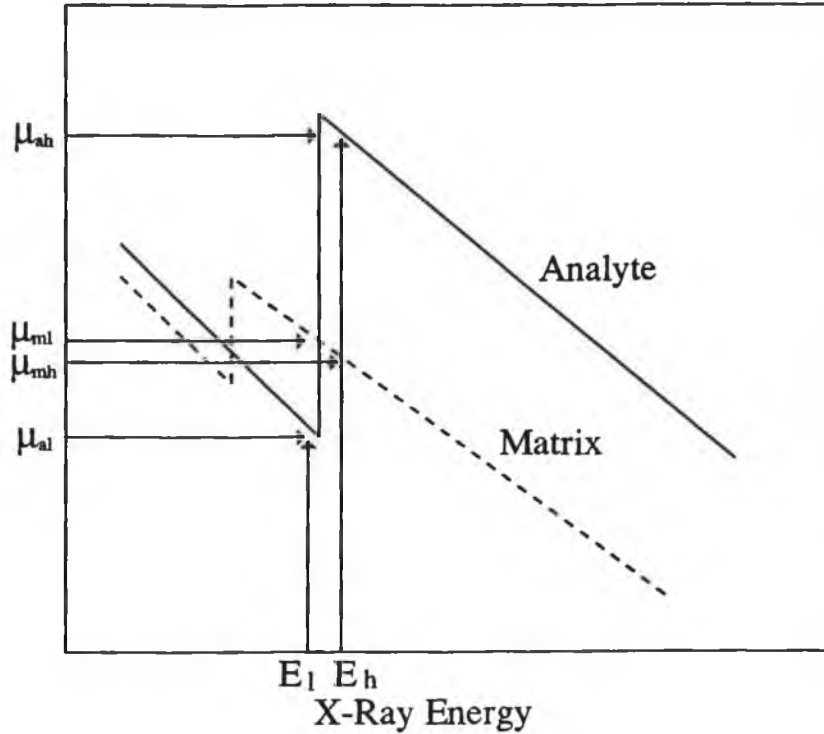
Figure 2.06
Variation of the mass attenuation coefficient of the analyte and matrix near the K-edge.

$$t_a = W_a t = \ln\left(\frac{N_l N_{oh}}{N_h N_{ol}}\right)\left(\mu_{ah} - \mu_{al}\right)^{-1} \qquad (2.17)$$

The difference between equation 2.16 and 2.17 is the term

$$t_m \left(\frac{\mu_{mh} - \mu_{ml}}{\mu_{ah} - \mu_{al}}\right) \qquad (2.18)$$

which gives the effect the matrix has on the equivalent thickness of the analyte. Near the K-edge $(\mu_{ah} - \mu_{al})$ is positive while $(\mu_{mh} - \mu_{ml})$ is negative, the effect being to reduce the analyte equivalent thickness.

To obtain an accurate value of the analyte concentration, an accurate value of $(\mu_{ah} - \mu_{al})$ is needed, and also that $(\mu_{mh} - \mu_{ml}) = 0$. The latter condition will be satisfied if the two X-ray energies are very close to the K-edge, but, because of absorption fine structure, an accurate value for the difference in analyte mass

35

attenuation coefficient may not be available. Unless the matrix effect is negligible either because the matrix concentration is relatively low or because it consists of elements with a low average mass attenuation coefficient, corrections will have to be made to the projection data.

2.2.3 Techniques to Correct for Matrix Effects.

Two methods to correct for matrix effects in the determination of analyte equivalent thickness will now be discussed. In the first method, it is assumed that the analyte can be added to the matrix after an initial scan of the matrix alone. When no analyte is present, then

$$\frac{N_{ml}}{N_{mh}} = \frac{N_{ol}}{N_{oh}} \exp\left\{\left(\mu_{mh} - \mu_{ml}\right)t_m\right\}$$

(2.19)

Substituting this into equation 2.15 gives

$$t_a = \ln\left(\frac{N_l N_{ml}}{N_h N_{mh}}\right) \cdot \left(\mu_{ah} - \mu_{al}\right)^{-1}$$

(2.20)

Here, the transmitted fluences from the matrix-only scan are used as if they were the incident fluences at the low and high energies.

The second method requires only one scan of the object. Here four or more energies are selected, two on the high side and two on the low side of the K-edge and near the K-edge. The transmittance on the low and high side at the K-edge are obtained by extrapolation of the counts for the two energies on the low side and the two energies on the high side respectively. At the K-edge (μ_{mh} $- \mu_{ml}$) = 0, therefore the correct value for the attenuation coefficient is obtained. Generally a linear extrapolation will suffice. Also, more than four energies will improve the extrapolation value.

2.3   *Reconstruction Algorithms.*

2.3.1 Introduction to Reconstruction Algorithms.

The aim of CT is to obtain information regarding the nature of the material at a specific location inside a body. In current CT scanners this information is obtained by "reconstructing" individual cross sections of the body by measuring the intensity of X-ray beams transmitted through the body. The total X-ray attenuation along a line is determined by the sum of the linear attenuation coefficients at individual points along that line. Since different tissue/tumour types have different linear attenuation coefficients, knowledge of the distribution of linear attenuation coefficients in the cross section provides the type of information required. Therefore, the problem is to find a method that when given the total X-ray attenuation along a large number of lines in the cross section, yields the linear attenuation coefficient at various points in the body.

A reconstruction algorithm is a collection of step - by - step instructions that allow conversion of the total X-ray attenuation along given lines into the linear attenuation coefficient at selected points. The reconstruction algorithms described here deal only with the case of parallel data collection as opposed to fan-beam data collection and reconstruction. In parallel data collection, only one detector measures the output from the source at one particular time. This is shown in figure 2.07 and is by far the simplest case to study. In this mode, either the body is stepped / rotated or the source-detector system is stepped / rotated. This is the method by which data was collected and simulated in the course of the work presented here. There are three main reconstruction algorithms used in CT; Fourier Transform Reconstruction, Iterative Reconstruction Techniques, and Filtered Backprojection. Filtered backprojection is the method used throughout this work, because of the ease of implementation and the speed in reproducing an image.

ART offers the advantage of a less noisy image and it is also easy to implement, however, it takes approximately 40 times longer to produce an image compared to filtered backprojection. Fourier transform reconstruction has the benefit of easy selective spatial frequency enhancement but it is by far the most complex to implement. Therefore, filtered backprojection will be explained in some detail with descriptions of the ART and fourier transform reconstruction algorithms being given in appendix 5.
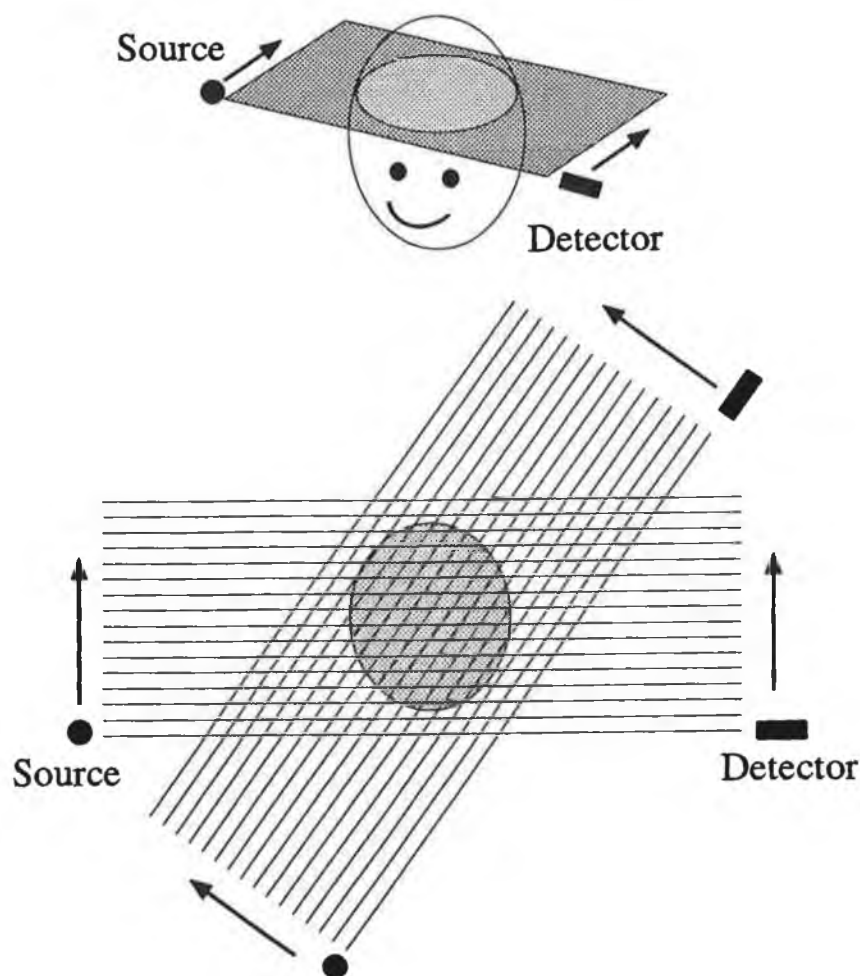
Figure 2.07

Parallel mode of data collection. The source and detector are moved in linear steps. The scan plane is then rotated and the process repeated.

2.3.2 Filtered Backprojection.

Backprojecting the image is the opposite process to that of obtaining the projection data, in that a one - dimensional function (ie. the projection data) forms a two

- dimensional distribution $T_\phi[x,y]$ by smearing the one - dimensional function, $G_\phi(x)$, uniformly over all space in the direction perpendicular to the y direction. This process is shown for several sets of projection data for a cylindrically symmetric object, in figure 2.08. The thickness of the lines is proportional to the amplitude of the fractional transmittance. However, backprojection is not the true inverse of the projection operation. Projection followed by backprojection does not reconstruct the original object.
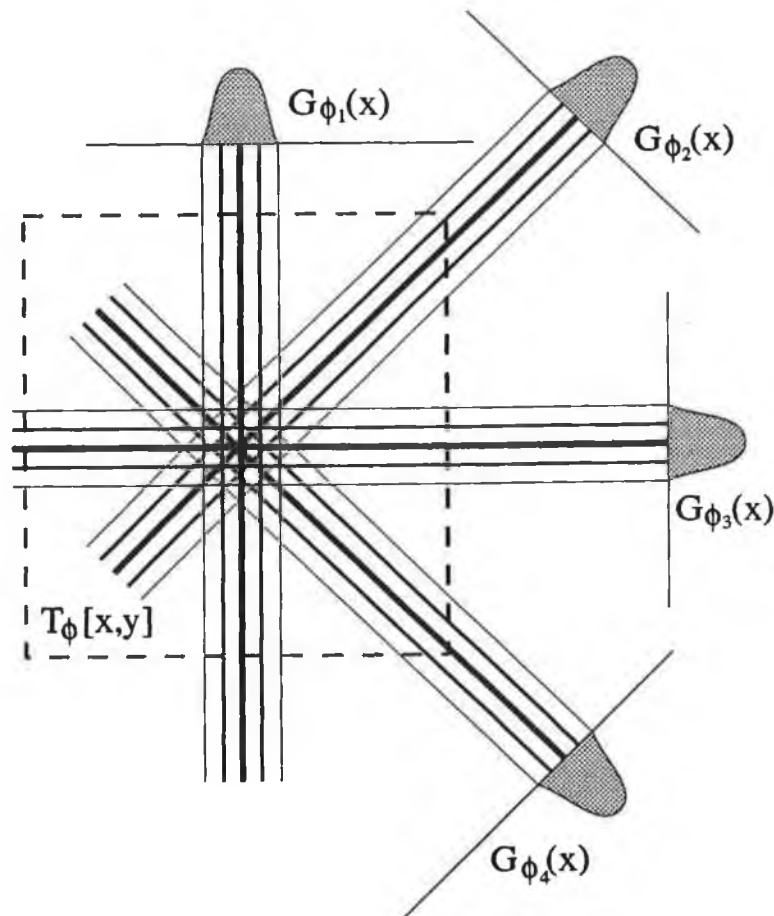
Figure 2.08

Demonstration of the backprojection process. Shown are four projections and the summation image which is formed by summing the four corresponding backprojections.

The process of combining many backprojections creates a new two - dimensional image, called the summation image. If a number of backprojections are taken at angles Φ_i, where i is the backprojection number, this summation image is just the arithmetic sum of these backprojections. If

this image is denoted by $B_d(r,\theta)$, $B_d(x,y)$, etc. as appropriate, then

$$B_d(x,y) = \sum_i T_\phi[x,y] = \sum_i \mathbb{G}_{\phi i}(x) \qquad (2.21)$$

which in polar form is given by

$$= \sum_i \mathbb{G}_{\phi i}(r.\cos(\theta - \phi_i)) \qquad (2.22)$$

In the case of a continuous data set, the summation image, written in polar form, is given by

$$B_d(r,\theta) = \frac{1}{\pi} \int_0^\pi \mathbb{G}_\phi(r.\cos(\theta - \phi)) \, d\phi \qquad (2.23)$$

The ϕ integration extends to a range π and not 2π because all necessary information is available in this range of projection angles. Occasionally, the name *layergram* is also used to describe $B_d(r,\theta)$ [14].

If $\mu(x,y)$ is the original object, then

$$B_d(x,y) = \frac{1}{\pi} \int_0^\pi \int_{-\infty}^\infty \mu(x,y) \, dy \, d\phi \qquad (2.24)$$

If the special case of a point object located at the origin is considered, the object is represented by $\mu_\delta(x,y) = \delta(x)\delta(y)$ where $\delta()$ is the Dirac delta function. The resulting expression for $B_d(r,\theta)$ will be the point spread function $P_u(r,\theta)$ (where u denotes unfiltered) given by

$$P_u(r,\theta) = \frac{1}{\pi} \int_0^\pi \int_{-\infty}^\infty \delta(x)\delta(y) \, dy \, d\phi \qquad (2.25)$$

$$= \frac{1}{\pi} \int_0^\pi \delta(x) \, d\phi \qquad (2.26)$$

$$= \frac{1}{\pi} \int_0^\pi \delta(r.\cos(\theta - \phi)) \, d\phi \qquad (2.27)$$

To evaluate this integral, use is made of the fact that

$$\delta[f(x)] = \sum_i \left|\frac{df}{dx}\right|_{x=x_i}^{-1} \delta(x - x_i) \qquad (2.28)$$

where $f(x_i) = 0$ for a delta function (see Appendix 5). Here $f(\phi) = r.\cos(\theta - \phi) = 0$ has only one root θ in the range of integration $0 - \Pi$, ie. $\cos(\theta - \phi) = 0 \Rightarrow \phi = \theta + \pi/2$,

$$\Rightarrow P_u(r,\theta) = \frac{1}{\pi|r.\sin(\theta - \phi_i)|} \int_0^\pi \delta(\theta - \phi_i) \, d\phi \qquad (2.29)$$

$$= \frac{1}{\pi |r.\sin(\theta - \phi_1)|} = \frac{1}{\pi r} \qquad (2.30)$$

since $\cos(\theta - \phi_1) = 0$ then $|\sin(\theta - \phi_1)| = 1$. This result can be understood by considering the image formed from a large number of line delta functions passing through the origin, see figure 2.09. The increasing density of lines toward the centre represents the point spread function and accounts for the 1/r distribution.
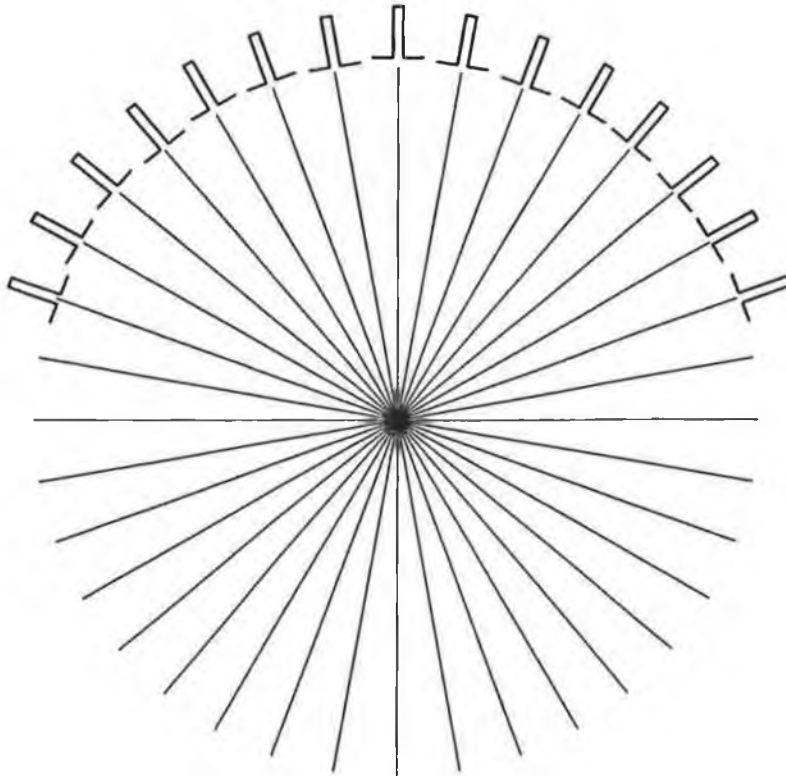
Figure 2.09
**A large number of backprojected delta functions which result
in a point spread function that approaches the 1/r functional form
form as indicated by the increasing line density toward the
centre of the pattern.**

A general distribution of the attenuation coefficient $\mu(r,\theta)$ is given by

$$B_d(r,\theta) = \mu(r,\theta) \ ** \ P_u(r,\theta) = \mu(r,\theta) \ ** \ (1/\pi r) \qquad (2.31)$$

where the symbol ** represents a two - dimensional convolution. Consequently, this 1/r blurring will result in a very badly blurred image.

It has just been shown that the unfiltered summation image is equivalent to the object convolved with a 1/r

point spread function. Therefore, simply backprojecting the data will yield a blurred version of the image. By appropriately filtering the summation image, the quality of the reconstructed image can improve. Summation and filtering are both linear operators and thus it is possible to filter the data before summation. This filtering is one - dimensional since it is applied to a one - dimensional function $G_\phi(x)$, the projection data.

The method requires that each projection be convolved with a filter function q(x) giving

$$G_\phi^+(x) = \int_{-\infty}^{\infty} G_\phi(x') \cdot q(x-x') \, dx' \equiv G_\phi(x) ** q(x) \qquad (2.32)$$

These filtered projections are now backprojected to yield the summation image;

$$\hat{\mu}(r,\theta) = \frac{1}{\pi} \int_0^\pi \left[G_\phi(x) ** q(x) \right] d\phi \qquad (2.33)$$

This converted to polar co-ordinates and put in terms of the attenuation coefficient gives,

$$\hat{\mu}(r,\theta) = \frac{1}{\pi} \int_0^\pi \int_{-\infty}^{\infty} \int_{-\infty}^{\infty} \mu[x,x'] \cdot q(r \cdot \cos(\theta-\phi)-x) \, dydx'd\phi$$

$$(2.34)$$

The filter function must have negative side lobes. Only then can the resulting point spread function be compacted [15]. The filter function most widely used in this thesis is that of the Ramachandran - Lakashminarayanan (Ram-Lak) filter given by

$$Q(s) = \frac{1}{4d} \qquad \text{for } s = 0$$
$$= \frac{1}{(\pi sd)^2} \qquad \text{for } s = \text{odd integer}$$
$$= 0 \qquad \text{for } s = \text{even integer.}$$

in its discrete form [16]. The continuous and discrete form of this filter function are shown in figure 2.10. The Ram-Lak filter is especially suited for images containing small high spatial frequency objects whereas the Hann filter [17] is good for large low contrast features. A third, the Shepp-Logan filter [18] is a compromise between two other functions.

To illustrate how convolution / filtered backprojection is implemented, consider the image of the rod shown in figure 2.11a. Figure 2.11b shows the

42

(A) Continuous Form.
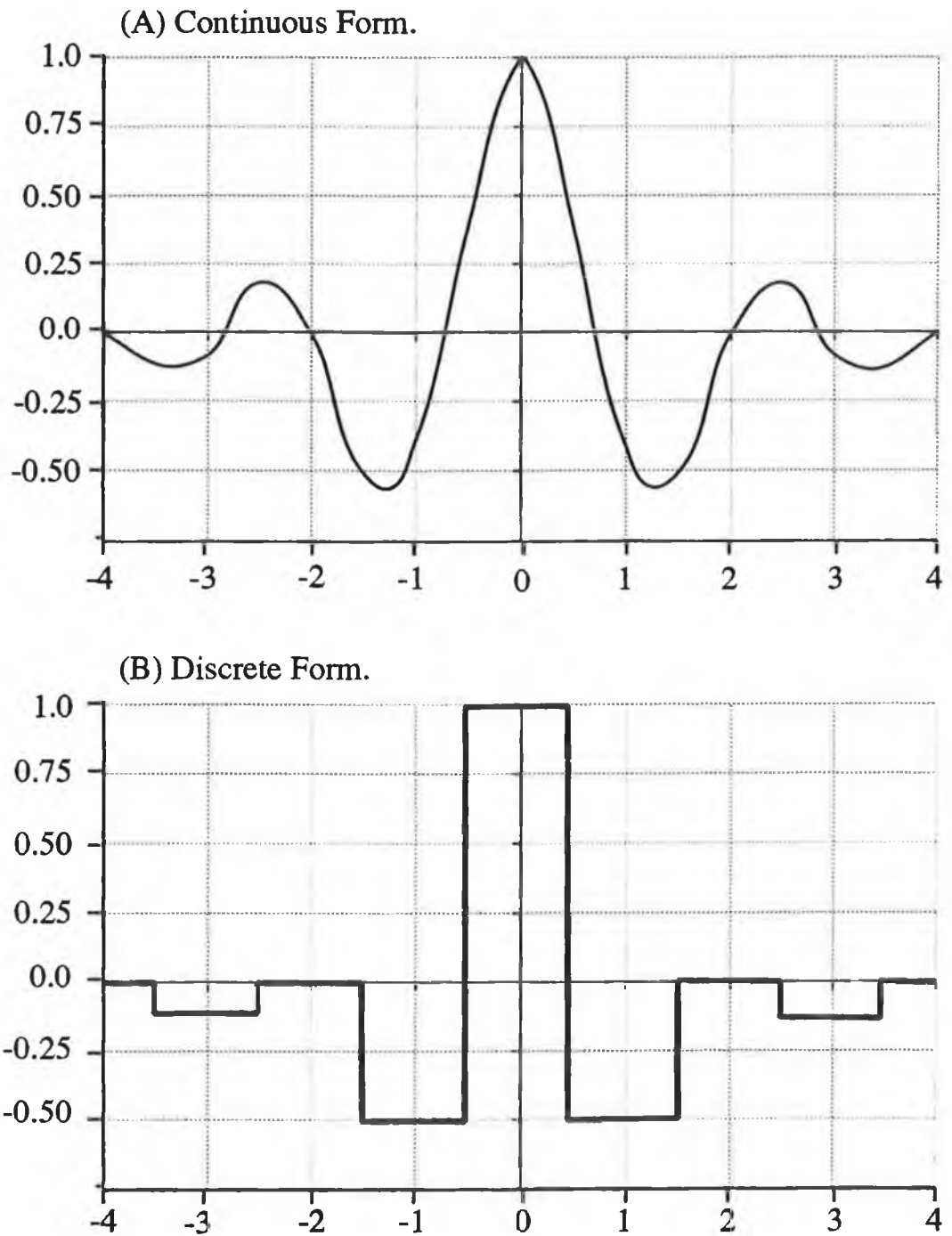
(B) Discrete Form.

Figure 2.10

The continuous (a) and the discrete (b) form of the Ramachandran - lakshminarayanan filter.

(A) Transmitted Intensity

(B) $Ln(I_o/I)$

Ram-Lak Filter Function

(C)

Moves one step at a time.

F_4 F_2 F_1
F_5
F_3

(D) Filtered Projection Data

M_5
M_3
M_1
M_4
M_2
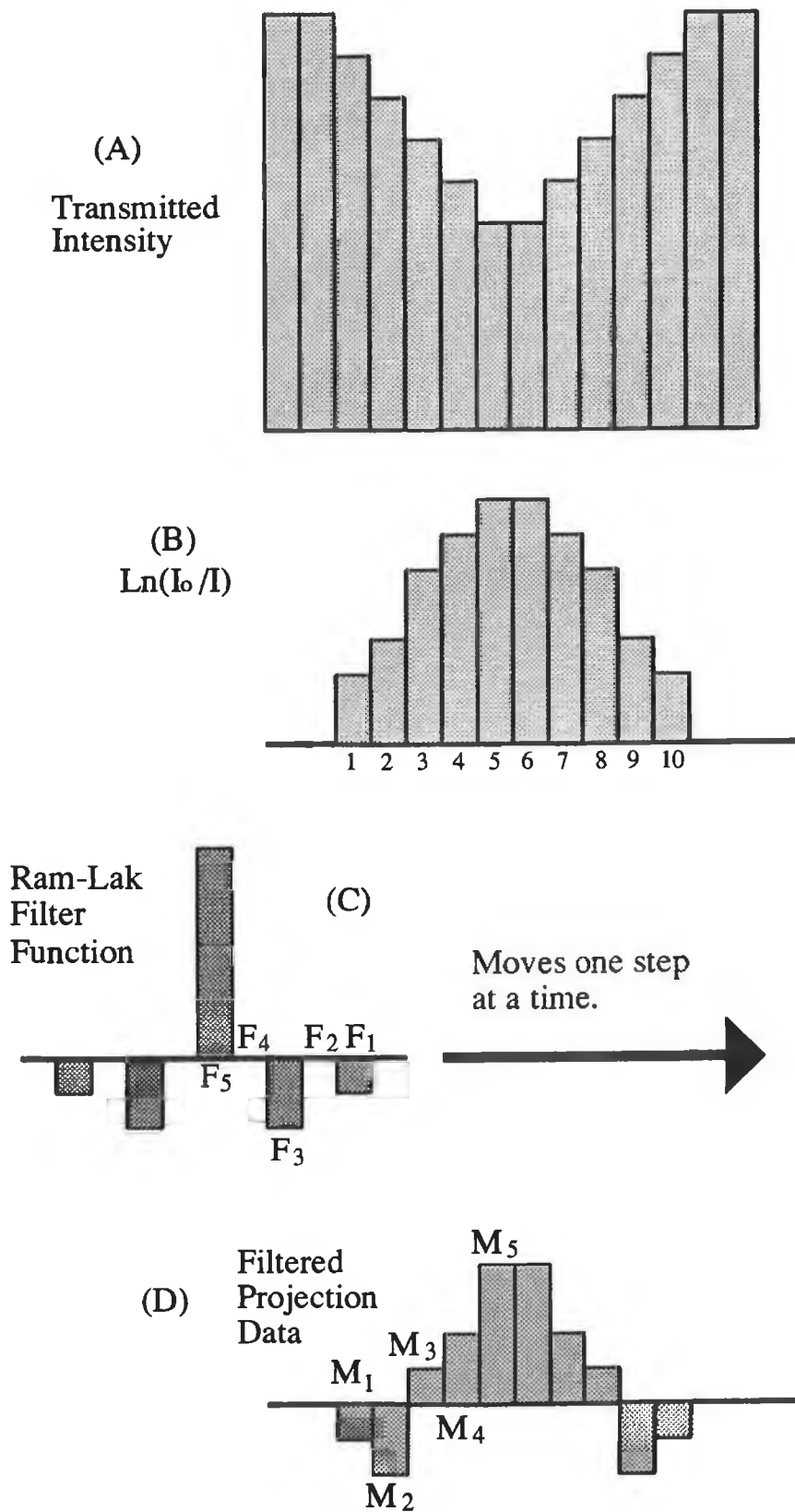
Figure 2.11
The process of filtering the projection data.

projected scan profile ($G_\phi(x,y)$ = $\ln(I_o/I)$)with the
discrete form of the Ram-Lak filter shown in figure 2.11c.

To obtain the filtered projection data, each of the
values in (b) are multiplied by the corresponding values
of the filter function (c). For example, the first value
in the filtered projection data is given by

$$M_1 = (1 * F_1) + (2 * 0) + (3 * 0) + ...$$

The filter function is now moved one step to the right and
the process repeated, eg

$$M_2 = (1 * F_2) + (2 * F_1) + (3 * 0) + ...$$
$$M_3 = (1 * F_3) + (2 * F_2) + (3 * F_3) + (4 * 0) + ...$$

etc.

Repeating the process across the profile (b) results in
the profile (d). It is quite different from the original
profile. This profile is now backprojected to obtain the
final image.

2.4 *Errors Inherent in CT Systems.*

The quality of a CT image is very dependent on the data acquisition and reconstruction methods. Some of the limitations and errors occurring in a CT image will now be discussed in brief. The limitations imposed by the data acquisition procedures include

1) Beam profile
2) Number of projections
3) Angular distribution of projections
4) Detector malfunctions
5) Motion artifacts

while the errors introduced by reconstruction methods include

1) Pixel size
2) Aliasing
3) Gibbs phenomenon
4) Reconstruction filters
5) Beam hardening

Data Acquisition Limitations:

1) *Beam Profile:* The profile of the incident X-ray beam places a fundamental limitation on the spatial resolution achievable. Two small features separated by less than the FWHM of the beam cannot be distinguished from a larger single feature [19]. This is known as the *Partial Volume Effect.*

2) *Number of Projections:* It has been shown by Brooks and DiChiro [14] that if for each projection there are n rotational data points, then the ideal number of projections is given by

$$M_o >= n\pi/4$$

Note: In the work presented in this thesis, the number of rotations is equal to the number of projections, thereby satisfying the above condition.

If more than M_o projections are obtained, the image is said to be overdetermined. Here the image represents the average of the excess and necessary information. If fewer than M_o projections are available, the image is said

46

to be underdetermined. The iterative reconstruction techniques described in appendix 5 handle under determined data better than analytic techniques, converging the image to the smoothest possible solution [14]. Generally commercial scanners work with overdetermined images.

3) *Angular distribution of projections:* Normally the projections need only span 180 degrees with the measurements between 180 and 360 degrees being redundant. If the projections are asymmetric with respect to the centre of rotation, or the centre of rotation has been misidentified, then projections spanning 360 degrees can suppress the artifacts arising from these problems [19]. However, rather than risk not detecting a misallignment, projections should be performed over 180 degrees. The system can then be readjusted.

4) *Detector Malfunctions:* In all but the first generation scanners, if one or more detector should fail during operation, a ring artifact is produced in the image. A similar effect occurs even if the response of the detectors is not uniform among the detectors. This effect is generally alleviated by pre-imaging calibration scans.

5) *Motion Artifacts:* The most common example of these occur in scans of the abdomen where the movement of gas bubbles in the intestines give rise to artifacts. If an air pocket moves during the scan, inconsistent data is presented for reconstruction usually resulting in black lines (low attenuation) emanating from the region of the gas bubble.

Reconstruction Limitations:

The above limitations are intrinsic to the data acquisition and equipment. The following effects occur due to the reconstruction procedures.

1) *Pixel Size:* The size of the pixel in the matrix onto which the data is reconstructed should be equal to or less than the sample spacing [19] otherwise information is lost due to averaging of the data.

2) *Aliasing:* If the Nyquist condition is not satisfied (ie. the object is not sampled at a frequency greater than or equal to twice the highest spatial frequency present),

then high frequency components appear artificially as lower spatial frequency components. This effect is similar to the Moire pattern visible on a TV image of a stripped shirt. The effect is generally small, but may be noticeable at sharp boundaries, and is minimised by the use of selective low pass filtering [17].

3) *Gibbs Phenomenon:* Due to the finite bandwidth or frequency response of the system, edges can exhibit an overshoot or ringing response, called the Gibbs phenomenon. The range or the spacing of these oscillations decrease as the cutoff frequency increases. This effect can be reduced by using a frequency response or filter function which does not have a sharp cutoff frequency, but rolls off at higher frequencies [14].

4) *Reconstruction Filters:* If filtered backprojection is being used as the reconstruction algorithm, then the choice of convolution / reconstruction filter will determine the type of image obtained. Of the three main filters used, ie. Ram-Lak, Shepp-Logan and Hann, it cannot be said that one is superior to the others. If large low – contrast features are of interest, then the Hann filter is preferable; if small high – contrast features are required, then the Ram-Lak filter is superior. The Shepp-Logan offers a compromise between the two [19].

5) *Beam Hardening:* When a polychromatic source is used, as X-rays pass through the body, low-energy photons are preferentially absorbed making the beam richer in higher energies and thus more penetrating or harder. A "harder" beam gives a lower effective attenuation coefficient. Therefore rays passing through the centre of a patient give a lower attenuation for tissue than rays passing through the edges of the patient. The partial solution to this problem is to pre-process the data such that $Ln(N_0/N)$ is a linear function of increasing thickness for a polychromatic beam [17].

References

[1] Roentgen, W.C.
"On a New Form of Radiation."
The Electrician, Jan. 24, pp.415-417, 1896

[2] R.E. Lapp, H.L. Andrews,
Nuclear Radiation Physics, Prentice-Hall Inc., New Jersey,
1972.

[3] Moseley, H.G.
"High - Frequency Spectra of the Elements."
Phil. Mag., Vol. 26, pp.1024-1034, 1913.

[4] Gifford, D.,
"A handbook of physics for radiologists and radiographers."
Wiley & Sons, 1984.

[5] Sanders, J.M., Spyrou, N.M.
"Suitability of Detectors for Imaging Applications."
Nucl. Inst. Methds. Vol. 193, pp. 79-86, 1982.

[6] Tsoulfanidis, N.
"Measurement and Detection of Radiation."
McGraw - Hill series in Nuclear Engineering, New York,
1983.

[7] "An Introduction to Radiation Protection"
A. Martin, S. Harbison, Chapman & Hall, New York, 1990

[8] Barkla, C.G., Sadler, C.A.
"Absorption of Roentgen Rays."
Phil. Mag., Vol. 17, pp.739-760, 1909.

[9] Glocker, R., Fronhnmeyer, W.,
"Roentgen - Spectroscopic Determination of the Quantity of
an Element in Mixtures."
Ann. Phys., Vol. 76, pp.369-395, 1925.

[10] Engstrom, A.,
"Quantitative micro- and histo-chemical elementary
analysis by Roentgen absorption spectrography."
Acta. Radiol., Vol. 69, 1946

[11] Jacobson, B., Heedman, P.A.,
"Thyroid iodine determined by X-ray spectrophotometry."
Jour. Clin. Endo. & Metabol., Vol. 24, pp.246-253, 1964

[12] Atkins, H.L., Hauser, W., Kraner, H.W.
"Absorption Edge Transmission Scanning."
Am. Jour. Roent., Vol. 114, No.1, pp.176-180, 1972

[13] Mistretta, C.A., Ort, M.G., Kelcz, F., et. al.,
"Absorption edge fluoroscopy using quasi-monoenergetic
X-ray beams."
Invest. Radiol., Vol. 8, No.6, pp.402-412, 1973.

[14] Brooks, R.A., DiChiro, G.,
"Principles of Computer Assisted Tomography (CAT) in
Radiographic and Radioisotopic Imaging."
Phys. Med. Biol., Vol. 21, No.5, pp.689-732, 1976.

[15] Barrett, H.H., Swindell, W.
"Radiological Imaging, Vol.2", Academic Press, 1981.

[16] Ramachandran, G.N., Lakshminarayanan, A.V.,
"Three dimensional reconstruction from radiography &
electron micrographs: Part III - Description &
Applications of the convolution method.", Ind. Jour. Pure
& Appl. Phys., Vol. 9, pp.997-1003, 1971.

[17] Waggener, R.G., Kereiakes, J.G., Shalek, R.J.
"Handbook of Medical Physics. Volume II."
CRC Press, Florida, 1984

[18] Shepp, L.A., Logan, B.F.,
"The Fourier reconstruction of a head section."
IEEE Trans. Nucl. Sci., Vol. NS-21, pp.21-43, 1974

[19] Taylor, T., Lupton, L.,
"Resolution, Artifacts and the Design of Computed
Tomography Systems."
Nucl. Inst. & Meth. in Phys. Res., Vol. A242, pp.603-609,
1986.

Chapter III
Sensitivities of Contrast Agents for use in Computerised Tomography of the Myocardium.

3.1 Introduction.

Note: A glossary of medical terms is provided in appendix 2 for easy reference.

"Cardiovascular disease continues to be the leading cause of death in the United States. An estimated 40 million Americans have diseases of the heart and blood vessels, resulting in a large burden of acute and chronic illness and disability. The total direct cost of heart diseases is approximately 12 billion dollars each year and the indirect costs have been estimated at a factor of 4 higher.

These statistics tend to indicate the relative inadequacy of current diagnostic methods to detect heart disease until it has progressed to a late stage".

The above extract from Boyd and Lipton's paper from 1983 [1] shows roughly the scale of the problem heart disease presents.

The traditional gold standard for cardiac diagnosis is cardiac catheterisation and angiography. However, this is an invasive procedure and has as such inherent problems. During recent years rapid developments have been made in the use of nuclear medicine techniques for imaging the heart. Several nuclear medicine techniques are proving useful in the evaluation of the patient with known or suspected heart disease. These include myocardial perfusion scintigraphy, gated-blood-pool radioangiography and left-to-right shunt studies [2]. However, these modalities are limited by their poor spatial resolution, eg. of the order of 1 cm.

Ultrasound has also been utilised in the study of the heart, by means of echocardiography. However, since

ultrasound energy is transmitted poorly through the air in the lungs, only a limited extent of the heart can be imaged.

These, and several other common methods, are described in more detail in the following section. However, CT has the advantage that very small density changes can be accurately detected. These small changes in density may be associated with some forms of myocardial disease. Contrast agents enhance this ability.

The following study will determine which element is most suitable for use as a contrast agent when used in computerised tomography. The study will consist of three sections; 1) investigation into existing theoretical work, 2) computed simulations to check these results and to make predictions on the results achieved with polychromatic spectra on a commercial scanner, and 3) experimental investigation of these results on a commercial scanner. The case to be studied is that of imaging the myocardium (heart wall) inside the thorax (chest).

3.1.1 Various Methods for Imaging the Heart.

The following are the normally used methods for imaging the heart and associated regions. A brief description of each method will be given for the purpose of providing a background to the use of contrast-enhanced computerised tomography.

Electrocardiography: Electrocardiography (ECG) is not an imaging method, but it does provide some information about coronary blood flow. Narrowing of the coronary arteries leads to inadequate perfusion of the heart muscle which result in changes in the electrical activity of the conduction tissue and of the muscle cells . These changes are most likely to occur after a work load has been placed on the heart. This activity is picked up using surface electrodes. In suspected cases, ECG's are obtained under standard conditions of exercise-induced stress. This approach is sensitive to severe forms of coronary artery disease, but it is plagued by both false-negative and false-positive results [3].

Ultrasound: Echocardiography refers to the non-invasive visualisation of the cardiac walls, valves and supporting structures, based on the reflection of ultrasonic waves from fluid-tissue interfaces. Normal M-mode scans and more recently 2-D high resolution scans provide a great deal of information about the heart. Very accurate measurements may be made of the ventricular cavity dimensions, arterial size, wall thickness and intra ventricular thickness. Recently, Doppler ultrasound has been utilised in the measuring of myocardial blood flow. Colour - coded Doppler imaging is particularly useful in this respect.

Nuclear Medicine: Cardiovascular nuclear medicine, in the early 80's, filled a previously existing vacuum in the early diagnosis of cardiac disease. In cardiac scintigraphy, a radiopharmaceutical is administered to the patient and will localise in a particular area of the body. This localisation of the drug can be imaged, both planely and tomographically, by gamma cameras.

Localisation of the radioactivity in the diseased area of the myocardium can be most helpful in the detection of myocardial infarction. Some radiopharmaceuticals localise in areas of normal heart muscle, but will not be taken up in areas of abnormal blood flow to the heart muscle. These procedures enable the diagnosis of myocardial ischemia. [4].

^{99m}Tc-pyrophosphate is utilised to access acute myocardial infarction. No patient preparation is required; 15 mCi of the radiopharmaceutical is administered intravenously and images are obtained after 1 to 2 hrs by a gamma camera. A low-energy, high resolution collimator is used and multiple views are obtained to evaluate the various segments of the left ventricular myocardium.

Thallium-201 has also proved useful in the imaging of the myocardium. It is suitable for rest-exercise or exercise-redistribution imaging using readily available scintillation cameras [2]. Following an intravenous injection, it is rapidly extracted by the tissues. The initial distribution of activity is proportional to

regional blood at the time of injection. Soon after this initial distribution (sec to mins), redistribution occurs such that the distribution more closely reflects the myocardial muscle mass.

Of the two ventricles of the heart, the left ventricle is much more prone to develop myocardial infarction. Therefore, most clinical nuclear medicine efforts are directed toward the left ventricle anatomical and functional assessment. However, right ventricle disorders can also be verified by this modality.

NMR: Unlike ferromagnetic materials, dia- and paramagnetic materials do not retain their magnetization when the magnetizing field is removed. However, for nuclear paramagnetism, the effect of the orbital electrons is to shield the nucleus from the effect of other magnetic moments, such as those due from other nuclei. Thus, when a magnetic field is removed from the material, nuclear magnetism persists for times from 0.1 to 1 sec. in the case of hydrogen nuclei, as compared to 1 X 10^{-6}sec. for electron paramagnetism [5].

It is thus possible to measure the rate of growth and the subsequent decay of the magnetisation of a material on removal of a magnetising field, by means of a radio-frequency signal emitted by the nuclear magnetic moments arising from the angular precession imposed upon them by the magnetising field applied.

When a field is applied to an unmagnetised specimen of magnetic material, of which the nuclear magnetic moments are in random orientations, the magnetic moments will tend to become aligned in the direction of the field, two states being possible, parallel or anti-parallel to this field. The stronger the field, the greater the number of magnetic moments that will be aligned with the field.

However, as the magnetic moments arise from nuclear spin, they do not align themselves precisely with the magnetic field, but precess around the direction of the field with a frequency of precession known as the Larmor frequency ω where

$$\omega = \gamma H \qquad (3.01)$$

54

where H is the field strength and γ the gyromagnetic constant. To obtain an image the procedure is as follows. If a combination of magnetic field gradients is utilised, a chosen volume element can be selected from within the specimen having a particular value of ω. This frequency, which by the choice of the appropriate value of the magnetic field, will be in the radio-frequency range, is applied in short bursts which excite the precessing nuclear magnetic moments. The radio-frequency magnetic field can impart enough energy to individual magnetic moments to rotate them through either 90° or 180° in relation to the main magnetic field, thus reducing the magnetisation of the system.

As the magnetic moments precess about the field, they emit an rf signal of the same frequency as the Larmor frequency. If they have received sufficient energy from the field, then this signal can be detected. There are a number of ways of scanning the tissue so as to form an image. Since the Larmor frequency is characteristic of the nucleus and the static magnetic field, a gradient can be applied to this constant field. This will define a *plane section* within the chosen volume. If a second magnetic gradient is applied at right angles to the first, elements are selected along a line in the plane section. This line can in turn be scanned by a third magnetic gradient applied at right angles to the first two, or the line can be scanned by sweeping across it with a range of Larmor frequencies appropriate to the nuclide of interest.

One of the advantages of NMR as an imaging technique is that there are several measurement options available. These include

T_1	Spin - lattice relaxation time
T_2	Spin - spin relaxation time
ρ	Nuclear Density.
S	Chemical shift.

At present most interest is directed towards obtaining spin density distribution of ^{1}H and the measurement of relaxation time T_1 and T_2. These options and how they are measured are explained in appendix 3.

The status of coronary blood flow can be inferred

from the concentration of the energy-rich substrates, phosphocreatine and adenosine triphosphate. The imaging of these compounds, using NMR, makes possible the assessment of energy metabolism and intercellular pH [6]. This information is of great importance in as much as there is incomplete understanding of the relationship between the severity of a stenosis of a coronary artery and the metabolic status of the muscle cells in the territory of that vessel.

Nuclear Magnetic Resonance has been used to produce cross-sectional images that provide detailed information about the structure and function of the central circulation, as well as about blood flow in major vessels. However, for cardiac studies it is both too slow and the resolution is inferior to other quicker methods [7].

Positron Emission Tomography (PET): Another radionuclide technique that has been developed recently is that of PET. Neutron-poor isotopes of carbon, nitrogen, oxygen and fluorine are incorporated within molecules such as water, glucose, oxygen, etc. These decay by positron-emission, which encounter electrons in the near vicinity and subsequently annihilate to give pairs of gamma photons travelling in opposite directions. These are detected by scintillation crystals mounted in a ring about the patient. The technique provides information about position and concentration of the isotope and allows image reconstruction tomographically. The method is especially well suited for metabolic studies related to the uptake of specific substances. It is also useful for the visualisation of myocardial scars. Because of the relatively poor spatial resolution, about 5-10 mm and slow imaging time, the method is not suitable for cardiac visualisation [3].

Coronary Arteriography: The standard approach to coronary X-ray imaging is based upon the direct injection of Iodine-containing contrast agents into the orifice of the coronary artery. The method produces excellent images of even the small branches of the coronary arteries. The

risks of the procedure limit its use to patients suspected of having far-advanced disease. About 1 in 100 suffers a significant complication and about 1 in 500 die as a consequence of the test [3].

Digital Subtraction Angiography (DSA): In recent years, DSA based upon images taken at different times or at different energy ranges, has been introduced into clinical practice [3]. This approach has allowed large and medium size arteries to be imaged without the need for arterial invasion. The use of dual energies has also improved the quality of DSAs, but the inadequate photon flux obtained from conventional sources by filtering has diminished the performance of this technique. The optimum approach would be to use intense monoenergetic beams, like those available in a synchrotron.

The principle use of this technique is the noninvasive study of blood vessels. With invasive procedures where catheters are inserted into vessels, large amounts of iodinated contrast material are present. In noninvasive studies, however, the iodine concentration is insufficient to be seen in a normal X-Ray image. Therefore, subtraction techniques are used to remove the extra tissue background so that only the iodine is imaged and limited in visibility by noise. In the subtraction process, an image is taken both before and after the administration of the contrast material. The two images are then subtracted with the difference signal, ie. the contrast material, left remaining.

Let $\mu_t(x,y,z)$ be the attenuation coefficient of the tissue and $\mu_c(x,y,z)$, the attenuation coefficient of the administered contrast agent. The subtraction operation involves first taking the logs of the measured intensities to derive the desired line integrals and then subtracting. The measured intensities, assuming monochromatic parallel X-rays are

$$I_1 = I_o \exp\left[-\int \mu_t(x,y,z)dz\right] \qquad (3.02)$$

$$I_2 = I_o \exp\left[-\int(\mu_t(x,y,z) + \mu_c(x,y,z))dz\right] \qquad (3.03)$$

By dividing both sides by I_0 and taking the natural logarithm gives;

$$\ln\left(\frac{I_0}{I_1}\right) = \int\mu_t(x,y,z)dz \qquad (3.04)$$

$$\ln\left(\frac{I_0}{I_2}\right) = \int(\mu_t(x,y,z) + \mu_c(x,y,z))dz \qquad (3.05)$$

Subtracting the logs, we have

$$\ln\left(\frac{I_0}{I_2}\right) - \ln\left(\frac{I_0}{I_1}\right) = \int\mu_c(x,y,z)dz \qquad (3.06)$$

the desired projection image of the contrast agent alone.

Computed Tomography: The principles of CT have already been explained extensively in chapters 1 & 2. The relevance of CT when imaging the heart will now be examined.

Conventional CT images of the thorax can provide useful information about the condition of the myocardium and the major blood vessels. Small changes in tissue density can be enhanced by intravascular contrast media administration. If contrast media is administered, areas of ischemic tissue or infarction are imaged as regions of lower density compared to the normal myocardium. However, during certain stages in the progression of ischemic myocardial disease, a further phenomenon is observed. If a scan is performed 20-30 mins after injection, a positive contrast agent density is observed in the region of infarction [1,8]. This delayed retention of contrast media shows abnormalities in the diffusion of the material through the myocardium.

Conventional CT images, without the use of contrast material, show little structure. The heart appears as a blurred shape within the lung field, with little or no apparent shape. However, in most conventional CT images, a contrast material is administered , usually in a vein in the arm. An injection of 25 ml of an iodinated compound, gives a CT enhancement of 5-10 percent in the heart, a sufficient change to give good images of the cardiac chambers and large cardiac vessels [9]. Lipton et al.

found that disease of the pericardium, lungs and pleura could be observed without contrast material but that disease of the cardiac chambers and myocardium requires administration of a contrast agent [9].

Present day scanners are too slow to image the heart without blurring, due to cardiac motion. Various methods have been developed to image the heart so as to remove this blurring. The first of these methods was gated CT. In this method, a series of scans are performed during steady state condition (ie. constant administration of a contrast material). ECG signals are simultaneously recorded and used retrospectively to sort out the projection data into corresponding phases of the cardiac cycle. A series of images are then reconstructed for each phase of the cardiac cycle [10,11]. It has the advantage that it requires very little modification to existing equipment, but the scan times are long (of the order of 1 minute) and the dose is consequently higher.

Redington proposed the use of multiple X-ray tubes [12]. There, he used three rotating tubes and three rotating fan-beam detectors. In such a system the angular range is reduced by 1/3 and the X-ray power is increased by 3. The same concept could be used with a stationary detector ring and three rotating sources, powered by slip-rings [1]. The Mayo Clinic's DSR (Dynamic Spatial Reconstructor) scanner took this multiple tube concept a stage further by the use of 28 X-ray tubes that may be electronically switched in sequence [13,14]. The DSR differs from commercial scanners in that it scans a volume, rather than a slice, using its video imaging system. It has a scan time of the order of 0.01 sec.

An alternative approach to high speed CT is based on the used of magnetic deflection of an electron beam to replace mechanical motion. The best example of this technique is the CVCT (Cardiovascular Computed Tomography) scanner, shown in figure 3.01 [1,15]. The CVCT consists of an electron beam scan tube, a stationary detector array, and a data-acquisition, reconstruction and display system. The modified Pierce-diode electron gun produces a 1000mA beam at 120kV. The beam is swept along a tungsten target

through an angle of 210 degrees. It has a scan time of
approximately 50 msec.
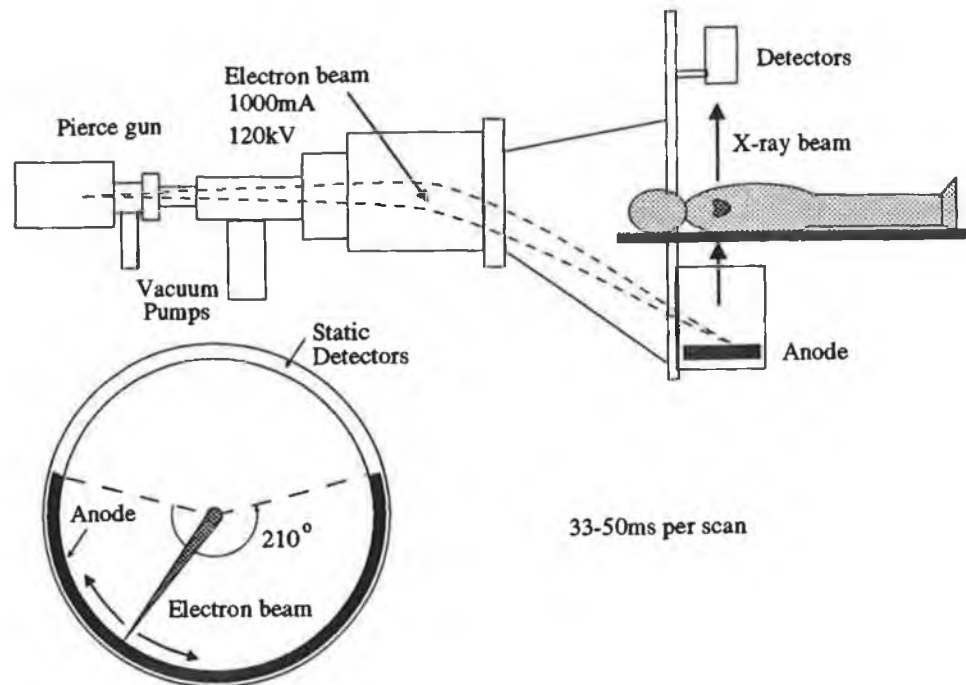
Figure 3.01
**Diagram of the Cardiovascular Computed Tomography
Scanner (CVCT).**

These two methods of ultrafast CT (DSR and CVCT) will
provide highly detailed examination of the left
ventricular aneurysms [16], myocardial blood flow [17], LV
mass and function [16], myocardial infarction extent [18]
etc., which are not adequately available on existing
scanners.

3.1.2 Reasons for this Study.

At present, the most commonly used contrast material
for various forms of X-ray imaging, is that of Iodine. For
a contrast - enhanced CT scan, it is usually given in
concentrations of 5 mg/cc depending on body weight, area
of the body to be imaged, etc. Lumbroso et al. found that
iodine was an excellent opacifying agent in the energy
range 50 to 80 kVp [19]. This is due to the maximum of

60

absorption of iodine lying at the peak energy of these incident spectrums. These are the energies most widely used in examinations like intravenous urography, carotid arteriography and digital angiography.

However, the question arises as to what is the optimum element to use as a CT contrast agent in terms of the minimum concentration that is necessary to be visible in the image. Adverse reactions to intravascular contrast media are relatively common, and occur in about 5% of investigations with a significant mortality rate (about 500 deaths per year in the USA alone) [20]. Therefore, a study will be made to determine whether or not iodine is the optimum element for use as a contrast agent when imaging the myocardium using CT. Various situations will be studied using theoretical, simulated and experimental methods. Figure 3.02 gives an easy reference to these situations and the methods used to investigate them.

	Subtraction	Theoretical	Simulation	Experimental
Monochromatic Scanning: Analyte contained in the full cylinder.	Yes	Yes	Yes	No
K-Edge Scanning: Analyte contained in the full cylinder.	Yes	Yes	Yes	No
Scanning with a Polychromatic Spectrum: Analyte contained in the full cylinder.	Yes	No	Yes	No
Scanning with a Polychromatic Spectrum: Analyte contained in the Myocardium Ring.	No	No	Yes	Yes
Scanning with a Polychromatic Spectrum: Analyte contained in the Myocardium Ring.	Yes	No	Yes	No

Figure 3.02
Figure showing the various cases studied and which methods were used to investigate these cases.

3.2.1   Introduction.

In this section the contrast agent will be referred to as the analyte because only a few of the atomic elements to be studied have any potential as in-vivo contrast agents. This is mainly due to toxicity problems, but also to a lesser extent, cost. The object to be scanned is designed to give an indication of the sensitivity for analyte detection in a structure of similar size to the myocardium in a human thorax. The scan geometry is shown in figure 3.03.
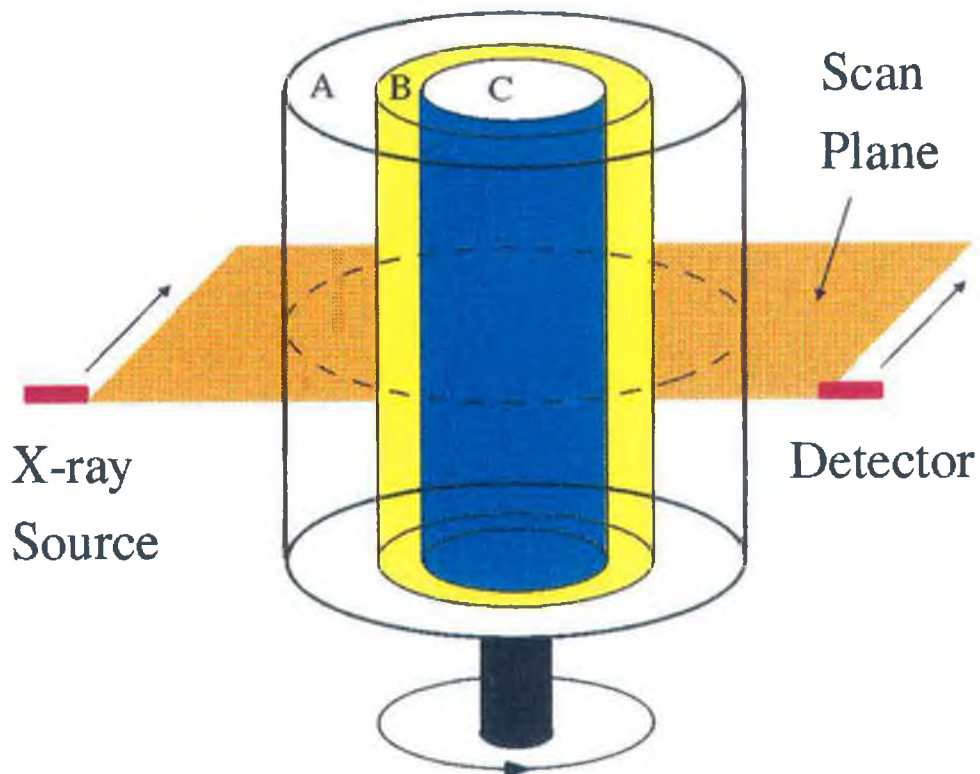
Figure 3.03
Schematic diagram of the phantom used in both the simulations and the experiments.

The cylindrical structure is considered to be filled with water. The complete scan of the object consists of M linear steps at M rotation angles between 0 and 180°. For the theoretical work , in which the minimum detectable concentrations are determined by calculation, the object is taken to be a cylinder in which the water and analyte

are homogeneously mixed. This cylinder is taken to be the outer cylinder in figure 3.03 with the inner partitions removed. The calculations for this situation give a rough idea of what may be expected when simulated images are generated for the full object which consists of the three concentric cylinders as shown, with the analyte added to the middle ring B. These calculations will also provide a means of testing the validity of the computer simulation technique by performing simulations for the full cylinder case. For the theoretical (and simulation) work, the diameters on figure 3.03 are A = 0.24m, B = 0.104m and C = 0.078m.

3.2.2 Monochromatic Beams.

There are three basic ways in which analytes can be imaged using monochromatic radiation.

Method 1:

The simplest method is to scan the object with a monoenergetic beam and to rely on the attenuation due to the analyte being sufficiently different from that of the matrix so that the analyte shows clearly in the final image. A drawback with this method is that it can only be used when a single analyte is present, otherwise another analyte of slightly lower attenuation, but present in a higher concentration, could yield an identical image. This situation will not be considered further because maximum sensitivity for the imaging of an analyte is obtained in the following two methods.

Method 2:

In some cases it is possible to scan the object before and after the analyte is added. The images are then subtracted to yield a final image of the analyte alone. This situation has been analysed by McCarthy and Fryar [21]. There it is shown that the minimum concentration observable in a cylindrical matrix, the diameter of which is X_m mean free paths at the X-ray energy used, is given by

$$C_a = \frac{\Delta U / U_m}{\left[\frac{\rho_a \mu_a}{\rho_m \mu_m} - 1 - \frac{\Delta U}{U_m} \right]} \rho_a \qquad (3.07)$$

$$\text{where,} \qquad \frac{\Delta U}{U_m} = \frac{6\sqrt{M}}{\sqrt{N_{ot}}} \; F \qquad\qquad (3.08)$$

$$\text{and } F = \frac{\exp[0.5(0.0275 + 0.762X_m - 0.0279X_m^2)]}{(0.762X_m - 0.0558X_m^2)} \qquad (3.09)$$

N_{ot} is the total number of incident photons for each complete scan and M is the number of linear steps per scan angle. U_m is the linear attenuation coefficient of the matrix and ΔU is the change in linear attenuation coefficient when the analyte is added. μ_m and μ_a are the respective mass attenuation coefficients for the matrix and the analyte. The attenuation coefficients are readily available from the literature [22,23]. ρ_m and ρ_a are the densities of the matrix and analyte respectively. It is assumed that the change in linear attenuation coefficient is solely due to the atomic element being imaged. At any energy, the maximum sensitivity is shown to occur when the diameter of the matrix approximately 3 mean free paths. This can be seen from the graph of $\Delta U/U$ vs. X shown in figure 3.04.
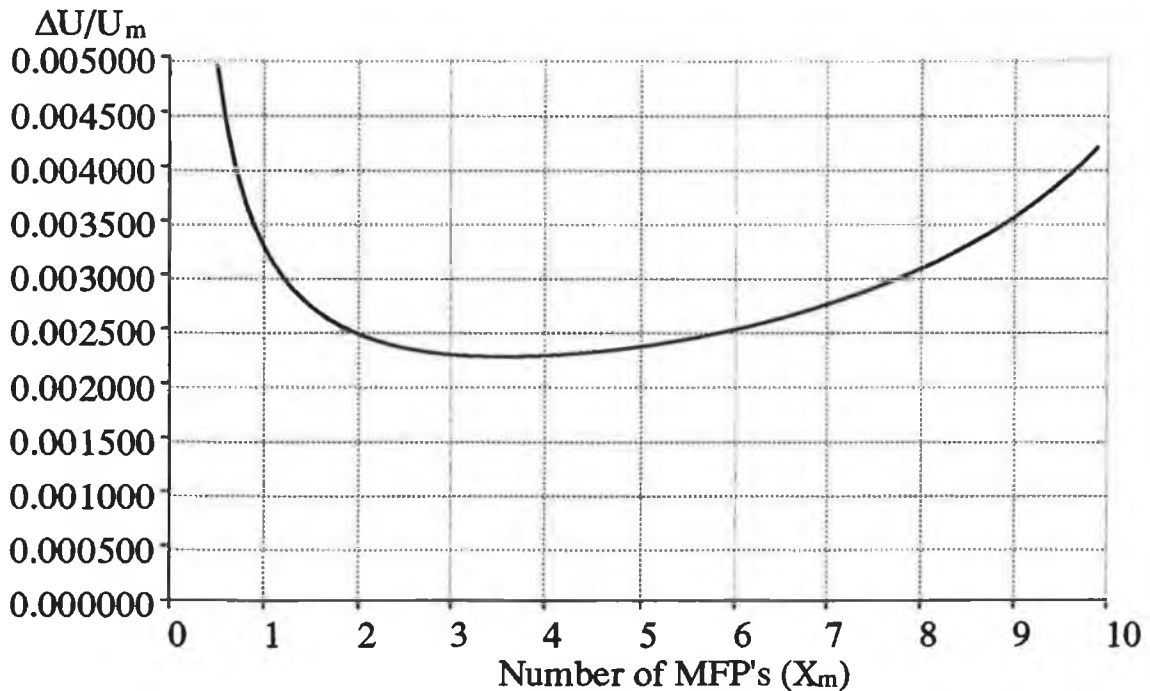
Figure 3.04

Minimum detectable change in attenuation coefficient as a function of the number of mean free paths through the matrix. These results are obtained from eqns. 3.08 and 3.09 (M=256, N_{ot} = 1E10).

Minimum Concentration (mg/cc)
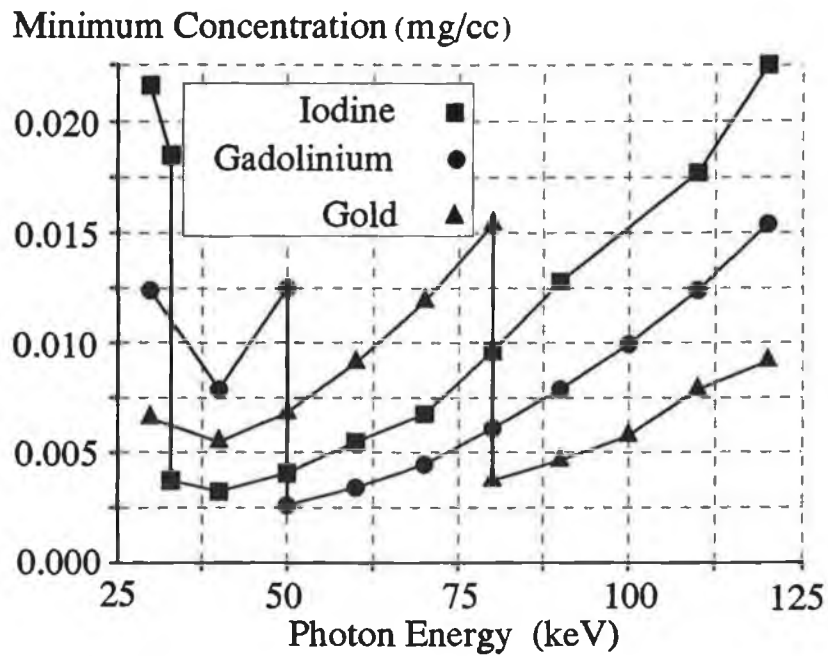
Figure 3.05
Minimum detectable concentrations of Iodine, Gadolinium and Gold as determined by eqn. 3.07. The object was a cylindrical matrix, 0.24m in diameter, scanned by a single monochromatic beam. N_{ot} = 1E10 photons and M = 256 projections.
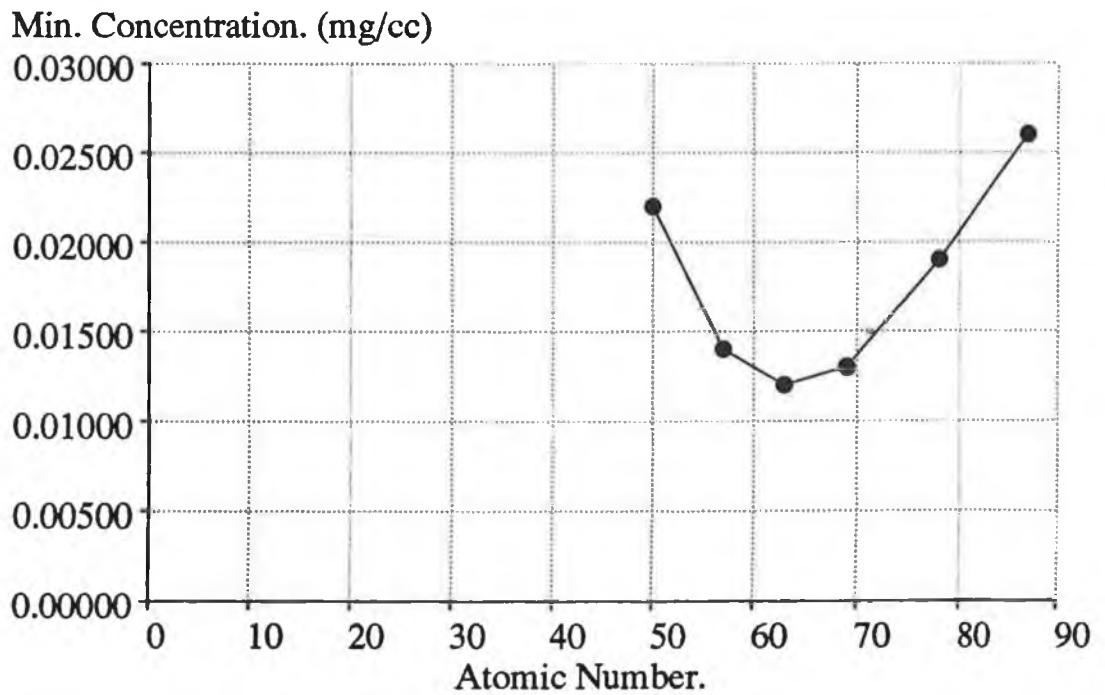
Figure 3.06
Minimum concentration values for various atomic numbers as given by eqn. 3.07, with N_{ot} = 1E10 photons and M = 40 projections.

Here equation 3.07 is applied to the case where the matrix is a cylinder of water 0.26m in diameter. The analyte is added homogeneously to the full cylinder. In figure 3.05, results are shown for the minimum concentration visible for iodine, gadolinium and gold. In these cases it is seen that the maximum sensitivity occurs for an X-ray energy just above the K-edge of the analyte. Figure 3.06 shows the minimum concentration as a function of atomic number for energies which are just above the K-edge energy for each element. It is seen that for this case the highest sensitivity occurs in the vicinity of gadolinium (Z=64).

Method 3:

It is possible to preferentially image the analyte even when the matrix and analyte cannot be separated. Images are produced for two monochromatic beams which have energies just below and just above the K (or L) absorption edge of the analyte. The images (or the projection data) are subtracted to give an image which is almost exclusively analyte.

Absorption-edge (or K-edge) imaging is a well known elemental imaging technique. However, a basic problem with this technique is to create the required energy spectrum. Various methods have been used to create or separate the desired beam energies including filtered X-ray beams [24,25], secondary fluorescence targets in X-ray beams [26,27], diffraction gratings [28], high resolution semiconductor detectors [26,29,30,31,32] and radioactive sources [33].

The methods of diffraction gratings and secondary fluorescence targets have not proven significant for absorption-edge imaging using computerised tomography because of low photon flux output resulting in increased exposure time, excessive tube loading, motion artifacts, etc. However three methods have proven successful, although not commercially available. The first of these is the filtered beam approach. Here two (or three) separate spectra are used, with the peaks straddling the K-edge of the analyte. This is the system described by Riederer and Mistretta [34,35]. The choice between a two spectrum and a

three spectrum technique depends on the anticipated complexity of the situation. In general a two spectrum technique cannot provide a complete separation of the attenuation information due to three materials such as bone, analyte and tissue like substances. In a three spectrum technique, simultaneous cancellation of two K-edge substances such as fat and bone can be achieved. However, the problem here, is that the beam is heavily filtered thus giving rise to the problem mentioned above for the other techniques, but to a somewhat lesser extent.

The second approach that has proven successful is imaging using a synchrotron. Synchrotron radiation sources can provide a better source of X-rays than a tube source since they produce very intense, naturally collimated (usually less than 1 mrad divergence), narrow bandwidth and tunable photon beams. Many authors have reported excellent results in CT imaging of a contrast agent using a synchrotron [36,37,38,39,40]. They also possess the added advantage of the absence of beam hardening artifacts and minimum radiation dose by selecting the proper wavelength. However, they do have two major disadvantages: their cost is far in excess of normal (not research) hospital budgets at present and because of their size, the source cannot be rotated, therefore the patient must be rotated. This is not practical for scans greater than about 5 sec.

The third approach is to use a high energy resolution detector and a normal broad band X-ray source. Here two energies are selected, above and below the K-edge of the analyte. This approach has been adopted by McCarthy and Fryar [29,30,31] who utilise this technique to perform multielement imaging in a single scan. The major drawback with this technique is the fact that it only uses a single Si(Li) detector, resulting in excessively long scan times. However, a multielement Si(Li) detector has been developed [32], comprising 60 regions each 0.4 mm in width and a centre-to-centre spacing of 0.5 mm.

A fourth method currently under development [41] employs a low resolution detector and a tube source of X-rays. The X-ray spectrum is swept past the K-edge and

from changes in the total number of counts, the jump in the absorption, and thus the concentration of the analyte, can be inferred.

Fryar et al. [29] have derived an equation which allows one to determine the minimum detectable concentration for the case where a polychromatic beam is used and the results for monochromatic beams is determined by extrapolation, of the counts in the region of interest, to the absorption edge. It is this equation which is now applied to the present case. It is assumed here, that the two energies are close to the absorption edge and thus no extrapolation is required. The concentration is given by

$$C_a = \frac{U_m}{\left[\mu_{ah} - \mu_{al}\right]} \frac{6\sqrt{M}}{\sqrt{N_{ot}}} F \qquad (3.10)$$

where U_m is the linear attenuation coefficient of the matrix at the K-edge energy of the analyte, M is the number of projections in the scan, N_{ot} is the total number of incident photons and F is given by equation 3.09. $\mu_{ah} - \mu_{al}$ is the jump in the mass attenuation coefficient of the analyte across the K-edge. In this method the energies must be close to the K-edge energy of the analyte.

Minimum Concentration (mg/cc)
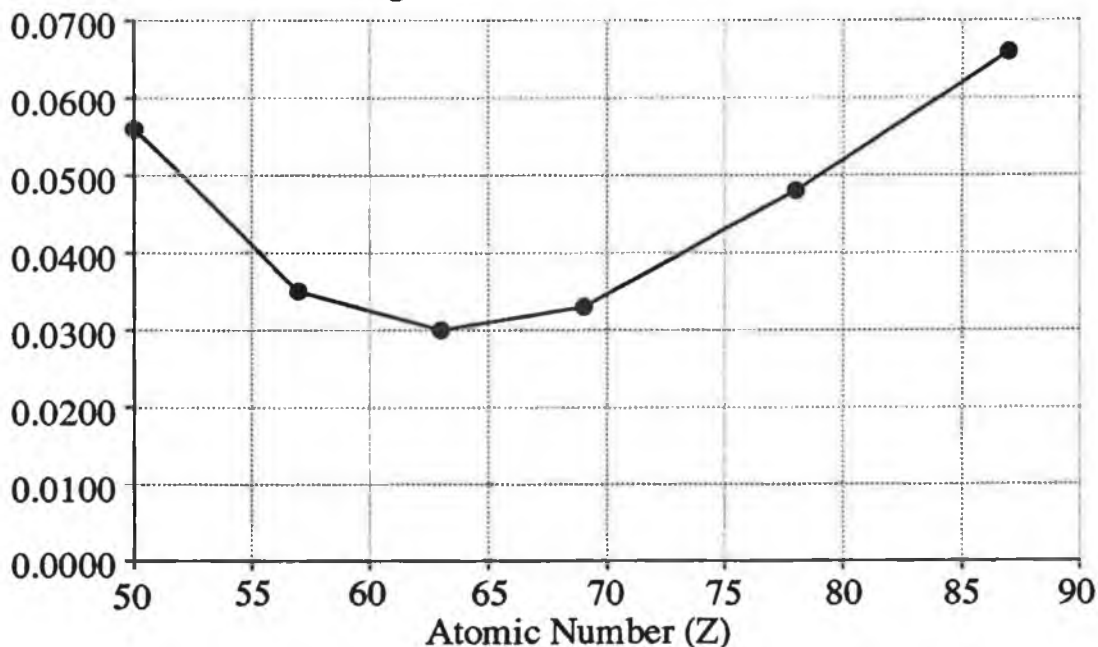
Figure 3.07

Minimum concentration visible vs. atomic number for the dual-energy case. These results are obtained from eqn. 3.10 with N_{ot} = 1E10 photons and M=256 steps.

Note: for heavier analytes it might be possible to work at the L-edge.

Figure 3.07 shows the results obtained when equation 3.10 is applied to the case of a water matrix of diameter 0.24m. The plot is of minimum detectable concentration against atomic number. As before, the minimum concentration occurs in the vicinity of gadolinium. For elements with atomic numbers between 50 and 80 the sensitivity varies by less than a factor of 2. If the beam energy is changed so that projection data is accumulated near the absorption edges of more than one element, then images can be produced for each analyte. This allows for the possible use of more than one contrast agent at the same time [29,31]. The ideal X-ray source for such studies is the synchrotron although it is possible to use tube sources or X-rays from radioactive sources [29,42,30].

3.2.3 Polychromatic Beams.

Due to the complexity of the spectra for polychromatic beams (eg. account has to be taken of filtration, characteristic lines of the target, etc) no theoretical equation has been developed that will yield a value for the minimum detectable concentration visible in the myocardium or some similar situation. Therefore, this situation will only be studied by computer simulation and experiment.

3.3 Simulations.

3.3.1 Introduction.

The simple equations, as given above, allow the minimum detectable concentration to be determined for monochromatic, or pseudo-monochromatic beams, for the case where the analyte is homogeneously dispersed throughout the matrix. They give some idea as to what might be expected in more complex situations. Since no theoretical equations exist that will provide the minimum detectable concentration of analyte present in the myocardium, computer simulations will be utilised to obtain a value for this concentration. In this section the production of computer simulated images for both monochromatic and polychromatic beams is discussed.

The object initially used for the simulations was that of a cylinder 0.26m in diameter (the approx. size of the chest/thorax). For each beam position the number of transmitted photons was determined. Poisson noise was added and the images were reconstructed using filtered backprojection with a Ram-Lak filter. Where relevant the projection data was subtracted before reconstruction. A visibility criterion was developed to remove any observer subjectivity. The simulations were performed on an Acorn Archimedes A440, a 32-bit RISC processor microcomputer. The calculation of the projection data, adding of the noise and reconstruction of the image for a 40 X 40 matrix took approximately 30 mins, and anything up to 30 images needed to be calculated to yield a value of minimum detectable concentration for one element.

3.3.2 Dummy Data:

To generate the dummy data for the scans in the computer simulations, the following approaches were adopted.

Analyte added to complete cylinder:

The beam path length through the matrix can be given by Pythagoras' theorem as

$$P = 2.\sqrt{R^2 - ((S-0.5)^2 dx^2)} \qquad (3.11)$$

where S is the step position with respect to the centre of rotation, R is the radius of the cylinder and dx is the step width, see figure 3.08.
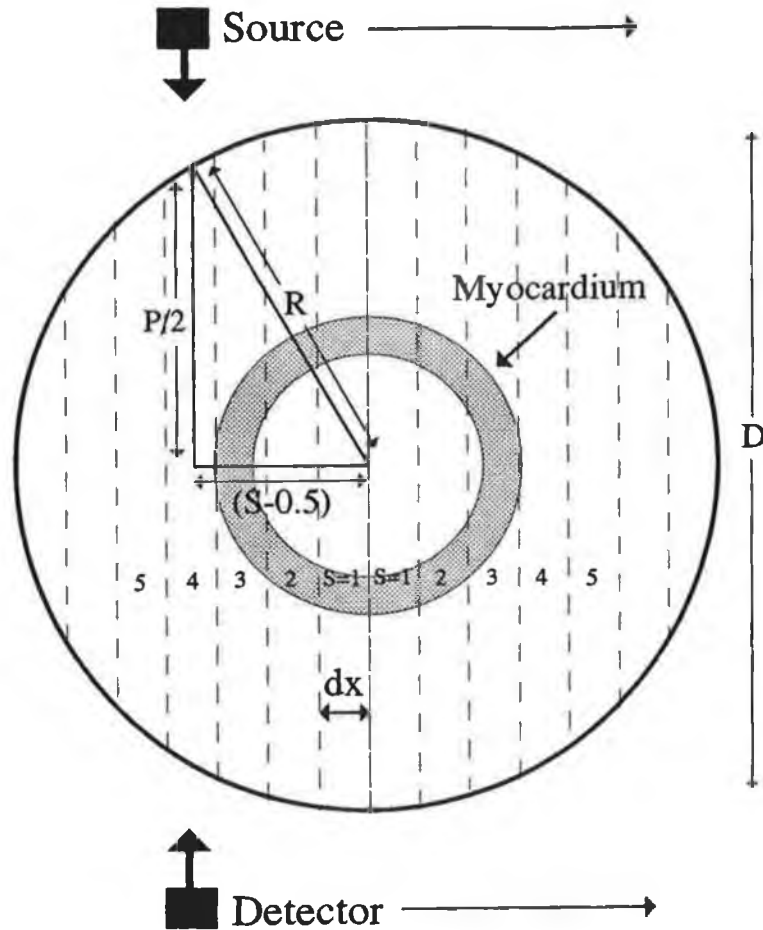
Figure 3.08
The scan geometry used in the simulations and theory.
D is the cylinder diameter.

The transmitted number of photons after passing through a path length P of an object, in the absence of scattering, is given by Beer's Law as

$$N = N_o \exp\left[-U_t . P \right] \qquad (3.12)$$

where U_t is the combined linear attenuation coefficient of the analyte and matrix. The total value of the linear attenuation coefficient is given by the addition of the component values,

$$U_t = U_a + U_m \qquad (3.13)$$

However, the linear attenuation coefficient of an element

can be defined as $U = \mu C$, where C is the element concentration and μ is the mass attenuation coefficient. Therefore 3.12 becomes,

$$U_t = C_a\mu_a + C_m\mu_m \qquad (3.14)$$

where μ_m and μ_a are the mass attenuation coefficients of the matrix and analyte respectively.

When C_a is small, then $C_m = \rho_m$, where ρ_m is the density of the matrix, therefore

$$U_t = C_a\mu_a + \rho_m\mu_m \qquad (3.15)$$

Substituting this into eqn 3.12 gives

$$N = N_0\exp\left[-2.\left(C_a\mu_a + \rho_m\mu_m\right)\sqrt{R^2 - ((S-0.5)^2dx^2)} \right] \qquad (3.16)$$

From this equation the number of photons (N) emerging through the object at any step position can be determined.

Analyte added to ring only:

This situation is similar to that described above, except that the above process is split into three sections, cf figure 3.08. First the attenuation due to the matrix outside the ring is determined. This is given by

$$A_1 = N/N_0 = \exp\left[-2.\rho_m\mu_m\left\{\sqrt{R^2 - ((S-0.5)^2dx^2)} \right.\right.$$

$$\left.\left. -\sqrt{r^2 - ((S-0.5)^2dx^2)} \right\} \right] \qquad (3.17)$$

Second, the attenuation due to the matrix and analyte in the ring is determined.

$$A_2 = N/N_0 = \exp\left[-2.(C_a\mu_a+\rho_m\mu_m).\left\{\sqrt{R^2 - ((S-0.5)^2dx^2)} \right.\right.$$

$$\left.\left. -\sqrt{(r-t)^2 - ((S-0.5)^2dx^2)} \right\} \right] \qquad (3.18)$$

where r is the outside radius of the internal ring and t is the thickness of the ring. Lastly, the attenuation due to the matrix only, inside the ring is determined.

$$A_3 = N/N_0 = \exp\left[-2.\rho_m\mu_m\sqrt{(r-t)^2 - ((S-0.5)^2dx^2)} \right] \qquad (3.19)$$

The total attenuation is now given by the product of these attenuations;

$$A_t = A_1.A_2.A_3 \qquad (3.20)$$

72

Therefore, the number of photons emerging is now given by

$$N = N_o.At \qquad (3.21)$$

The object simulated was radially symmetric so only one set of projection data was determined for a fixed angle. This data was reused as many times as there were scan angles but Poisson noise was separately generated for each beam position. The program to generate this dummy data, add Poisson noise and reconstruct the image is called "c.simscan", and is shown in appendix 1.

3.3.3 Poisson Noise:

The normal distribution was first discovered by DeMoivre in 1721 and later by Gauss in 1809, however, it is now generally credited to Gauss and it is now frequently called the Gaussian distribution. As with earlier binomial and later Poisson distributions, it describes the deviations of the values of a statistic from the 'true' or average value. The normal distribution has the general form

$$P(x) = \frac{1}{(2\pi\sigma^2)^{1/2}} \exp\left(\frac{(x-\mu)^2}{2\sigma^2}\right) \qquad (3.22)$$

where $x = (n-\mu)$ {n is the actual value and μ the mean value}, and σ is the standard deviation.

Now, if $\mu = 0$ and $\sigma = n^{1/2}$ (true for Poisson statistics), then

$$P(x) = \frac{1}{(2\pi n)^{1/2}} \exp\left(-\frac{x^2}{2\sigma^2}\right) \qquad (3.23)$$

These equations are for the Gaussian distribution, not the Poisson distribution. The Poisson distribution differs in two important respects from the Gaussian. First, it refers to a discrete value r,

$$P(r,\mu) = \frac{e^{-\mu}.\mu^r}{r!} \qquad (3.24)$$

that can only take zero or positive integral values, unlike the continuous distribution of the Gaussian. Secondly, it is not symmetrical. When μ is small (ie. < 10), the asymmetry is very marked, but as μ is increased it becomes more symmetrical. For $\mu \geq 10$, the Gaussian shape is a good approximation to the Poisson, therefore, since in the present case $\mu \gg 10$, the Gaussian

73

distribution will be used. [61].

   To produce noisy data, a random number between 0 and
1 is chosen, representing a certain area under the
Gaussian curve. Using the trapezoidal rule of integration,
equation 3.22 is integrated from 3 standard deviations to
the left of the mean until the integrated value is greater
than or equal to the random number. *Note: The Gaussian is
normalised, such that the area under the curve equals 1.*
This value of x (ie. when $\int P(x)dx \geq$ random number) is then
added to the actual value inputted to the function to
yield the 'noisy' value. This process is carried out by
the function 'noisel' contained in the program 'simscan'
shown in appendix 1.

   The algorithm was checked as follows. The routine was
called 10000 times with the same value, 10000. The number
of occurrences of each noisy value around 10000 is plotted
in figure 3.09. From the data, it was determined that the
results had a standard deviation of $\simeq$ 110, which is in
good agreement with the predicted value of 100.

No. of Occurances.

Actual Value
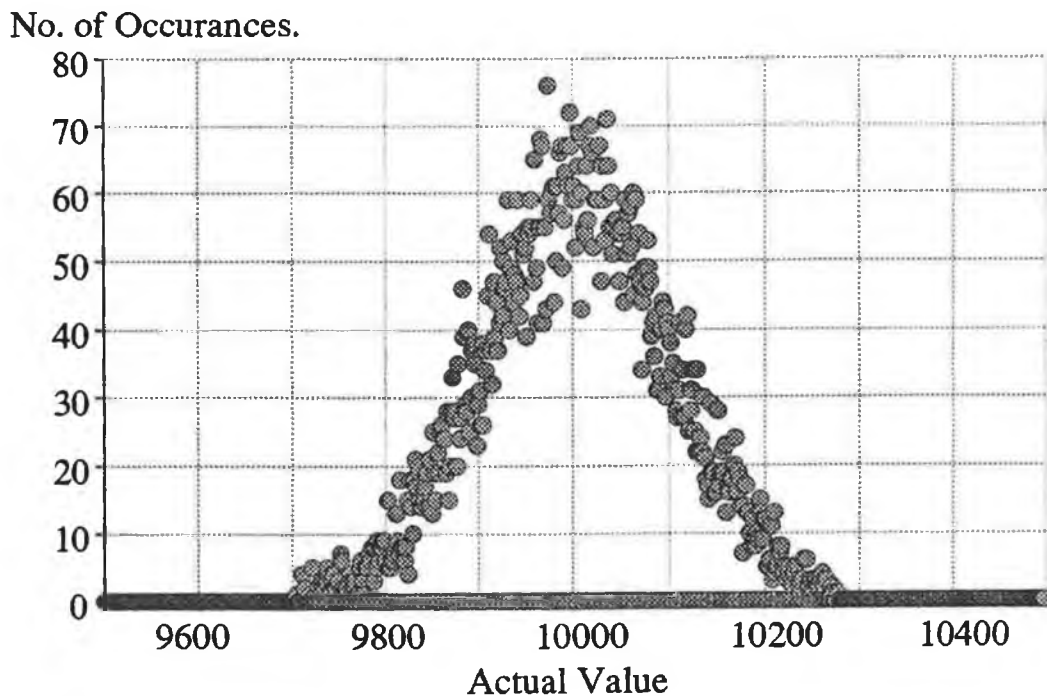
Figure 3.09

**Results obtained from the noise generation algorithm. The value
10000 was inputted 10000 times into the routine.**

74

3.3.4 Image Subtraction:

An image with no analyte was produced for each element and subtracted from the original image in an attempt to take out only the image due to the analyte. The subtraction method involved obtaining the projection data for the two objects, one with the analyte present, the other void of any analyte. Noise was added to both these sets of data, the logarithm was taken and they were then subtracted pixel by pixel and a third file was produced with these subtracted values. This file was reconstructed and displayed. The effect of this will now be derived.

The line integral for one beam is given by

$$\ln \left(-\frac{I_o}{I}\right) = \int \mu \ dy. \qquad (3.25)$$

Now, subtracting two sets of data, one with the analyte and the other without, gives

$$\ln \left(-\frac{I_{o1}(n)}{I_1(n)}\right) - \ln \left(-\frac{I_{o2}(n)}{I_2(n)}\right) = \int \mu_1 dy - \int \mu_2 dy \qquad (3.26)$$

where n is a particular step/rotation. Rearranging gives

$$\ln \left(-\frac{I_{o1}(n)}{I_1(n)}\right) - \ln \left(-\frac{I_{o2}(n)}{I_2(n)}\right) = \int (\mu_1 - \mu_2) \ dy \qquad (3.27)$$

ie., the image is that of the difference in attenuation coefficient, which is assumed to be due solely to the analyte.

Note: It is also possible to subtract the two reconstructed images. A comparison of these methods was made for a cylinder containing water and KI, mixed homogeneously, with a 40kV monochromatic spectrum. For 3E9 incident photons and 40 steps/rotations, the pre-reconstructed method gave a value for the minimum visible concentration of 5E-3 mg/cc. For the same conditions, the post-reconstruction subtraction method gave a value of 2 mg/cc. The reason for the difference is due to the amplification of noise by the reconstruction algorithm and the non-perfect filtering performed by the point-spread filter, eg. Ram-Lak filter.

3.3.5 Perception of Images.

When viewing an image (CT or otherwise), a general axiom applies: prior knowledge of what the object should look like makes it is easier to see the object. This is certainly the case with the work presented here. Thus a visibility condition will be derived (see section 3.3.6) which yields a clearly visible image of the disc/ring. The area of image visibility is closely related to human perception, and this area of human perception of images will now be discussed briefly.

Several important factors influence human perception of images. These include (1) contrast-luminance limitations, (2) spatial frequency characteristics, and (3) information density (noise) limitations.

Contrast is a measure of the relative difference in luminance between the signal and background. It may be defined as:

$$C = \frac{L_s - L_b}{L_s} \qquad (3.28)$$

where C is contrast and L_s and L_b are the respective luminance levels of the signal and the background regions. The overall perceived contrast depends on the size of the signal and the luminance of the display function. Viewing conditions affect the perception of contrast. As the intensity of the light reaching the eye increases, so does the eye's ability to see small changes in contrast. [43].

To understand some of the additional considerations of human perception, the human visual response to more complex variations in luminance such as edge gradients and variations in luminance backgrounds levels must be investigated.

As in most optical systems, it is reasonable to begin the investigation of the response of the human visual imaging system by considering the response of the system to isolated point sources of light. It is understood that more complex patterns can be considered as a composition of point sources, each with its own relative intensity. Under certain conditions of linear systems analysis [44] the total output can then be predicted by convolving the complex input pattern of intensity-weighted point sources

76

with the appropriate point spread function (PSF) that describes the system response to an isolated point source. The modulation transfer function (MTF) describes the relative ability of a system to transfer the sinusoidal wave of a given frequency. The MTF can therefore be used to predict the resultant image under certain conditions of positional independence and system linearity [44]. For example, if the imaging system is unable to reproduce or transfer high frequency components, the resultant image will tend to lack sharp, clear edge information, such as an image produced with a defocussed lens.

Brightness is a perceptual equivalent of light intensity or luminance. The brightness of an object depends not on the intensity of light in the retinal image of that particular object alone, but rather on the relationships among the various intensities in the overall image [45].
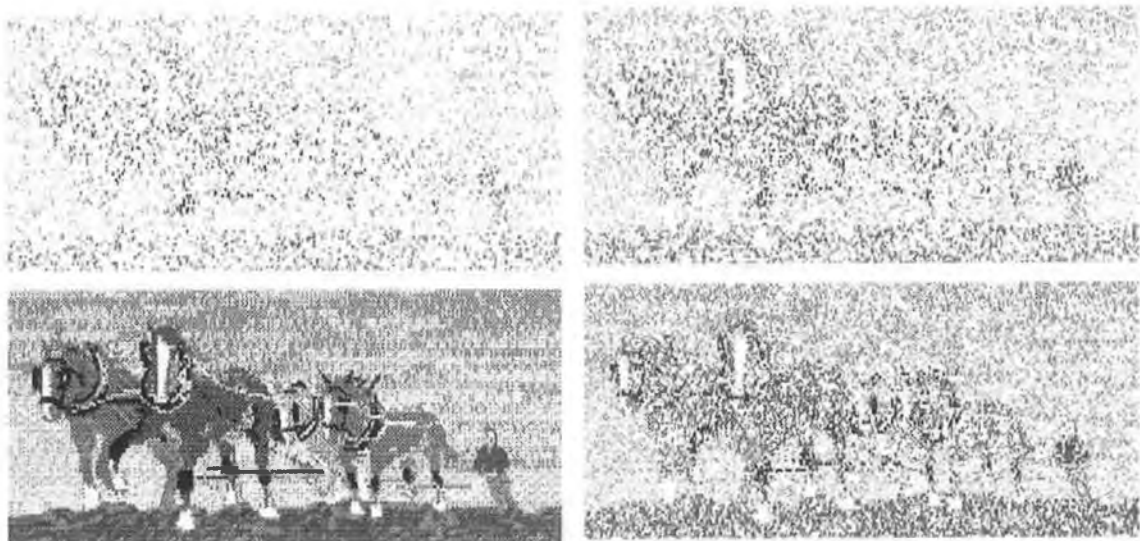
Figure 3.10
Result of increasing the number of information containing pixels forming an image. From top left and working clockwise: 30000, 60000, 90000 and 200000.

The perceived information in a picture is also a function of the number of discrete visible specks making up the picture [46]. Figure 3.10 provides a graphic illustration of increased information as the number of

discrete visible specks (photons) is increased. In the sense that the number of discrete specks in a CT image is fundamentally limited by the number of X-rays detected by the CT system, it is clear from the analysis of figure 3.10 that the perceived information in a CT image will be likewise limited.

CT images are generally spatially quantized or digitised into discrete pixel values. Harmon and Julesz [47] found that recognition of certain pictorial images is difficult when the images have been coarsely sampled and quantised. They suggest that high-frequency noise introduced by sampling may be removed by smoothing (low-pass spatial frequency filtering) processes to improve signal recognition. Smoothing is well known in medical imaging. Even though the procedure blurs the image, it can be argued that in certain instances in which high-frequency noise components are present the deleterious effects of blurring edge information are compensated by reducing or blurring the high-frequency noise components.

Most medical X-ray images, including those of CT, are not statistically limited, or 'noisy', because of intrinsic fluctuations of visible light photons from the display system. The statistical limitation is a result of the finite number of X-rays used in the measurements to reconstruct the image.

3.3.6 Visibility Criterion:

To check the validity of the simulation technique at determining the minimum detectable concentration, dual-energy scans were simulated with the analyte homogeneously dispersed throughout the object and the results compared to those predicted by equations 3.07. The results of these are shown in figure 3.11. It is obvious from this graph that the simulations do not concur with the predicted results.

When determining the minimum visible concentration, the images were compared to each other by viewing the image and making decisions by visual inspection. Two images could have the same concentration but appear

different on the screen. This is due to the auto-scaling display routine in the program 'testdisp' and noise

Minimum Concentration (mg/cc).

Atomic Number (Z).
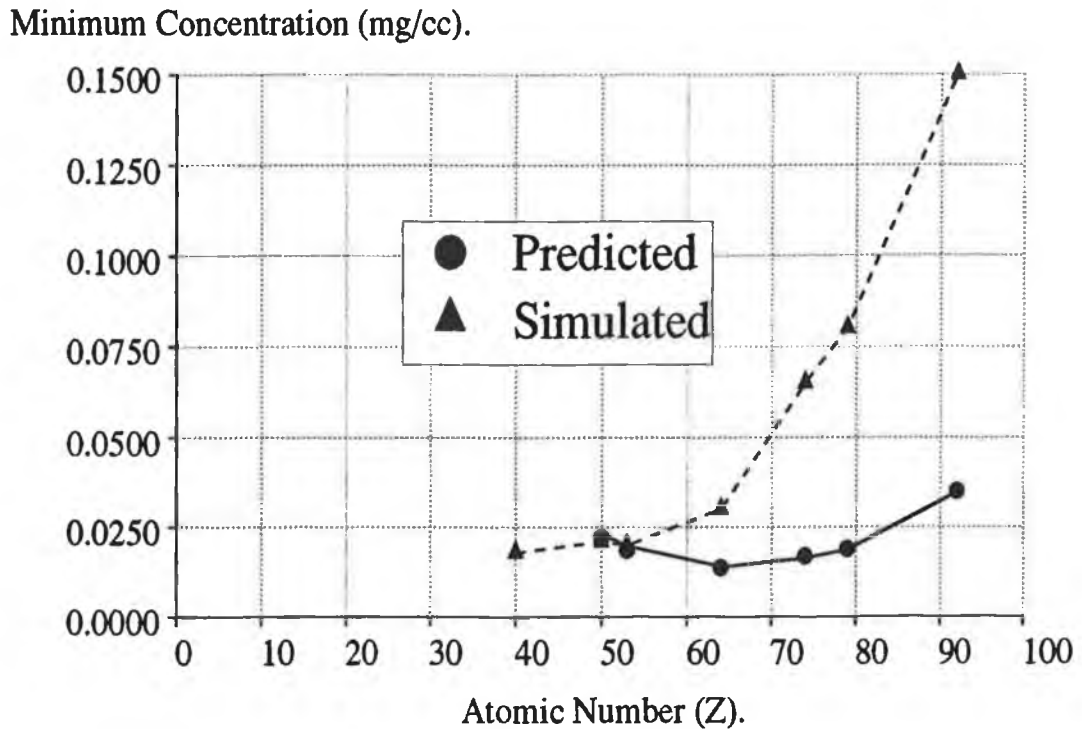
Figure 3.11
Predicted and simulated results for the minimum concentration using the visual method of determination.

fluctuations, ie. a random large value pixel could suppress the image making it appear darker then another similar image. Also, another factor that will lead to discrepancy is due to the image perception factors mentioned above, ie. how bright is the object compared to the background?, is the object broken into a small number of large fragments or visa versa, etc.

To overcome these human visualisation problems, some automated visibility criterion needed to be developed. After several attempts, the parameter that held a reasonably linear relationship with increasing concentration was the difference in the mean of the object and the mean of the background. The relationship between the visibility parameter and concentration is shown in figure 3.12. This linear relationship held only at the lower end of the concentration values range. To be valid for all elements, the reconstruction values had to be normalised between 0 and 1. The minimum value, for

visibility of the image, chosen for this parameter was 0.14. In reality this value of 0.14 normally yielded a visible image without any image processing. Using the image processing techniques available in the 'testdisp' program, it would be possible to obtain a visible image with this parameter set lower than 0.14, resulting in correspondingly lower minimum concentrations.

Visibility Parameter.
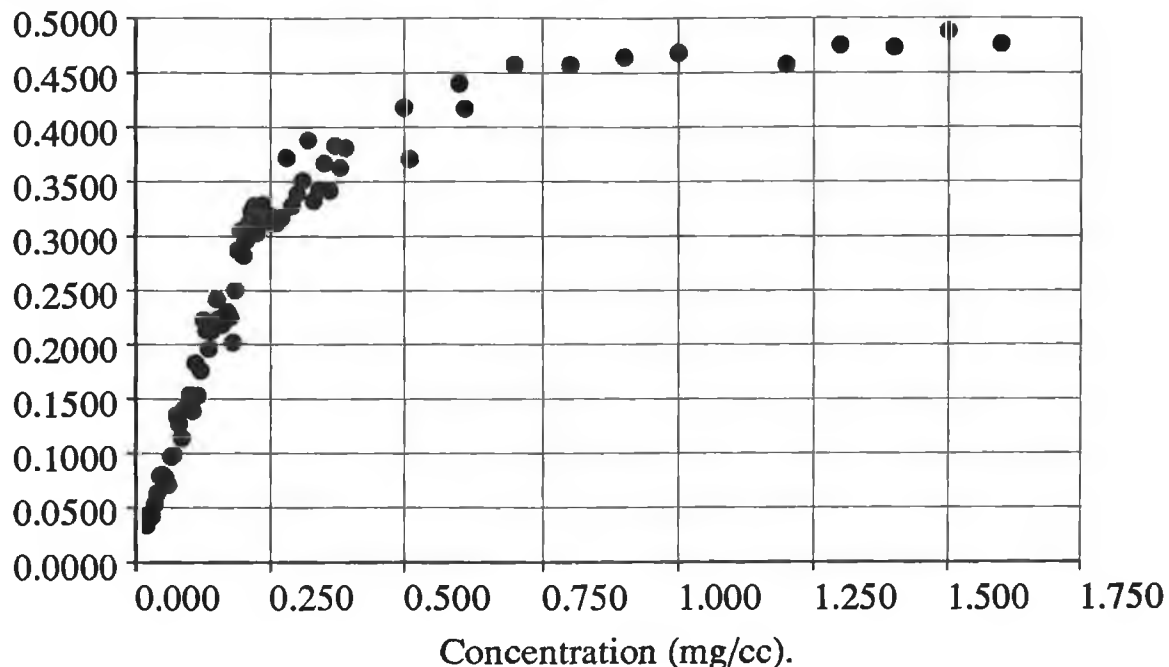
Figure 3.12
Graph of the value of the visibility parameter vs. concentration of Tin in water. M = 40 and Not = 1E10 photons.

3.3.7 Single Energy Simulations:

Figure 3.13 shows the results of these simulations when applied to gold for the case of a single monochromatic beam being used. Separate sets of projection data are produced for the matrix and the matrix plus analyte. These sets of data were subtracted and the image reconstructed as per section 3.3.4. The concentration of the analyte was adjusted until the analyte was visible as per the visibility criterion given in section 3.3.6. Figure 3.14 shows the minimum concentration values as a function of atomic number for simulated images. The theoretical results are also given. The results show that

the simulated result is approximately 3 times higher than the calculated result. This is partly due to the fact that the criterion used resulted in clearly visible analyte in our system, whereas the theory prediction was on the limits of visibility, ie. only a difference of three standard deviations was used to predict whether a particular pixel was visible. It is clear from figure 3.13 that maximum sensitivity occurs just to the high side of the K-edge and that for the graph of sensitivity vs. atomic number, the maximum sensitivity occurs for Gadolinium (Z = 64).

Minimum Concentration. (mg/cc)

Photon Energy (keV).
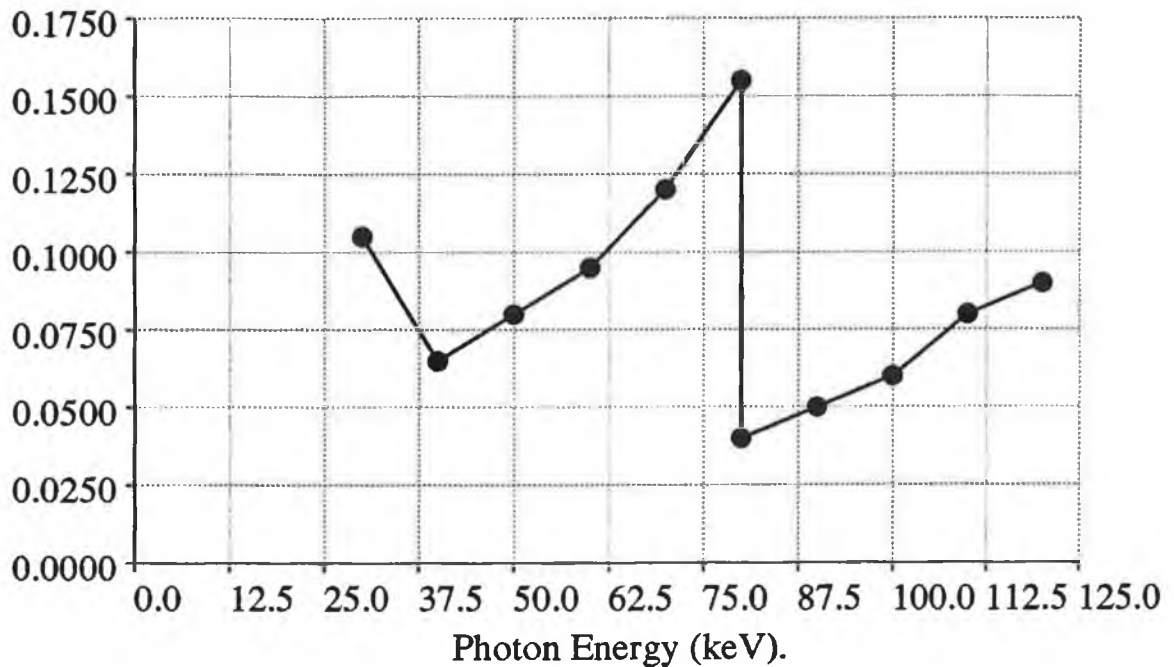
Figure 3.13
Simulated results for the minimum concentration vs. energy for Gold in a water matrix using a single energy spectrum. Not=1E10 and M=40.

3.3.8 Dual-Energy Simulations (K-Edge Subtraction):

Here the matrix and analyte are considered inseparable. The object was considered to be scanned by two monochromatic beams: one beam had an energy just below the K-edge of the analyte and the other had an energy which was just above, both beams being less than 100 eV from the K-edge. Poisson noise was added to both sets of projection data and these sets were subsequently

81

Minimum Concentration (mg/cc).
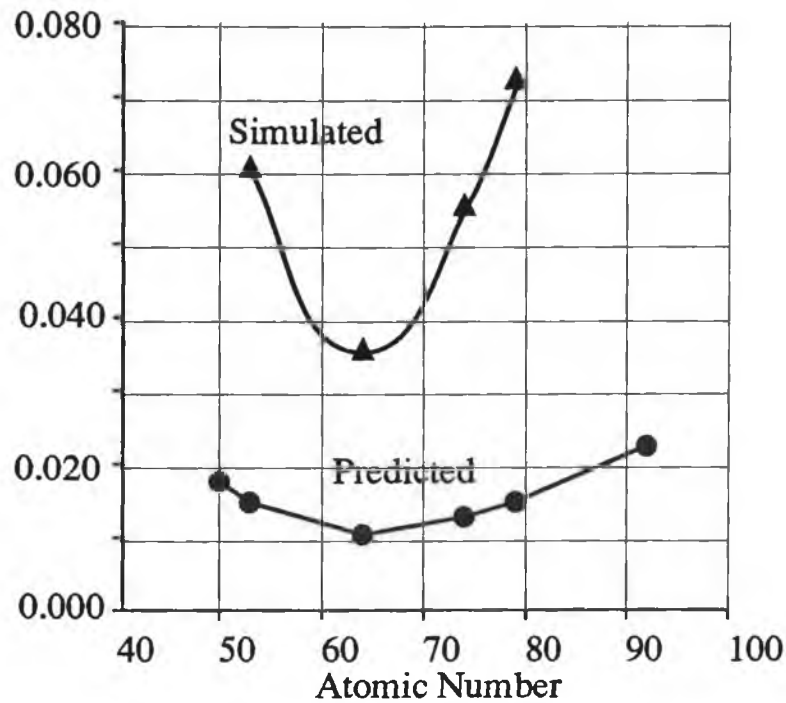
Figure 3.14
Eqn. 3.08 for a single energy beam, applied to a cylindrical matrix (water) 0.24 in diameter. The results are compared with the results of simulations. N_{ot} = 1E10 and M = 40.

Minimum Concentration (mg/cc).
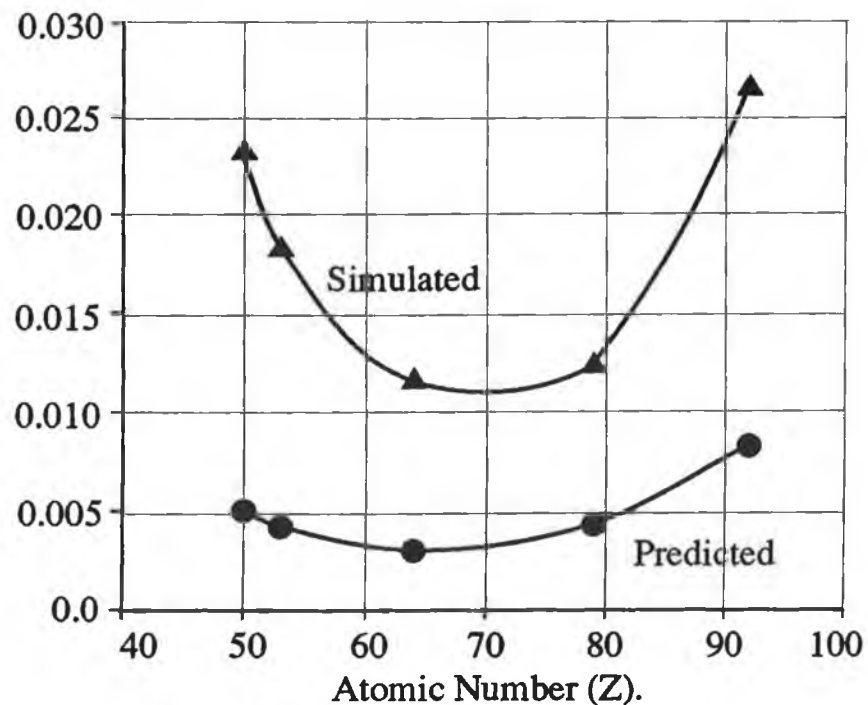
Figure 3.15
Equation 3.10 for dual-energy beams, applied to a cylindrical matrix (water), 0.24m in diameter. The results are compared with the results of simulations with N_{ot} = 1E10 photons and M=40 projections.

subtracted and the result reconstructed. This process was repeated and the resultant minimum visible concentration determined. Figure 3.15 shows the simulated results for several elements between atomic numbers 50 (tin) and 92 (uranium) and can be compared to the predicted results. Again the simulated results are approximately a factor of 3 higher than the predicted results. As with the monochromatic energy case, Gadolinium has again the maximum sensitivity, being a factor of 1.5 more sensitive then Iodine.

3.3.9 Number of Incident Photons / Projections Scaling:

It is evident from equations 3.07, 3.08 and 3.10 that for both cases of monochromatically imaging an analyte, the concentration scales as $M^{1/2}$, where M is the number of steps/rotations, and scales as $N_{ot}^{-1/2}$, where N_{ot} is the number of incident photons. This scaling had not been tested rigorously by McCarthy [48]. Since the final results required that M = 256 or 512 (ie. the number of projections on a commercial CT scanner) depending on the scan mode, and the number of incident photons from the commercial scanner was not yet determined, the M and N_{ot} dependence needed to be verified. Also, because of time limitations, it would be impractical to perform simulations for M = 256 or 512 for each set of data, eg. each 256 X 256 image takes approximately 4 hrs to complete. The results of the simulations to check these dependencies are shown in figures 3.16 and 3.17. The slope of figure 3.17 is +1/2 and figure 3.16 has a slope of -1/2. These results are in perfect agreement with the theory. Thus, this agreement, as well as confirming the number of projections and number of photons scaling, also confirms the validity of the simulations as the results for these scaling factors were determined using a method totally independent of the theory.

3.3.10 Polychromatic Spectra Simulations for the Full Disc Case:

The simulations performed in the previous two cases were for monochromatic spectra. With these simulations

83
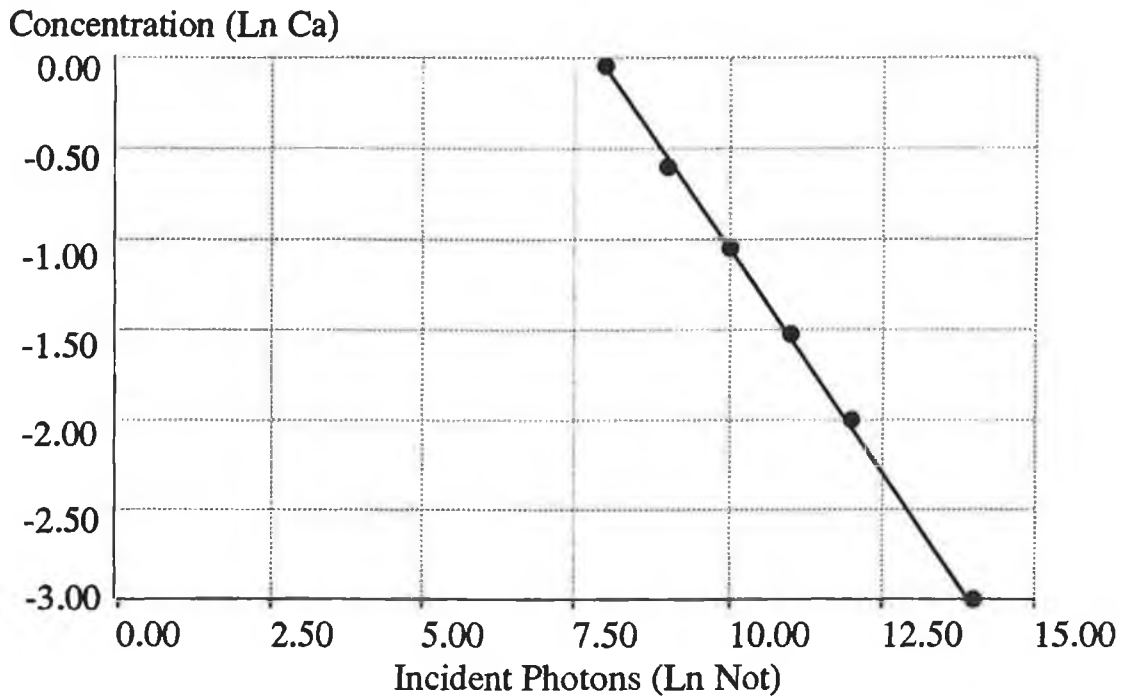
Figure 3.16
Simulation results for minimum concentration vs. incident photons for Gold in a Water matrix at 120keV.
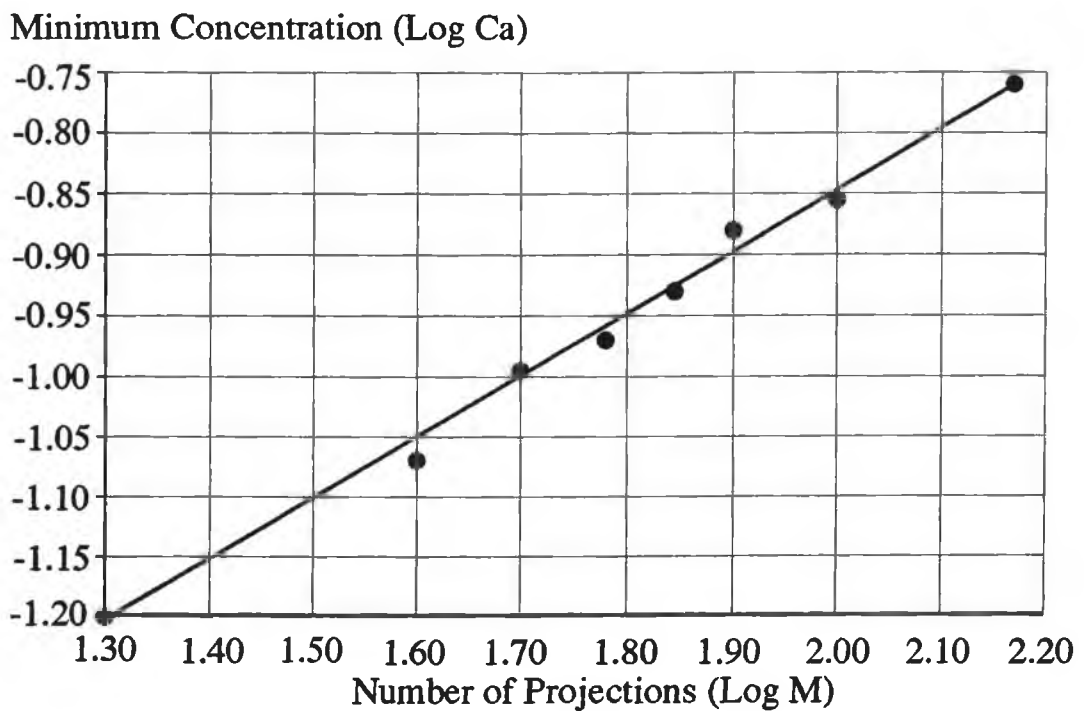
Figure 3.17
Graph of the minimum concentration vs. number of projections.

showing good agreement with the theoretical results, it could be assumed that the processes involved in the simulation programs were valid. Although the simulated results were larger then the theoretical results by a factor of approximately 3, this is deemed good agreement because the simulated results produced a clearly visible image without the need of any image processing, whereas the theoretical results are the absolute limits on detectability. The process was now taken a stage further, the modification of the program to perform simulations for polychromatic spectra. This was achieved as follows.

Data files for the projection data were produced at eleven energies with equal separation over the 120keV spectrum range, ie. 20,30,40,...120 keV, using the known mass attenuation coefficients at these energies [22]. These files were then combined into a single file by adding each beam intensity to its corresponding value in the other files, weighted by the known intensity of a 120keV tungsten target tube, (filtered by 2.5mm Al and 0.4mm Cu) at each energy interval. The weighting values are given in figure 3.18.

Relative Number of Photons.
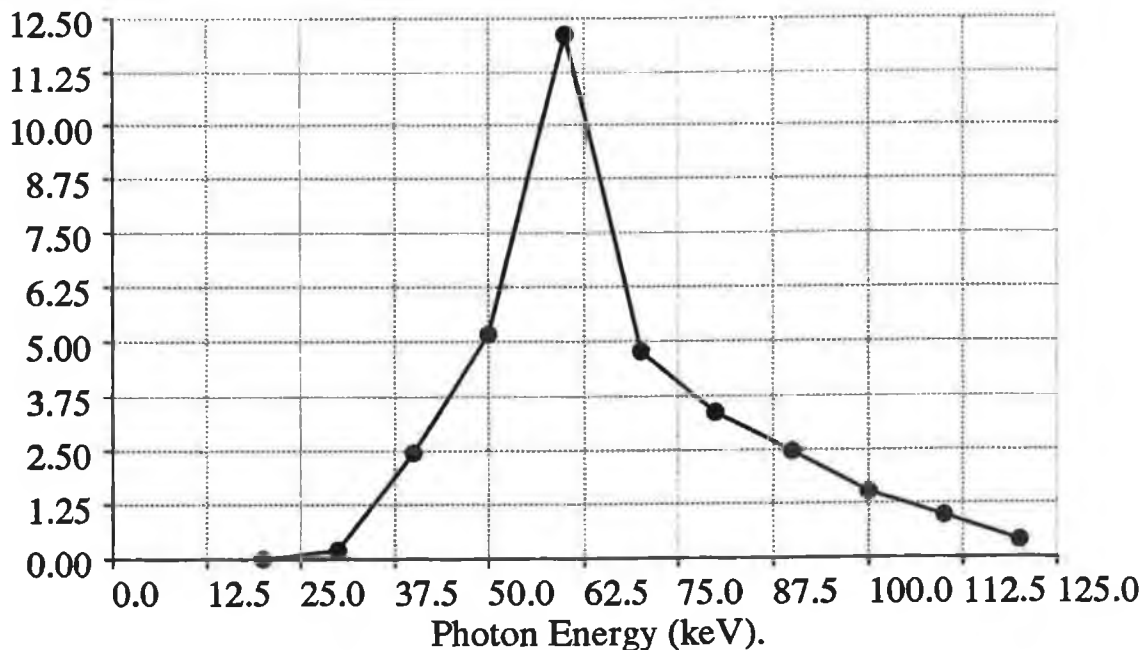
Figure 3.18

Graph of incident filtered spectrum used in simulations and calculations. Source is a 120 kVp X-Ray tube.
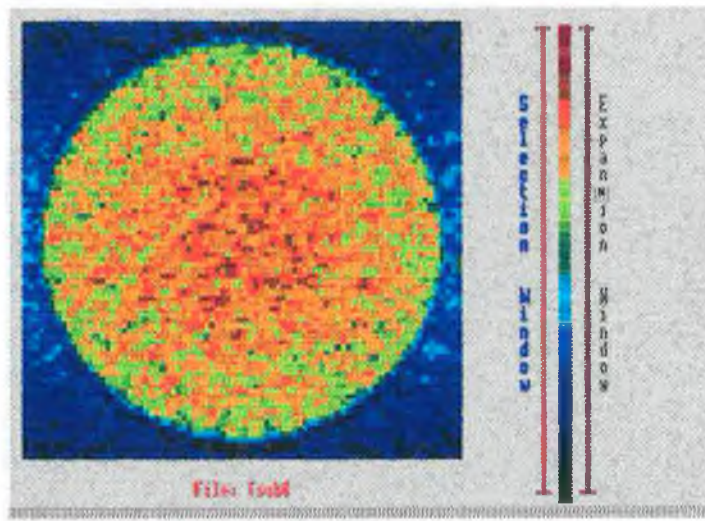
Figure 3.19
CT simulated image of a cylindrical phantom containing a water-only matrix.
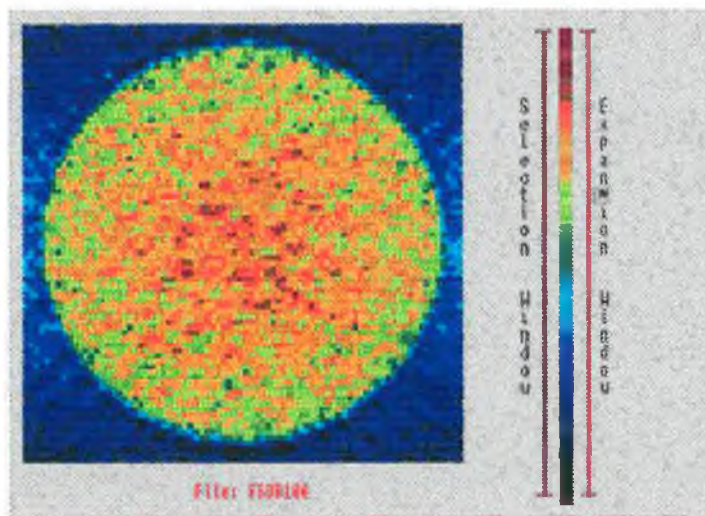
Figure 3.20
CT simulated image of cylindrical phantom containing a water matrix and analyte mixed homogenousely throughout the matrix. No subtraction of the images performed.
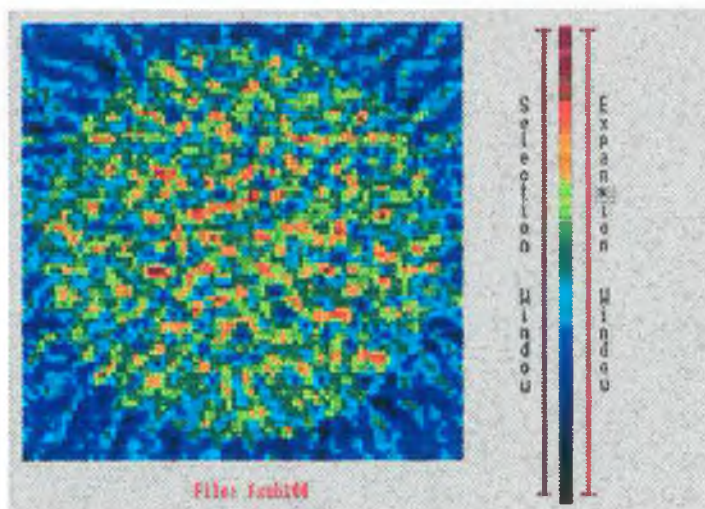
Figure 3.21
CT simulated subtraction image of water-only and water & analyte data. The above image results from the subtraction of the data in figures 3.19 and 3.20.

Thus one file was produced with the attenuation of all the individual files combined. The data in this file was multiplied by the number of photons per beam, Poisson noise was added and the data reconstructed using the backprojection algorithm.

Two sets of projection data were produced, one containing the analyte at a certain concentration, the other containing no analyte, only matrix (water). Before reconstruction these two sets of data were subtracted as per 3.3.4 to yield the final image of only the analyte.

For the case where the analyte was added to the full cylinder homogeneously, only the subtraction modality could be implemented. This is because it is impossible to visualise the analyte when it cannot be spatially compared to the matrix, ie. the intensity distribution across the image would remain constant, no matter what concentration of the analyte was present. This is of course assuming that an autoscaling display algorithm is being used. However, when the images are subtracted then the distribution of the analyte alone can be compared to the background outside the object. Figures 3.20 and 3.21 contain the same amount of analyte. However, it is impossible to state whether figure 3.18 (a matrix only image) or figure 3.19 contains the analyte. In figure 3.21, the analyte can be clearly visualised against the background.

The results of these simulations can be seen in figure 3.22 which shows the minimum concentration visible vs. atomic number (Z) for Z = 35 (Bromine) to Z = 82 (lead). It is obvious that the trend is similar to that of the monochromatic case, see figure 3.14, with the lowest concentration visible occurring at Z = 64 (Gadolinium).

3.3.11 Polychromatic Spectra Simulations for Thorax / Myocardium Phantom: No Subtraction.

In the experimental section 3.4, images are produced using the thorax/myocardium phantom (Plate 3.1) in the Somatom-2 scanner. No image subtraction is performed, so simulations of the sensitivity of the Somatom-2 scanner under this condition are now discussed.

87

Min. Concentration (mg/cc).
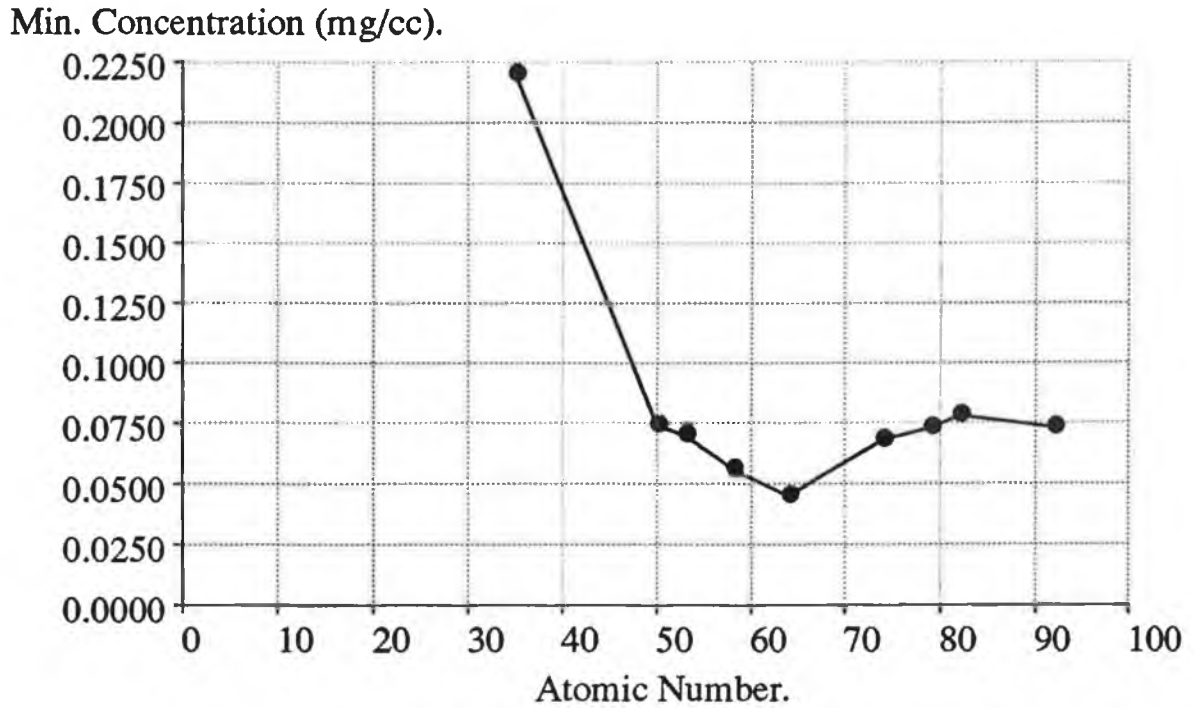
Figure 3.22
The results of simulations of subtracted images for the X-ray tube operating at 120 kV. The analyte is homogenously dispersed throughout the phantom. Not = 1E10 photons and M = 40 steps.

Concentration (mg/cc).
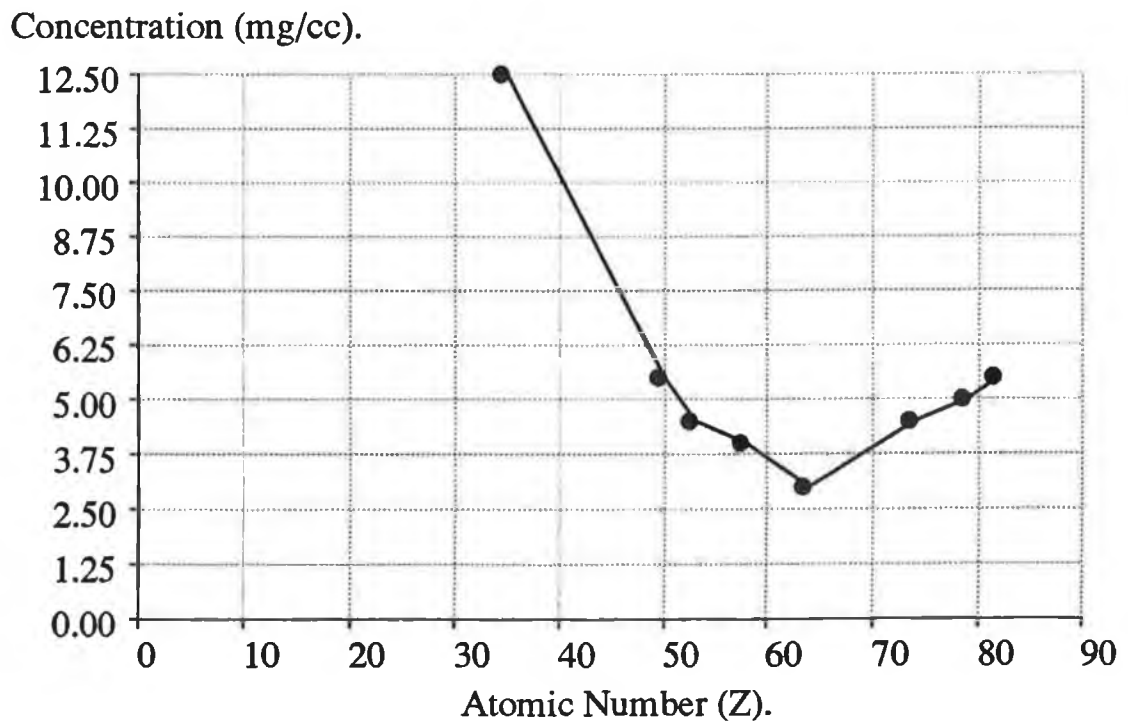
Figure 3.23
The results of simulations for the case where the analyte is contained in the central ring, but with no subtraction of the images performed. Not = 1E10 photons and M = 40 steps.

Simulated images were generated for the X-ray tube working at 120keV with a 40 X 40 pixel display / data acquisition array. The total number of incident photons used was 1E10. Dummy projection data was determined using the algorithm shown in the program 'c.simscan' (Appendix 1) for analyte contained in a ring, itself contained in a larger cylinder, ie. simulating the heart wall (myocardium) inside the chest (thorax). Poisson noise was added to the projection data and the images were reconstructed using the backprojection algorithm. The minimum concentration visible of that analyte was determined using the previously described visibility condition 3.3.6. The estimated minimum detectable concentration for these conditions is shown in figure 3.23 as a function of atomic number. Again the maximum sensitivity occurs in the vicinity of Gadolinium.

Min. Concentration (mg/cc).

Atomic Number.
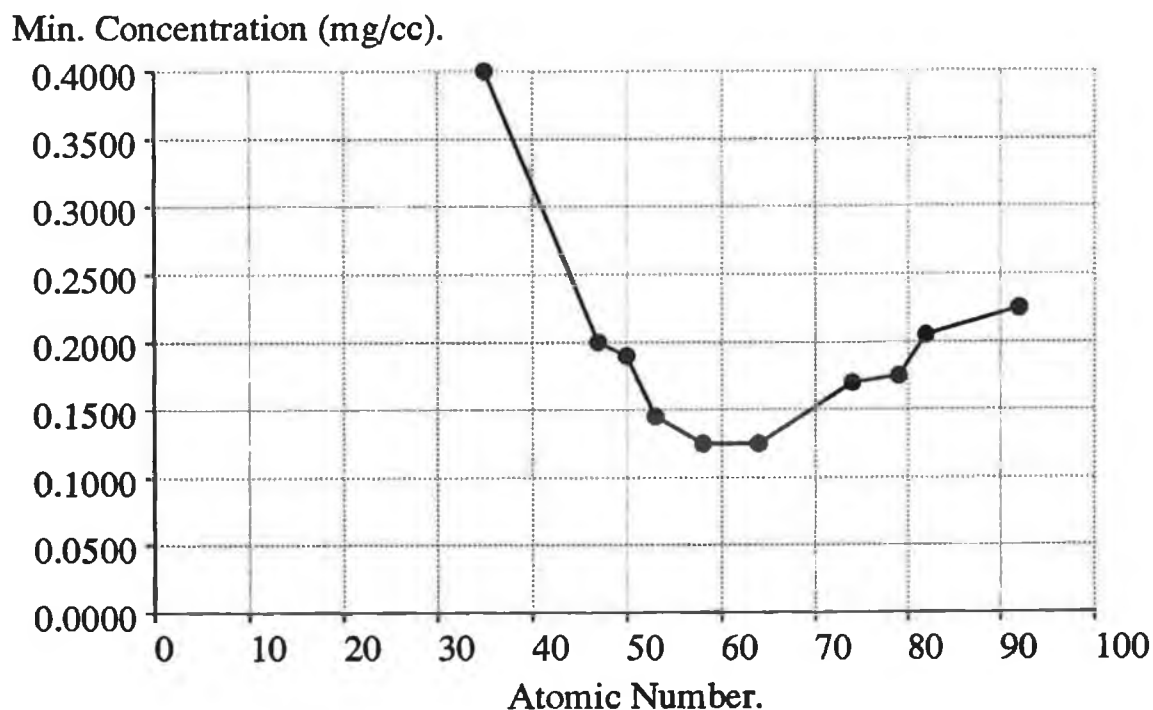
Figure 3.24
The results of simulations of subtracted images for the X-ray tube operating at 120 kV with the analyte present in the central ring only. The sensitivity is about 30 times better than for the non-subtracted case. Not = 1E10 photons and M = 40 steps.

3.3.12 Polychromatic Spectra Simulations for Thorax / Myocardium Phantom (Subtraction case).

The situation where the analyte is added to the central ring and the data subtracted from a scan with no analyte, could not be studied experimentally using the Somatom-2 scanner. However, this case was investigated using computer simulations. The minimum concentration visible was determined for various elements and the results are shown in figure 3.24. Here also, the maximum sensitivity occurs when gadolinium is used. From comparison with figure 3.23(the case where the analyte is in the central ring but no subtraction is performed) it is evident that the sensitivity is a factor of approximately 30 higher than that of the non-subtracted case.

3.4 Experimental Results.

The results of this section divide into two parts.

a) Determination of the number of incident photons and the number of projections / steps used in the commercial scanner utilised. These are used to scale the simulation predictions to the experimental conditions.

b) Experimental images obtained using a cylindrical phantom modeling the myocardium in the thorax.

This enables a direct comparison between the simulation predictions and the experimental results.

3.4.1 Determination of the Number of Incident Photons and the Detector Efficiency.

For the simulations to give an accurate result, the number of incident photons from the scanner at a particular voltage, slice thickness, tube current, must be known. This information was not supplied in the technical reference manual for the Somatom-2 scanner, therefore, the following is a calculation for the number of incident photons from the information supplied about the scanner. All scans were performed using 720 projections, with the tube set at 125 kVp and 230mAs and a slice thickness of 2mm. It was also known that the initial spectrum was filtered with 2.5mm of Al and 0.4 mm of Cu. From Figure 3.25, it was known that the peak of this graph corresponds to 8.405×10^5 photons/mm^2.mAs per 2 keV at 0.75m [18]. It was assumed that this was the same distance from tube to phantom in the commercial CT scanner.

The summation of the graph yields a total number of photons as 7.69×10^6 photons/mm^2.mAs. Filtering this spectrum with 0.4 mm Cu at 50 points at 2keV intervals, yields a value of 3.37×10^6 photons/mm^2.mAs. Knowing the tube current and the surface area onto which the beam is impinging, the total number of incident photons can be calculated. The dose due to these photons was now calculated by knowing the dose per 3600 photons/cm^2.s, figure 3.26. The calculated dose is in good agreement with the stated dose from the reference manual, ie. the total

91

Relative No. Photons.
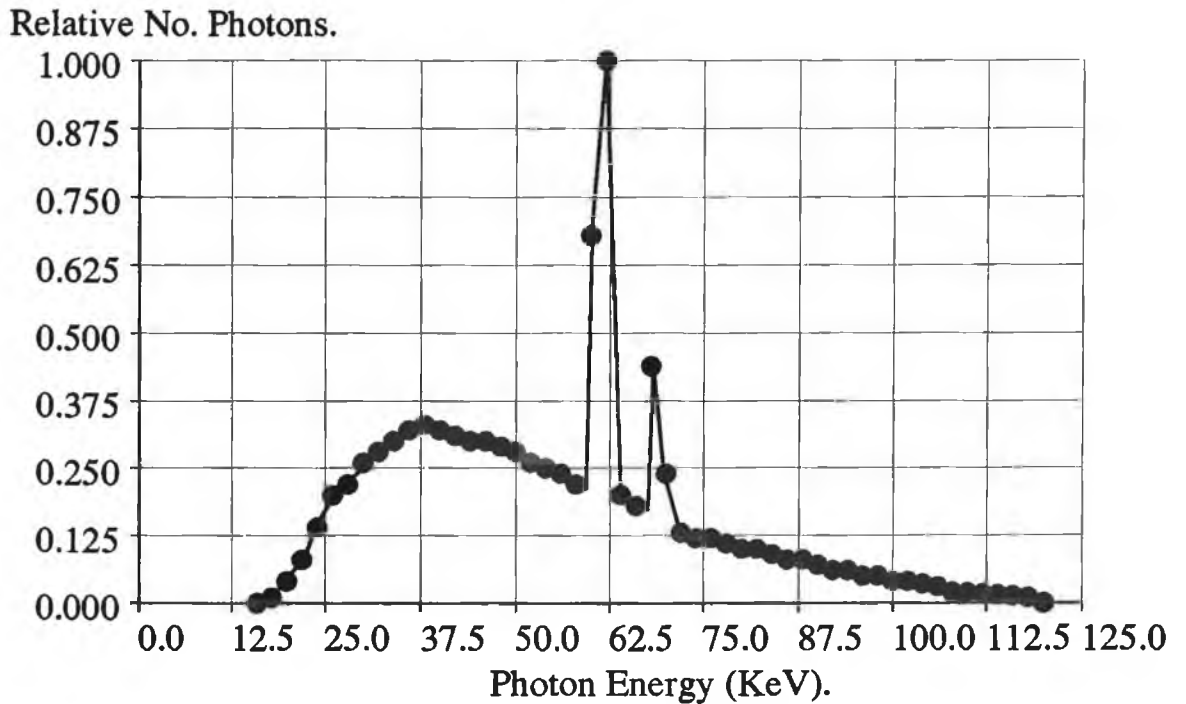
Figure 3.25
Incident energy spectrum in terms of relative number of photons for
a 120 kVp X-ray tube source, filtered by 2.5 mm Al.
(Gifford, "A handbook of physics for Radiologists and Radiographers",
Wiley & Sons, 1984)

mR/h per Photon/cm^2.s
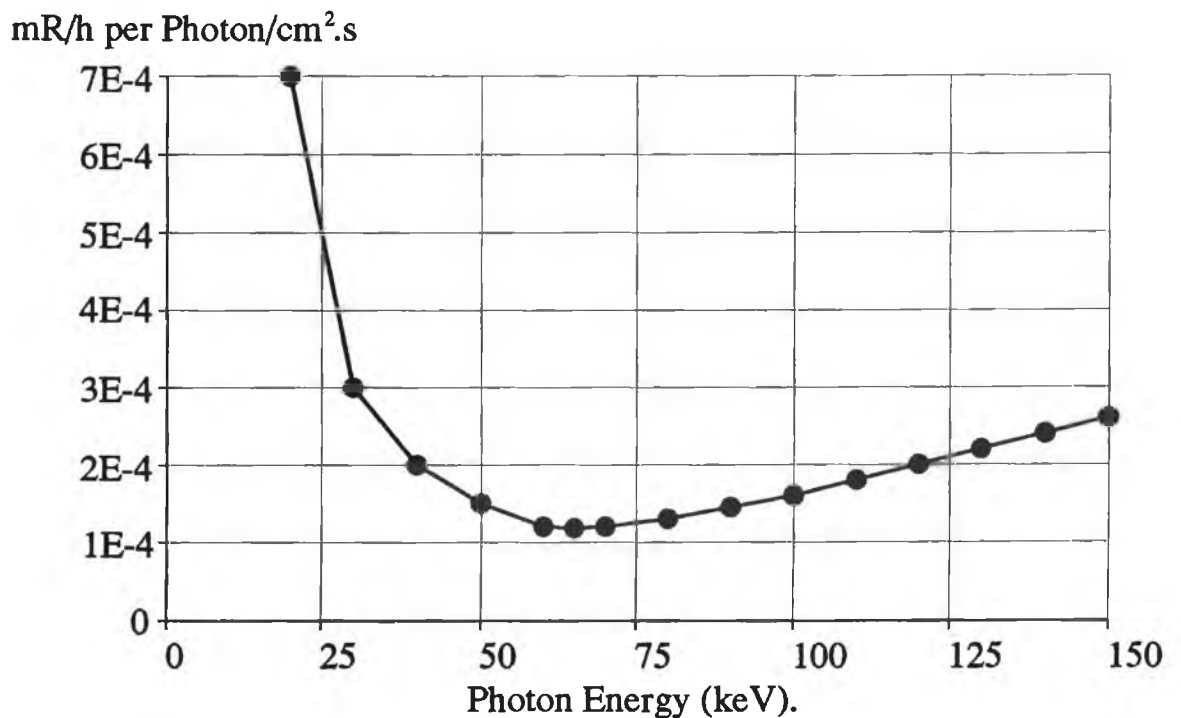
Figure 3.26
Exposure rate as a function of X-ray photon energy.
(From BS 4094, Part 1: 1966).

number of photons is estimated at 0.8 X 10^{12} for a 0.26m diameter phantom and a slice thickness of 2mm. This converts to a surface dose of 2.95 mGray (295 mRad) which compares well to the measured dose of 2.9 mGray.

In both the initial theoretical calculations and more importantly, in the computer simulations of an actual CT scan, it was assumed that the detector had a 100% efficiency, ie. no photons were lost due to the detector's conversion efficiency. It was decided to theoretically check this assumption because a non 100% efficiency would lead to disagreement between the simulated results and the experimental results.

The efficiency was determined at two extreme points. The first when there is no object attenuating the beam and the second taken when the beam is through the centre of the phantom, ie. the maximum attenuation of the beam. From the information derived from the Siemans technical manual for Somatom 2 scanner, it is known that the detector is a CsI crystal of 0.5 cm thick, connected to a near UV photodiode. It was felt that due to the small thickness of the crystal, that the crystal, and not the photodiode, would be the largest contributor to the inefficiency. The photodiode was operated in current mode on the CT scanner.

For the first case, the attenuation due to the CsI crystal is determined for each energy division using the tabled values of mass attenuation coefficient [22], see appendix 7. Using these values, the number of incident photons absorbed by the detector is calculated and from this the ratio of incident to detected photons is calculated, ie. the efficiency. For this case, the efficiency was found to be 99.76% Fig 3.27 shows the graph of the number of photons undetected by the crystal as a function of energy.

For the second case, where the object was in place and the beam traversed the centre of the phantom, a similar procedure was followed. However the attenuation of the beam by the object was also taken into account. Here, the percentage of incident photons that were detected was found to be 99.48%.

From the above two calculated values for the detector

93

efficiency, it can be concluded that the initial
assumption of an efficiency of 100% is valid.

Photons Undetected.
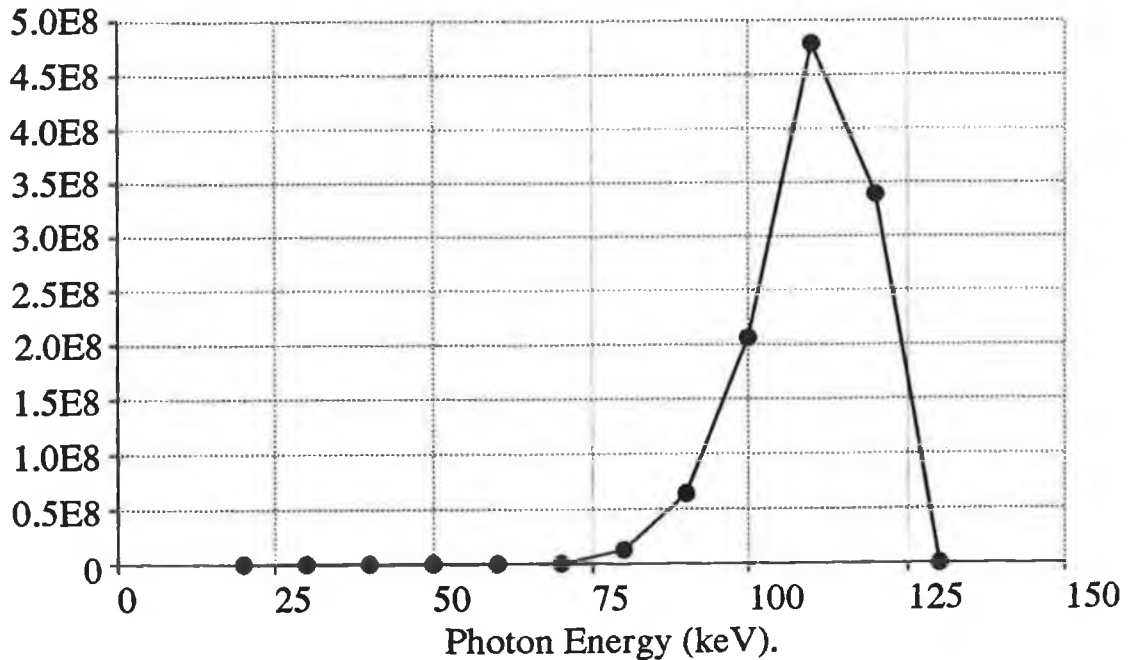
Figure 3.27
**Graph of the number of photons undetected by the CsI crystal as a
function of photon energy. The total number of photons incident on
the detector was 8.0E11.**

3.4.2 Determination of the Number of Steps/Rotations Performed on Somatom-2 Scanner.

Several modes of operation were available on the
scanner, with a choice between 4 tube current settings
(115, 153, 230, 300 mAs) , 2 voltage settings (96kV,
120kV) and 3 projection settings (256, 512, 720). The mode
of operation that was chosen was 120kV, 230 mAs and 720
projections, ie. normal head scan mode. However, the scan
size in head mode was approximately 0.24 m. For 720
projection, this would yield a resolution of 0.0003 m.
This value is highly improbable since the maximum
resolution with modern commercially available hospital
scanners is 0.001m. The Somatom-2 scanner is approximately
10 years old. It could not be determined from the
manufacturer how the 720 projections were generated,
therefore, the resolution of the image was determined from

the printed image using a travelling microscope. It was found that the image is made up of 256 X 256 pixels. Thus, our calculations were based upon this value for the number of steps and not 720 as originally thought.

3.4.3 Scaled Simulation Predictions.

With both the number of incident photons in a typical scan known as well as the assumed number of projections, predictions can be made as to the values of the minimum concentration visible that will be achieved for the elements scanned in the Somatom-2 scanner. The results of these predictions are shown in figure 3.28. The scaling of these values is based on equations 3.07 and 3.08 and the results achieved in section 3.3.11.

Min. Concentration (mg/cc).
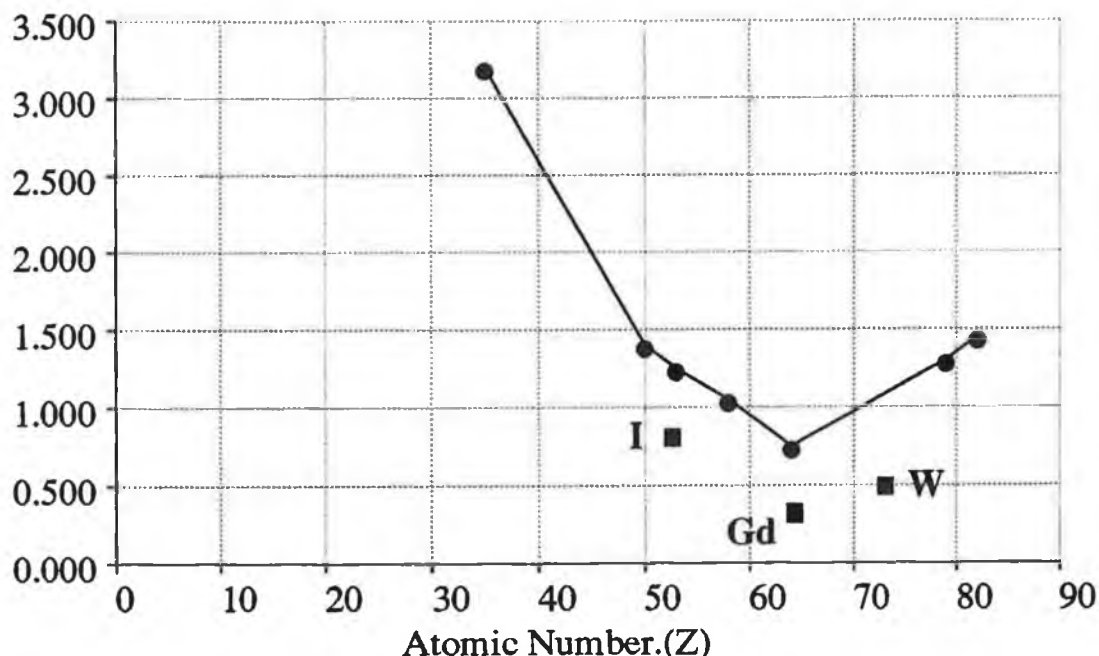
Figure 3.28
Results of simulations of single scans with a tube operating at 120 kV and Not=1E12 photons. These are simulations of the Soamtom-2 scanner operating at 230mAs. The experimental results for Iodine, Gadolinium and Tungsten are shown.(■)

3.4.4 Experimental Phantom.

The predictions for the minimum concentration visible had to be verified experimentally. Scans were performed of a phantom in a Somatom-2 scanner running at 125kV and 230mAs. The phantom was constructed in a similar fashion

to that shown in figure 3.03. An image of the phantom is shown in plate 3.1. The outer cylinder was made from polymethyl methacrylate and was 0.26m in diameter with a wall thickness of 3mm. The inner cylinders were made from polyethylene terephthalate, 0.086m and 0.052m in diameter with an approximate wall thickness of 0.25mm. The region between the two cylinders was partitioned to give two distinct regions. The regions A and C (figure 3.03) were filled with water, as was part of the middle ring B. The remaining section of B was filled with the analyte dissolved in water.

3.4.5 Preparation of Chemicals.

Three analytes were used in the experimental scans performed on the Somatom-2 scanner; Gadolinium, Iodine and Tungsten. The analytes were made up initially in 10 mg/cc solutions with the idea of diluting them to lower concentrations to reach the concentration visibility limit. The solutions were all made up as follows:

Using Gadolinium as an example; the soluble compound of Gadolinium is $Gd_2SO_48H_2O$ (gadolinium sulphate octahydride). Its molecular weight is 746.81, assuming that there is only one Gd ion per chelate:

$\Rightarrow$ 1g Gd $\equiv$ 746.81 / 157.25 g $\equiv$ 4.7492g of $Gd_2SO_48H_2O$.

$\Rightarrow$ 300cc of 10 mg/cc $\equiv$ 4.7492 X 10E-3 X 300 g

$= 14.25$ g.

Using de-ionized water, both the iodine (Potassium Iodine) and the tungsten (tungsten sulphate dihydride) $Na_2WO_42H_2O$, dissolved without any difficulty. However, the gadolinium failed to dissolve totally in de-ionized water. To overcome this problem some Nitric acid was added to the solution, (about 1-2cc) and this successfully dissolved the gadolinium.

3.4.6 Results.

Various concentrations of Iodine, Gadolinium and Tungsten solutions were scanned in the Somatom-2 scanner and the limits of visibility judged by eye from the monitor attached. Fig. 3.28 shows the results of these

experiments compared to the simulated results for single scans with a tube operating at 120kV and Not=1E12 photons. This graph shows that in both the simulated and experimental results, gadolinium is the optimum element to use as a contrast agent in the range of elements used for this study and that good agreement exists in terms of the trends of the minimum concentration vs. atomic number for both graphs. It can be used in concentrations a factor of approximately twice lower than iodine, the currently used contrast agent. The experimental results are lower than the simulated results with roughly equal visibility of the images in both cases. One reason for this could be due to errors in determining the number of incident photons. No measurement of this value could be made directly due to limited access to the scanner. The data used in the determination of this value was made on the information available from the technical manual and not on measurements taken from this particular machine. Plates 3.1 show typical images of the phantom with varying amounts of analyte present.

SOMATOM 2   MATER HOSPITAL, DUBLIN
03-JAN-90   13:17 TS/010   I: 4 E3*
0.125 MG GD   256
1   FRONT
                                + 150
                               RIGHT
                                + 22

                                - 106
S 2
T 10
V 96
D 150
G 1
P 0
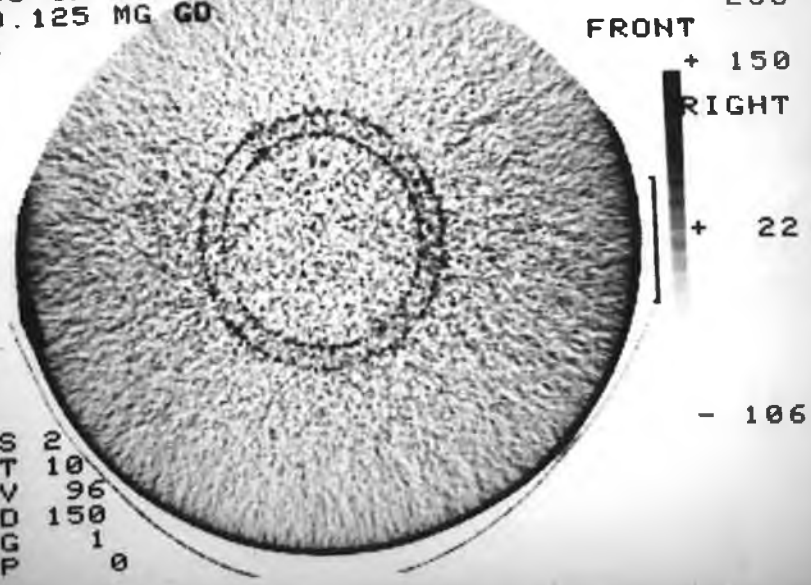
SOMATOM 2   MATER HOSPITAL, DUBLIN
03-JAN-90   12:58 TS/063   I: 2 E3*
0.5 MG GD   256
1   FRONT
                                + 155
                               RIGHT
                                + 27

                                - 101
S 2
T 10
V 125
D 115
G 0
P 0
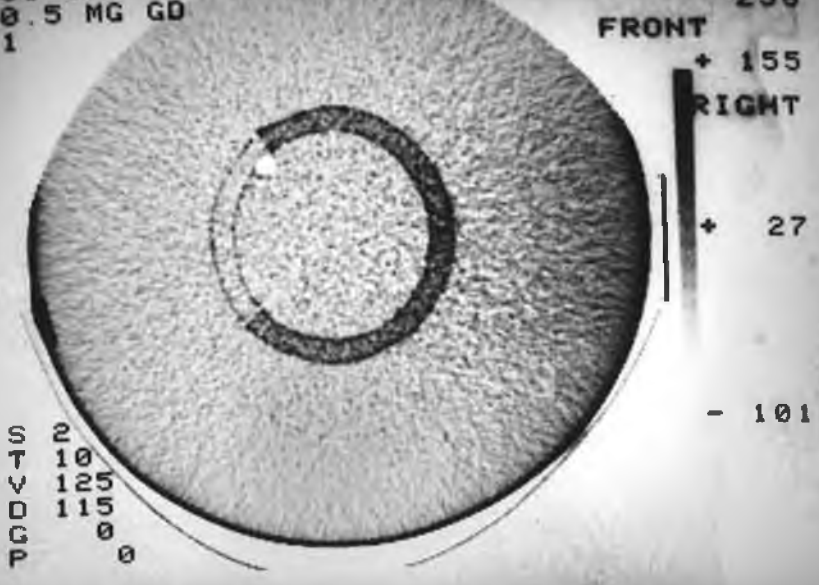
than theory would predict. It should be noted that according to the simulated images the minimum concentration of gadolinium obtained for 10^{12} photons is approximately 0.01 mg/cc. A similar result is seen in the single-monochromatic-energy scans (3.5.2).

3.5.4 Single Polychromatic Scan.

Results were simulated for a scan of the phantom with the analyte already present in the middle ring, see figure 3.23. No subtraction was performed. The total number of incident photons was 10^{10} as for the monochromatic cases. In figure 3.28 results of simulations are compared with measurements made in the Somatom-2 scanner set at 125kV and 230 mAs. This gives about 10^{12} photons. In both simulated and experimental results the maximum sensitivity occurs for gadolinium with a predicted sensitivity of about 0.7 mg/cc. This is approximately 80 times less sensitive than the monochromatic scans with image subtraction, performed on the phantom with the analyte evenly dispersed throughout.

3.5.5 Two-fixed Voltage Polychromatic Scans with Image Subtraction.

This work was based purely on simulations. If the analyte can be added to the matrix after an initial scan then the predicted minimum detectable concentrations are shown in figure 3.24. If we compare the results in figure 3.24 with the results in figure 3.23 it is seen that image subtraction will give about a 30 fold increase in sensitivity. It is interesting to note that on comparing figures 3.14 to 3.22, there is little to be gained by using monochromatic beams with image subtraction.

3.5.6 Gd-DTPA.

No drug is completely safe. Even water, if given in a large enough dose, can induce intoxication and death. For this reason, safety has to be defined in terms of the ratio of risks to benefits [49]. To be considered safe, the contrast agent must therefore exhibit far greater benefit in terms of diagnostic information, than unwanted

side effects.

The above results indicate that Iodine is not the most sensitive element to use as a contrast agent. These results indicate that for the spectral ranges used in CT, Gadolinium gives the optimum sensitivity. Iodine has been used clinically for cardiac and general X-ray/CT imaging because of its low toxicity and relatively good opacity. However, considerable interest has been generated by clinical and laboratory reports describing the applications of diethylenetriamine pentaacitic acid (DTPA) complex of gadolinium. The free Gd ion is poorly tolerated and tends to be retained in the body for long periods and also to have undesirable side effects [50,51]. A common strategy to encourage more rapid elimination of this element is chelation (derived from the Greek word for 'claw'). Some chelating agents (organic acids) form stable complexes with the ion. Chelation causes a dramatic change in the properties of a metal ion. One of the most common of these chelating agents is DTPA, shown in figure 3.29. Although free Gd is poorly tolerated, there is no evidence of in-vivo disassociation of the Gd-DTPA complex [49].
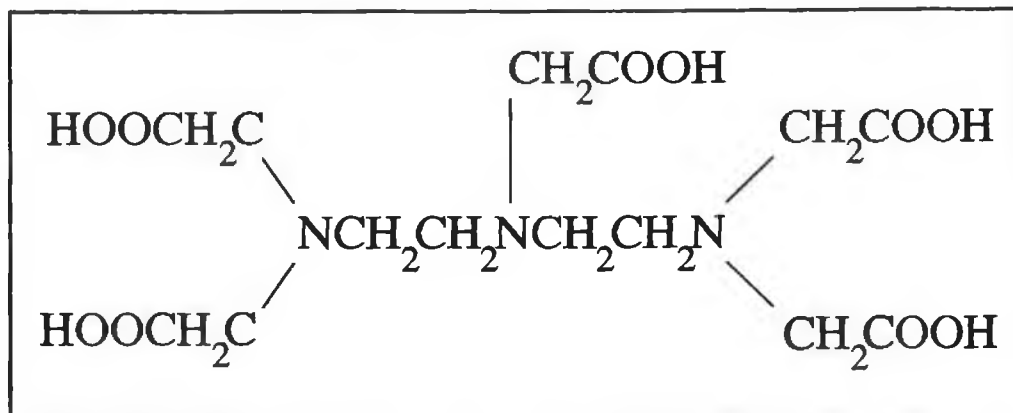
Figure 3.29
Chemical formula for Diethylenetriamine Pentaacetic Acid (DTPA).

The pharmockinetic behavior of intravenously delivered Gd-DTPA is similar to that of the iodinated contrast agents used in urography and angiography. Studies of toxicity in animals indicate high tolerance, a result supported by the findings of many clinical trials on

humans [49,52,53,54,55,56,57].

With regard to the potential use of Gd-DTPA as a contrast agent for cardiac imaging, Eichstadt et al. [58] published a study of 38 patients with a confirmed history of myocardial infarction. According to these results, acute infarctions (less than 7 days old) can be recognised by an increased accumulation of the contrast agent in the NMR image. On the other hand, sub-acute (7-21 days old) and chronic infarctions (over 21 days) are characterised by the absence of contrast enhancement or a reduced accumulation of contrast agent compared to normal myocardium.

Gd-DTPA therefore seems to have good potential as a contrast agent for use in CT imaging of the heart. However, no clinical trials have yet been performed using Gd-DTPA in CT. It does however posses low toxicity and high tolerability and therefore should be investigated further.

3.6 Conclusion:

It has been shown in the work presented here, that for the energy range applicable to CT scans of the myocardium, gadolinium is the best element to use as a contrast agent, in terms of the minimum concentration required for a certain visibility. This is contrary to current clinical practice of using Iodine in virtually all contrast-enhanced scans. Gadolinium is at present used as a contrast agent in Magnetic Resonance Imaging when chelated to DTPA, therefore its toxicity effects are within reasonable limits. This fact therefore suggests the use of Gd-DTPA as a contrast agent in CT. This has not been clinically tested yet.

However, in the energy range 50-80kVp, Lumbroso and Dick [19] found that Iodine was the optimum element for use as a contrast agent. Thus, for specific examinations, with a need for extra contrast in the image, it would be better to select the best element for each examination. This can be explained by the fact that the peak intensity for a 80 KVp spectrum occurs at an energy close to the

K-edge of Iodine. At CT spectrum energies, ie. 120 kVp, the peak occurs in the vicinity of gadolinium's K absorption edge.

Also, in the work presented in this chapter, it has been found that if image subtraction could be performed on a commercial CT scanner, before reconstruction, then the sensitivity achieved by this method would be similar to that currently available by synchrotron. This process, if implemented, would have a dramatic effect on reducing the toxicity effects of currently administered contrast agents as lower concentrations could be utilised.

References

[1] Boyd, D., Li[ton, M.,
"Cardiac Computed Tomography.", Proc. IEEE, Vol. 71, No. 3, pp.298-307, 1983.

[2] Hamilton, G.W.,
"Myocardial imaging with Thallium-201: The controversy over its clinical usefulness in ishemic heart disease.", Jour. Nucl. Med., Vol. 220, pp.1201-1205, 1979.

[3] Rubenstein, E.,
"Medical Imaging with Synchrotron Radiation.", Nuclear Instruments and Methods in Physics Research, No. 222, pp.302-307, 1984

[4] Waggener, R., Kereiakes, J., Shalek, R.,
"Handbook of Medical Physics: Volume III", CRC Press Inc., Boca Raton, Florida. (1983)

[5] Gifford, D.,
"A Handbook of Physics for Radiologists and Radiographers.", 1984, John Wiley & Sons.

[6] Haselgrovem, J., Harihara Subramanian, V., Leigh, J., et al. "In vivo One-Dimensional Imaging of Phosphorous Metabolites by Ph-31 Nuclear Magnetic Resonance.", Science, Vol. 220, pp.1170, 1983

[7] Bates, R., Garden, K., Peters, T.,
"Overview of computerised tomography with emphasis on future developments.", Proc. IEEE, Vol. 71, No. 3, pp.356-372, 1983.

[8] Higgins, C., Sovak, M., Schmidt, W., et. al.,
"Differential accumulation of radiopaque contrast material in acute myocardial infarction.", Amer. Jour. Cardiol., Vol. 43, pp.47-51, 1979

[9] Lipton, M., Brundage, B., Doherty, P., et. al.,
"Contrast medium-enhanced computed tomography for evaluating ischemic heart disease.", Cardiovasc. Med., Vol. 4, pp.1219 ,1979

[10] Berninger, W., Redington, R., Doherty, P., et. al.,
"Gated cardiac scanning in normal and experimentally infarcted canines.", Jour. Comput. Assis. Tomo., Vol. 32, pp.155-163, 1979.

[11] Sagel, S., Weiss, W., Gillard, R., et. al.,
"Gated computed tomography of the human heart.", Invest. Radio., Vol. 12, pp.563-566, 1979.

[12] Redington, R.,
"CT scanner designs of the future.", Current development in medical imaging - An evaluation., Proc. Symp., Colorado Springs, Aug 5-7, pp.49-58, 1980.

[13] Robb, R., Ritman, E., Gilbert, B., et. al.,
"Ths DSR: A high-speed three dimensional X-ray computed
tomography system for dynamic spatial reconstruction of
the heart and circulation.", IEEE Trans. Nucl. Sci., Vol.
NS-26, pp.2713-2717, 1979.

[14] Behrenbeck, T., Kinsey, J., Harris, L., et. al.,
"Three-dimensional spatial, density, and temporal
resolution of the dynamic spatial reconstructor.", Jour.
Comput. Assis. Tomog., Vol. 6, No. 6, pp.1138-1147, 1982.

[15] Boyd, D.,
"Computerised transmission tomography of the heart using
scanning electron beams.", CTT of the Heart: Experimental
evaluation and Clinical applications., Futura Press, New
York.

[16] Diethelm, L., Simonsen, J., et. al.,
"Determination of LV mass by ultrafast CT and 2-D
echocardiography.", Radiology, Vol. 171, pp.213-217, 1989.

[17] Wang, T., Wu, X., Chung, N., Ritman, E.,
"Myocardial blood flow estimated by synchronous
multislice, high-speed computed tomography.", IEEE Trans.
Med. Imag., Vol. 8, No. 1, pp.70-77, 1989

[18] Himelman, R., Abbort, J., Lipton, M., et. al.,
"Cine computed tomography compared with echocardiography
in the evaluation of cardiac function in emphysema.",
Amer. Jour. Card. Imag., Vol. 2, No. 4, pp.283-291, 1988.

[19] Lumbroso, P., Dick, C.E.,
"X-ray attenuation properties of radiographic contrast
media.", Medical Physics, Vol. 14, No. 5, pp.752-758, Oct
1987.

[20] Skowrinski, G., Runciman, W., Crawford, C., et. al.,
"Acute systemic reactions in intravascular contrast media
- a planned approach.", Australas Radiol., Vol. 31,
pp.186-191, 1987.

[21] McCarthy, K., Fryar, J.,
"Sensitivities for Contrast Agent Imaging in CT Scans
using Single Energy Synchrotron Radiation", Nucl. Inst.
and Meth. in Phys. Res., Vol. A287, pp.613-618, 1990.

[22] Hubbell, J.H.,
"Mass Attenuation and Energy Absorption Coefficients from
1keV to 20 MeV." , Int. J. Appl. Radiat. Isot., Vol 33, pp
1269-1290, 1982.

[23] Muller, E.A.,
"Archiv fear Technicians Messen und Industrielle
Messtechnik". R. Oldenbourg, Munich 1956.

[24] Jacobson, B.,
"Dichromatic Absorption Radiography. Diochromography.",
Acta Radiol., Vol. 39, pp.437-452, 1953.

[25] Mistretta, C., Ort, M., Kelcz, F., et. al.,
"Absorption - edge fluoroscopy using quasi -monoenergetic
X-ray beams.", Invest. Radiol., Vol. 8, pp.402 - 412, 1973.

[26] Atkins, H., Hauser, W., Kraner, W.,
"Absorption - edge transmission scanning.", American Jour.
Roentgenology, Vol. 114, pp.176-180, 1972.

[27] Oldendorf, W., Phelps, M., Hoffer, P.,
"An inherently stable system for measuring tissue iodine
using its K-absorption edge.", American Jour.
Roentgenology, Vol. 120, pp.583-588, 1974.

[28] Rose, H., Flick, D.,
"Assay of iodine content of thyroid extract by X-ray
absorption edge analysis.", J. Pharmacol. Sci., Vol. 53,
pp.1153-1156, 1964.

[29] Fryar, J., McCarthy, K., Fenelon, A.,
"Differential X-Ray Absorptiometry Applied to Computerised
X-Ray Tomography.", Nucl. Inst. and Methods., A259,
pp.557-565, 1987.

[30] Fryar, J., McCarthy, K., Fenelon, A.,
"Multielement Imaging in Computerised X-Ray Tomography.",
Nucl. Inst and Meth., A271, pp.671-677, 1988.

[31] Fryar, J., McCarthy, K.,
"Multielement Imaging in CT using a tube source of
X-Rays.", IEEE Trans. Nucl. Sci., Vol 136, No.1,
pp.1138-1143, 1989.

[32] Zeman, H., Hughes, E., Campbell Finman, L., et. al.,
"Evaluation of synchrotron X-rays for transverse coronary
angiography.", Nucl. Inst. & Meth., Vol. 222, pp.308-318,
1984.

[33] Sorenson, J.,
"Absorption - edge transmission technique using Ce-139 for
measurement of stable iodine concentration.", Jour. Nucl.
Med., Vol. 20, pp.1286-1293, 1979.

[34] Riederer, S., Mistretta, C., Kruger, R.,
"Relative properties of tomography, K-edge imaging, and
K-edge tomography.", Medical Physics, Vol 4, No. 3,
pp.244-249, 1977.

[35] Riederer, S., Mistretta, C.,
"Selective iodine imaging using K-edge energies in
computerised X-ray tomography.", Medical Physics, Vol. 4,
No. 6, pp.474-481, 1977.

[36] Thompson, A., Lacer, J., Campbell Finman, L.,
"Computed tomography with Synchrotron radiation.", Nuclear
Inst. and Meth., Vol. 222, pp.319-323, 1984

[37] Rubenstein, E.,
"Medical imaging with synchrotron radiation.", Nucl. Inst.
& Meth., Vol. 222, pp.302-307, 1984

[38] Suzuki, Y., Usami, K., Sakamoto, K., et. al.,
"X-Ray computed tomography using monochromated synchrotron radiation.", Jap. Jour. Appl. Phys., Vol 27, No. 3, pp.461-464, 1988

[39] Hughes, E., Rubenstein, E., Zeeman, H.,
"The Angiography program at Stanford.", Nucl. Inst. & Meth., Vol A246, pp.719-725, 1986

[40] Rubenstein, E., Brown, G., Gorden, H., et. al.,
"Angiography by synchrotron radiation.", Physica Scripta, Vol. T19, pp.487-490, 1987.

[41] Markham, C.,
"Dual element imaging using a low resulution detector and tube source of X-rays.", Ph.D. work in progress.

[42] Cesareo, R.,
"Principles and Applications of Differential Tomography.", Nucl. Inst. and Meth., A270, pp.572-577, 1988.

[43] Blackwell, H.,
"Contrast thresholds of the human eye.", J. Opt. Soc. Am., Vol 36, pp.624-643, 1946.

[44] Rossman, K.,
"Point spread function, line spread-function, and modulation transfer function: tools for the study of imaging systems.", Radiology, Vol.93, pp.257-272, 1969.

[45] Cornsweet, T.N.,
"Visual Perception.", New York, 1970, Academic Press, Inc.

[46] Rose, A.,
"Vision: human and electronic.", New York, 1973, Plenum Press Corp.

[47] Harmon, L., Julesz, B.,
"Masking in visual recognition; effects of two-dimensional filtered noise.", Science, Vol. 180, pp.1194-1197, 1973.

[48] McCarthy, K.J.,
"A Study of the Imaging of Atomic Elements by Computerised Axial Tomography"., Ph.D Thesis, 1989, Dublin City University.

[49] Brasch, R.C.,
"An Overview of Contrast Agents for Magnetic Resonance Imaging." (Quoted in:"Contrast Agents in Magnetic Resonance Imaging.", Excerpta Medica, Princeton, pp.11-13, 1986.)

[50] Christiensen, H.E.,
"Registry of Toxic Effects on Chemical Substances.", Rockville, National Institute of Occupational Safety and Health, 1975.

[51] Browning, E.,
"Toxicity of Industrial Metals.", New York, Appleton-Century-Crofts, 1975.

[52] McNamara, M., Higgins, C., Ehman, R., et. al.,
"Acute Myocardial Ischemia: Magnetic resonance contrast
enhancement with Gd-DTPA.", Radiology, Vol. 153,
pp.157-163, 1984.

[53] Weinmann, H., Brasch, R., Press, W., et. al.,
"Characteristics of Gd-DPTA complex: A potential MRI
contrast agent.", Am. Jour. Roentgenology, Vol 142, pp.619
,1984.

[54] Carr, D., Brown, J., Bydder, G., et. al.,
"Intravenous chelated gadolinium as a contrast agent in
NMR imaging of cerebral tumors.", Lancet, Vol. 1, pp.484 ,
1984.

[55] Claussen, C., Laniado, M., Felix, R., et. al.,
"Application of contrast agents in CT and MRI (NMR). Their
potential in imaging brain tumors.", Neuroradiology, Vol.
27, pp.164 , 1985.

[56] Felix, R., Schorner, W., et. al.,
"Brain tumors: MRI imaging with Gd-DTPA.", Radiology, Vol.
156, pp.681 ,1985.

[57] Runge, V., Clanton, J., Price, A.,
"Evaluation of contrast-enhanced MRI imaging in a brain
abscess model.", Amer. Jour. Neuroradiology, Vol. 6,
pp.139 , 1985.

[58] Eichstadt, H., Felix, R., Dougherty, F., et. al.,
"Magnetic Resonance Imaging (MRI) in different stages of
myocardial infarction using the contrast agent Gd-DTPA.",
Clinical Cardiology, Vol. 9, pp.527 ,1986.

[61] Barford, N.C.,
Experimental Measurements: Precision, Error and Truth.",
Wiley & Sons, 1987.

Chapter IV
Determination of the Sensitivity of CT to contrast agents in cylinders.

4.1 Introduction

Previously, an investigation was performed on determining which element, when used as a radiographic contrast agent in CT, needed the lowest concentration for visibility to occur. It was found that for the particular case of imaging the myocardium using a commercial CT scanner, gadolinium was the optimum element. However, the question now arises, is this always the case? That is, if the contrast agent were administered into a capillary, would gadolinium still be the optimum element and how does the concentration vary as a function of the size of the region in which it is administered, relative to the size of the object in which the region is contained. These questions will be answered in the following work. Two situations will be studied; 1) In the first case the contrast agent can be added to the region after an initial scan of the object containing no contrast agent, the two scans being performed at any energy. The two sets of scan data are subtracted to yield an image of the analyte alone. 2) In the second case the contrast agent is already present in the region and a scan will be performed at two energies just above and below the K-absorption edge of the analyte. The only difference between these two images is due to the jump in the absorption coefficient of the analyte. Subtraction of these data sets will yield an image of only the analyte.

Several authors have studied similar cases, however in each of these works the case studied was that of adding the contrast agent / analyte to the complete object homogeneously. This is not the norm in routine CT scanning. Grodzins [1] studied the minimum detectable

concentration in terms of the photons passing through one pixel, the pixel size and composition, and the fraction of the atoms that were defined as "critical". Fryar and McCarthy [2,3] studied the minimum detectable concentration in a full CT image and developed a simple equation for the determination of this concentration. Here, as with Grodzins, the analyte was assumed to be homogeneously dispersed throughout the matrix. This is the first study performed on the situation where the analyte is not homogeneously dispersed throughout the matrix. This is the normal case in contrast enhanced CT imaging.
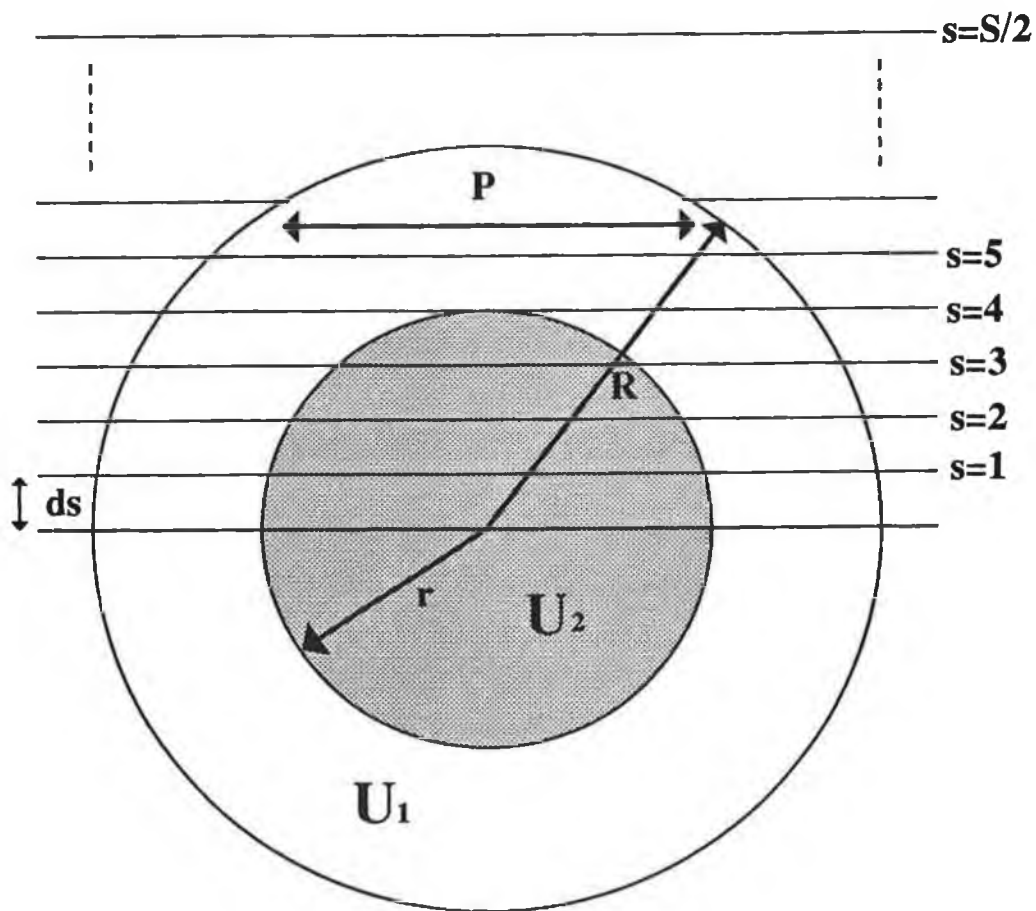
Figure 4.01
Diagram showing the geometry and parameters for the two cases studied.

4.2.1   The case where the analyte can be added to the matrix.

The object considered in both cases consists of two cylinders, one inside the other. This arrangement produces scan profiles which are similar for all rotation angles.

The path length through the cylinder at a given step position is given by the following equation,

$$P = 2.\left[R^2 - \left((s-0.5).\Delta x\right)^2 \right]^{1/2} \qquad (4.01)$$

where s is the step position with respect to the centre of rotation, Δx is the beam width and R is the radius of the cylinder. This is seen in Fig 4.01. In the object the two regions have linear attenuation coefficients U_1 and U_2. These, and other symbols common to both cases, are explained in Table 4.1.

M	=	Number of rotations in a scan.
S	=	Number of steps in a scan.
N_0	=	Incident number of photons per beam.
N_{ot}	=	Total number of incident photons in a complete scan.
N	=	Number of photons emerging from the object per beam.
U_1	=	Linear attenuation coefficient of matrix.
U_2	=	Linear attenuation coefficient of analyte.
R	=	Radius of the outer cylinder.
r	=	Radius of the inner cylinder.
f	=	Ratio of the radii, ie. f=r/R.
Δx	=	Beam width.
s	=	Step number in the scan.
X_1	=	Number of mean free paths through the cylinder containing the matrix only.
L_1	=	Mean free path of the matrix.
L_2	=	Mean free path of the analyte.
D	=	Number of standard deviations.
B	=	Reconstruction noise amplification factor.
N_m	=	Number of photons emerging from the complete scan of the matrix only.
N_{ma}	=	Number of photons emerging from the complete scan of the matrix and analyte.
ρ_a	=	Density of the analyte.
ρ_m	=	Density of the matrix.
μ_a	=	Mass attenuation coefficient of the analyte.
μ_m	=	Mass attenuation coefficient of the matrix.

Table 4.1 showing symbol definitions.

When no analyte is present in the object, the number of photons emerging through the object, given that N_0 photons are incident on the object at any step position in the object, is given by;

$$N = N_0.\exp\left[-2.U_1.\sqrt{R^2 - (s-0.5)^2.(\Delta x)^2}\right] \qquad (4.02)$$

where R is the radius of the large cylinder, Δx is the step size and s is the step position.

When analyte is present in the inner cylinder, the number of photons emerging from the object is given by;

$$N = N_0.\exp\left[-2.U_1\left(R^2 - (s-0.5)^2(\Delta x)^2\right)^{1/2}\Bigg|_{s \geq r}\right.$$

$$\left\{-2U_1\left(R^2 - (s-0.5)^2(\Delta x)^2\right)^{1/2} + 2U_1\left(r^2 - (s-0.5)^2(\Delta x)^2\right)^{1/2} -\right.$$

$$\left.\left.2U_2\left(r^2 - (s-0.5)^2(\Delta x)^2\right)\right\}\Bigg|_{s < r}\right] \qquad (4.03)$$

For a complete scan with S steps and M rotations, the total number of transmitted photons is given by

$$N_{ma} = 2.M.\sum_{s > r}^{\frac{S}{2}} N_0.\exp\left[-2.\left[\left(\frac{X_1 L_1}{2L_1}\right)^2 - (s-0.5)^2\left(\frac{X_1 L_1}{SL_1}\right)^2\right]^{1/2}\right]$$

$$+ 2.M.\sum_{s=1}^{r} N_0.\exp\left[-2.\left[\left(\frac{X_1 L_1}{2L_1}\right)^2 - (s-0.5)^2\left(\frac{X_1 L_1}{SL_1}\right)^2\right]^{1/2} + \right.$$

$$2.\left[\left(\frac{fX_1 L_1}{2L_1}\right)^2 - (s-0.5)^2\left(\frac{X_1 L_1}{SL_1}\right)^2\right]^{1/2}$$

$$\left. - 2.\left[\left(\frac{fX_1 L_1}{2L_2}\right)^2 - (s-0.5)^2\left(\frac{X_1 L_1}{SL_2}\right)^2\right]^{1/2}\right]$$

$$(4.04)$$

Here, use is made of the fact that R = D/2 and that Δx, the step size, = D/S. The diameter D = X_1L_1, where L_1 is the mean free path of the matrix at that energy and X_1 is the number of mean free paths through the object of diameter D. This equation can be reduced to the following by simple cancellation. *Note:* $L_1 = 1/U_1$.

$$
N_{ma} = 2.M.\sum_{s>r}^{\frac{S}{2}} N_0.\exp\left[-X_1\left(1 - \frac{4.(s-0.5)^2}{S^2}\right)^{1/2}\right] +
$$

$$
2.M.\sum_{s=1}^{r} N_0.\exp\left[-X_1\left(1 - \frac{4.(s-0.5)^2}{S^2}\right)^{1/2}\right. +
$$

$$
X_1\left(f^2 - \frac{4.(s-0.5)^2}{S^2}\right)^{1/2} -
$$

$$
\left.\frac{X_1 U_2}{U_1}\left(f^2 - \frac{4.(s-0.5)^2}{S^2}\right)^{1/2}\right]
$$

$$(4.05)$$

For a scan performed with no analyte present, the number of photons emerging is given by

$$
N_m = 2.M.\sum_{s=1}^{r} N_0.\exp\left[- X_1.\left(1 - \frac{4.(s-0.5)^2}{S^2}\right)^{1/2}\right]
$$

$$
+ 2.M.\sum_{s\geq r}^{S/2} N_0.\exp\left[- X_1.\left(1 - \frac{4.(s-0.5)^2}{S^2}\right)^{1/2}\right]
$$

$$(4.06)$$

If two scans are done, the first of the object containing no analyte and the second of the object with the analyte now present, and the data of the scans are subtracted from each other, then the following gives the total number of photons transmitted for the resulting subtracted image.

113

$$N_m - N_{ma} = 2.M. \sum_{s=1}^{r} N_o.\exp\left[-X_1\left(1 - \frac{(s-0.5)^2.4}{s^2}\right)^{1/2}\right]$$

$$- 2.M. \sum_{s=1}^{r} N_o.\exp\left[-X_1\left(1 - \frac{(s-0.5)^2 4}{s^2}\right)^{1/2}\right.$$

$$+ X_1\left(f^2 - \frac{(s-0.5)^2 4}{s^2}\right)^{1/2}$$

$$\left. - \frac{X_1 U_2}{U_1}\left(f^2 - \frac{(s-0.5)^2 4}{s^2}\right)^{1/2}\right]$$

(4.07)

where N_m is the number of counts from scanning the object with the matrix alone and N_{ma} is the number of counts from the matrix and analyte. Rearranging the above equation gives the following where $\Delta U = U_2 - U_1$ and $N_{oT} = S.M.N_o$ (N_{ot} is the total number of incident photons in a complete scan).

$$N_m - N_{ma} = N_{ot} \sum_{s=1}^{r} \frac{2}{S}.\exp\left[-X_1\left(1 - \frac{(s-0.5)^2.4}{s^2}\right)^{1/2}\right]$$

$$- N_{ot} \sum_{s=1}^{r} \frac{2}{S}.\exp\left[-X_1\left(1 - \frac{(s-0.5)^2 4}{s^2}\right)^{1/2}\right.$$

$$\left. - \frac{\Delta U.X_1}{U_1}\left(f^2 - \frac{(s-0.5)^2 4}{s^2}\right)^{1/2}\right]$$

(4.08)

The above equation will yield the difference in the number of photons from two scans, one with analyte and the other without. The analyte can be detected (ie. visible in the final image) if this difference is sufficiently large.

It can be said that the analyte is statistically detectable if the difference in the number of counts is

114

greater than D standard deviations where D is a number usually between 2 and 5. The standard deviation is given by

$$\sigma = \sqrt{N_m} = \sqrt{N_{ma}} \qquad (4.09)$$

where $N_m \simeq N_{ma}$ when the concentration of the analyte is low. Considering an image made up of S X S pixels, then on average, the number of photons which pass through a pixel is N_m/S or N_{ma}/S. However, the region of interest here is where the analyte is added, therefore, for the difference term the photons pass through f.S pixels. On average, the analyte will be seen if the difference count per pixel is greater than or equal to D standard deviations of the mean pixel value in the region of interest.

$$\Rightarrow \qquad \frac{N_m - N_{ma}}{f.S} \geq D.\sqrt{N_m/(f.S)} \qquad (4.10)$$

However, this does not take into account the noise amplification due to the reconstruction algorithm;

Generally, the noise present in a CT image occurs from two main sources (assuming that no artifacts are present due to misalignment, insufficient number of projection, etc.); 1) noise inherent on the projection data and 2) noise amplification by the reconstruction algorithm.

The noise in the projection data arises from Poisson statistical fluctuations in the number of counts measured and also scattering which may occur with non-perfect collimation. The above equation takes account of this noise in diminishing the detectability of the system. Fryar and McCarthy found that D needed to be at least 3 such that detection of the analyte occurred [2].

This inherent noise is amplified when the projection data is processed by the reconstruction algorithm. This case has been studied by Chesler and Flannery et al. [4,5]. They both introduced a constant multiplier on the noise, the factor B shown below. Chesler found that for a very good filtered backprojection algorithm using the Hann filter, the factor B = 2.3 [4].

$$\Rightarrow \qquad \frac{N_m - N_{ma}}{f.S} \geq B.D.\sqrt{N_m/(f.S)} \qquad (4.11)$$

115

Substituting equations 4.06 and 4.07 into the above equation gives;

$$
\text{Not} \sum_{s=1}^{r} (2/S).\exp\left[- X_1\left(1 - \frac{(s-0.5)^2.4}{S^2}\right)^{1/2}\right] -
$$

$$
\text{Not} \sum_{s=1}^{r} (2/S).\exp\left[- X_1\left(1 - \frac{(s-0.5)^2.4}{S^2}\right)^{1/2}\right.
$$

$$
\left. - \frac{\Delta U X_1}{U_1}\left(f^2 - \frac{(s-0.5)^2.4}{S^2}\right)^{1/2}\right]
$$

$$
\geq B.D.\sqrt{S.f} . \left\{ \text{Not}. \sum_{s=1}^{r} (2/S)\exp\left[-X_1\left(1 - \frac{(s-0.5)^2.4}{S^2}\right)^{1/2}\right]\right\}^{1/2}
$$

$$(4.12)$$

Now, dividing both sides by N_oT gives

$$
\sum_{s=1}^{r} (2/S).\exp\left[-X_1\left(1 - \frac{(s-0.5)^2.4}{S^2}\right)^{1/2}\right] -
$$

$$
\sum_{s=1}^{r} (2/S).\exp\left[-X_1\left(1 - \frac{(s-0.5)^2.4}{S^2}\right)^{1/2}\right.
$$

$$
\left. - \frac{\Delta U X_1}{U_1}\left(f^2 - \frac{(s-0.5)^2.4}{S^2}\right)^{1/2}\right]
$$

$$
\geq \frac{B.D.\sqrt{S.f}}{\text{N}_{o\,t}} . \left\{ \text{Not}. \sum_{s=1}^{r} (2/S).\exp\left[-X_1\left(1 - \frac{(s-0.5)^2.4}{S^2}\right)^{1/2}\right]\right\}^{1/2}
$$

$$(4.13)$$

Thus

$$
\sum_{s=1}^{r} (2/S).\exp\left[- X_1\left(1 - \frac{(s-0.5)^2.4}{S^2}\right)^{1/2}\right] -
$$

$$
\sum_{s=1}^{r} (2/S).\exp\left[-X_1\left(1 - \frac{(s-0.5)^2.4}{S^2}\right)^{1/2}\right.
$$

$$
\left. - \frac{\Delta U X_1}{U_1}\left(f^2 - \frac{(s-0.5)^2.4}{S^2}\right)^{1/2}\right]
$$

116

$$\geq \ P.\left\{ \sum_{s=1}^{r} (2/S).\exp\left[-X_1\left(1 - \frac{(s-0.5)^2.4}{s^2}\right)^{1/2}\right]\right\}^{1/2}$$

(4.14)

where,

$$P \ = \ \frac{Q.(f.S)^{1/2}}{N_o t^{1/2}} \quad \text{and} \quad Q = D.B \quad (4.15)$$

Solution of the above equation will yield a value for ΔU, the smallest change in the linear attenuation coefficient that is visible.

4.2.2 Determination of Concentration:

An equation to convert the $\Delta U/U_1$ quantity into actual analyte concentration will now be determined.

If only the internal cylinder is considered, then this has a volume V_m and a density ρ_m before the analyte is added. If we add a volume V_a of analyte, which has a density ρ_a, the concentration of the analyte and the matrix is given by

$$C_a \ = \ \frac{(\rho_a V_a)}{(V_a + V_m)} \quad \text{and} \quad C_m \ = \ \frac{(\rho_m V_m)}{(V_a + V_m)} \quad (4.16, \ 4.17)$$

Dividing one by the other yields

$$C_a \ = \ \frac{(V_a \rho_a C_m)}{(V_m \rho_m)} \quad (4.18)$$

The change in the linear attenuation coefficient can be written as follows,

$$dU = U_{a+m} - U_m \ = \ (C_a \mu_a + C_m \mu_m) - \rho_m \mu_m \quad (4.19)$$

where μ's are the mass attenuation coefficients and the C's the respective concentrations. Using the above equations for the concentrations the following equation can be derived,

$$dU \ = \ \left(\frac{V_a}{(V_a + V_m)}\right)\left(\rho_a \mu_m - \rho_m \mu_m\right) \quad (4.20)$$

Dividing both sides by the linear attenuation coefficient of the matrix ($U_m = \rho_m \mu_m$) and rearranging will yield

117

$$\frac{V_a}{V_m} = \frac{\left(\frac{dU}{U_m}\right)}{\left(\frac{\rho_a \mu_a}{\rho_m \mu_m}\right) - 1 - \left(\frac{dU}{U_m}\right)} \qquad (4.21)$$

Substituting this into equation 4.18 will give an equation giving the minimum analyte concentration visible in a CT scan.

$$C_a = \frac{\rho_a \left(\frac{dU}{U_m}\right)}{\left(\frac{\rho_a \mu_a}{\rho_m \mu_m}\right) - 1 - \left(\frac{dU}{U_m}\right)} \qquad (4.22)$$

This is identical to that obtained by Fryar and McCarthy [3].

4.2.3   Multi-Element Compounds.

The analyte considered, may form part of a compound (eg. Iodine in Potassium Iodide). Account must also be taken for the other elements of the compound. Here the matrix has a volume V_m and density ρ_m. A volume V_a of analyte, having density ρ_a, is added to this cylinder. The total volume is now given as $V_a + V_m$. The concentration of the analyte is now given by

$$C_a = \frac{\rho_a V_a}{V_a + V_m} \qquad (4.23)$$

Now, if the analyte can be divided into n basic elements, the concentration of each element is given by

$$C_1 = \frac{\rho_1 V_1}{V_m + \sum_{i=1}^{n} V_i} \ , \ \ C_2 = \frac{\rho_2 V_2}{V_m + \sum_{i=1}^{n} V_i} \ \ ....C_n = \frac{\rho_n V_n}{V_m + \sum_{i=1}^{n} V_i}$$

$$(4.24)$$

The change in the linear attenuation coefficient can be written as

$$\Delta U = U_{tot} - U_m \qquad (4.25)$$

where U_{tot} is the linear attenuation coefficient of the matrix plus analyte(s) and U_m is the linear attenuation coefficient of the matrix.

$$\Rightarrow \quad \Delta U = \left(\sum_{i=1}^{n} U_i + U_m\right) - U_m$$

118

$$= \sum_{i=1}^{n} U_i \tag{4.26}$$

However, the linear attenuation coefficient can be defined as $U = C.\mu$, where C is the element concentration and μ the mass attenuation coefficient.

$$\Rightarrow \quad \Delta U = \sum_{i=1}^{n} C_i \mu_i = \sum_{i=1}^{n} \frac{\rho_i V_i \mu_i}{V_t} \tag{4.27}$$

where $V_t = V_m + \sum_{i=1}^{n} V_i$. Dividing both sides by U_m gives

$$\frac{\Delta \mu}{U_m} = \sum_{i=1}^{n} \frac{\rho_i V_i \mu_i}{V_t (\rho_m \mu_m)} \tag{4.28}$$

However,

$$\rho_i V_i = M_i \tag{4.29}$$

where M_i is the mass of element i.

Substituting this equation for the concentration, equation 4.28 becomes

$$\frac{\Delta U}{U_m} = \sum_{i=1}^{n} \frac{M_i \mu_i}{V_t \rho_m \mu_m} \tag{4.30}$$

$$\Rightarrow \quad \sum_{i=1}^{n} M_i \mu_i = V_t \rho_m \mu_m \left(\frac{\Delta U}{U_m} \right) \tag{4.31}$$

Now, if the mass of the individual elements can be defined as $M_i = R_i M_t$, where M_t is the total mass of the compound and R_i are the relative masses of the elements, then

$$M_t = \frac{V_t \rho_m \mu_m \left(\dfrac{\Delta U}{U_m} \right)}{\sum_{i=1}^{n} R_i \mu_i} \tag{4.32}$$

Thus, the above equation will give the amount of the compound necessary to be diluted in a volume of the matrix (V_t) such that it is visible in a CT scan with the parameters set so as to obtain the value $\Delta U/U_m$ from equation 4.14.

4.2.4   The case where the analyte cannot be added to the matrix. (K-Edge Scanning).

In the case now to be studied, the analyte is already present in the matrix and thus two scans (one with and one without the analyte as in the first case) cannot be done. A different method for the detection of the analyte has to be used. That method used will be that differential absorptiometry, ie. K-edge jumping. In this method two scans are done, one on the high side of the K-absorption edge of the analyte and one on the low side. These two images are subtracted to yield an image of just the analyte because the attenuation coefficient of the matrix will vary only slightly across the K-edge if we work very close to the K-edge. The theoretical equation for the determination of the minimum concentration of analyte visible in a scan using this method will now be derived. Table 4.2 shows the commonly used symbols pertaining to this section not already given in table 4.1.

N_l = Number of photons on the low side of the K-edge emerging from a complete scan.
N_h = Number of photons on the high side of the K-edge.
U_{ml} = Linear attenuation coefficient (LAC) of the matrix on the low-side of the K-edge.
U_{mh} = LAC of the matrix on the high-side of the K-edge.
U_{al} = LAC of the analyte on the low-side of the K-edge.
U_{ah} = LAC of the analyte on the high-side of the K-edge.
U_{cl} = LAC of the compound on the low side, ie. combination of analyte and matrix.
U_{ch} = LAC of the compound on the high side of the K-edge.
X_{ml} = Number of mean free paths through the matrix on the low-side.
X_{mh} = Number of mean free paths through the matrix on the high-side.
μ_{al} = Mass attenuation coefficient (MAC) of the analyte on the low-side.
μ_{ah} = MAC of the analyte on the high-side.
μ_{ml} = MAC of the matrix on the low-side.
μ_{mh} = MAC of the matrix on the high-side.
C_a = Concentration of the analyte.

Table 4.2 showing symbol definitions.

Two beams are passed through the object, one on the low side and the other just to high side of the K

120

absorption edge of the analyte. The number of photons emerging from the object at these energies are given by the following equations.

$$N_l = N_o \exp\left[-2.U_{ml}.\left(R^2 - (s-0.5)^2.(\Delta x)^2\right)^{1/2}\right]_{s>r}$$

$$N_o \exp\left[-2.U_{ml}\left(R^2 - (s-0.5)^2(\Delta x)^2\right)^{1/2} + \right.$$

$$2.U_{ml}\left(r^2 - (s-0.5)^2(\Delta x)^2\right)^{1/2} -$$

$$\left. 2.U_{cl}\left(r^2 - (s-0.5)^2.(\Delta x)^2\right)^{1/2}\right]_{s\leq r} \qquad (4.33)$$

$$N_h = N_o \exp\left[-2.U_{mh}.\left(R^2 - (s-0.5)^2.(\Delta x)^2\right)^{1/2}\right]_{s>r}$$

$$N_o \exp\left[-2.U_{mh}\left(R^2 - (s-0.5)^2(\Delta x)^2\right)^{1/2} + \right.$$

$$2.U_{mh}\left(r^2 - (s-0.5)^2(\Delta x)^2\right)^{1/2} -$$

$$\left. 2.U_{ch}\left(r^2 - (s-0.5)^2.(\Delta x)^2\right)^{1/2}\right]_{s\leq r} \qquad (4.34)$$

where U_{ml}, U_{mh}, U_{cl} and U_{ch} and the linear attenuation coefficients of the matrix and compound (ie. analyte and matrix) at the low and high energy sides of the K-edge. The radius of the internal cylinder is given by r and R is the radius of the outer cylinder. The step size is Δx and N_o is the number of photons incident on the object per beam.

Now knowing that $\Delta x = D/S = (2.R)/S$, $r = f.R$ and $R = (X_{ml}.L_{ml})/2$ and substituting into the above equations, we get the following;

$$N_l = N_{ol} \exp\left[-X_{ml}.\left(1 - \frac{4.(s-0.5)^2}{s^2}\right)^{1/2}\right]_{s>r}$$

$$N_{ol} \exp\left[-X_{ml}.\left(1 - \frac{4.(s-0.5)^2}{s^2}\right)^{1/2} + \right.$$

121

$$\left(X_{ml} - \frac{X_{ml} \cdot U_{cl}}{U_{ml}}\right)\left(f^2 - \frac{4 \cdot (s-0.5)^2}{s^2}\right)^{1/2}\Bigg]_{s \leq r}$$

$$(4.35)$$

$$N_h = N_{oh} \exp\left[-X_{mh} \cdot \left(1 - \frac{4 \cdot (s-0.5)^2}{s^2}\right)^{1/2}\right]_{s > r}$$

$$N_{oh} \exp\left[-X_{mh} \cdot \left(1 - \frac{4 \cdot (s-0.5)^2}{s^2}\right)^{1/2} +\right.$$

$$\left(X_{mh} - \frac{X_{mh} \cdot U_{ch}}{U_{mh}}\right)\left(f^2 - \frac{4 \cdot (s-0.5)^2}{s^2}\right)^{1/2}\Bigg]_{s \leq r}$$

$$(4.36)$$

U_{cl} and U_{ch} refer to the linear attenuation coefficients of the compound contained in the centre cylinder. This compound is in fact a combination of two attenuation coefficients, that of the matrix and that of the contrast agent, as both form a mixture which constitutes the centre cylinder analyte. We can add the mass attenuation coefficients of two elements using the following formula;

$$\mu_c = W_a \mu_a + W_m \mu_m \qquad\qquad (4.37)$$

where W_c and W_m are the weight fractions of the contrast agent and matrix respectively.

$$\Rightarrow \qquad U_c = \rho \cdot \mu_c = \rho\,(W_a \mu_a + W_m \mu_m) \qquad (4.38)$$

where ρ = density of the combination. When the concentration of the contrast agent is low then ρ is in effect the density of the matrix.

$$\Rightarrow \qquad U_{cl} = C_a \mu_{al} + \rho_m \mu_{ml} \qquad\qquad (4.39)$$

$$\Rightarrow \qquad \frac{U_{cl}}{U_{ml}} = \frac{C_a \mu_{al}}{\rho \cdot \mu_{ml}} + 1 \qquad\qquad (4.40)$$

Substituting equation 4.40 into equation 4.35 and the corresponding equation into 4.36

$$N_l = N_{ol} \exp\left[-X_{ml} \cdot \left(1 - \frac{4 \cdot (s-0.5)^2}{s^2}\right)^{1/2}\right]_{s > r}$$

$$N_{ol} \exp\left[-X_{ml} \cdot \left(1 - \frac{4 \cdot (s-0.5)^2}{s^2}\right)^{1/2} -\right.$$

122

$$\left(\frac{X_{ml}.C_a.\mu_{al}}{\rho_m.\mu_{ml}}\right)\left(f^2 - \frac{4.(s-0.5)^2}{s^2}\right)^{1/2}\Bigg]_{s\leq r}$$

$$(4.41)$$

$$N_h = N_{oh}\exp\left[-X_{mh}.\left(1 - \frac{4.(s-0.5)^2}{s^2}\right)^{1/2}\right]_{s>r}$$

$$N_{oh}\exp\left[-X_{mh}.\left(1 - \frac{4.(s-0.5)^2}{s^2}\right)^{1/2} - \right.$$

$$\left(\frac{X_{mh}.C_a.\mu_{ah}}{\rho_m.\mu_{mh}}\right)\left(f^2 - \frac{4.(s-0.5)^2}{s^2}\right)^{1/2}\Bigg]_{s\leq r}$$

$$(4.42)$$

If these two quantities are subtracted, then the following expression will yield the number of transmitted photons resulting from this subtraction.

$$N_l - N_h = N_{ol}\exp\left[-X_{ml}\left\{1 - \frac{4.(s-0.5)^2}{s^2}\right\}^{1/2} - \right.$$

$$\left(\frac{X_{ml}C_a\mu_{al}}{\rho_m.\mu_{ml}}\right)\left\{f^2 - \frac{4.(s-0.5)^2}{s^2}\right\}^{1/2}\Bigg]_{s\leq r}$$

$$- N_{oh}\exp\left[-X_{mh}\left\{1 - \frac{4.(s-0.5)^2}{s^2}\right\}^{1/2} - \right.$$

$$\left(\frac{X_{mh}C_a\mu_{ah}}{\rho_m.\mu_{mh}}\right)\left\{f^2 - \frac{4.(s-0.5)^2}{s^2}\right\}^{1/2}\Bigg]_{s\leq r}$$

$$(4.43)$$

At or near the K-edge, $X_{ml} \cong X_{mh}$, therefore the terms giving the number of photons when s>r are equal and cancel each other. Following similar arguments to those given in section 4.2.1 a visibility criterion is arrived at given by

$$\frac{N_l - N_h}{f.S} \geq B.D.\left(\frac{N_l}{fS}\right)^{1/2} \qquad (4.44)$$

$$\Rightarrow \qquad N_l - N_h \geq B.D.(f.N_l.S)^{1/2} \qquad (4.45)$$

123

It is assumed that for low values of concentration that $N_l \cong N_h$. Using N_h in the square root sign will have the effect of making the equations slightly more sensitive. Substituting equations 4.41 and 4.43 into this equation and accounting for the complete scan gives;

$$\sum_{s=1}^{r} 2.N_{ol}.M.\exp\left[- X_{ml}\left(1 - \frac{4.(s-0.5)^2}{s^2}\right)^{1/2} - \left(\frac{X_{ml}.C_a.\mu_{al}}{\rho_m.\mu_{ml}}\right)\left(f^2 - \frac{4.(s-0.5)^2}{s^2}\right)^{1/2}\right]$$

$$- \sum_{s=1}^{r} 2.N_{oh}.M.\exp\left[- X_{mh}\left(1 - \frac{4.(s-0.5)^2}{s^2}\right)^{1/2} - \left(\frac{X_{mh}.C_a.\mu_{ah}}{\rho_m.\mu_{mh}}\right)\left(f^2 - \frac{4.(s-0.5)^2}{s^2}\right)^{1/2}\right]$$

$$\geq B.D.(S.f)^{1/2}.\left\{ \sum_{s=1}^{r} 2.N_{ol}.M.\exp\left[- X_{ml}\left(1 - \frac{4.(s-0.5)^2}{s^2}\right)^{1/2} - \left(\frac{X_{ml}.C_a.\mu_{al}}{\rho_m.\mu_{ml}}\right)\left(f^2 - \frac{4.(s-0.5)^2}{s^2}\right)^{1/2}\right]\right\}^{1/2}$$

$$(4.46)$$

The above equation is valid for a complete scan of S steps and M rotations. When scanning at or close to the K-edge, $N_{ol} \cong N_{oh}$ and knowing that $N_{ot} = S.M.N_{ol} = S.M.N_{oh}$, then dividing both sides by N_{ot} gives

$$\sum_{s=1}^{r} \frac{2}{S} \exp\left[- X_{ml}\left(1 - \frac{4.(s-0.5)^2}{s^2}\right)^{1/2} - \left(\frac{X_{ml}.C_a.\mu_{al}}{\rho_m.\mu_{ml}}\right)\left(f^2 - \frac{4.(s-0.5)^2}{s^2}\right)^{1/2}\right]$$

$$- \sum_{s=1}^{r} \frac{2}{S} \exp\left[- X_{mh}\left(1 - \frac{4.(s-0.5)^2}{s^2}\right)^{1/2} - \left(\frac{X_{mh}.C_a.\mu_{ah}}{\rho_m.\mu_{mh}}\right)\left(f^2 - \frac{4.(s-0.5)^2}{s^2}\right)^{1/2}\right]$$

124

$$\geq \frac{B.D.(f.S)^{1/2}}{N_{ot}^{1/2}} \cdot \left\{ \sum_{s=1}^{r} \frac{2}{S} \exp\left[-X_{ml}\left(1 - \frac{4.(s-0.5)^2}{S^2}\right)^{1/2} \right. \right.$$

$$\left. \left. - \left(\frac{X_{ml}.C_a.\mu_{al}}{\rho_m.\mu_{ml}}\right)\left(f^2 - \frac{4.(s-0.5)^2}{S^2}\right)^{1/2} \right] \right\}^{1/2}$$

<div align="right">(4.47)</div>

Here, $N_{ot} = N_{ol}.S.M$, ie. the total number of incident photons, and S is taken as equal to M which is applicable to the work presented in this thesis. Unlike the case described in section 4.2.1, the above equations will yield a value of C_a, the analyte concentration, directly that will solve this equality.

The above equation assumes that the measurements were carried out at the K-edge. However, this cannot be performed in practice, therefore two energy bands on either side of the K-edge were used and the results extrapolated to the K-edge. This introduces an extra error into the total detected photon count on both sides of the absorption edge as discussed by Fryar and McCarthy [2]. When this error is taken into account it results in a multiplication factor G to be included to the right hand side of the equation. At or close to the K-edge $X_{ml} \cong X_{mh} = X_m$ and $\mu_{ml} \cong \mu_{mh} = \mu_m$, then the above equations become;

$$\sum_{s=1}^{r} \frac{2}{S} \exp\left[-X_m\left(1 - \frac{4.(s-0.5)^2}{S^2}\right)^{1/2} - \right.$$

$$\left. \left(\frac{X_m.C_a.\mu_{al}}{\rho_m.\mu_m}\right)\left(f^2 - \frac{4.(s-0.5)^2}{S^2}\right)^{1/2} \right]$$

$$- \sum_{s=1}^{r} \frac{2}{S} \exp\left[-X_m\left(1 - \frac{4.(s-0.5)^2}{S^2}\right)^{1/2} - \right.$$

$$\left. \left(\frac{X_m.C_a.\mu_{ah}}{\rho_m.\mu_m}\right)\left(f^2 - \frac{4.(s-0.5)^2}{S^2}\right)^{1/2} \right]$$

$$= \frac{G.B.D.(S.f)^{1/2}}{N_{ot}^{1/2}} \left\{ \sum_{s=1}^{r} \exp\left[-X_m\left(1 - \frac{4.(s-0.5)^2}{S^2}\right)^{1/2} \right. \right.$$

$$- \left(\frac{X_m \cdot C_a \cdot \mu_{al}}{\rho_m \cdot \mu_m}\right) \left(f^2 - \frac{4 \cdot (s-0.5)^2}{s^2}\right)^{1/2} \left.\right]^{1/2} \right\}$$

(4.48)

Fryar and McCarthy found that this factor G was approximately 3, which states that the standard deviation in the extrapolated value is approximately three times the standard deviation in the counts in the band closest to the absorption edge.

4.2.5   Theoretical Results:

Both equations 4.14 (the monochromatic case) and 4.48 (the K-edge case) are of similar form and as such difficult to solve algebraically. The methods of finding dU/U or Ca that solved these equations was identical. An initial value of the dependent variable was assumed and each side of the equation was calculated. The value of the dependent variable was determined using the bisection method for finding roots.

Figure 4.02 is a three-dimensional graph showing the minimum detectable fractional difference in the linear attenuation coefficient as a function of X, the number of mean free paths through the matrix, and f, the ratio of the inner to the outer cylinder diameters. The results are for S=240 projections/steps and N_{ot}=1E10 incident photons. Figure 4.03 is equivalent to figure 4.02 except that the natural logarithm of the data is taken. It is obvious from figure 4.02 that dU/U as a function of X is similar to that achieved by Fryar and McCarthy [3]. Figure 4.04 is again a three-dimensional graph but this time showing the minimum detectable concentration as a function of X and f for the case of the K-edge scanning technique. Iodine was used as the analyte, contained in a water matrix. Here S=200 steps and N=1E11 incident photons. Figure 4.05 is the logged data of figure 4.04. Figure 4.06 and 4.07 are equivalent to figures 4.04 and 4.05 except that Gadolinium in a soft tissue matrix is now studied. The programs to calculate these values for both the monochromatic and K-edge cases are shown on pages 76 to 80 of appendix 1.

The monochromatic case and the K-edge case both follow the same dependence on S, the number of steps, and N_{ot}, the total number of incident photons, ie. the results scale as $\sqrt{S}$ and $1/\sqrt{N_{ot}}$. This S dependence holds true for S > 30 as the summation factors of the equations containing the S terms are independent of S above this value for the purposes of the work presented here. Figure
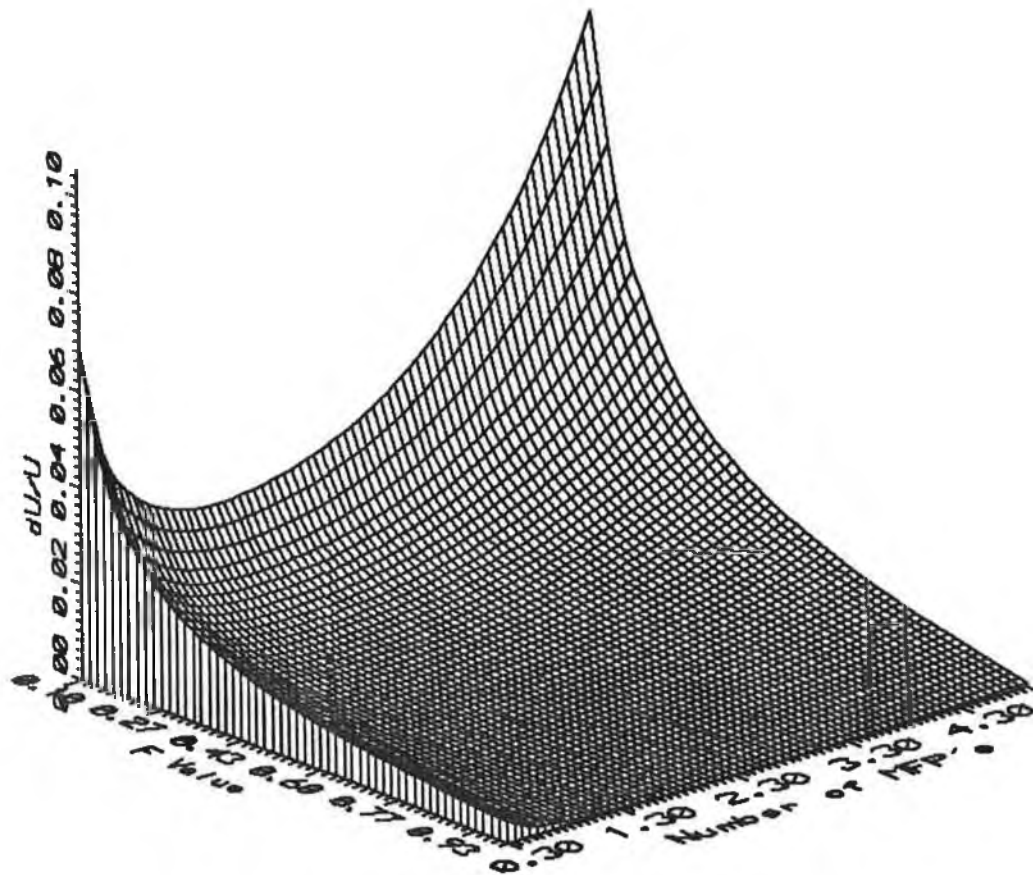
Figure 4.02: Three dimensional graph of dU/U vs. X vs. f for the monochromatic case. S = 240, N$_{ot}$ = 1E10.
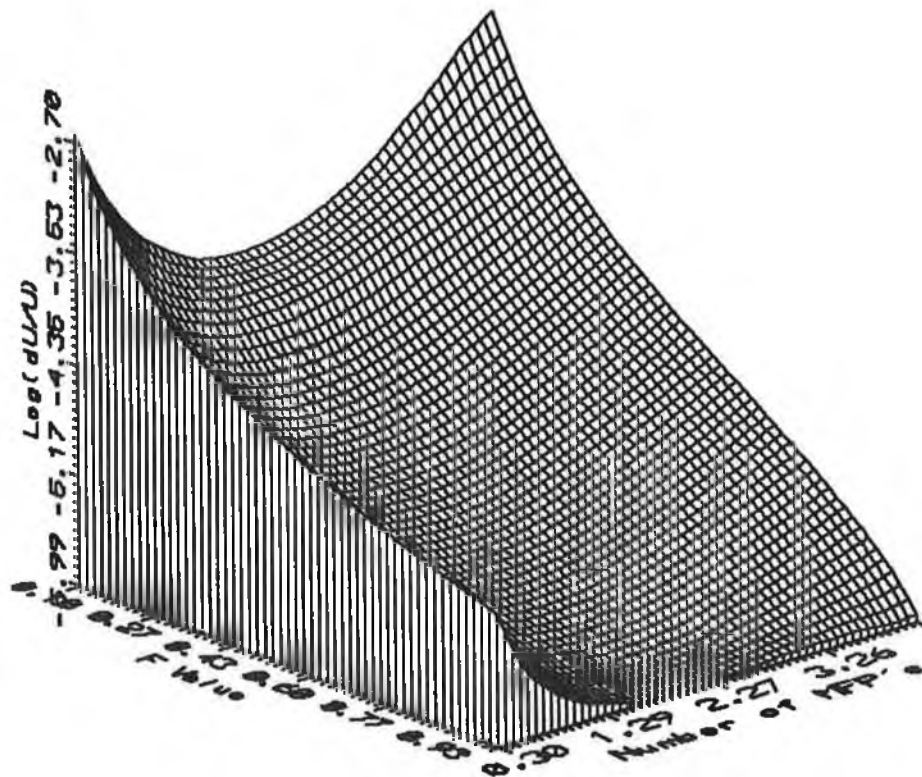
Figure 4.03: As figure 4.02 except the natural logarithm of the data taken.
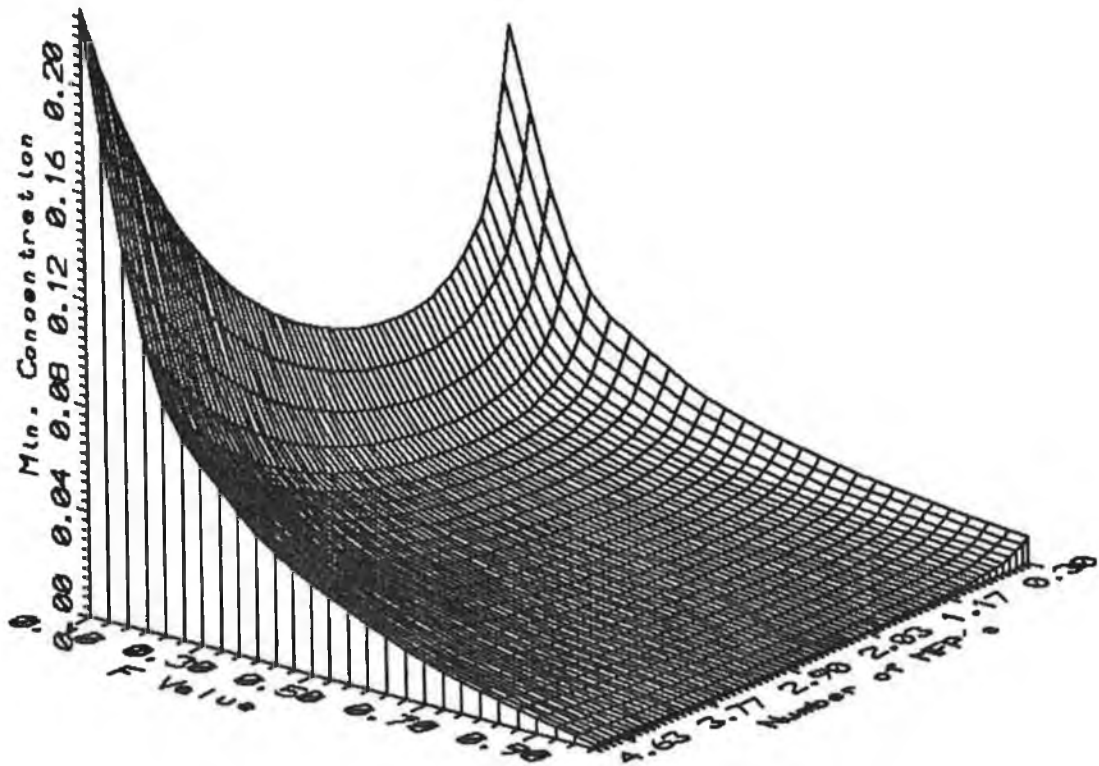
Figure 4.04: Graph of Ca vs. f vs. X for the K-edge case. Iodine in a water matrix, S = 200 and N_{ot} = 1E11.
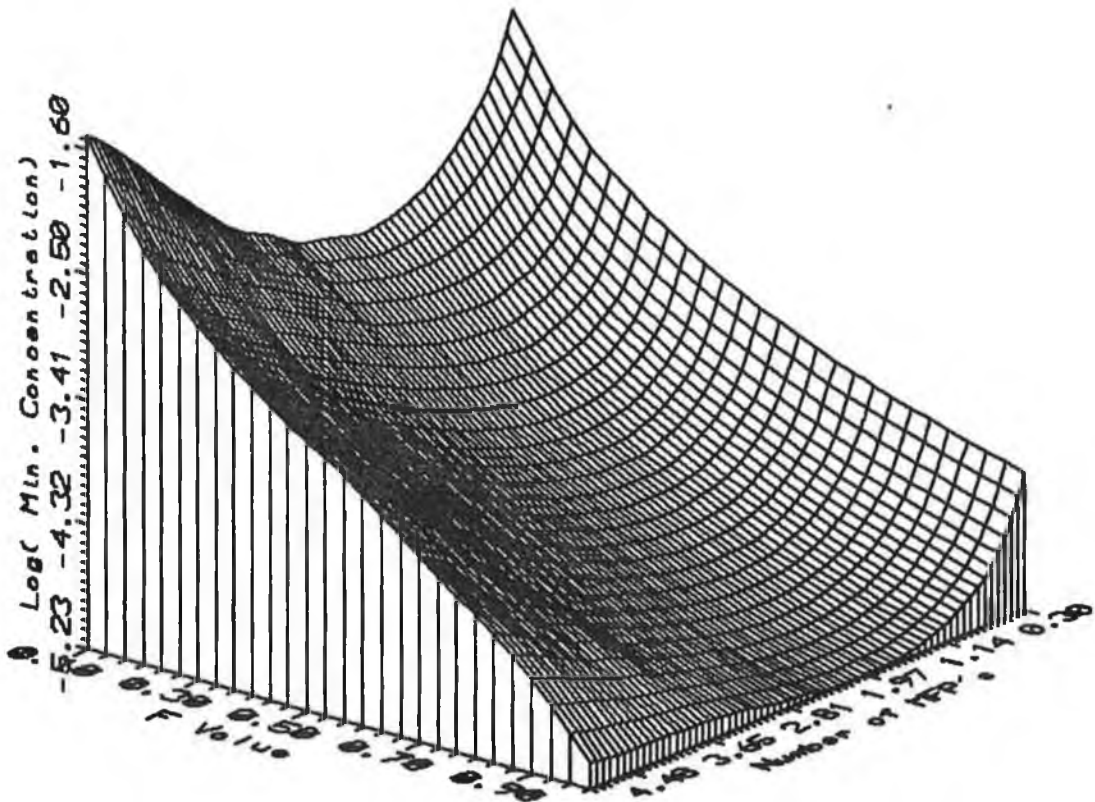
Figure 4.05: As figure 4.03 except natural logarithm of the data taken.
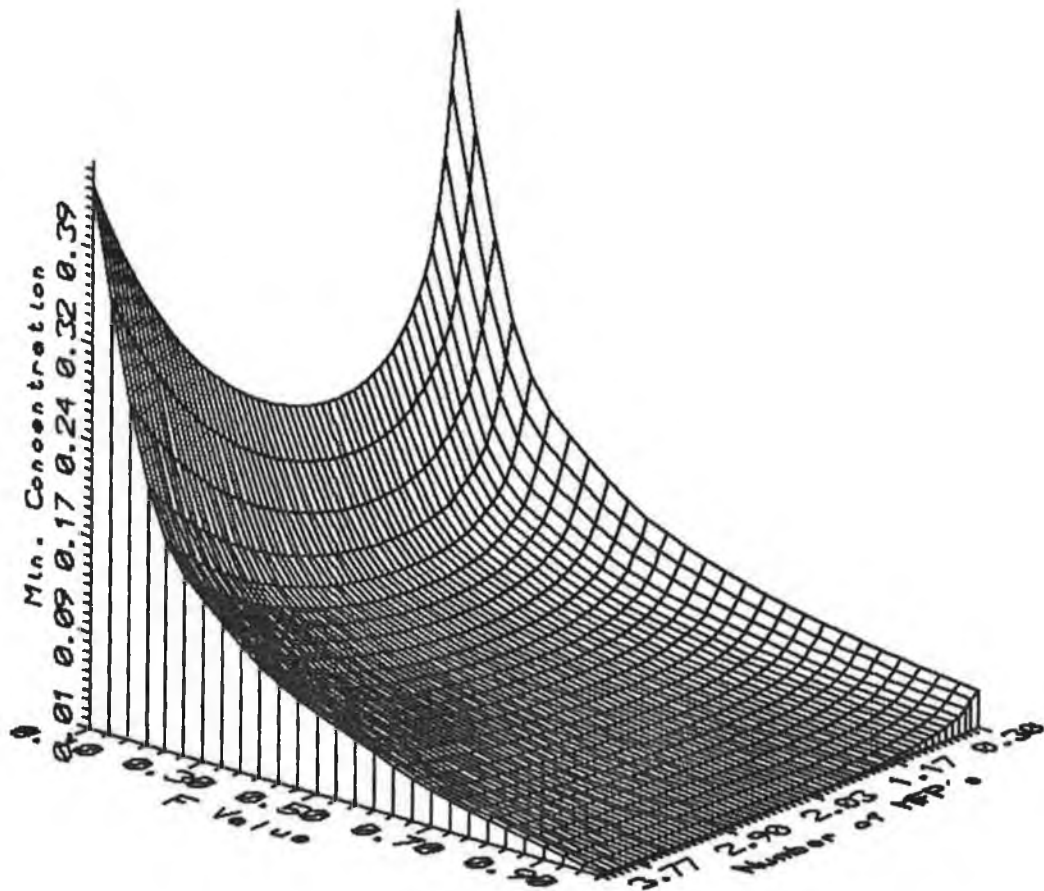
Figure 4.06: Graph of Ca vs. X vs. f for the K-edge case. Gadolinium in a tissue matrix. S = 100, N_{ot} = 1E10.
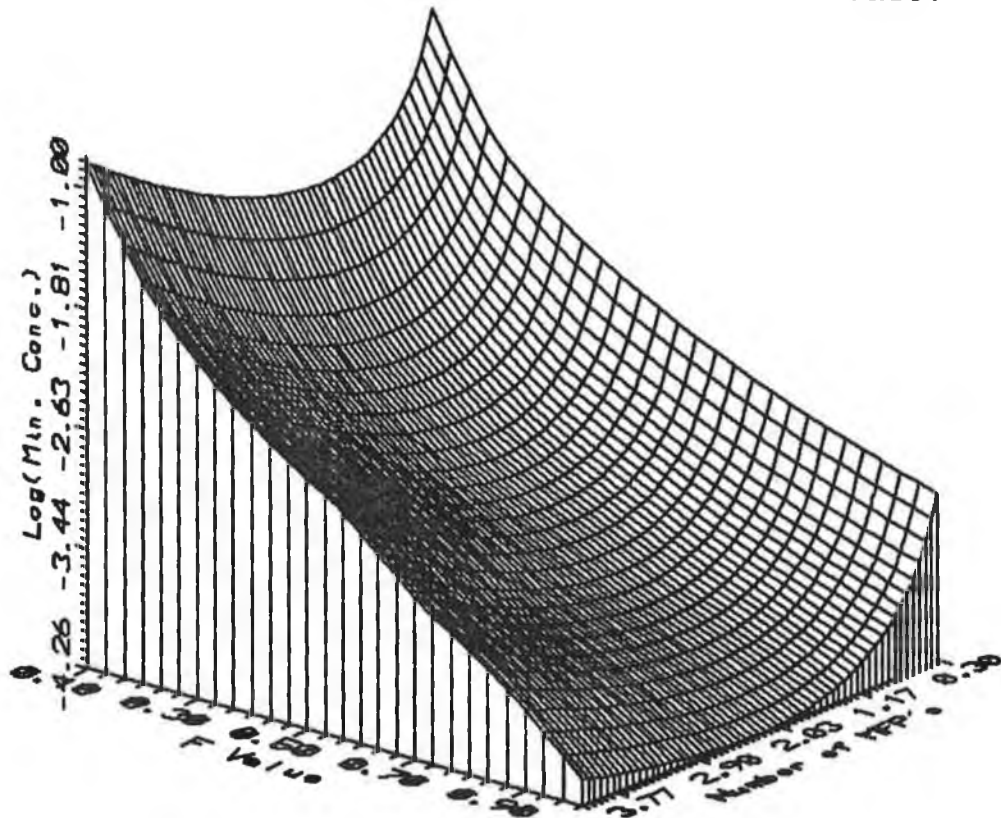
Figure 4.07: As figure 4.06 except that the natural logarithm of the data was taken.

4.08 and 4.09 show how the dU/U varies with S and N$_{ot}$ respectively. Figure 4.10 shows the variation of concentration with S at f = 0.1. A stepping pattern is evident particularly at low values of S. This is due to the number of steps contained in the inner cylinder not changing at low values of f as the number of steps in the scan increases, ie. integer value of 0.1 X 30 (f X S) = integer value of 0.1 X 38.
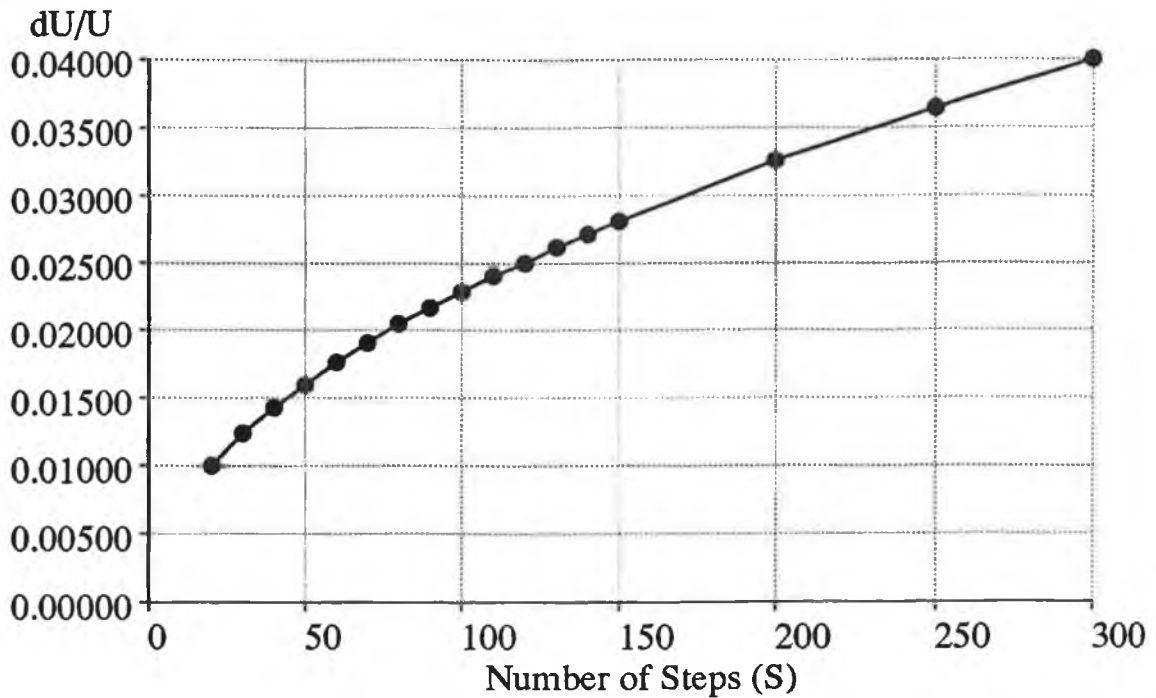
Figure 4.08
Graph showing the variation of dU/U as a function of the number of steps (S) in the scan. The above data is for f=0.8, X=2.5 and N$_{ot}$ = 1E8 incident photons. These results are for the monochromatic case.

The question that this chapter set out to answer, namely is gadolinium the optimum element to use as a contrast agent regardless of the size of the organ into which it was administered, is answered in figures 4.11 and 4.12 for the two scanning modalities utilised. These graphs show the minimum detectable concentration of analyte as a function of atomic number for selected elements ranging from tin to lead. In the K-edge case, the scans are performed just above and below the K absorption edge and in the monochromatic case the scans are performed just to the high side of the K-edge.
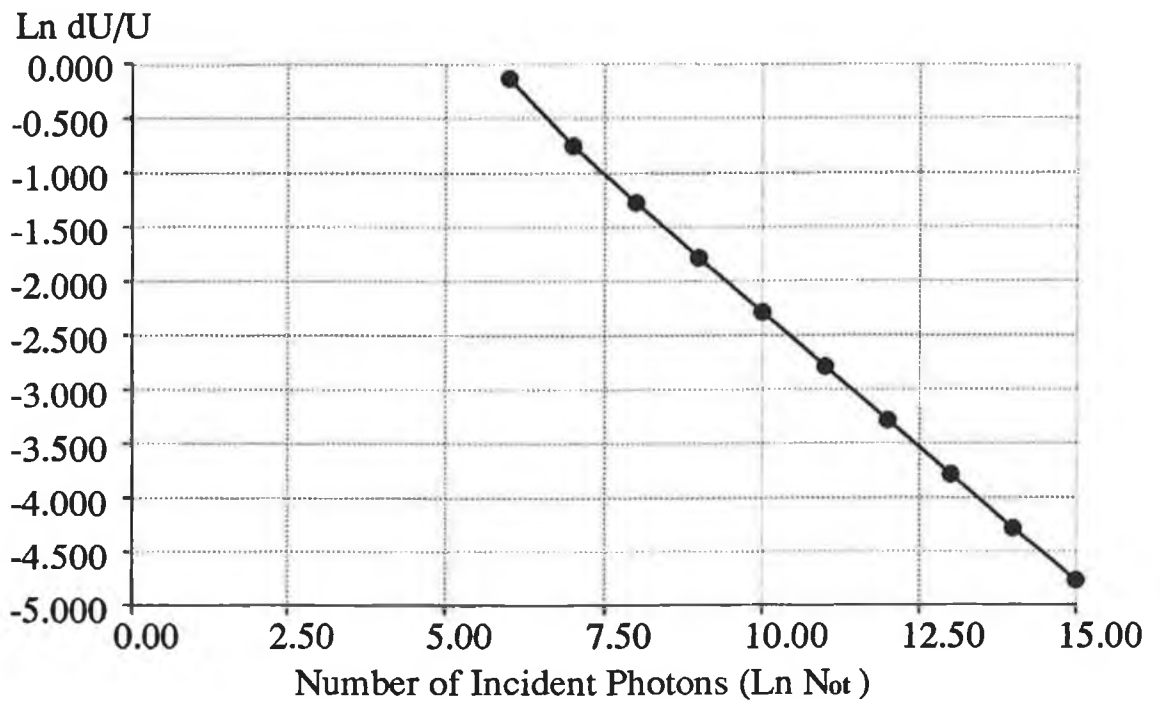
Figure 4.09
**Graph of the log of the number of incident photons vs. the log of the
minimum detectable fractional difference in linear attenuation
coefficient. S=100, f=0.5 and x=2.5. Monochromatic case.**
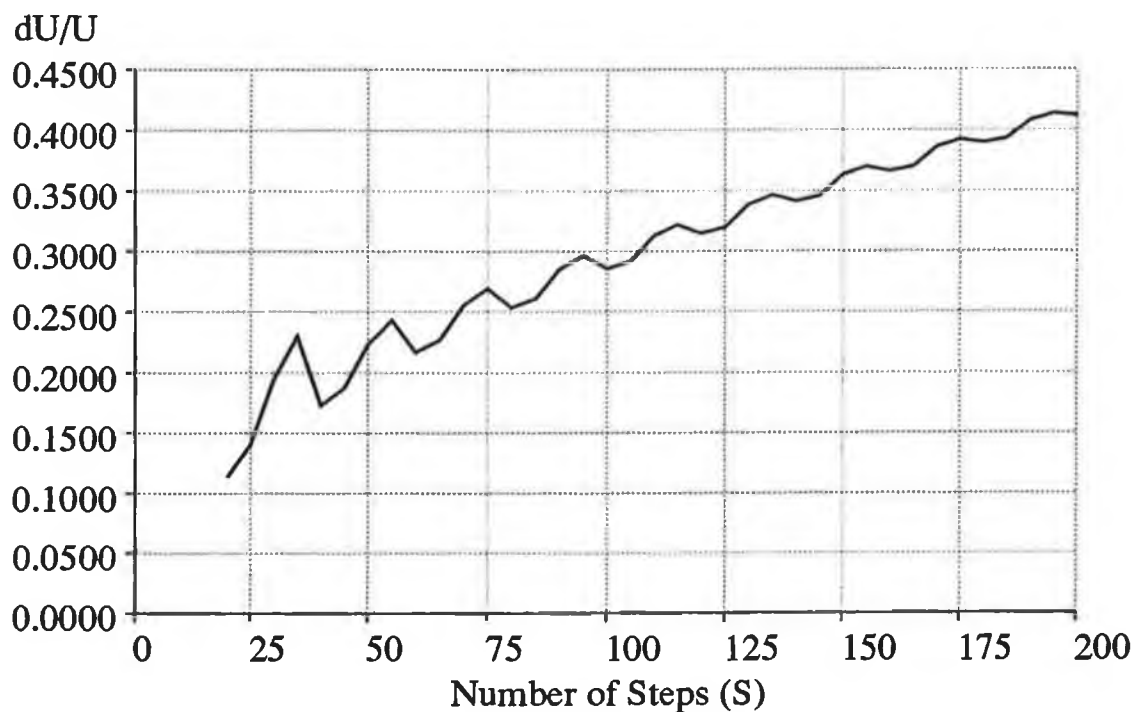
Figure 4.10
**Graph showing the quantisation effect of f on the value dU/U
for increasing number of steps (S). The above results are for
f=0.1, x (number of mfp's) = 2.5 and N_{ot} = 1E8 photons.
These results are for the monochromatic case.**

Minimum Concentration (mg/cc) — Atomic Number (Z) **(a)**

Minimum Concentration (mg/cc) — Atomic Number (Z) **(b)**

Minimum Concentration (mg/cc) — Atomic Number (Z) **(c)**
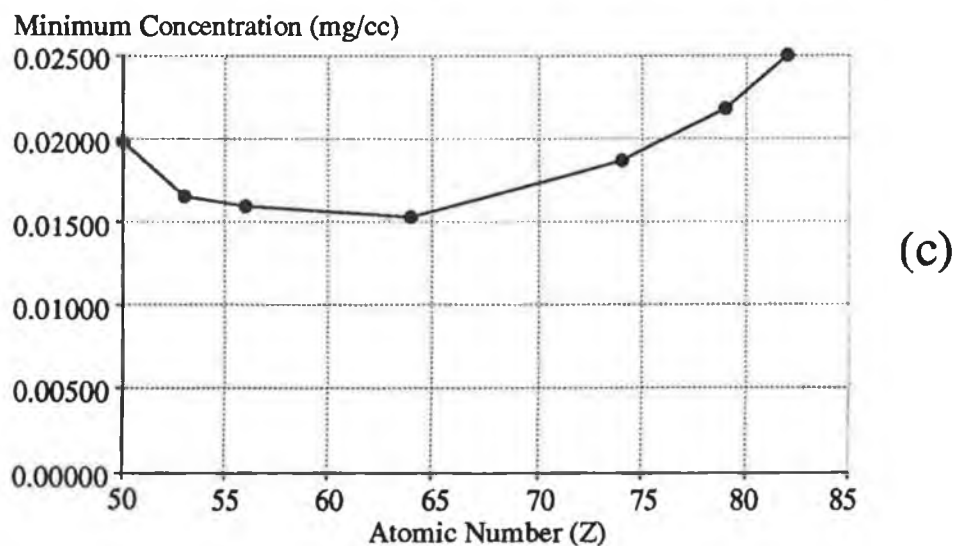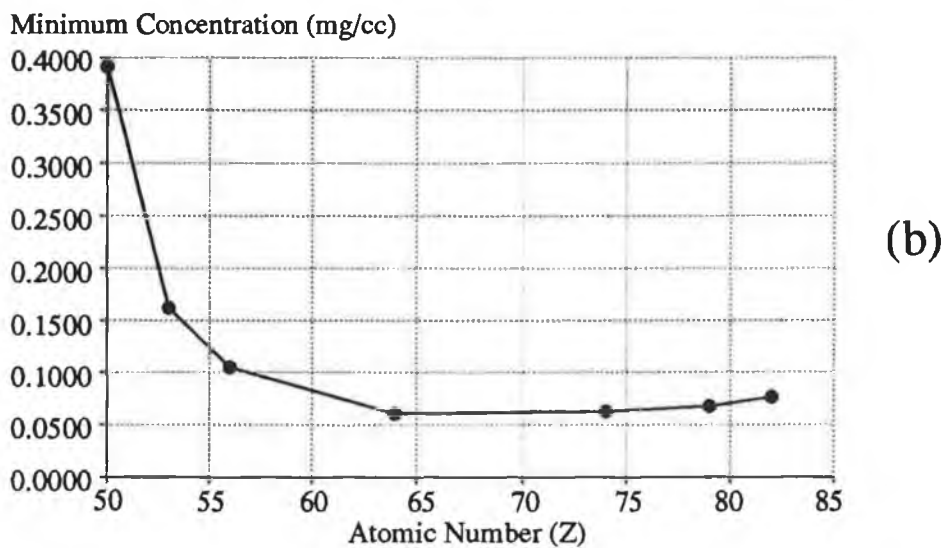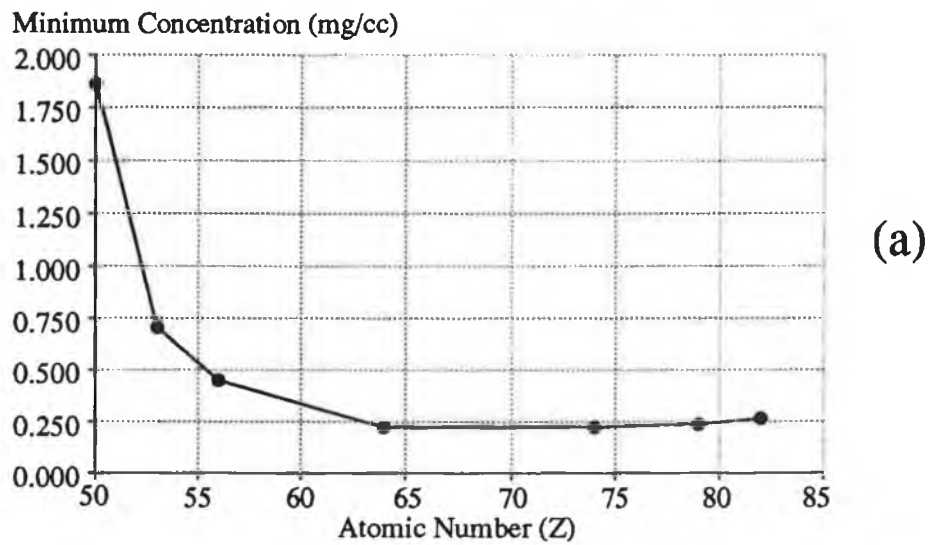
Figure 4.11
Three graphs showing the variation of the minimum detectable concentration as a function of atomic number (Z) for three cases: (a) f=0.2, (b) f=0.6 and (c) f=1.0. In all cases S = 50, N_{ot} = 1E9. These results are for the monochromatic case.
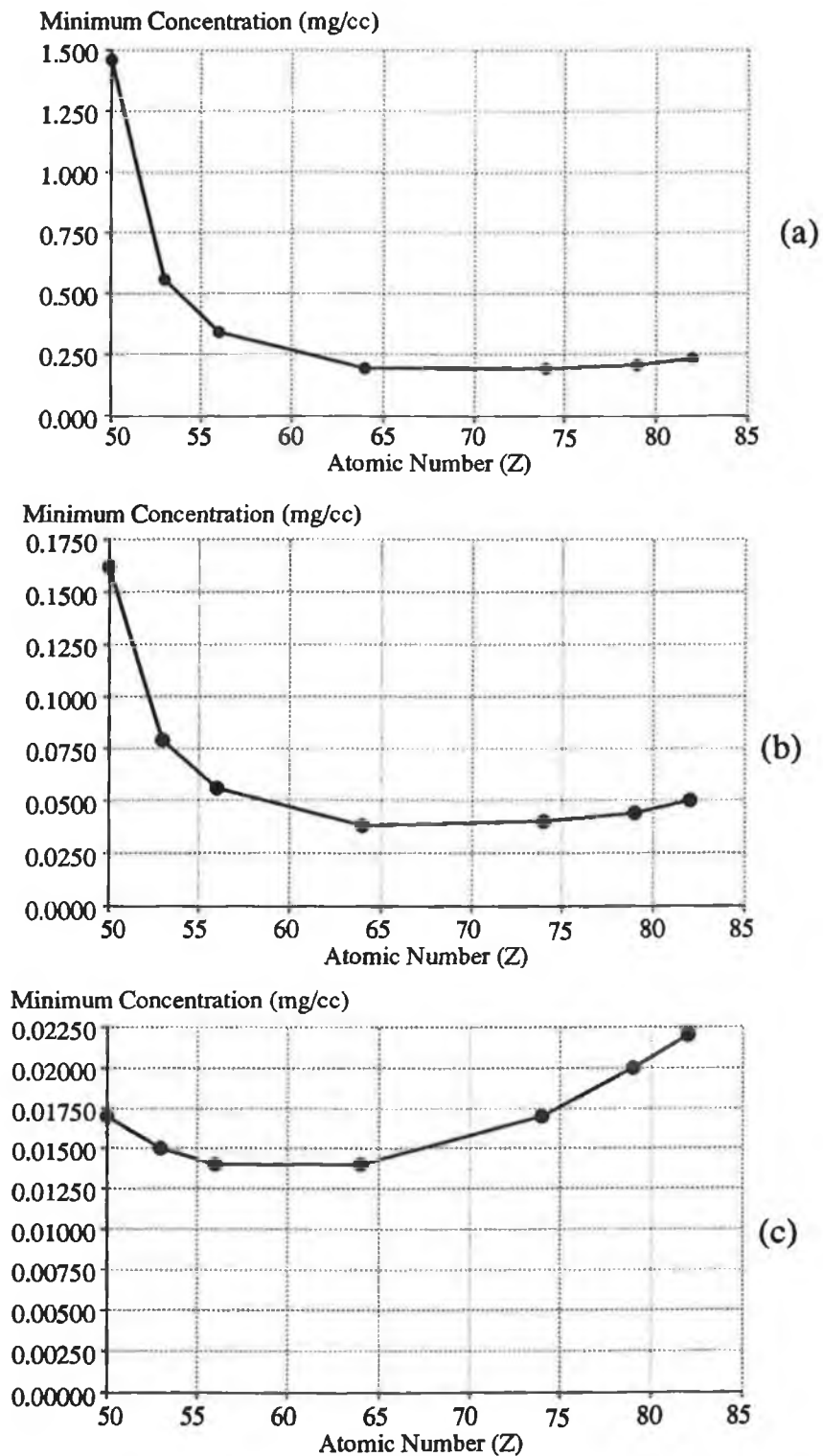
Figure 4.12
Three graphs showing the variation of the minimum detectable concentration as a function of atomic number (Z) for three cases; (a) f=0.2, (b) f=0.7 and (c) f=1.0. In all cases S=50, N_{ot} = 1E10. This is using the technique of K-edge imaging.

Both figures show that for medium to high values of f, gadolinium is the optimum element to use. However, at low values of f (eg. ≤ 0.2) there is a slight shift of the optimum element to higher atomic number elements. For f=0.2, in both graphs, the minimum concentration occurs somewhere in the range M = 64 to M = 74. Unfortunately mass attenuation coefficients data were not available for the elements between these values (ie. the rare-earth elements) so as to determine which of these elements is the optimum.

It must also be stated that at low values of f, the difference in minimum concentration between Iodine and Gadolinium is now a factor of approximately 3 in favor of Gadolinium. This compares to a difference of only approximately 1.1 at f = 1.0. This makes the case for using Gadolinium as a radiographic contrast medium, in preference to Iodine, stronger when scans are performed of small organs.

One means of testing these equations is the comparison of the results obtained at the limiting case of f=1.0 (ie. the inner diameter equals the outer diameter) with the results obtained from the equations derived by Fryar and McCarthy. Listed below are the results for three different cases for both scanning modalities. The results are obtained from eqns. 4.14 and 4.48. The results for the specific case (ie.f=1.0) derived by Fryar and McCarthy are given by eqn. 7 of [2] and 9 of [3].

Monochromatic Case:	General Eqn. (dU/U)	Specific Eqn. (dU/U)
1) S=100, N_{ot}=1E11, X=1.9	0.00031	0.00030
2) S=50, N_{ot}=1E7, X=2.5	0.021	0.021
3) S=250, N_{ot}=1E10, X=1.0	0.00191	0.00195

K-Edge Case:	General Eqn. (mg/cc)	Specific Eqn. (mg/cc)
1) S=250, N_{ot}=1E10, X=1.0		
μ_m=0.035, μ_{ah}=1.9, μ_{al}=0.4	0.135	0.137
2) S=100, N_{ot}=1E11, X=2.0		
μ_m=0.042, μ_{ah}=3.69, μ_{al}=.63	0.014	0.013
3) S=50, N_{ot}=1E8, X=4.0		
μ_m0.055, μ_{ah}=2.89, μ_{al}=.52	0.55	0.52

It is obvious from the above results that there is good agreement between the two sets of results. The slight discrepancy could be due to the curve fitting approximations used extensively by Fryar and McCarthy [2].

4.3.1   Introduction.

The results shown in section 4.2.5 give a feel for the variation of the minimum concentration as a function of the number of mean free paths, the ratio of the radii, the number of projections, etc. To verify a large portion of these results experimentally would be impractical due to the time required to perform scans. Therefore it was decided to check these results using computer simulations which are relatively much faster than the experimental scans to perform. The simulation results should then give a better value for the number of standard deviations needed for visibility times the reconstruction noise factor. The value for this product was initially chosen at 6 (ie. 3 (no. of standard deviations) X 2 (reconstruction noise factor)). However this value is dependent on the particular reconstruction algorithm used and the display techniques.

4.3.2   Visibility Parameter.

When performing computer simulations to determine the minimum concentration that is visible in a particular situation, it is preferable to have as little operator involvement as possible. Therefore some parameter is needed that determines whether or not an image is visible. This is the basis of the visibility parameter described in chapter 3. A similar parameter was investigated for the situation described in this chapter. However, because the object size was changing in certain situations (ie. minimum concentration as a function of f), the parameter needed to be reformulated. This proved to be difficult to achieve because image visibility depends on several factors;

1) Size of the scan, ie. the total number of pixels in the entire image.

2) Size of the object. It is easier to see a

large contrast enhanced area against a noisy background then an object of similar dimensions to the noisy clusters.

3) The noise in the background.

4) The percentage of pixels in the object area that are above the background mean.

5) Whether a gray scale or colour scale is used and how many levels are contained in either.

6) Whether any image processing has been performed on the image, eg. smoothing, level selection, etc.

No parameter could be easily found that accounts for these factors. It was therefore necessary to manually check whether an image was visible. This was performed as follows. A large range of images were generated and from visual inspection the minimum concentration that yielded a visible image was selected. Although this method is valid and yielded acceptable results, it is more susceptible to noise than the parameter method, ie. it is easier to see the object when what your looking for is known.

4.3.3   Number of Incident Photons Scaling.

It is obvious from equations 4.14 and 4.48 that the minimum concentration in both cases varies as $(1/N_{ot})^{1/2}$, where N_{ot} is the total number of incident photons for an entire scan. This dependence is shown in figure 4.09 for the monochromatic case and the results of simulations to check this dependence is shown in figure 4.13. The theoretical results are given for comparison. Excellent agreement exists confirming the scaling. Knowledge of this scaling is necessary since accumulation of 1E13 incident photons experimentally would be prohibitively long.

4.3.4   Number of Projections Scaling.

It has been shown previously that for the two cases the minimum concentration scales as the square root of the number of projections. Simulations were performed to investigate this property because to run simulations at
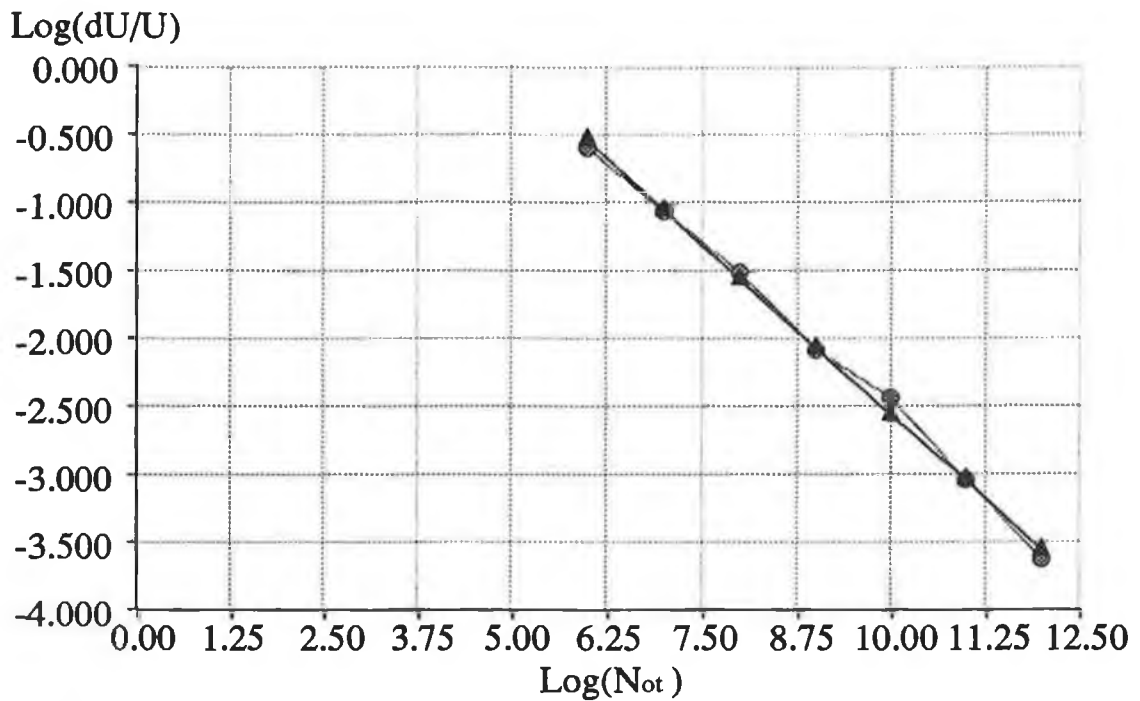
Figure 4.13
Graph showing the comparison between theoretical and simulated results for dU/U as a function of N_{ot}, the number of incident photons. ▲ = theoretical results and ◉ = simulated results. S=40, f=0.5 and X=2.5
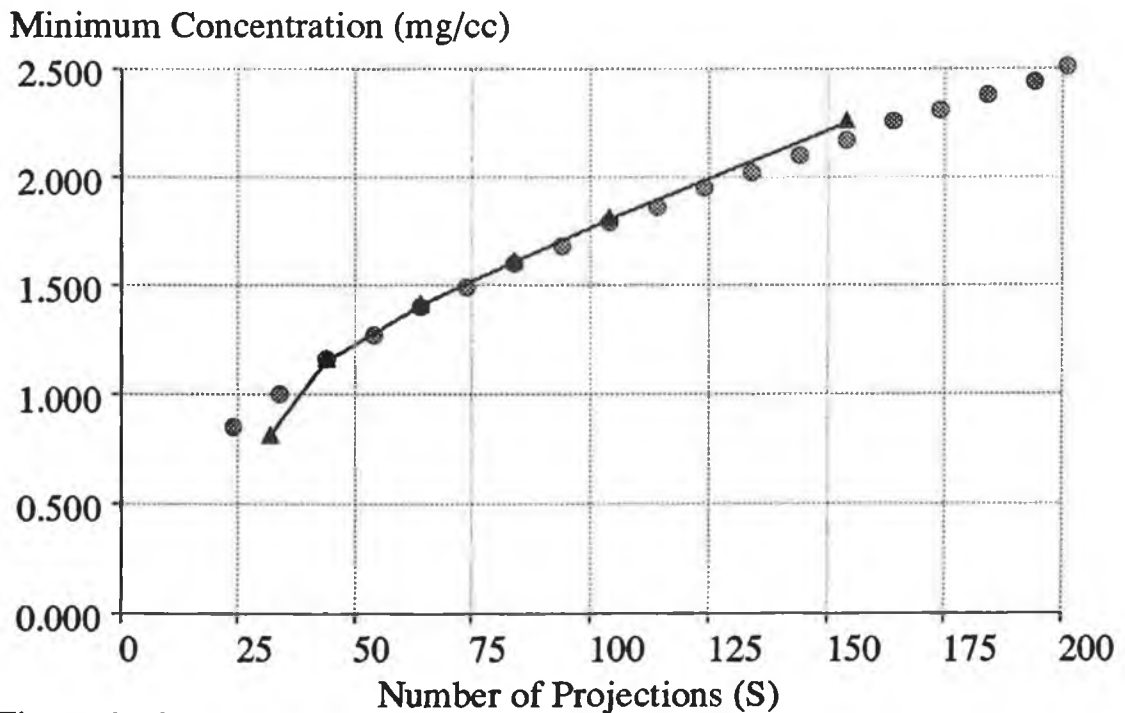
Figure 4.14
Graph showing the variation of the concentration with the number of projections / steps (S). The circles represent the theoretical results and the triangles, the simulated results. These results are for gadolinium in a water matrix imaged at 50 keV using the K-edge method. N_{ot} = 1E8.

scan sizes greater then 50 x 50 is prohibitively time consuming. If this property is shown to be correct, the results obtained for small scan sizes could be scaled-up to yield the correct values for $S \geq 256$, the normal commercial number of projections / rotations.

Figure 4.14 shows the results of these simulations (triangles) for various numbers of projections. The theoretical values for the case studied, ie. gadolinium in a water matrix, are also shown (circles) by way of a comparison. There is obviously good agreement between the two sets of data making the number of projections scaling valid. *Note: Simulations could not be performed when the number of projections was greater than 160 due to computer memory restrictions and at low numbers of projections, the coarseness of the image made decisions on the visibility of an image difficult.*

4.3.5   Minimum Concentration vs. F Simulations.

The situation that this study set out to investigate was how the minimum concentration varied as the size of the area into which the contrast agent was administered decreased. The results given in section 4.2.5 show this relationship. Simulations were performed to investigate this relationship for both cases. Figures 4.15 and 4.16 give the results of these simulations with the theoretical results given as a comparison. A value for Q of approximately 11 was needed for the theoretical results to agree with the simulations. It is obvious from figure 4.15 that although a value for Q of 11 was chosen as giving the best agreement, this is very much open to observer interpretation as can be observed by the theoretical curves for Q = 10, 11 and 12.

The simulation results were obtained by observing the images and making a decision as to their visibility. This method however, posses problems at low values (ie. $f \leq 0.1$) and high values ($f \geq 0.9$) of f. In figure 4.17(A), f=0.1. Here, if you know what to look for and where to look, this image would be deemed visible. However, if no prior information was available, the object might be considered

(A)   (B)
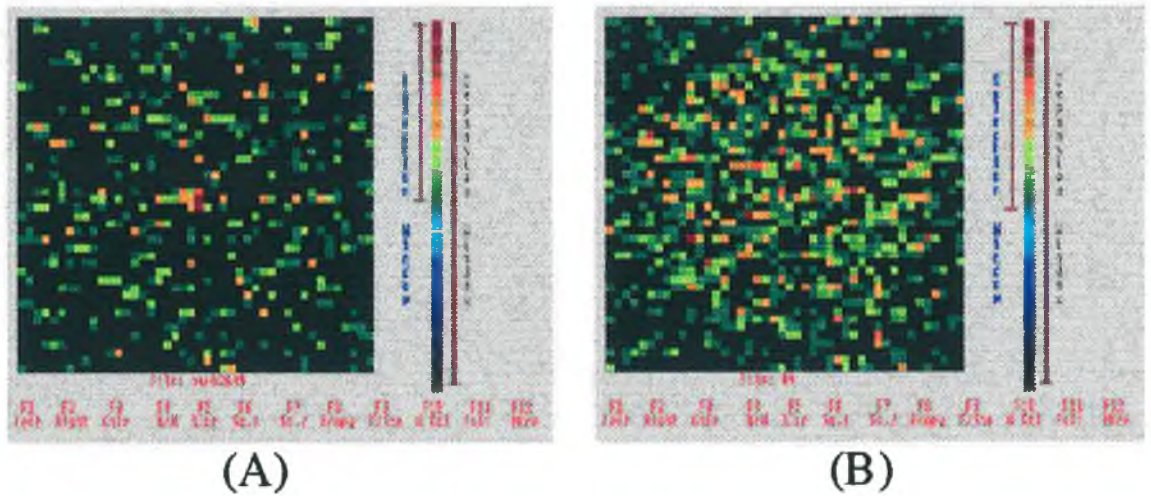
Figure 4.17
Diagram showing two simulated images. (A) Concentration = 2.8 mg/cc, S=44 and f=0.1. (B) Concentration = 0.5 mg/cc, S=44 and f=0.9.
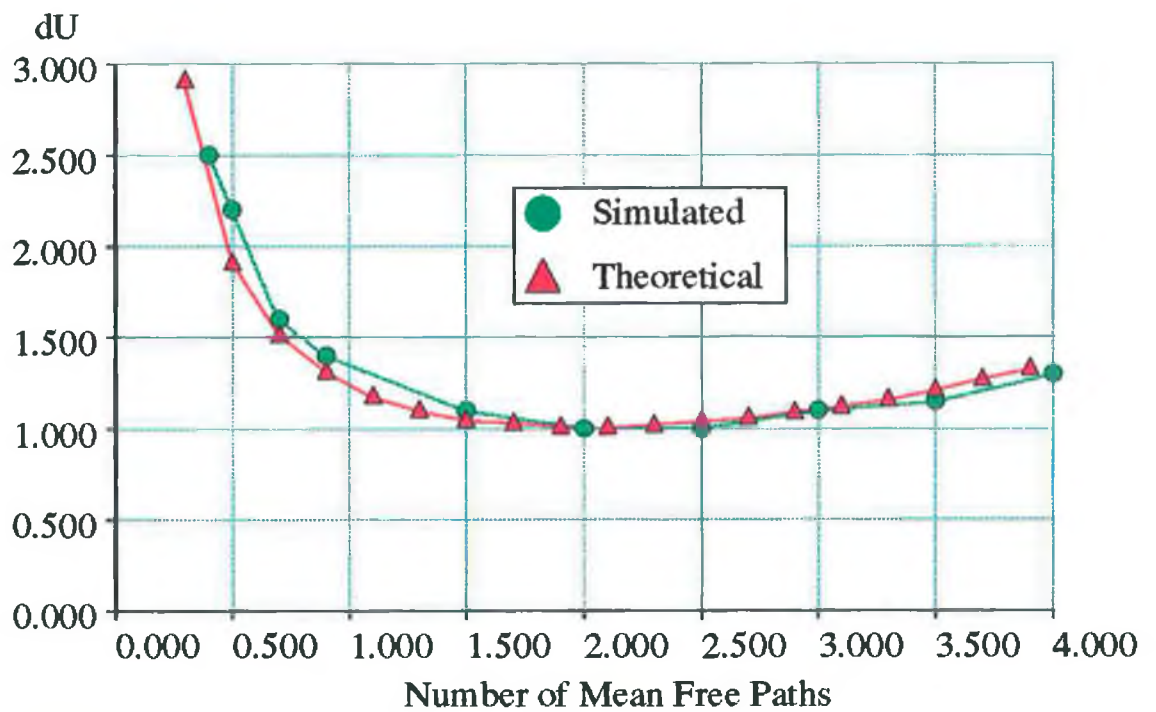
Figure 4.18
Graph showing the variation of the difference in linear attenuation coefficient with the thickness of the object in mean free paths. These results are for S=44, N_{ot} = 1E8, f=0.5 and Um = 0.042.

a noise cluster. This effect at low values of f tends to yield a lower minimum concentration that is visible than the equations predict. A similar effect can be seen in figure 4.17(B). Here f=0.9, and the object is hard to distinguish above the background as there is little background with which to compare it. This situation tends to increase the minimum concentration above the predicted value.

4.3.6   Number of Mean Free Paths Dependence.

The last parameter to investigate by way of simulations, is the number of mean free paths (X) dependence, ie. how does the minimum concentration vary as a function of X. Simulations were performed for the monochromatic case with the minimum difference in mass attenuation coefficient that was visible being determined for various object thicknesses. Figure 4.18 shows the results of these simulations. In these simulations the number of steps, the relative object size and the number of incident photons all remained constant. Thus a visibility parameter was used to determine whether an image was visible or not. This is similar to the parameter described in Chapter 3. If the mean pixel value in the object area minus the mean pixel value in the background area, with all the pixels normalised between 0 and 1, lay between 0.118 and 0.128, the image was deemed visible. The program was run so as to continually vary the concentration until the above condition was met. Shown in figure 4.18 are the theoretical results (Q=10.5). Good agreement exists between the simulated and theoretical results.

4.3.7   Determination of the Q value.

In both the monochromatic and K-edge cases, the value for the minimum detectable concentration is dependent on the value of Q. Q is the product of the reconstruction noise factor and the number of standard deviations difference between two pixels needed for detection. Fryar
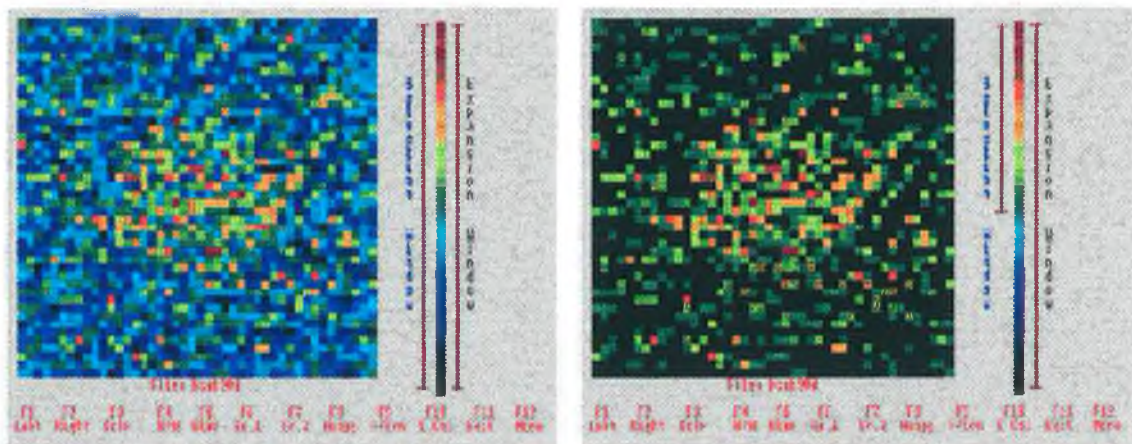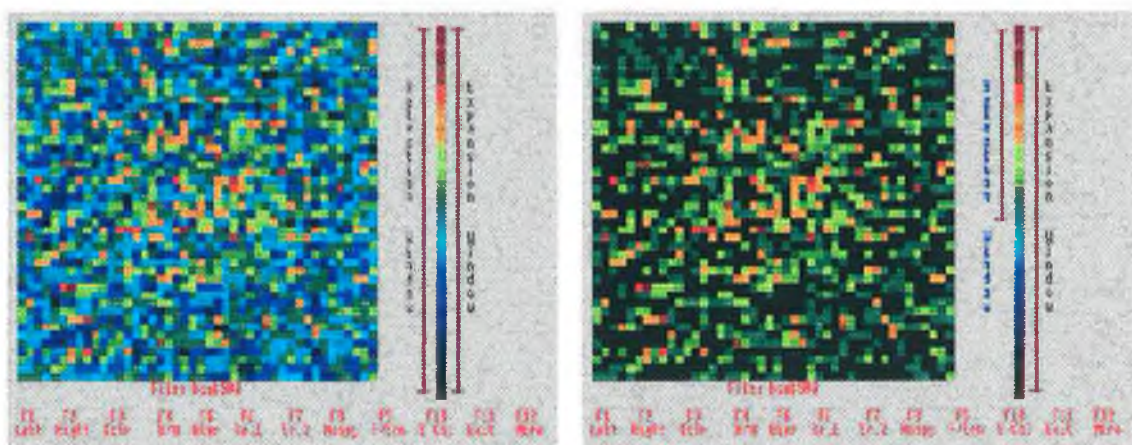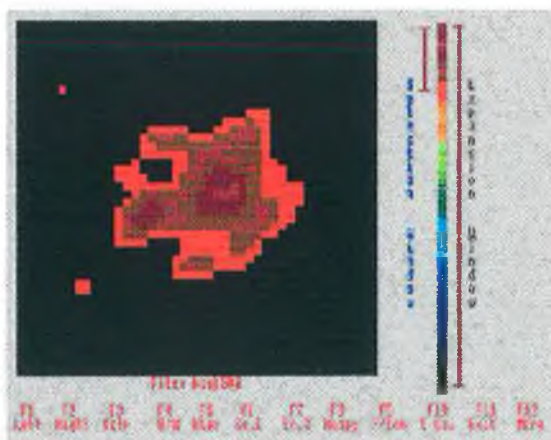
Figure 4.19

Two sets of images showing a concentration deemed visible for simulation results and a one deemed not visible, but clearly visible after some image processing.

and McCarthy found that at least 3 standard deviations difference was necessary for detection to occur [2]. As was previously stated, Chesler et al., found that the reconstruction noise factor for a good algorithm was 2.3. Thus we have a theoretical lower limit on Q of approximately 7. In the process of this work it was found that Q had to be of the order of 11 for detection of the image to occur. However, this is for an unprocessed image. Figures 4.19 (A) and (B) show a concentration of 0.9 mg/cc of gadolinium in a water matrix imaged at 50 keV with S=44, N_{ot}= 1E8 and f=0.5. Image (B) is similar to (A) except that some of the background has been removed. This image would be deemed visible for simulation purposes.

Figure 4.19 (C) shows a concentration of 0.5 mg/cc. On first inspection the object is not visible above the background. Even with some of the background removed, ie. figure 4.19 (D), it is still not resolvable. However, with some image smoothing and further background removal, the object is clearly visible, as shown in figure 4.19 (E). The steps needed to obtain image (E) from image (C) are relatively simple but time consuming. Therefore this approach was not utilised for all the simulation results obtained. A value of 0.5 mg/cc corresponds to a Q value of 7.2.

<p style="text-align:center">4.4   *Summary*</p>

In this chapter equations were developed that allow the determination of the minimum concentration of any element that is necessary for visualisation, when the element is used as a contrast agent in computerised tomography. Two cases were studied, the monochromatic and the K-edge cases. In the monochromatic case the minimum change in the linear attenuation coefficient between the matrix and analyte that is needed for visibility is determined. This is then converted into a concentration. In the K-edge case the minimum concentration is determined directly. Chapter 3 deals with the specific case of imaging the myocardium where as in chapter 4 the equations deal with the general case of administering the analyte to

a variable size inner cylinder.

The results from these equations were first tested by comparison with the results obtained by Fryar and McCarthy at the limiting case of f=1.0. Excellent agreement resulted.

Finally, computer simulations were performed to further verify the results obtained from these equations. All the parameters utilised in the equations were investigated with good agreement resulting.

[1] Grodzins, L.
"Optimum Energies for X-ray Transmission Tomography of Small Samples.", Nucl. Inst. & Meths., Vol. 206, pp. 541-545, 1983.

[2] Fryar, J., McCarthy, K.J.,
"Multi-element Imaging in CT using a Tube Source of X-rays.", IEEE Trans. Nucl. Sci., Vol. 36, No.1, pp.1138-1143, 1989

[3] McCarthy, K.J., Fryar, J.,
"Sensitivities for Contrast Agents Imaging in CT Scans using Single Energy Synchrotron Radiation.", Nucl. Inst. & Meths. in Phys. Res., Vol. A287, pp. 613-618, 1990.

[4] Chesler, D., Riederer, S., Pelc, N.,
"Noise due to Photon Counting Statistics in Computed X-Ray Tomography.", Jour. Compt. Assis. Tomo., Vol. 1, No.1, pp.64-74, 1977.

[5] Flannery, B., Roberge, W.,
"Observational Strategies for Three-Dimensional Microtomography.", Jour. Appl. Phys., Vol. 62, No. 12, pp.4669-4674, 1987.

Chapter V
Experimental results on the sensitivity of CT to contrast agents in cylinders.

5.1   *Introduction*

In the previous chapter, equations were developed that predict the minimum concentration of an analyte that is visible when a CT scan is performed on a cylindrically symmetric object. Two cases were studied; the monochromatic case described by equation 4.14 and the K-edge case, described by equation 4.48. The results of these equations have been tested using computer simulations with good agreement resulting. The procedure and results obtained in verifying the equations experimentally will now be described along with the apparatus and software used in the experiments.

5.2   *Apparatus*

5.2.1   Overview of Apparatus

Shown in figure 5.01 is a block diagram of the apparatus used along with the connections between each element. Each of these elements will be explained further in the following sections. Also shown is the x-ray cabinet in greater detail. This contains the x-ray tube, scan table, detector, etc.

5.2.2   X-Ray Source & Shielding:

The x-ray source used in the determination of experimental results was an x-ray tube forming part of an
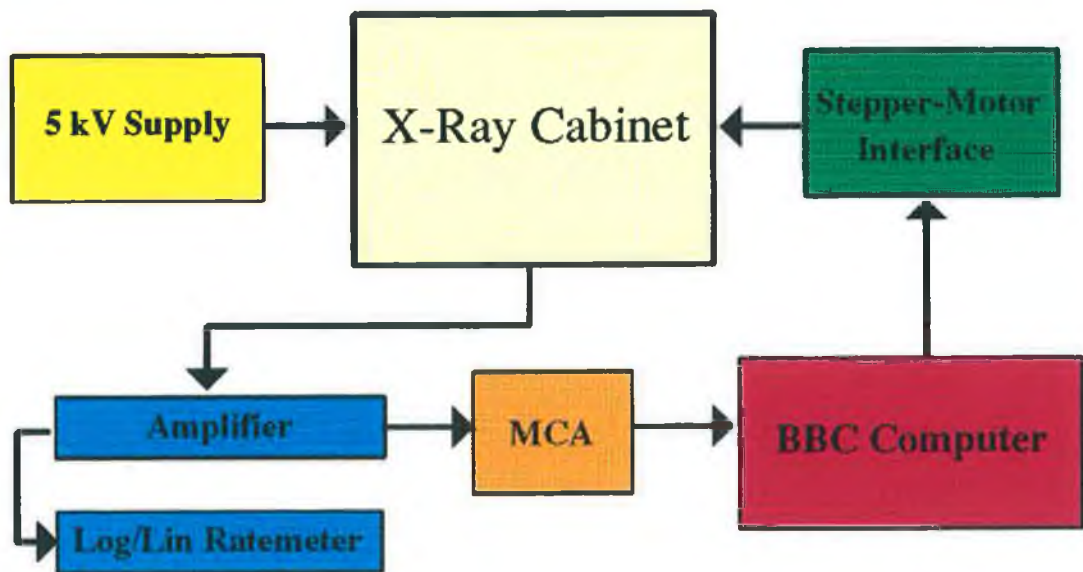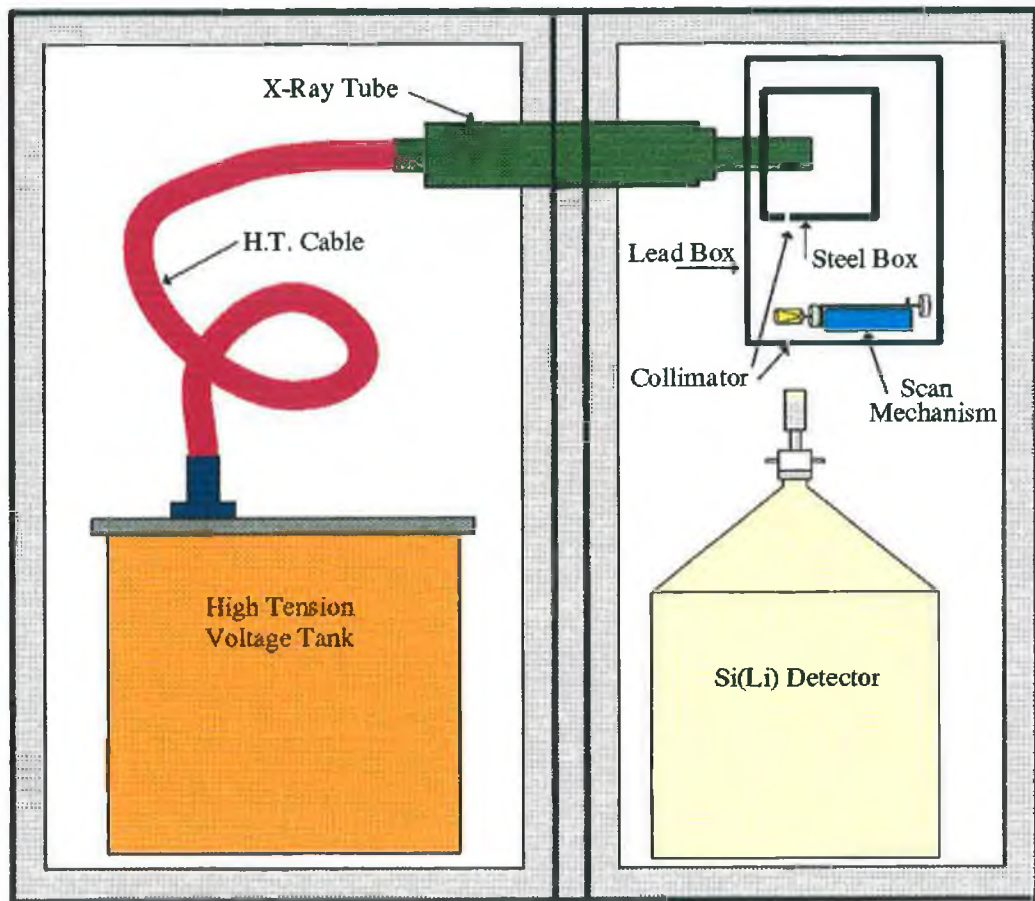
Figure 5.01

Diagram of the X-ray cabinet containing the tube, scan table, SiLi detector and shielding. Shown below is a schematic diagram of the apparatus interconnections.

old Philips PW 1270 automatic simultaneous x-ray spectrometer. The spectrometer had been significantly modified by Adrian Fenelon [01] with most of the components inside the analysing chamber being removed.

These have been replaced by a 3 mm thick lead box formed on a light steel frame. The box is closed with a tight fitting 3 mm thick lead lid which is pushed onto the open side of the box. This allows access to the interior of the box which includes the scan mechanism, beam filters and a further steel box, as shown in figure 5.01. A 10 mm thick welded steel box is mounted on a frame inside the lead box, and this steel box absorbed most of the non-beam x-rays. A collimation hole exists in both the steel and lead boxes. This provides the parallel beam of x-rays used in the recording of experimental data. The thickness of the lead box is sufficient to absorb the x-rays down to well below the annual dose limit, even in the absence of the steel box. A 1.5 mm thick lead shield is also attached to the inside walls and door of the analysing chamber.

All doors, as well as the lid of the lead box, have micro-switches attached, preventing the x-ray machine operating if any became open. The x-ray tube requires water cooling and this is supplied via the mains water supply. If the flow rate decreases excessively or stops, two flow-rate switches will shut-off the power to the tube. The tube has a voltage range from 20 to 60 keV, switchable in 10 keV steps. The tube current can be adjusted from 5 to 80 mA for each of these voltage settings. However, the maximum power allowed to be drawn by the tube is 3 kW, therefore at 60 keV, the maximum current that can be selected is 50 mA.

Fenelon [01] has calculated the radiation levels below the lead box, with no apertures or a steel box, as 10^{-3} mR/hr. With the steel box present, this value decreases to 10^{-10} mR/hr. With the aperture present he found that the dose-rate beneath the aperture was 2.5 x 10^3 mR/hr. He also found that the exposure rate of the scattered beam outside the chamber door was 5 x 10^{-10} mR/hr. One would need 2.3 x 10^8 years to accumulate the dose equivalent to one x-ray image in a hospital (ie.

approx. 1R). These calculations were for the maximum output of the x-ray tube, ie. 60 kV at 50 mA.

5.2.3   Si(Li) Detector.

Of the three types of x-ray detectors in common use, gas-filled, scintillation and semiconductor detectors, the Si(Li) semiconductor detector has the best energy resolution for x-rays. This fact is shown in figure 5.02 [02]. *Note, that only the Si(Li) detector can resolve the $K\alpha$ and K_β lines of the iron fluorescence spectrum.* The efficiency of the Si(Li) detector depends on the x-ray energy as shown in figure 5.03 and has a useful energy range from less than 1 keV to above 30 keV. The Si(Li) detector is usually mounted on a cryostat and operated at liquid nitrogen temperatures to reduce thermal noise. The detector used in the course of this work was an *EG&G Ortec* SLP - series detector, model SLP - 06180, with a quoted energy resolution of 200 eV at 5.9 keV. The detector had been modified to perform at $\geq$ 100,000 cps and 50 keV.

5.2.4   Multichannel Analyser.

To measure the energy spectrum of a radioactive source means to record the pulse-height distribution produced by the particles emitted from the source, which is achieved with the use of an instrument called the multichannel analyzer (MCA). Multichannel analyzers are used in either of two different modes; the *pulse-height analysis* (PHA) mode or the *multichannel scaling* (MCS) mode.

The PHA mode is the traditional function of a MCA and is used to sort out incoming pulses according to their height / energy and store the number of pulses of a particular height in a corresponding channel. In the PHA mode, a MCA performs the function of a series of SCAs (single channel analyser) placed adjacent to one another. The incoming pulse enters into an *analog-to-digital converter* (ADC). The ADC digitizes the pulse amplitude, it

151
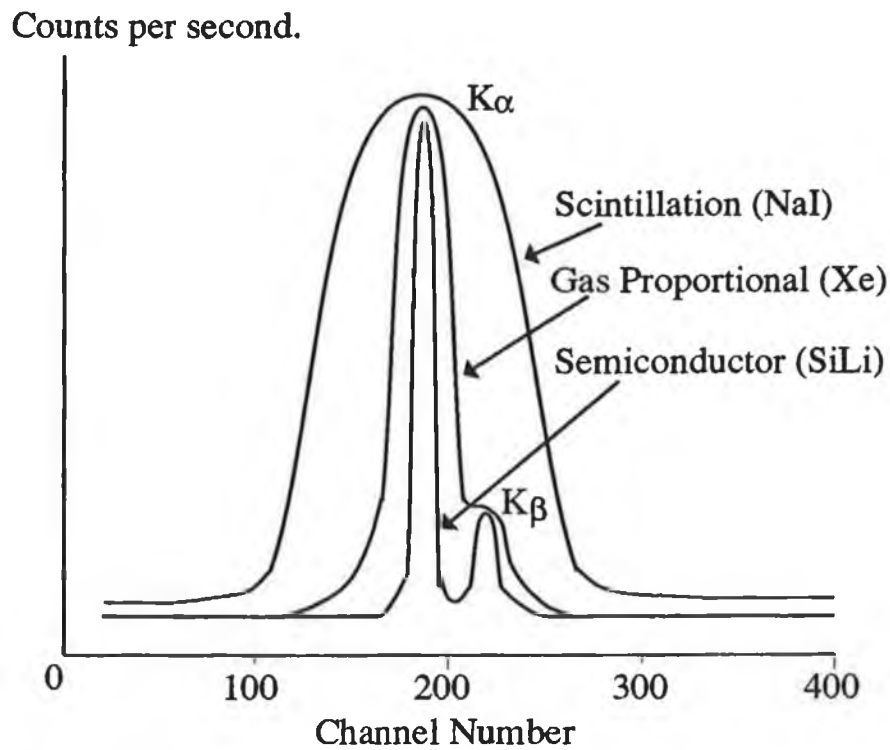
Figure 5.02
**Demonstration of the superior energy resolution of Si(Li)
detectors by showing the same peak recorded with a NaI(Tl)
scintillator and a gas-filled proportional counter.
(Tsoulfandis, "Measurement and Detection of Radiation")**
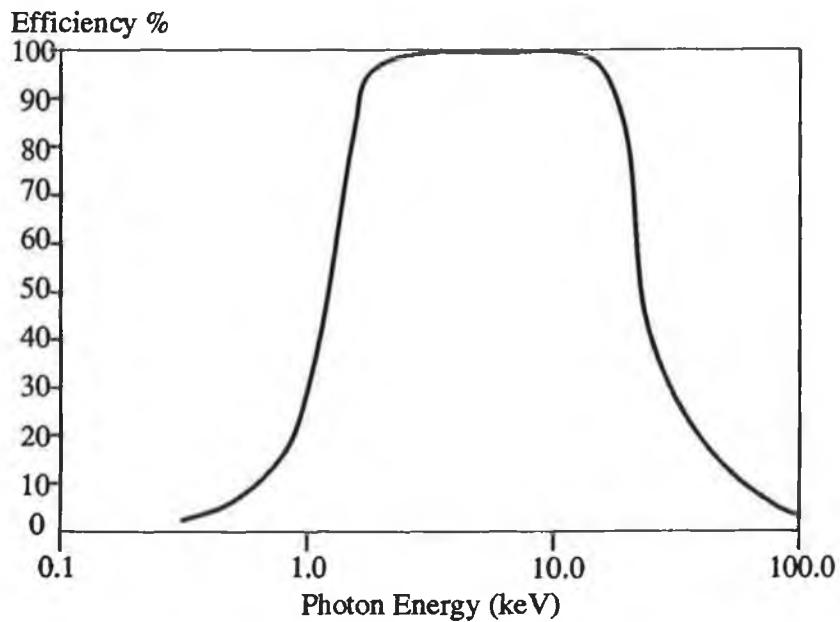
Figure 5.03
**Si(Li) detector efficiency as a function of x-ray energy.
(Tsoulfanidis, "Measurement and Detection of Radiation")**

then produces a number proportional to the height of the pulse, a number which determines the channel where the pulse is stored. The MCA available for this experiment had 1024 channels.

The MCS mode is used to count events as a function of time. The individual channels of the memory count all incoming pulses for a preset time Δt. After time Δt, the counting operation is switched automatically to the next channel in the memory. Thus if a radioactive source is a short lived isotope, the MCS mode will give the exponential decay curve that can be used for the measurement of the half-life of the isotope.

The Multichannel Analyser used in the course of this work was an *EG&G Ortec* 7100 and was used only in the Pulse Height Analysis mode.

5.2.5   NIM Modules.

In this section a brief description of each of the NIM modules used in this experiment is given without any regard for any of the internal electronic details. All NIM modules were powered by an *EG&G Ortec* 4001A NIM Bin.

Log/Lin Ratemeter: The ratemeter gives the average count rate for input pulses. These pulses come from the spectroscopy amplifier. There are 11 linear ranges available with full-scale values from 10 cps up to 10^6 cps. There is also a Log scale which can accommodate up 10^6 cps. A variety of time constants can be selected, each of which determines the amount of averaging/smoothing that is done for each measurement. For this project only the time constants of 0.3 and 1 sec were used. Any measured count-rate will be shown on the front-panel meter, however there is also a proportional voltage output available at the rear of the unit. The full scale range of this analogue output is 0 to 10 V. The input pulses should have a voltage rage from ±3V up to ±30V maximum. An *EG&G Ortec* 449 ratemeter was used for these experiments.

153

5 kV Detector Voltage Supply: The supply voltage for the detector was supplied by a *EG&G Ortec* 459 High Voltage Supply. This module gives a voltage of 0 to 5 kV of either polarity for use with a semiconductor detector or a low current scintillation detector. When using this in conjunction with the Si(Li) detector, the voltage must be applied slowly, ie. in 200V steps every 30 sec. It should also be a negative supply voltage. There is a 'remote shutdown' connection at the rear of the module which is used with the SiLi detector to turn the voltage off if the temperature of the detector rises above 80K.

Spectroscopy Amplifier: This amplifier has extremely low noise and a very wide gain range for use with high resolution spectroscopy. It accepts input pulses of either polarity and its single output can be switch-selected for either unipolar or bipolar pulse shapes. The unipolar format is usually used for spectroscopy arrangements while the bi-polar is normally used for fast counting. The gain range is continually adjustable from X5 up to X750. It accepts pulses up to a maximum of 20V. An *EG&G Ortec* 575 low-cost spectroscopy amplifier was used.

5.2.6 Pulse Shaping

The output signals from most detectors (except the Geiger-Muller tube), are of the order of 10^{-10} to 10^{-15} C per event. These signals need to be amplified and shaped such that fast counting equipment may be utilised. The output pulse from a typical detector is a current or voltage pulse having a very short rise time and a relatively long fall time. One of the essential requirements of pulse counting systems is that the individual pulses from the detector must be processed totally before the following pulse is incident on the system. With the long detector time constants, typically from 50 to 100μsec, the time required for a pulse to decay to the zero volt level can be of the order of 1 msec. At count rates in excess of a few hundred counts per second, *pile-up* of the pulses will occur. This effect of pile-up

154
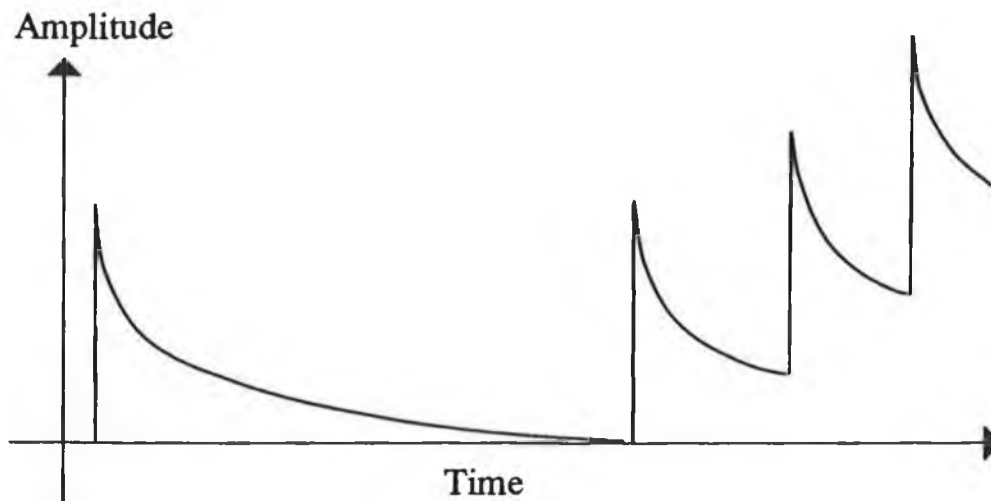
Figure 5.04
Pulses from a typical radiation detector showing the effect of pile-up on pulse heights.

is shown in figure 5.04. The effect of pile-up includes distortion of the energy resolution of the system and loss of counts due to dead-time effects.

These effects of pile-up can be reduced if the slowly decaying tails of these pulses are removed. This can be achieved by differentiating the pulse using a simple RC circuit, see figure 5.05a. Here the pulses are clipped and decay with a time constant τ that is determined by the product of the resistance and capacitance of the circuit. The pulse shape derived from this RC circuit, particularly the narrow width at its peak, is not well suited for processing by the pulse height analysis equipment. Additional shaping of the pulse can, however, be achieved by the use of an RC integrating circuit, the output peak amplitude of which is proportional to the energy deposited within the detector. Figure 5.05c shows the result of single differentiation and integration when the two RC circuits have equal time-constants. This combined circuit produces a pulse known as a unipolar pulse.

If this pulse is further differentiated, then a pulse having both positive and negative values is produced. This pulse, shown in figure 5.05d, is known as a bipolar pulse, with the areas of both the positive and negative lobes being equal, and their relative amplitudes determined by the RC time-constants of each stage.

155

(a) V_i C   R $V_o = R.C.\frac{dV_i}{dt}$

$\tau = C.R$

(b) V_i R   C $V_o = \frac{1}{R.C}\int V_i\, dt$

$\tau = C.R$

(c) C_D R_D Buffer R_I C_I

$\tau = R_D.C_D = R_I.C_I$

(d) C_D R_D Buffer R_I C_I C_D R_D

$\tau = R_D.C_D = R_I.C_I$
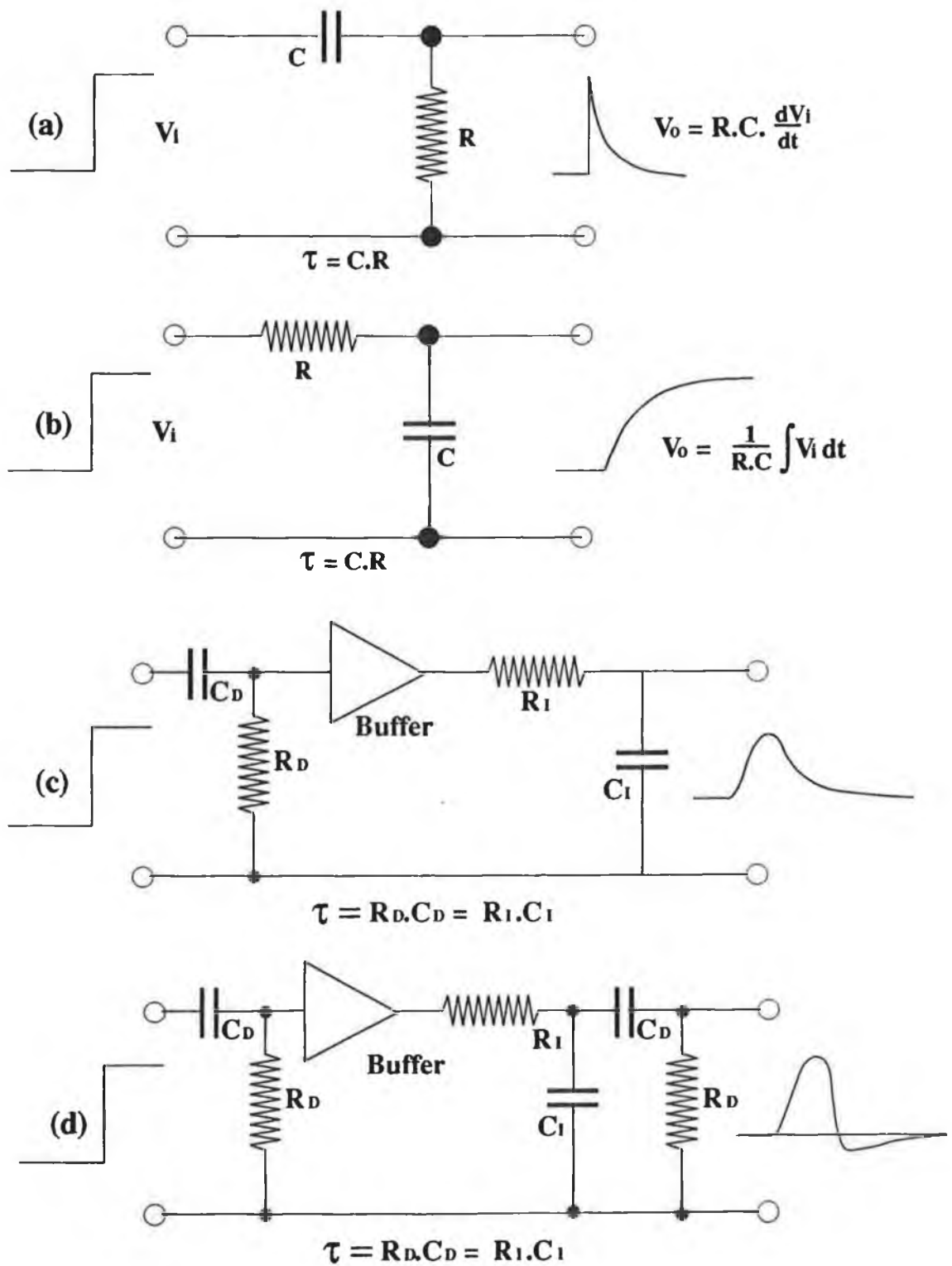
Figure 5.05
**RC Shaping networks and their effect on a step input: a) single RC
differentiation, b) single RC integration, c) combined differentiation
-integration and d) combined double differentiation and single
integration.**

In most radiation detectors, operated in pulse mode, a preamp is incorporated into the detector. This preamp has four main functions; 1) first-stage amplification of the pulse, 2) preliminary pulse-shaping, 3) matching of the detector output impedance with the input impedance of the main amplifier, and 4) charge-to-voltage conversion of the detector output pulse.

5.2.7 Counting Systems.

Initial experimental results to check the predictions of the equations given in sections 4.2.1 and 4.2.3 gave erroneous results. Having checked various parameters in the equation and experimental set-up, it was decided to measure the mass attenuation coefficient of water and compare this to the value quoted in the literature [03].

At 28 keV, the value for the mass attenuation coefficient is quoted at 0.042 m^2/kg [03]. Initial experiments to measure this value using various tube currents and water thicknesses gave values in the range 0.029 - 0.035 m^2/kg.

Using a faster counting system, incorporating a delay-line amplifier, the linearity of the source with increasing tube current was investigated. *Note: Although this new counting systems had a faster response, the energy resolution was not sufficient for testing of the theoretical predictions.* The source was heavily filtered to alleviate problems due to excessive count rates on the detector / counting system. This counting system is shown in figure 5.06 with the results of this investigation shown in figure 5.07. It is obvious from this graph that the x-ray output is very linear with increasing tube current. This, therefore, leads to the conclusion that the counting electronics were incapable of counting at high rates, ie. >1000 cps for the total spectrum. This system was altered such that bipolar pulses were used and a time-constant of 0.5 μsec was chosen on the spectroscopy amplifier. *Note: Bipolar pulses are faster than unipolar pulses because the charge is taken off the sensing capacitor by the negative lobe of the pulse.*
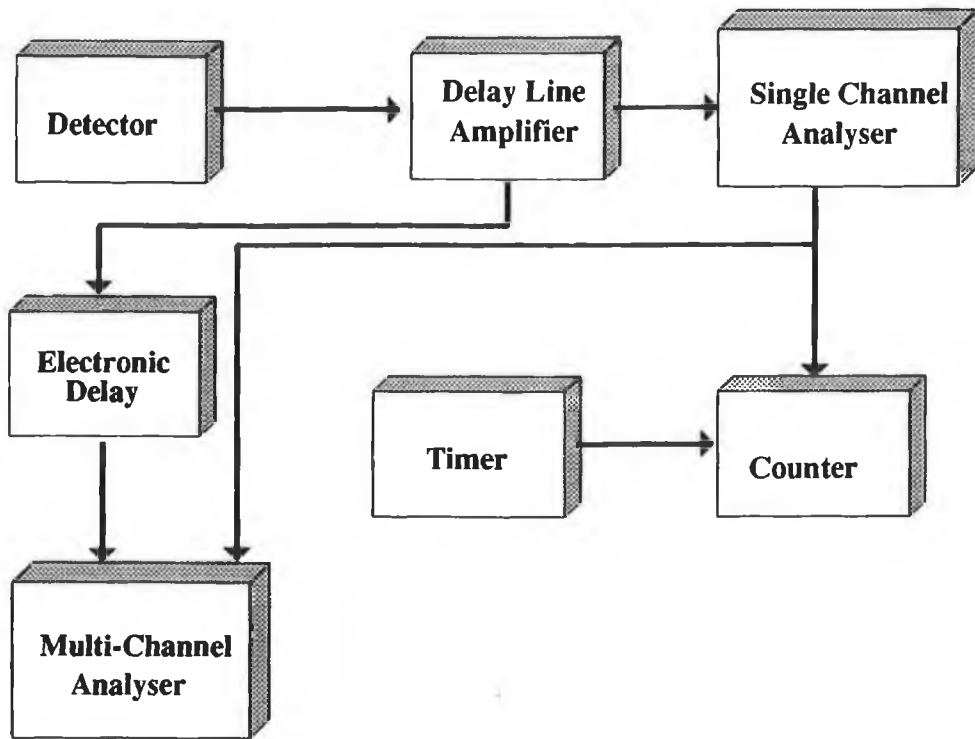
Figure 5.06
Block diagram of the fast - counting electronics system. The delay and the multi-channel analyser combination are used to set up the region of interest on the SCA.
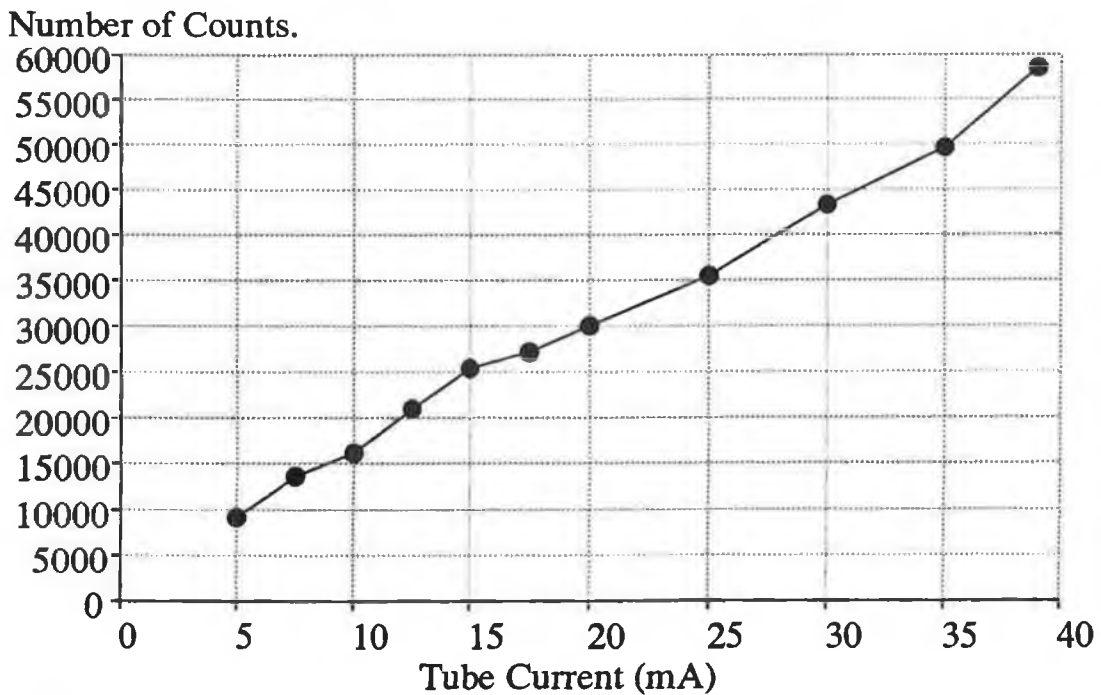
Figure 5.07
Graph of X-ray tube current vs. number of counts in a region of interest centered on 28 keV. The region of interest was approximately 0.5 keV wide and the counting time was 100 sec. The beam was heavily filtered with tin.

Using this set-up, results were taken for the mass attenuation coefficient of water at 28 keV vs. incident count rate, and the results are shown in figure 5.08. These results indicate that no dead-time or pile-up effects will be observed if the count-rate remains below 2500 cps for the total spectrum. The x-ray spectrum will therefore, be filtered to yield a maximum flux in the energy range 25 - 35 keV. This filtering of the spectrum will be covered in section 5.2.10.

Mass Attenuation Coefficient (m^2/kg)
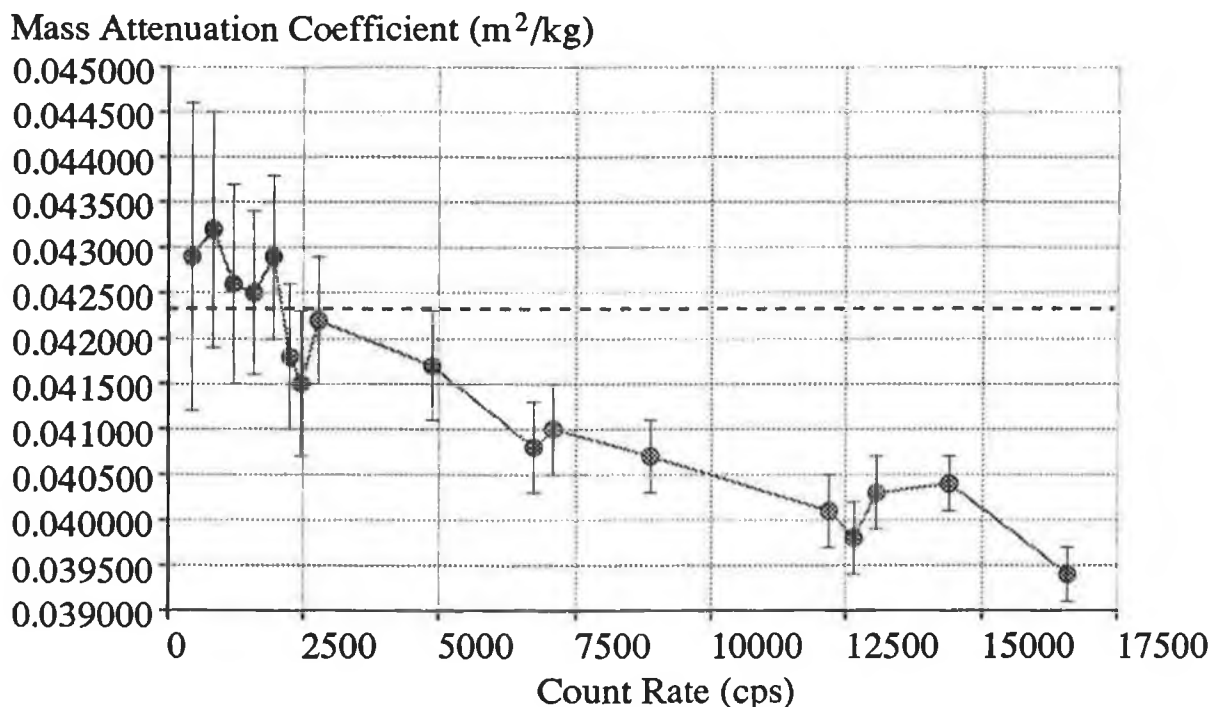
Figure 5.08
Graph showing the count rate vs. the mass attenuation coefficient of water at 28 keV. The published value is shown by the dashed line.

5.2.8   Scan Table / Stepper-Motor Interface

The phantom used in these experiments is shown in figure 5.09 and will be described in further detail in the next section. This phantom was imaged using a technique similar to the first generation CT scanners. However, in this case the object was rotated / translated as moving the source / detector combination around the object was impractical. The phantom was attached to the scan table which provided the necessary rotation and translation. The

scan table used was a converted *Feedback CNC*932 computer controlled drilling machine in which a further rotational stepper-motor was added to the existing x-y table. The three stepper-motors were controlled by the BBC computer via the stepper-motor interface unit. It's purpose was to decode the bit-pattern output on the *userport* of the BBC, so as to determine which motor to drive and in which direction. The interface unit also amplified these pulses as well as powering the stepper-motors.
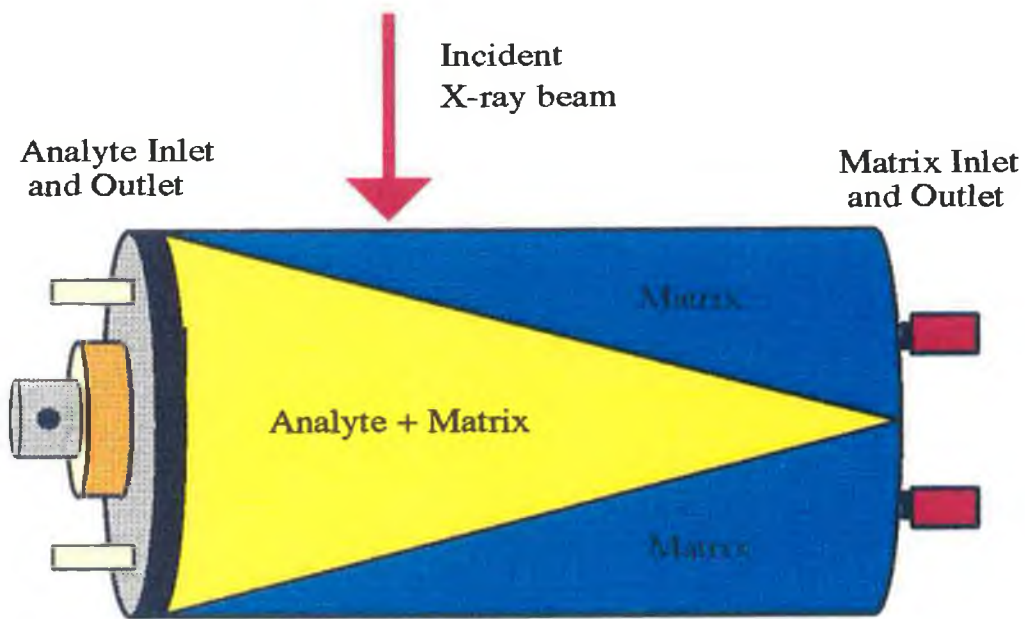
Figure 5.09
Diagram of the phantom used for experimental CT scans. By varying the position of the interrogating beam, the f-value in the equations could be changed.

5.2.9   Experimental Phantom

The experimental phantom used in the testing of the theoretical predictions is shown in figure 5.09. It consists of a closed cylinder made of Perspex of dimensions 4.00 cm in diameter and 8.00 cm in length. Contained inside this cylinder is a cone of polystyrene which is sealed to the outer cylinder at one end. Two apertures exist at either end to allow the insertion and removal of the matrix and the matrix / analyte

160

combination. The cone is graduated to allow accurate positioning of the x-ray beam. Fixed to one end is a connection to allow the phantom to be fixed to the scanning table.

5.2.10   Filtering the X-ray Beam.

As outlined in section 5.2.7, the counting system must not be used at count rates greater than 2500 cps. Therefore, to maximise the count rate in the region of interest, the x-ray spectrum will be filtered in such a way as to achieve this objective. Shown in figure 5.10 is the unfiltered 30 keV spectrum emitted from the x-ray tube. Using the program *c.simula*, written by Charles Markham, the incident spectrum was filtered with various elements and thicknesses of these elements. The best achievable spectrum is shown in figure 5.11. Here the incident spectrum is filtered by 0.7 kg/m^2 of Tin, 0.3 kg/m^2 of copper and 0.6 kg/m^2 of Bromine. From the graph it is obvious that the majority of the photons reside in the energy band 20 - 30 keV. This is in marked contrast to figure 5.10 where the majority of the photons reside in the band 7 - 25 keV. The energy range 20 - 30 keV is used in the experiments described herein because in this band the mass attenuation coefficient of the matrix is sufficiently low to allow concentrations of the order of a few mg/cc to be imaged. At energies lower then 20 keV, concentrations needed for visibility increase dramatically causing problems in regard to analyte solubility in the matrix used, ie. water. Also shown in figure 5.12 is the result of the above filtration on the 40 keV incident spectrum.
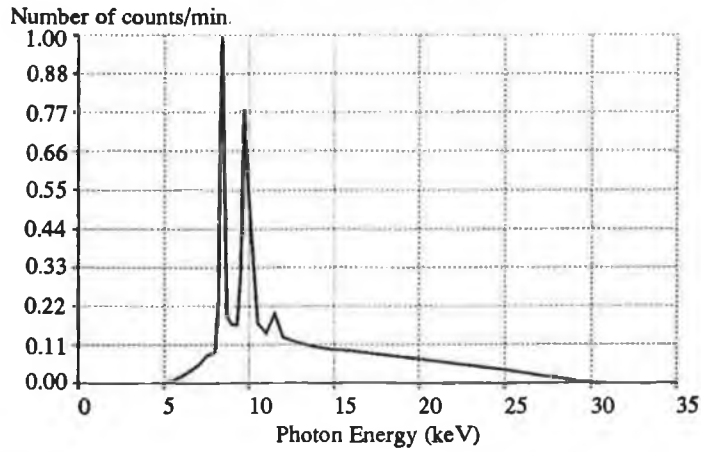
Figure 5.10

Graph of the photon output vs. energy for the unfiltered 30 keV x-ray spectrum used in the experimental section.
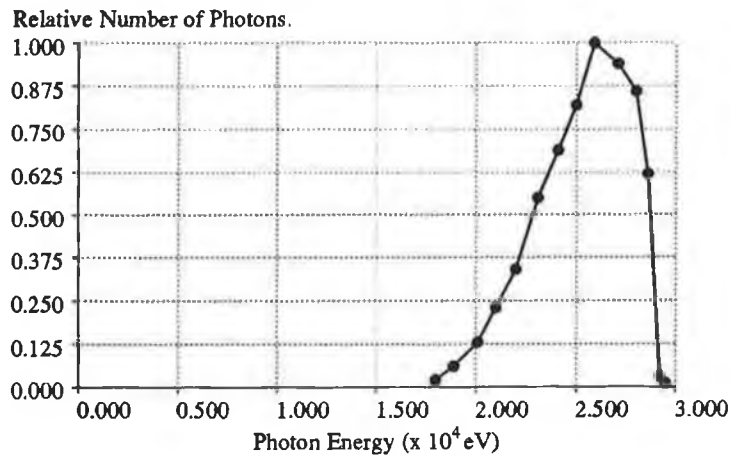
Figure 5.11

Graph of relative photon output as a function of energy for a 30 keV x-ray spectrum filtered by 0.7 kg/m^2 of tin, 0.3 kg/m^2 of copper and 0.6 kg/m^2 of bromine.
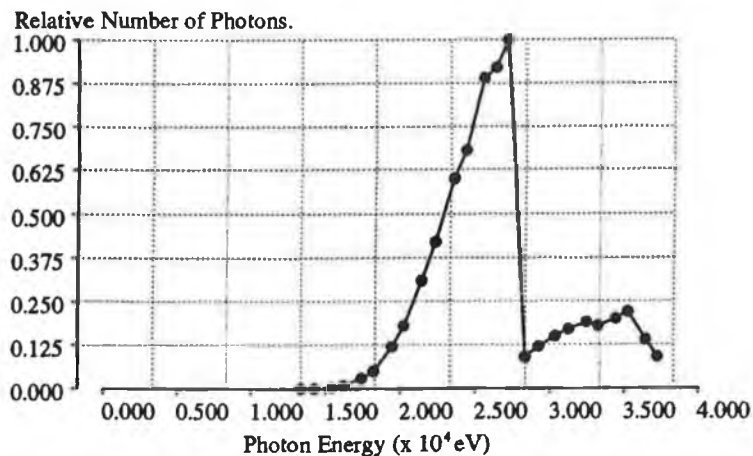
Figure 5.12

Graph of the relative photon output as a function of energy for a 40 keV x-ray spectrum filtered by 0.7 kg/m^2 of tin, 0.3 kg/m^2 of copper and 0.6 kg/m^2 of bromine.

5.3 *Software*

5.3.1   Scanning Program.

The program shown on pages 52-56 of appendix 1 contains the stepper-motor driving functions and the MCA - data collection functions necessary to perform an experimental scan. It is written in BASIC and runs on the BBC micro. The program shown is for a 24 x 24 step/rotate scan, but it is simply modified to perform any other size of scan, eg 40 x 40. The major steps will now be described.

Lines 1 - 120 are the main controlling section of the program. Here all the other subroutines necessary for the program to run are called.

Lines 130 - 180: (Procloaddata) Here the variables controlling the size of the scan and the step size used are defined.

Lines 190 - 280: (Procscan) This subroutine calls the three functions proccount, procrotate and procstep in the correct order to complete the scan.

Lines 390 - 520: (Procstep(S)) This routine moves the translate stepper motor by S number of steps.

Lines 530 - 610: (Procrotate, Procreturn) These subroutines cause the rotate stepper motor to move for each of the angles. When the 180 degrees are covered, the object is then rotated back around to the zero degree angle in preparation for the next data set.

Lines 620 - 720: (Proccount) In this routine the MCA is controlled to count for a preset number of seconds live - time, and then to transfer the data to the BBC. First the various baud rates are set up by the routine procsetup (lines 810-870). The MCA is then cleared of any data that might be already present by the routine procclear (1210 - 1260). The command sequence to tell the MCA to start counting is then sent by the routine procstartpha (880 - 1020). As the MCA outputs no signal to signify completion of counting, the BBC waits for a specified time before sending the sequence to transfer the data (proctransfer,

163

730 - 800). When transferring the data, an assembly language routine (1660 - 2290) is used to read the data and store it in memory. This memory is later interrogated to yield the various counts from within the data stream sent by the MCA, which contains various control codes as well as the count data. This assembly routine has inherent error - checking routines on the data received.

Once these processes have been repeated M x M number of times, the data is saved and the program terminates.

5.3.2 Transferring Data.

Once the projection data has been collected by the BBC computer, it must be transferred to the Archimedes 440 computer for reconstruction. The program shown on page 1 of appendix 1 performs this task. This program is executed on both computers, with the user selecting which computer is the 'sender' and which is the 'receiver'. The program basically works as follows: 1)both the receive and send baud rates are set to 2400 baud, 2)the logical output device on the sender and the logical input device on the receiver are redirected to the RS423 port, 3)the sender opens the user-selected file, reads in each number and prints it to the RS423, 4) the receiver reads each number and saves it to a user-selected file. Finally, line 310 returns the logical input device of the receiver to the keyboard.

5.3.3 Reconstruct / Shift-Data Program.

The transferred projection data now requires reconstruction. The program *c.reconst*1 (pp 4-8, appendix 1) performs this reconstruction by implementing the filtered backprojection algorithm. Of the three main reconstruction algorithms, (ART, Filtered backprojection and fourier transform reconstruction), filtered backprojection is by far the quickest in yielding a reconstructed image and was therefore the algorithm that was implemented in the work presented here. The program will now be explained without going into too much detail.

The first section is the declaration and initialisation of the variables utilised in the program. The various arrays are initialised such that a data set of up to 80 x 80 can be accommodated. In C all variables must be initialised to zero or some other pre-set value because, unlike BASIC, the variables can hold any value in the range applicable to its declaration class.

The projection data is then read in from the user selected file and the size of the array is determined. The projection data is now converted into the natural log of the fractional transmittance for each value. If the file is not in ASCII format, then a program called *C. convertbbc* supplied by Adrian Geissel (pp. 2-3, Appendix 1) was implemented, which converts BBC-type random access files into ASCII format and then re-runs the reconstruction program.

If the rotation centre does not coincide with the centre position of the scan travel distance, streaming artifacts occur in the image similar to those shown in figure 5.13a. A solution to this problem was developed by simply moving each set of the translate projection data by some user-supplied fraction of a complete step. Two pixel were combined in the ratios given by this fraction with wrap-around of the data occurring at either ends. The routine to perform this "shifting of the data" is given on page 6, appendix 1. The results of this shifting algorithm can be seen in figure 5.13b.

The projection, having now been converted to the log of the fractional transmittance and shifted (if necessary), now requires to be reconstructed. First the data is filtered using the Ram-Lak filter (page 6, appendix 1). To do this the data was copied into an array called stp[c] with each transverse data set having side lobes added to it which contain zeros. This is necessary for filtering since the filter is five steps wide on either side. The discrete form of the Ram-Lak filter is used. The values obtained for this filter beyond five steps wide are negligible in comparison to the other values. The single dimensional array stp[c] is then reformatted into a two-dimensional array called

165
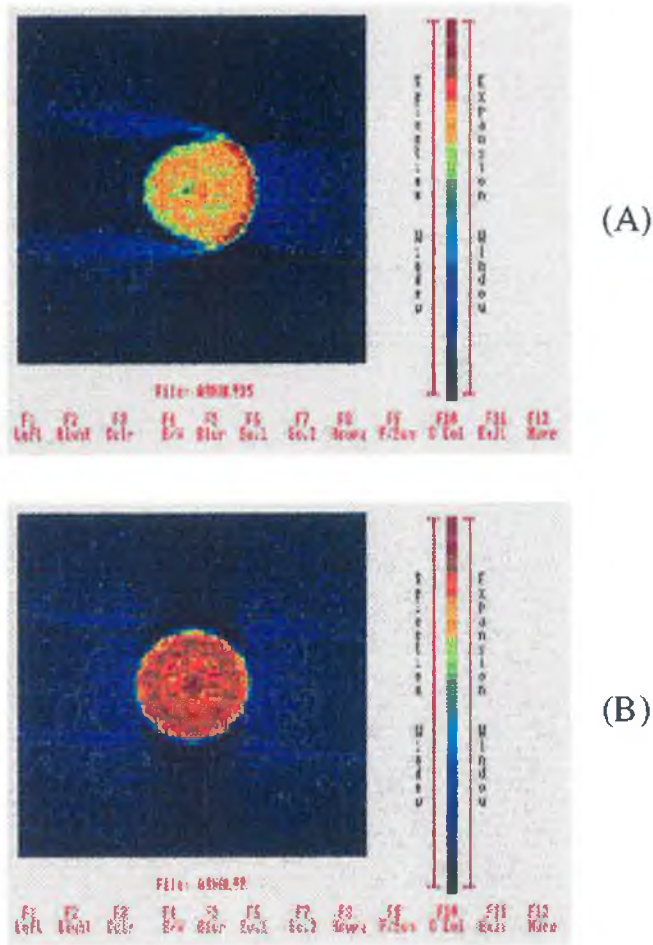
Figure 5.13
Two images showing the effect of the "shift data" routine.
(A) Original off-centre image, (B) image obtained with
the data shifted 1.5 steps left.

lambda[ind][ind] where ind is the array size.

   In the reconstruction algorithm, first the angle of a
particular beam with respect to the reconstruction grid is
calculated. If the data formed a M x M data array, it was
found by McCarthy [04] that if the reconstruction grid was
twice the size, ie. 2M x 2M (the original pixels were
split into four equal segments), then an improvement in
the reconstructed image ensued. Now, the pixel quarters
that intersect with a particular beam are determined. If a
particular pixel does overlap with the beam, then it is
assigned a fraction of the transmission measurement for
this beam. This process is repeated for all steps in this
rotation, and then for all other rotations.

Once this process has been completed, the reconstructed array is saved on disk, with the maximum value being first determined and saved as the first value in the file. This is necessary for the display routine.

5.3.4 Display Program.

Once the image has been reconstructed, it now needs to be displayed with possibly some image manipulation being performed. The program *c.testdisp* performs this displaying function along with a host of image manipulation functions. This program will now be described without going into great detail.

The program listing is given on pages 11 to 51 of appendix 1. The first two sections declare and initialise the various variables and arrays necessary for use in the program. All the functions used are declared and defined and the screensize, necessary for multiple screen displays, is set.

The data is then read in from the user - selected file and its size determined. If the file is in non - ASCII format, it is converted using the program *c.convertbbc*, supplied by Adrian Geissel. Both the colour palette and the display mode are then set up and the image then formed on screen 2, while displaying screen 1. When the image has been formed, viewing is switched to screen 2. The program now enters an infinite *while* loop containing the various image manipulation routines.

The first of these routines allows the image to be shifted up, down, left or right any number of pixels with wrap - around occurring at the edges. This function is useful for subtracting two reconstructed images that don't correspond exactly to each other with respect to the centre of the scan. Once the image has been moved to the desired position, the resultant image data file is saved for subsequent use. This process is shown in figure 5.14b where the image has been moved left 4 pixels and up 4 pixels. The original simulated image is shown in figure 5.14a

The next six function (pp 16 - 19) select and control

167
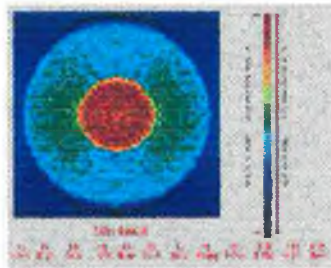
(A) Normal display of a simulated image of a cylinder containing water with iodine contained in the central cylinder.
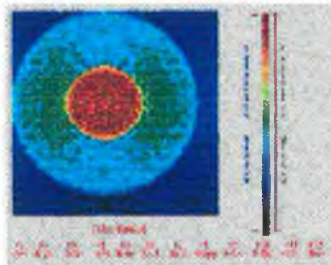
(B) Original image moved four pixels left and four pixels up.
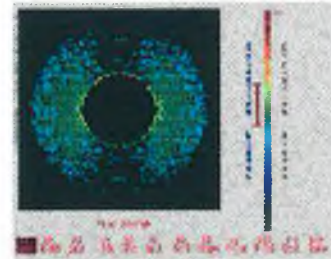
(C) An image showing the effect of the left "selection" arrow on the original image.
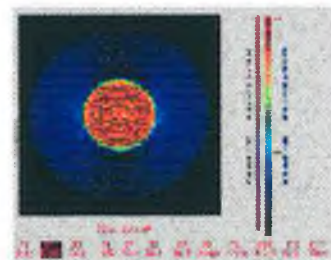
(D) An image showing the effect of the right "expansion" arrow on the original image.
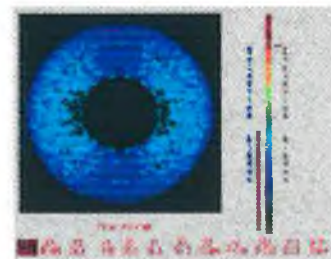
(E) An image showing the result when the effects of both arrows are combined.
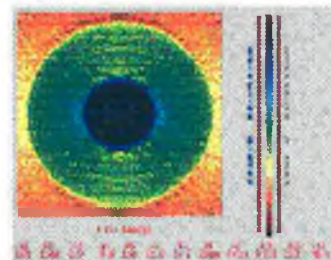
(F) The original image displayed using the inverted colour scale.

Figure 5.14

Various images showing the effects of some of the image processing functions available in the display program.

the colour - selection display scale and the colour - selection expansion scale. The first of these displays only the range of colours between the ends of the arrows on the left arrow. This function is shown in figure 5.14c. The second of the functions expands out the range of colours / values selected by the right arrow into the full scale of colours and displays either the full scale or just that portion selected by the left arrow, figure 5.14d, 5.14e.

The two routines shown on pages 19 - 20, displays the image in either 63 colour levels or 16 grey shades. All manipulation functions work in either of these two modes.

The next routine, *Blur the Display* (pp. 20 - 21), produces an effect similar to viewing the image slightly out of focus. This is useful in aiding viewing of small low-contrast objects contained on a noisy background. The effect is implemented as follows. First the M x M image array is copied into a 3M x 3M array, with each original pixel value being copied into 9 pixels in the new array. A 3 x 3 smoothing matrix is convolved with the new array to yield the new blurred image. This new image is then displayed.

-1	-1	-1
2	2	2
-1	-1	-1

Horizontal Line Detection

-1	0	1
-2	0	2
-1	0	1

followed by

-1	-2	-1
0	0	0
1	2	1

yields the GRADIENT image, ie. the first derivative of the image which gives good detection of edges.

Figure 5.15

Depiction of some commonly used edge and line detection matrices. These are convolved with the initial image.

The routine *Detect the Edges of the Image* (pp. 22 - 24) allow the user to convolve a 3 x 3 matrix with the image matrix. The values of the 3 x 3 matrix have to be inputted by the user and the matrix can convolve with either the original image or the previous convolved image. By selecting the array, various functions can be performed, eg. figure 5.15.

The routine to *sharpen the image* (pp 24 - 25) causes a point - detection matrix to be convolved with the image to reverse the operation of the blurring algorithm. It calls the function *sharpenimage( )* to perform this operation.

During the program, pressing F12 causes selection of the function - key menu to toggle between two sets of options. This is carried out by the routine shown on page 25. When menu 1 has been selected, F6 will cause screen 1 to be displayed and F7 causes screen 2 to be displayed.

It is sometimes helpful to invert the colour / grey - shade scales such that high values are represented by normally low value colours / grey-shades. The routine to perform this is shown on page 26 and it's effect is shown in figure 5.14f.

The next routine *Read Normalised CT Numbers* calls the function *procmouse( )* which displays the mouse cursor on the screen and allows particular pixel coordinates to the read. Also, by selecting a known air region, the routine can display approximate CT values for the image. The function procmouse() is given on page 47.

The routines shown on pages 27 and 28 enable the image to be displayed using an exponential or logarithmic colour / grey-shade scale. These functions are useful to see small changes contained in either the top end or bottom end of the scale.

If the image has been modified or processed in any way, the routine shown on pages 28 - 29 will redraw the original unprocessed image. Also, the image display usually accounts for approximately two-thirds of the available screen size. The function shown on page 29 will display an image on the full screen size while not displaying any menus or colour shades.

The *Multi File Display* routine shown on pages 29 - 31 will allow up to four images to be viewed on screen simultaneously. Each image is viewed at approximately one third its original size. This facility is extremely useful when comparing similar images. The next function shown on pages 31 - 35 allows two images to be subtracted from one another. The two images are first normalised to between 0 and 1 and then subtracted pixel by pixel. The resultant array is then normalised and displayed as normal. The function also contains the ability to move one of the images before subtraction by any number of pixels in any direction.

This marks the end of the main body of the program. The subroutines shown on pages 35 - 51 are those called by the main body of the program to perform the processing function mentioned above. These include the display routine, the function - key names and the mouse driver routines.

5.5   *Experimental Results.*

5.4.1   Monochromatic Results.

In this section the results predicted by the monochromatic equation (eqn 4.14) will be verified experimentally. Two separate elements will be imaged at different number of incident photons using two different methods of verification. In the first case the one concentration will be imaged at three different values of f. The image at the low value should not be visible, the image at the medium value should just be visible and the image obtained at the high f value should be well visible. In the second case three different concentrations will be imaged at the one f value. Again the low concentration should not be visible, the medium concentration just visible and the high concentration definitely visible.

In both of these cases the total incident count was in the range 1E7 to 1E8 photons. In all cases (both monochromatic and K-edge) the number of projections was 44 with the step size being 1 mm. This corresponds to an incident count per beam of approximately 26000. With the narrow energy bands selected on the multi-channel analyser, and taking into account the count rate limitations of section 5.2.7, this corresponded to a counting time of approximately 1000 sec per beam. For a complete scan , ie. 44 steps each with 44 rotations, this would entail a scan time of 540 hrs or 22 days per scan. In an attempt to alleviate this excessive time requirement, the following procedure was adopted.

Only one linear scan was performed with no rotations. Since the object is cylindrically symmetric this data set was used 44 times with noise added to each of the data sets using the poisson noise algorithm described in section 3.3.3. This cut the scan time down to 13 hours. Running at lower incident count rates would result in larger concentrations necessary for visibility. This caused problems in regard to the solubility of the analyte. Although this method proved adequate it has one

172

major drawback. A statistically low count at one of the step positions resulted in a ring being formed in the final image due to this statistically low value being taken as the 'true' value and having poisson noise added. These ring artifacts are obvious to some degree in all the images. *Note: All data regarding mass attenuation coefficients are obtained from published tables* [03] *and the extrapolation program provided by C. Markham.*

CASE 1: Here sodium tungstate (NaW) was imaged at 25 keV using the monochromatic method of scanning. First the multichannel analyser / detector / amplifier combination was calibrated with the variable x-ray fluorescence source (Amersham AMC.2084 Am^{241}) using the K_α lines of terbium (44.23 keV) and molybdenum (17.44 keV). With the MCA calibrated and energy band of approximately 200 eV wide was set up as a region interest. Three scans were performed at f=0.2, f=0.4 and f=0.6 with no analyte present. From these scans it was known that the total number of incident photons for a complete scan was 6E7, The following are the results and calculations obtained from eqn. 4.14 and 4.32 to calculate the necessary concentration of NaW needed for visibility at f=0.4. *Note: Q was assigned the value 11 as per results from the simulations.*

$$S = 44, \ N_{ot} = 6E7, \ \mu_m = 0.0523 \ m^2/kg$$
$$\text{Therefore} \quad \Delta U \ (f=0.4) = 3.0 \quad (\text{from eqn. 4.14})$$

NaW: Na – $\mu_1 = 0.113 \ m^2/kg$ R1 = 0.112

W – $\mu_2 = 3.627 \ m^2/kg$ R2 = 0.888

$$\Rightarrow \quad \text{Conc.} = M_t/V = \frac{\Delta U}{\sum R_i \mu_i} = 3.0/2.053 = 1.34 \ mg/cc$$

Three scans were now performed at f=0.2, f=0.4 and f=0.6 with this concentration (1.3 mg/cc NaW) present in the inner cone, see figure 5.09. These six data sets were then transferred to the Archimedes computer where they were converted into a 44 x 44 data point sets with poisson noise being added to each set. The corresponding data sets
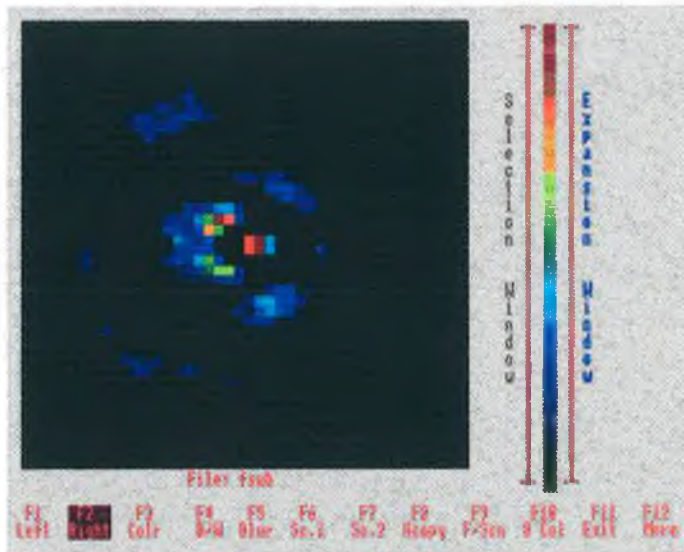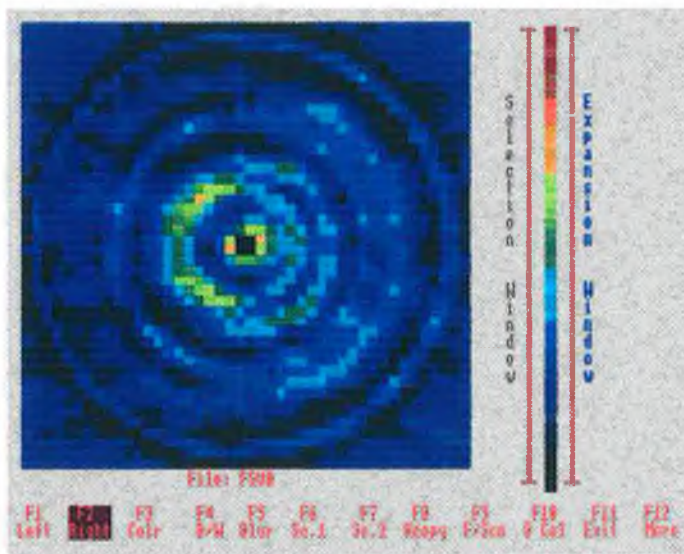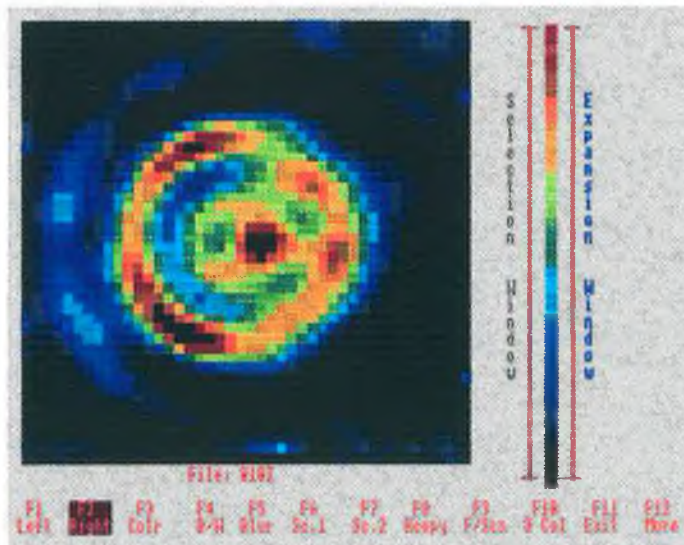
Figure 5.16

Three experimental scans of one concentration (1.3 mg/cc NaW) at various inner cylinder diameters. A: f=0.2, B: f=0.4 and C: f=0.6. These results are for S=44, Nₒₜ =6.0E7, @ 25keV. Water matrix. These scans are obtained using the monochromatic method of scanning.
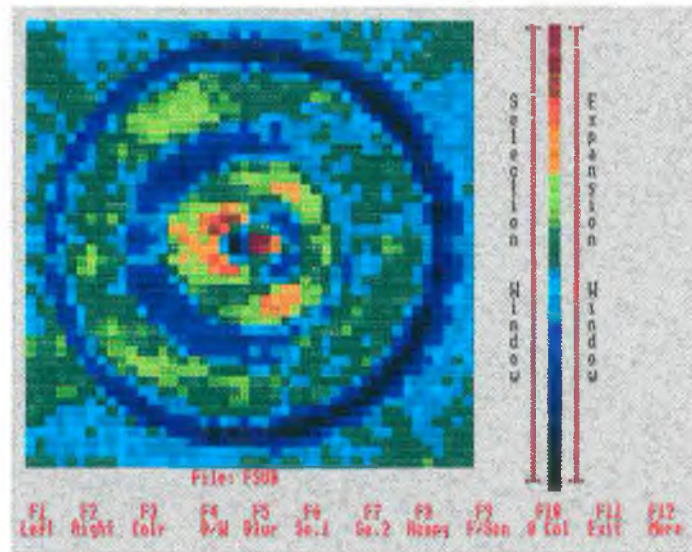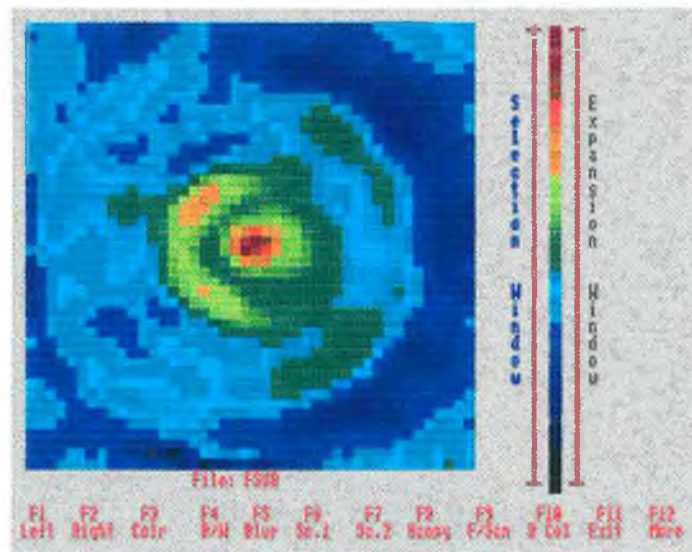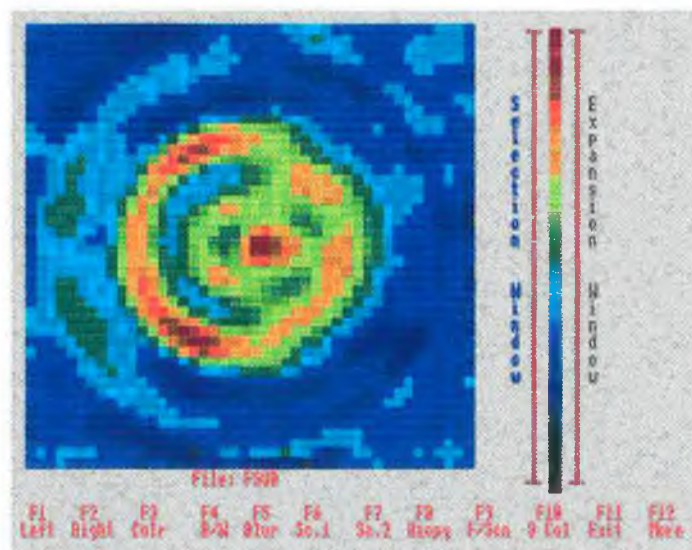
Figure 5.17
Three experimental scans of one concentration (1.3 mg/cc NaW)
at various inner cylinder diameters. A: f=0.2, B: f=0.4 and C: f=0.6.
These results were obtained using the monochromatic method of
scanning with S=44, N_{ot} = 6E7.

were then subtracted and reconstructed to yield the images shown in figure 5.16.

It is obvious from figure 5.16c that the image obtained at f=0.6 is clearly visible and it could be said from figures 5.16a and 5.16b that f=0.2 is not visible and f=0.4 is just visible. However, present in all images are ring artifacts caused by a statistically low point in the original data set. Also present in the images are artifacts that occur due to misalignment of the two data sets that were subtracted. Shifting of the data to reduce this misalignment was performed and the images shown are the best achievable results. In an attempt to determine whether at f=0.2 the image is purely due to ring artifacts, and at f=0.4 the image is due to the contrast agent and not ring artifacts, the following procedure was followed. First the image data was scaled to between 0 and 1 for display. This has the effect of increasing the information contained in the background and lessening the effect of one or two high pixel values on the original scaling. Secondly, the image will be smoothed slightly to try and enhance large scale structure (ie. contrast agent) and smear out small scale structure (ie. ring artifacts). The results of these processes are shown in figure 5.17. It can be seen from figure 5.17b that the f=0.4 image is now just visible compared to the background whereas in figure 5.17a no definite image of f=0.2 could be observed in comparison to the large noisy background.

Case 2: In this case three different concentrations will be scanned at the same f value, ie. f=0.5. Potassium iodide (KI) was imaged at 27 keV with the total number of incident photons being 3.5E7. The number of projections will remain at 44. Again image subtraction is performed with a no-analyte scan being carried out prior to the analyte scans. The following are the calculations to determine what is the necessary concentration of KI for visibility at f=0.5.

At 27 keV, $\mu_m = 0.0455 \text{ m}^2/\text{kg}$

$\Rightarrow$ $\Delta U = 2.5$ is necessary for visibility

176
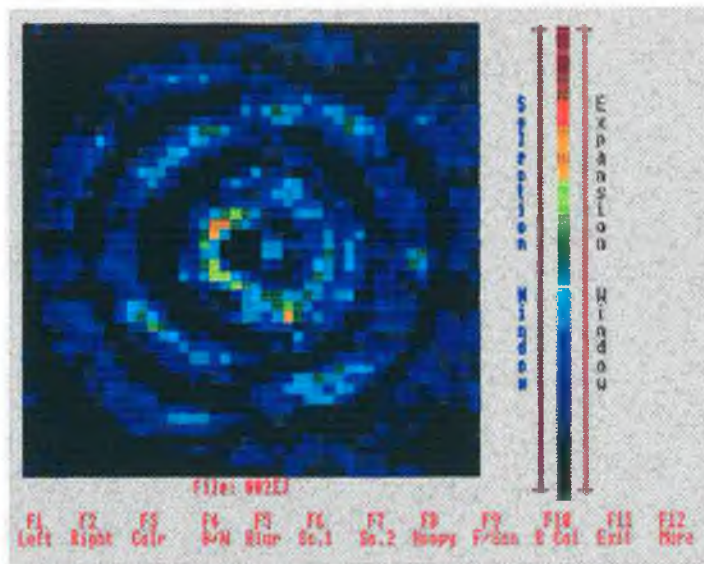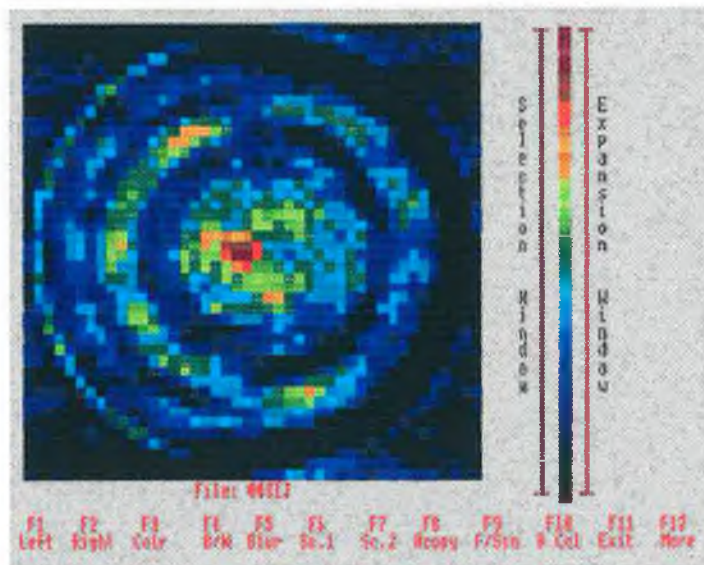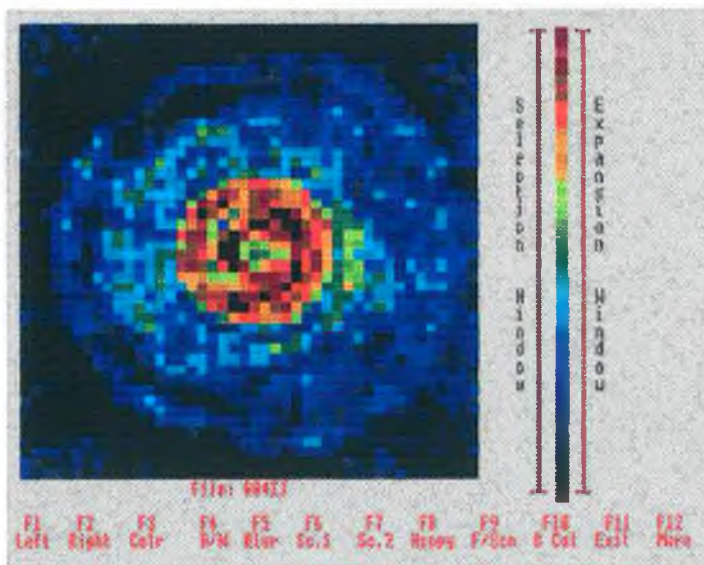
Figure 5.18
Three scans performed with three different concentrations at the same inner cylinder size, ie. f=0.5. A: 1.00mg/cc KI, B: 2.5 mg/cc KI, and C: 4.0 mg/cc KI. S=44, N_{ot} =3.5E7 @ 27 keV. These scans are obtained using the monochromatic method of scanning.

KI: K - μ_1 = 0.453 m^2/kg   R$_1$ = 0.236

            I - μ_2 = 1.103 m^2/kg   R$_2$ = 0.764

     ⇒   Conc. = 2.5/0.95 = 2.63 mg/cc KI

Therefore three scans will be performed at

ΔU   =   1.0   -   conc. =   1.05 mg/cc

ΔU   =   2.5   -   conc. =   2.63 mg/cc

ΔU   =   4.0   -   conc. =   4.20 mg/cc

Figure 5.18 shows the results of these scans. It is obvious from figure 5.18a that the concentration of 1.05 mg/cc is not visible. Figure 5.18b shows the concentration of 2.63 mg/cc just visible and the concentration of 4.2 mg/cc is clearly visible in figure 5.18c. No image processing was performed except shifting of the data to decrease the misalignment of the two data sets for subtraction.

5.4.2   K-edge Results.

In this section the results predicted by eqn. 4.48 are checked experimentally. Two different situations are studied using different elements as the analyte. In both cases two energy bands above and below the K absorption edge of the element were selected on the multichannel analyser. The counts from the two low bands were used to extrapolate to the count on the low side at the K-edge. This processes was repeated to yield the high side K-edge count. These counts were subtracted to yield the data attributable only to the analyte, ie. the difference in counts when scanning only the matrix should be negligible in comparison. Since only one scan is performed, no misalignment between the two data sets (above and below the K-edge) exists. This should significantly reduce ring artifacts. However other artifacts that exist in both the monochromatic and K-edge scans now become apparent. These artifacts are due to the misalignment of the centre of the scan with the centre of rotation. Again these artifacts can be reduced by shifting the subtraction data.
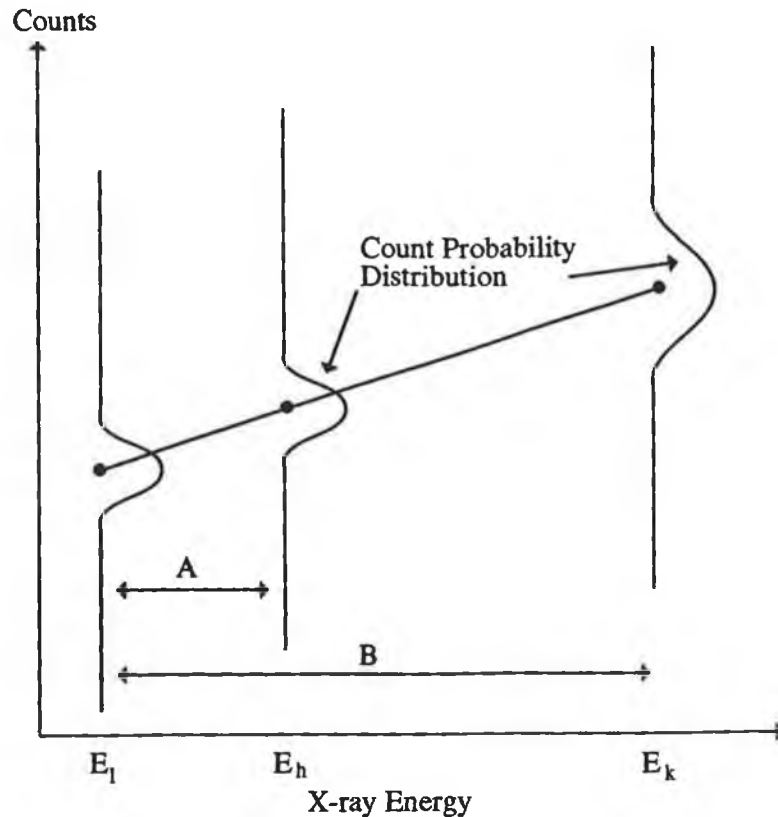
Figure 5.19
Extrapolation of the statistical variation in the photon counts in the two narrow energy bands, E_l and E_h, to the K-edge, E_k. The standard deviation in the extrapolated value is a factor G times the standard deviation in the narrow energy bands. G is given by the ratio B/A.
(McCarthy, "A study of the imaging of atomic elements by computerised axial tomography.")

McCarthy found that the factor G was given by the ratio B/A [04], see figure 5.19, where B is the distance in keV between the low energy band and the K-edge and A is the distance between the two energy bands used. For both cases studied using this method, the factor G was approximately equal to 1.9. This was therefore the value used in equation 4.48 in determining the minimum concentration.

Case 3: Here cadmium, forming part of the chemical cadmium sulphate, was imaged at 26.7 keV. Three different concentrations were imaged at an f value of 0.4. The

following are the theoretical predictions as obtained from eqn. 4.48, for the minimum concentration that is visible at f=0.4.

$$S = 44, \; N_{ot} = 1E8, \; \mu_{al} = 0.794 \; m^2/kg,$$
$$\mu_{ah} = 5.265 \; m^2/kg, \; \mu_{m} = 0.0465 \; m^2/kg$$

Eqn. 4.48 predicts concentration = 0.7 mg/cc of Cd. Cadmium forms part of the chemical cadmium sulphate (crystals), ie. $3CdSO_4.8H_2O$.

⇒   0.7 mg/cc ≡ 1.6 mg/cc of cadmium sulphate.

Three scans were performed at concentrations of 3.6 mg/cc, 1.6 mg/cc and 0.7 mg/cc of cadmium sulphate. The results are shown in figure 5.20. It is clear from these images that the lower concentration is not visible, the middle concentration is just visible and the high concentration is clearly visible. This is again in good agreement with the predicted results.

Case 4: In the final situation studied, silver nitrate was imaged at 25.5 kev (the K-edge of silver) using three different numbers of total incident photons. The object was imaged at f=0.7 and S=44. The total number of photons used was 1E6, 1E7 and 1E8. The following are the predicted results.

$$S = 44, \; N_{ot} = 1E7, \; \mu_{al} = 0.872 \; m^2/kg,$$
$$\mu_{ah} = 5.895 \; m^2/kg, \; \mu_{m} = 0.0505 \; m^2/kg$$

Equation 4.48 predicts a concentration of 1.26 mg/cc of silver necessary for visualisation. The silver forms part of the chemical silver nitrate which must be dissolved in distilled water as it precipitates out the chlorine in tap water as silver chloride.

⇒   1.26 mg/cc of silver ≡ 2.34 mg/cc of $AgNO_3$

The results are shown in figure 5.21. Again it is clear that the trend in visibility follows that which is predicted theoretically with the image for N_{ot} = 1E6 not being visible, the image at N_{ot} = 1E7 being just visible
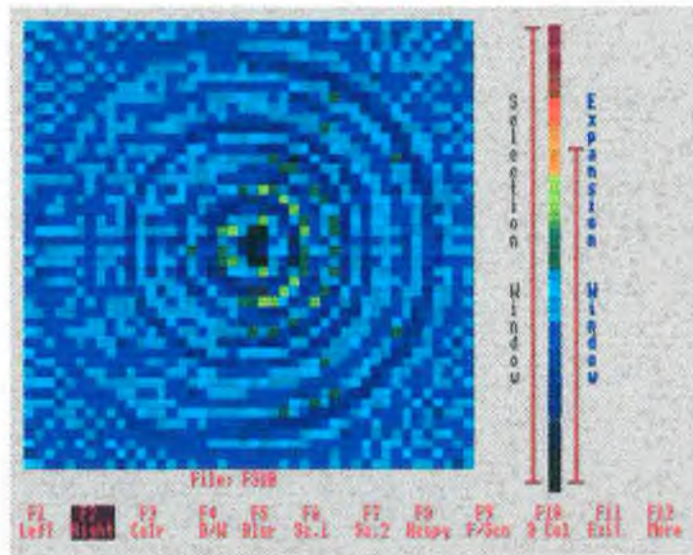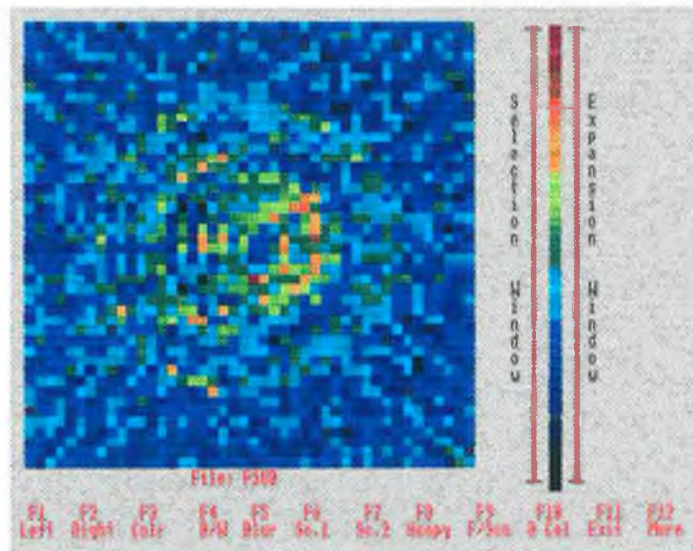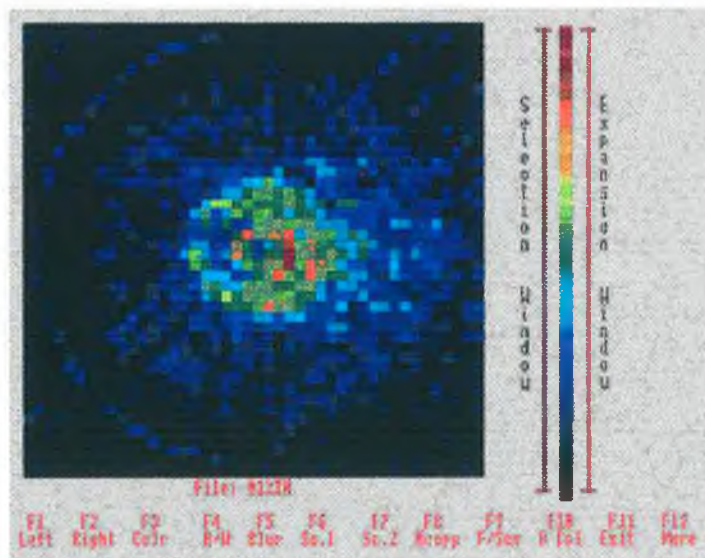
Figure 5.20
Three scans performed using the K-edge technique on Cadmium.
Here f=0.4, S=44 and N$_{ot}$ = 1E8 photons. A: 0.7 mg/cc, B: 1.6 mg/cc
and C: 3.6 mg/cc of cadmium sulphate. These images are obtained
using the K-edge method of scanning.
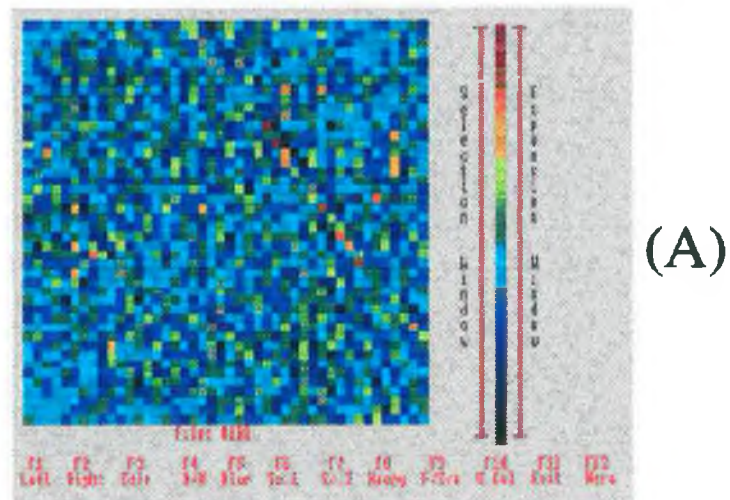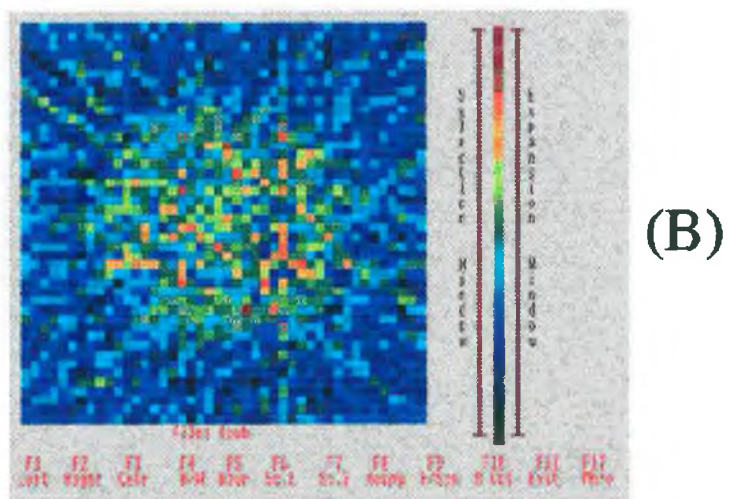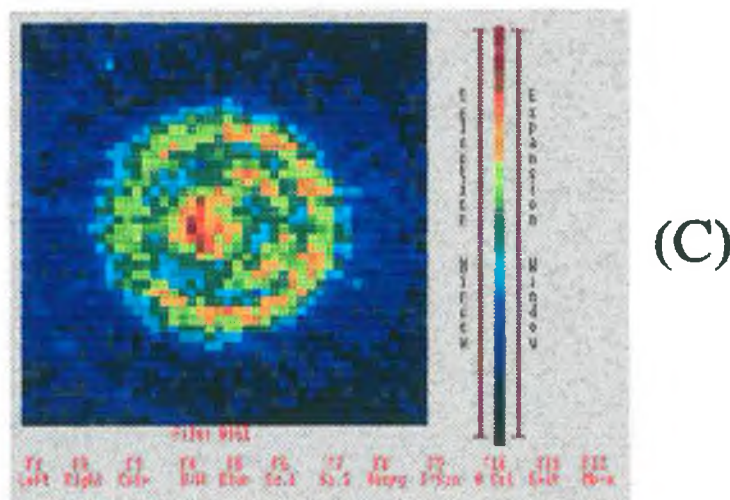
Figure 5.21
Three scans performed on the one concentration (2.3 mg/cc
AgNO₃) at f=0.7 with three different number of incident photons.
A: N_{ot} = 1E6, B: N_{ot} = 1E7 and C: N_{ot} = 1E8. These images are
obtained using the K-edge technique.

and the image at N_{ot} = 1E8 being clearly visible. For the image with N_{ot} = 1E6, a complete scan was performed, ie 44 steps each with 44 rotations as the counting time was only 14 sec per position. It is obvious that no ring artifacts are present.

5.5 *Summary*

In this chapter the theoretical predictions of the monochromatic case, described by eqn. 4.14, and the K-edge case, eqn. 4.48, were checked experimentally. In the situations studied good agreement existed between the theoretical, simulation and experimental results. It was not possible / practical to investigate all the parameters associated with eqns. 4.14 and 4.48, the two reasons being scan time limitations and experimental apparatus. Ideally the predictions should be verified at various numbers of projections / rotations and at a greater range of energies than could be achieved. Nevertheless, the ability of the equations to predict the minimum concentration of an element that is visible has been proven to be good in the range of situations studied. This is bearing in mind that the equations were developed with no initial assumptions as to the values of the various parameters.

References

[01] Fenelon, A.G.,
"X-ray Scanning Machine for Imaging Atomic Elements.",
M.Sc. Thesis, Dublin City University, 1988.

[02] Tsoulfandis, N.,
"Measurement and Detection of Radiation", McGraw-Hill, New
York, 1983.

[03] Hubble, J.H.,
"Mass Attenuation and Energy Absorption Coefficients from
1 keV to 20 MeV.", In. Jour. Appl. Rad. Isot., Vol. 33.,
pp. 1269-1290, 1982.

[04] McCarthy, K.J.,
"A Study of the Imaging of Atomic Elements by Computerised
Axial Tomography".
Ph.D. Thesis, Dublin City University, 1989.

Chapter VI

Conclusion and future work.

This thesis deals with the suitability of various atomic elements as radiographic contrast agents when used in contrast-enhanced computerised tomography. Iodine is almost universally used as a contrast agent in CT. However the results obtained in the course of this work show that for the energies associated with CT imaging, iodine is not the best element to use in terms of the concentration needed for visibility.

In the first case studied, the results clearly show that in CT scans of an object, which is approximately the size of the myocardium contained in the thorax, the greatest sensitivity is for gadolinium. This would suggest that the contrast agent Gd-DTPA, as used in MRI, has the potential for use in CT imaging. Several situations were studied including fixed monochromatic-energy scans with image subtraction, K-edge subtraction using monochromatic beams, single polychromatic scans (the normal medical CT imaging method) and two polychromatic scans with image subtraction. It was shown that a single polychromatic scan is approximately 80 times less sensitive than the monochromatic scans with image subtraction with the analyte evenly dispersed throughout the phantom. However if image subtraction is used with polychromatic scans of the myocardium, it will give about a 30 fold increase in sensitivity over the single polychromatic scan case.

The above results were obtained for the case of imaging the myocardium. In the second case studied, equations were derived that yielded the minimum concentration required for a particular element, when used as a contrast agent in a cylinder contained inside a

larger cylinder of some matrix. The equations take into account that the two cylinders can be of any absolute or relative size. They also accounted for the total number of incident photons, the number of projections and the energy used for the scan. Two situations were studied: 1) monochromatic scans at any energy with image subtraction and 2) K-edge scans across the K-absorption edge of the contrast agent. Thus the work can be used to estimate the concentration of an element necessary for visualisation in different size organs, blood vessels, etc.

The results show that as the size of the inner cylinder decreases, the most optimum element shifts to high atomic number transition elements. Another important result was that at low values of this inner cylinder diameter, the difference in sensitivity between iodine and gadolinium increases dramatically, making the case for using Gd-DTPA, a known biologically tolerated contrast agent, stronger. The results of this work were extensively checked by computer simulations and by experimental scans on a cylindrical phantom.

The results presented in this thesis therefore show that iodine is not the best element to use as a contrast agent in contrast-enhanced CT. Gadolinium, or other transition elements, are better suited in regards to the concentration required. It must be pointed out however that this result is only applicable to physical characteristics and this result does not take into account biological constraints, availability or cost.

Future Work: It has been previously stated that image subtraction using two polychromatic scans gives a 30 fold increase in sensitivity. This has not been performed in practice and would require modification of an existing CT scanner. However this is indeed possible and a similar technique in conventional radiography, Digital Subtraction Angiography, is used extensively with excellent results. To perform this routine, two scans are performed on the patient, one with and one without the contrast agent. The two data sets are subtracted and the resultant data set reconstructed to yield an image of the contrast agent

alone. Any patient movement between scans would introduce artifacts into the image.

A second technique that should be attempted is dual element subtraction imaging. Here two contrast agents are administered to the patient via the blood supply. The blood accumulates in the heart. Only one of the contrast agents, agent A, can cross the boundary and remain resident in the heart wall. Two CT images are obtained; one of element A alone and one of element B alone using K-edge imaging. Since element A will be contained in the heart and heart wall and element B will be contained only in the heart blood, subtraction to these two images will yield a sharper image of the heart wall that if only element A were imaged. This has not been attempted.

ACKNOWLEDGMENTS

List of Appendices

Appendix 1:   Computer Programs

Appendix 2:   Glossary of Medical terms.

Appendix 3:   Altered equations to account for object
                extent.

Appendix 4:   MRI Imaging methods.

Appendix 5:   Reconstruction algorithms and associated
                maths.

Appendix 6:   Radiation detectors.

Appendix 7:   Mass attenuation coefficients and periodic
                table of elements.

Appendix 1
Computer Programs

TRANSFER

```
10 REM The following program accepts and saves data or
20 REM reads and sends data to or from the Archimedes
30 REM or the BBC.
40 CLS
50 MODE 0
60 P.:P.:INPUT "Is this the receiver or sender (S/R):";A$
70 IF A$="R" THEN GOTO 100 ELSE GOTO 250
80 GOTO 50
90 CLS
100 P.:P.:INPUT "Input the name of the saved file: ";NAME$
110 *FX7,5
120 *FX2,1
130 XX=OPENOUT NAME$
140 FOR T=1 TO 1600: REM Number of points
150    INPUT "" GHJ$
160    IF GHJ$="" GOTO 150
170    PRINT#XX, GHJ$
180 NEXT T
190 CLOSE#0
200 GOTO 320
210 CLS:P.:P.
220 INPUT "Input the name of the file to be sent:";NAME$
230 *FX8,5
240 *FX3,1
250 XX=OPENIN NAME$
260 FOR C=1 TO 1600
270    INPUT#XX,FGJ
280    PRINT FGH
290 NEXT C
300 CLOSE#0
310 PRINT "*FX2":*FX3
320 END
```

c.ConvertBBC

```
/*********************************************************/
/*                                                       */
/*      The following program converts BBC format random- */
/* access files to ASCII format data files written in C. */
/*                                                       */
/*              Written By: Adrian Geissel               */
/*                                                       */
/*********************************************************/


#include <stdio.h>
#include <math.h>
#include <Arthur.h>
#include <stdlib.h>
#include <float>
#include <string.h>
#include <time.h>

#define STRINGLEN 10

void main(void)
{


        int             i,f,ch,temp;
        signed int      loop,exponent,sign=+1;

        double          b[53000],maxx.beebreal(FILE*);
        double          mantissa=0.0,result;

        char            Instring[STRINGLEN],abc[10];

        FILE            *beebfile,*fp;

        void            cls(void);


        abc[0]='S'; abc[1]='\0';
        cls();
        printf("\n\n\n\t File is non-ascii. Conversion taking
                place\n");
        printf("\n\tFile name will have an S appended too its
                name. \n\n\n");
        system("*.");
        printf("\n\n\n\nInput the file name: ");
        fgets(Instring,STRINGLEN,stdin);
        strncat(abc,Instring,7);
        fp = fopen(abc,"w");
        beebfile = fopen(Instring,"r");
        rewind(beebfile);
        if(beebfile==NULL)
        {
            printf("\tError opening input file %s",beebfile);
            exit(0);
        }
```

```
        i=0;
        fgetc(beebfile);
        maxx=beebreal(beebfile);
        fprintf(fp,"%f\n",maxx);
        while((ch=fgetc(beebfile))!=EOF)
        {
                for(loop=4;loop>=2;mantissa+=pow(0.00390625,
                    loop--)*fgetc(beebfile));
                temp=fgetc(beebfile);
                if (temp>128) sign=-1; else temp+=128;
                mantissa+=0.00390625*temp;
                exponent=fgetc(beebfile)-127;
                result=0.5*mantissa*pow(2,exponent)*sign;
                temp=0;
                loop=exponent=sign=+1;
                b[i++]=result;
                result=mantissa=0.0;
                fprintf(fp,"%f\n",b[i-1]);
                if(i>53000) {fclose(beebfile); exit(0);}
        }

        fclose(beebfile);
        fclose(fp);
        remove(Instring);
        free(b);
        system("*run p.testdisp");

}


double    beebreal(FILE *beebfile)
{

        signed int      loop,exponent,sign=+1;
        int             temp;
        double          mantissa=0.0,result;

        for(loop=4;loop>=2;mantissa+=pow(0.00390625,
            loop--)*fgetc(beebfile));
        temp=fgetc(beebfile);
        if(temp>128) sign=-1; else temp+=128;
        mantissa+=0.00390625*temp;
        exponent=fgetc(beebfile)-127;
        result=0.5*mantissa*pow(2,exponent)*sign;
        return(result);
}
```

3

```
/****************************************************/
/*                                                  */
/*   The following program yields an image for any sized */
/*     matrix using data in ASCII format. It uses the   */
/*             backprojection algorithm.            */
/*                                                  */
/*           Written By: Neil O'Hare                */
/*                                                  */
/****************************************************/


#include <stdio.h>
#include <math.h>
#include <Arthur.h>
#include <stdlib.h>
#include <float>
#include <string.h>
#include <time.h>

#define STRINGLEN 10

void main(void)
{

/*****************************************************/
/*                                                   */
/*    Declaration and initalisation of variables.    */
/*                                                   */
/*****************************************************/



        int       j,cc,dsa,t,n,p,i,k,r,s,ch,move;
        int       sl,rl,a,z,ff,rotate,step;
        int       tim,jj[2000],kk[2000],ind;

        float     fx[81][81],sum,vb,ill,ii,mean,top;
        float     ffr,minutes,minnl,minn2,maxx,mn[83];
        float     xl[4001],xx[81][81],l[4001],yy[81][81];
        float     f[161][161],corrct[4200],lambda[81][81];
        float     stp[4200],diff,vv[2000],standev,oldstd;
        float     theta,phi,cosphi,tanphi,range,cept,shift;
        float     xl,v,correct,correctl,x,y,jc,sum1,abd;

        double    cos(double),tan(double),fabs(float);
        double    log(double);

        FILE      *fp;

        char      Instring[STRINGLEN],buffer[3];


        j=cc=dsa=n=p=i=k=r=s=sl=rl=a=z=ff=rotate=step=tim=0;
        sum2=vb=ill=ii=mean=ffr=minutes=minnl=minn2=maxx=0.0;
        difstandev=oldstd=theta=phi=cosphi=tanphi=range=0.0;
        cept=xl=v=x=y=jc=sum1=correct=correctl=0.0;
```

4

```
for(i=1;i<2000;i++) { jj[i]=kk[i]=0; vv[i]=0.0; }
for(i=1;i<4200;i++) { corrct[i]=stp[i]=0.0;
for(k=1; k<=81;k++) {
                         mn[k]=0.0;
                         for(j=1;j<=81;j++)
                         {
                         fx[j][k]=xx[j][k]=yy[j][k]=0.0;
                         lambda[j][k]=0.0;
                         }

                      }
for(k=1;k<=4001;k++) l[k]=0.0;
for(k=1;k<=161;k++)
  for(j=1;j<=161;j++) f[j][k]=0.0;


/*****************************************************/
/*                                                   */
/*      Reading the data from the chosen file.       */
/*                                                   */
/*****************************************************/


cls();
system("*.");
printf("\n\n\n\tInput the file name:  ");
gets(Instring);

fp=fopen(Instring,"r");
rewind(fp);
ch=fgetc(fp);
if(ch==128) cc=2; else cc=1;
rewind(fp);
fclose(fp);

if(cc==2) system("*run p.convertbbc");
else
{
    fp=fopen(Instring,"r");
    i=1;
    rewind(fp);
    while((fscanf(fp,"%f",&xl[i++])!=EOF))
        { if(i>53000) {fclose(fp); exit(0);}}
    fclose(fp);
    top=sqrt(i*1.0);
    ind=(int)top;
    printf("\n\t--- File Now Closed ---\n\n\n");
}

maxx=0;
for(i=1;i<=ind*ind;i++)
{
    maxx=(xl[i]>maxx)?xl[i]:maxx;
}
for(i=1;i<=ind*ind;i++) l[i]=log(maxx/xl[i]);
cc=1;
maxx=0.0;
for(rotate=0;rotate<ind;rotate++)
  for(step=1;step<=ind;step++)
```

5

```
                xx[rotate][step]=l[cc++];

        for(j=1;j<=ind;j++)
            for(k=1;k<=ind;k++) yy[j][k]=0.0;
/****************************************************/
/*                                                  */
/*        Shifting the data by a chosen amount.     */
/*                                                  */
/****************************************************/
        printf("Input the shifting factor (ie, 0.5) :- ");
        scanf(" %f",&x1);
        shift=x1;
        correct=x1;
        if (correct>=0.0) dsa=-1; else dsa=1;
        correct=(correct<0.0)?(correct*-1.0):correct;
        correct1=1.0-correct;
        i=1;
        for(rotate=1;rotate<=ind;rotate++)
        {
            for(step=1;step<=ind;step++)
            {
              if((step+dsa)>ind) yy[rotate][step]=0.0;
              yy[rotate][step]=(correct1*xx[rotate][step])+
                            (correct*xx[rotate][step+dsa]);
              l[i++]=yy[rotate][step];
            }
        }




/*****************************************************/
/*                                                   */
/*           The Backprojection Algorithim.          */
/*                                                   */
/*****************************************************/
        i=1;
        for(r=0;r<=ind-1;r++)
        {
          for(t=((r*(ind+10))+1);t<=((r*(ind+10))+5;t++)
                stp[t]=0.0;
          for(t=((r*(ind+10))+ind+6;t<=((r*(ind+10))+ind+10);
                t++) stp[t]=0.0;
          for(t=((r*(ind+10))+6;t<=((r*(ind+10))+ind+5);t++)
                stp[t]=l[i++];
        }

        for(r=0;r<=ind;r++)
        {
          for(k=(rr*(ind+10))+6;k<=(r*(ind+10))+ind+5;k++)
            corrct[k]=(stp[k]*0.25) - ((stp[k-1]*0.101) +
                    (stp[k+1]*0.101)) - ((stp[k-3]*.0112)
                    + (stp[k+3]*.0112)) - ((stp[k-5]*.004)
                    + (stp[k+5]*.004));
        }
        for(r=0r<=ind;r++)
          for(k=(r*(ind+10))+6;k<=(r*(ind+10))+ind+5;k++)
            lambda[(k-(r*(ind+10)))-5][r]=corrct[k];
```

6

```c
theta=3.14159/(ind*1.0);
for(r=0;r<=ind-1;r++)
{
    phi=r*theta;
    cosphi=cos(phi);
    tanphi=tan(phi);
    if(r==(int)(ind/2.0))
    {
        for(s=1;s<=(ind*2);s++)
        {
            p=((s+1.0)/2.0);
            for(j=1;j<=(ind*2);j++)
                    f[s][j]+=(lambda[p][r]/(ind*2.0));
        }
        continue;
    }

    range=fabs(0.5/cosphi);
    if(range>ind) range=ind;
    for(s=1;s<=(ind*2);s++)
    {
        cept=((ind+0.5)-s)/cosphi;
        for(x=-(ind*1.0-0.5);x<=(ind*1.0+0.5);x++)
        {
            y=(x*tanphi)+cept;
            k=(int)(ind+1)+x;
            jc=(ind+1)*1.0-y;
            if((jc>(ind*2.0+7.0))||(jc<7.0)) continue;
            for(j=(jc-range);j<=(jc+range);j++)
            {
                if((j<0)||(j>(ind*2))) continue;
                p=((s+1.0)/2.0);
                f[k][j]+=(lambda[p][r]/(ind*2.0));
            }
        }
    }
    printf("   %d  ",r);
}


/*****************************************************/
/*                                                   */
/*        Saving the Reconstructed Image.            */
/*                                                   */
/*****************************************************/

    if(shift<0.0) shift*=-1.0;
    sl=(int)(shift*100.0);
    sprintf(buffer,"%d\n",sl);
    strcat(Instring,buffer);

    fp=fopen(Instring,"w");
    i=1;
    maxx=0.0;
    for(j=1;j<=(ind*2);j++)
     for(k=1;k<=(ind*2);k++)
         maxx=(f[k][j]>maxx)?f[k][j]:maxx;
```

```
        fprintf(fp,"%f\n",maxx);
        for(j=1;j<=(ind*2);j++)
          for(k=1;k<=(ind*2);k++)
            fprintf(fp,"%f\n",f[k][j]
        fclose(fp);
        cls();
        printf("\n\n\n\n\n\n\tFinished Backprojection\n\n");
        system("*run p.testdisp");

}
```

```
 10 *FX4,1
 20 CLS
 30 INPUT TAB(2,12) "Size of step in X direction (48/mm)",S
 40 CLS
 50 PRINT "Use Edit keys to position scan"
 60 PRINT "Small Step Up", CHR$(94)
 70 PRINT "Small step down", CHR$(86)
 80 PRINT "Change step size: ","C"
 90 PRINT "QUIT                    ","Q"
100 Q$=GET$
110  IF  Q$<>CHR$(&8B)  AND  Q$<>CHR$(&8A)  AND  Q$<>"Q"  AND
    Q$<>"C" THEN GOTO 40
120 IF Q$="Q" THEN GOTO 260
130 IF Q$="C" THEN GOTO 20
140 IF Q$=CHR$(&8A) THEN PROCDEF1
150 IF Q$=CHR$(&8B) THEN PROCDEF2
160 PROCSTEP(S)
170 *FX21,0
180 SOUND 1,-15,101,4
190 GOTO 40
200 DEF PROCDEF2
210 D=112:R=96
220 ENDPROC
230 DEF PROCDEF1
240 D=48:R=32
250 END PROC
260 *FX4,1
270 CLS
280 INPUT TAB(1,12) "Angle step size (3deg = 10pulses)",S
290 CLS
300 PRINT "Use edit keys to rotate scan"
310 PRINT "Clockwise Rotation", CHR$(93)
320 PRINT "Anticlockwise Rotation", CHR$(91)
330 PRINT "Change Angle Step",    "C"
340 PRINT "Return to X-Drive",    "R"
350 PRINT "            (QUIT) ",   "Q"
360 Q$=GET$
370  IF  Q$<>CHR$(&88)  AND  Q$<>CHR$(&89)  AND  Q$<>"Q"  AND
     Q$<>"C"  AND  Q$<>"R"  THEN GOTO 290
380 IF Q$="Q" THEN GOTO 460
390 IF Q$="C" THEN GOTO 270
400 IF Q$="R" THEN GOTO 20
410 IF Q$=CHR$(&89) THEN PROCROT1
420 IF Q$=CHR$(&88) THEN PROCROT2
430 PROCSTEP(S)
440 *FX21,0
450 GOTO 290
460 CLS
470 INPUT TAB(1,12) "Size of Z-Step (48 pulses/mm)",S
480 CLS
490 PRINT "Use edit keys to move table forward/backward"
500 PRINT "Table forwards ",CHR$(86)
510 PRINT "Table backwards",CHR$(94)
520 PRINT "Change step size ",    "C"
530 PRINT "Return to X-drive",    "X"
540 PRINT "Return to Y-drive",    "Y"
```

```
550 PRINT "     (QUIT)          ",     "Q"
560 Q$=GET$
570  IF  Q$<>CHR$(&8B)  AND  Q$<>CHR$(&8A)  AND  Q$<>"Q"  AND
       Q$<>"C"  AND  Q$<>"X"  AND  Q$<>"Y"  GOTO 480
580 IF  Q$="Q"  THEN  GOTO 870
590 IF  Q$="C"  THEN  GOTO 460
600 IF  Q$="X"  THEN  GOTO 20
610 IF  Q$="Y"  THEN  GOTO 270
620 IF  Q$=CHR$(&8B)  THEN  PROCROT1
630 IF  Q$=CHR$(&8A)  THEN  PROCROT2
640 PROCSTEP(S)
650 *FX21,0
660 GOTO 480
670 DEF PROCSTEP(S)
680 B=&FE60
690 ?(B+2)=255
700 FOR N=1 TO S
710 ?B=D
720 Q=TIME+5
730 REPEAT
740 UNTIL TIME>=Q
750 ?B=R
760 Q=TIME+5
770 REPEAT
780 UNTIL TIME>=Q
790 NEXT N
800 ENDPROC
810 DEF PROCROT1
820 D=14:R=12
830 ENDPROC
840 DEF PROCROT2
850 D=6:R=4
860 ENDPROC
870 *FX4,0
880 CLS
890 END
```

```
/**********************************************************/
/*                                                        */
/*     Program to display and manipulate images, etc.     */
/*                                                        */
/*              Written By:  Neil O'Hare                  */
/*                                                        */
/**********************************************************/

#include <stdio.h>
#include <math.h>
#include <Arthur.h>
#include <float.h>
#incldue <stdlib.h>
#include <string.h>
#include <time.h>

#define   STRINGLEN   10
#define   PI          3.14159

void label(void);

int    flg;
int    beebint(FILE *);
float beebreal(FILE *);
char   *beebstring(FILE *,char *);

void main(void)
{
        int    f,g,ind,i,step,cc,ch,indm[4],pixel,dist;
        int    alenght1,alenght2,aheight1,aheight2;
        int    top1,top2,bottom1,bottom2,bfg,blur,choice;
        int    f1,f2,f3,f4,f5,f6,f7,f8,f9,f10,f11,f12;
        int    togglescreen,invert,fcount,multdisp,moved;
        int    xm,ym,bm,line,positon,sharp,stp,moveno;
        int    xx[100][100];

        float      a[200][200],maxx[4],x,b[45000],c[693][693];
        float      ii,d[4][200][200],maxs,mins,dmy[4][693];
        float      outside[3],mmm[3],e[260][260],grid[4][4];
        float      diff;

        double     angle;

        char       Instring[STRINGLEN],onelet;


        void       rectanglefill(int,int,int,int);
        void       arrow1(int,int);
        void       arrow2(int,int);
        void       icons1(int,int,int,int,int,int,int,int,int,
                        int,int,int,char *);
        void       icons2(int,int,int,int,int,int,int,int,int,
                        int,int,int,char *);
        void       gcol(int,int);
        void       mode(int);
        void       cls(void);
```

11

```
void       tab(int,int);
void       tint(int,int);
void       colour(int);
void       cursor(int);
void       vduq(int,int,int,int,int,int,int,int,int);
void       palette(int,int,int,int,int);

int        inkey(int);
int        mouseX(void);
int        mouseY(void);
int        mouseB(void);

char       findfile(int,int);
```

```
/*******************************************************/
/*                                                     */
/*         Initial Declaration and RMA setup.      */
/*                                                     */
/*******************************************************/

system("*configure screensize 12");
vduq(23,1,0,0,0,0,0,0,0);
mode(15);

while(1)
{

f1=f2=f3=f4=f5=f6=f7=f8=f9=f10=f11=f12=1;
toglescreen=invert=step=ind=multdisp=sharp=blur=1;
fcount=0;
for(f=1;f<=260;f++) for(g=1;g<=260;g++) e[f][g]=0.0;

mode(0);
cls();
system("*.");
printf("\n\n\n\tInput the file name: ");
fgets(Instring,STRINGLEN,stdin);
```

```
/*******************************************************/
/*                                                     */
/*         Select file type and input data.        */
/*                                                     */
/*******************************************************/

if((fp=fopen(Instring,"rb"))==NULL)
{
    cls();
    printf("ERROR - cannot open file");
    system("*run p.testdisp");
}
rewind(fp);
ch=fgetc(fp);
if(ch==128) cc=2; else cc=1;
fclose(fp);
```

12

```
        if(cc==2)
        {
            free(a); free(b); free(c); free(d);
            system("*run p.convertbbc");
        }
        else
        {
            system("*fx113,1");
            system("*fx112,1");
            mode(15);
            cls();
            colour(12);
            tab(20,12);
            printf("Loading Data");
            cousor(0);

            fp=fopen(Instring,"r");
            i=0; rewind(fp);
            fscanf(fp,"%f",&maxx[1]);
            while((fscanf(fp,"%f",&b[i++]))!=EOF)
            { if(i>5300) {fclose(fp); exit(0); } }
            fclose(fp);
        }

/***********************************************************/
/*                                                         */
/*        Find Array size and Normalize data.         */
/*                                                         */
/***********************************************************/

    ii=i*1.0;
    x=sqrt(ii);
    int=(int)x;
    step=(int)(880.0/x);
    x=53.0/maxx[1];
    i=0;

    for(f=1;f<=ind;f++)
     for(g=1;g<=ind;g++)
      a[f][g]=b[i++];


/***********************************************************/
/*                                                         */
/*            Plot data on screen 2.                   */
/*                                                         */
/***********************************************************/

    system("*fx112,1");
    mode(15);
    vduq(23,17,2,0x00,0,0,0,0,0,0);
    tint(63,250);
    palette(63,16,250,250,250);
    colour(128+63);
    cls();
    colour(3);
    tab(20,12);
    printf(" Processing ");
    system("*fx112,2");
```

```
         cls();
         top1=top2=53;
         bottom1=bottom2=1;
         for(f=1;f<=ind;f++)
          for(g=1;g<=ind;g++)
           c[f][g]=a[f][g]*x;
         bfg=1;
         if(invert==1) display(c,top1,bottom1,top2,bottom2,ind
                              ,step,bfg,blur,fcount,sharp);
         if(invert==2) invdisplay(c,top1,bottom1,top2,bottom2,
                              ind,step,bfg,blur,fcount,sharp);
         system("*fx113,2");
         if(f12==1)  icons1(f1,f2,f3,f4,f5,f6,f7,f8,f9,
                              f10,f11,f12,Instring);
         else        icons2(f1,f2,f3,f4,f5,f6,f7,f8,f9,
                              f10,f11,f12,Instring);

         vduq(23,1,0,0,0,0,0,0,0,0);
         toglescreen=2;
         aheight1=136;
         aheight2=136;
         alength1=850;
         alength2=850;
         arrow1(alength1,aheight1);
         arrow2(alength2,aheight2);
         blur=1;
         flg=1;

while(1)
{

/***********************************************************/
/*                                                         */
/*          Move image and Save result.                    */
/*                                                         */
/***********************************************************/

         if((f12==2)&&(inkey(-21)))
         {
           moveno=0;
           moved=0;
           f4=2;
           if(f12==1) icons1(f1,f2,f3,f4,f5,f6,f7,f8,f9,
                              f10,f11,f12,Instring);
           else        Icons2(f1,f2,f3,f4,f5,f6,f7,f8,f9,
                              f10,f11,f12,Instring);
           while(1)
           {
             tab(70,9); printf("<== ==>");
             tab(69,12);printf("No = %d ",moveno);
             tab(70,15);printf("%c  v"94);
             tab(69,18);printf(No. = %d ",moved);

             if(inkey(-122))
             {
               moveno++;
               for(f=1;f<=ind;f++)
               {
```

14

```c
        for(g=1;g<=ind-1;g++) d[1][f][g+1]=a[f][g];

        d[1][f][1]=a[f][ind];
    }
    for(f=1;f<=ind;f++)
     for(g=1;g<=ind;g++) a[f][g]=d[1][f][g];
}

if(inkey(-26))
{
   moveno--;
   for(f=1;f<=ind;f++)
   {
       for(g=2;g<=ind;g++) d[1][f][g-1]=a[f][g];
       d[1][f][ind]=a[f][1];
   }
   for(f=1;f<=ind;f++)
    for(g=1;g<=ind;g++) a[f][g]=d[1][f][g];
}

if(inkey(-42))
{
   moved++;
   for(g=1;g<=ind;g++)
   {
       for(f=1;f<=ind-1;f++) d[1][f+1][g]=a[f][g];
       d[1][1][g]=a[ind][g];
   }
   for(f=1;f<=ind;f++)
    for(g=1;g<=ind;g++) a[f][g]=d[1][f][g];
}

if(inkey(-58))
{
   moved--;
   for(g=1;g<=ind;g++)
   {
       for(f=2;f<=ind;f++) d[1][f-1][g]=a[f][g];
       d[1][ind][g]=a[1][g];
   }
   for(f=1;f<=ind;f++)
    for(g=1;g<=ind;g++) a[f][g]=d[1][f][g];
}
for(i=1;i<=1e4;i++);
if(inkey(-74)) break;
}

for(f=1;f<=ind;f++)
 for(g=1;g<=ind;g++) a[f][g]=d[1][f][g];
fp=fopen("MOVED","w");
fprintf(fp,"%10.6f\n",maxx[1]);
for(f=1;f<=ind;f++)
for(g=1;g<=ind;g++) fprintf(fp,"%10.6f\n",a[f][g]);
fclose(fp);

f4=1;
if(f12==1) icons1(f1,f,f3,f4,f5,f6,f7,f87,f9,
                  f10,f11,f12,Instring);
else       icons2(f1,f2,f3,f4,f5,f6,f7,f8,f9,
                  f10,f11,f12,Instring);
```

15

```
        x=53.0/maxx[1];

        for(f=1;f<=ind;f++)
          for(g=1;g<=ind;g++) c[f][g]=a[f][g]*x;
        if(invert==1)    display(c.top1,bottom1,top2,
            bottom2,ind,step,bfg,blur,fcount,sharp);
        if(invert==2) invdisplay(c.top1,bottom1,top2,
            bottom2,ind,step,bfg,blur,fcount,sharp);
        colour(128+63);
        tab(70,9);  printf("                    ");
        tab(70,15); printf("                    ");
        tab(69,12); printf("                    ");
        tab(69,18); printf("                    ");
      }


/****************************************************/
/*                                                  */
/*           Left Arrow Selection Key.              */
/*                                                  */
/****************************************************/

      if((inkey(-114))&&(f12==1))
      {
        flg=1;  f1=2;  f2=1;
        label();
        if(f12==1) icons1(f1,f,f3,f4,f5,f6,f7,f87,f9,
                          f10,f11,f12,Instring);
        else       icons2(f1,f2,f3,f4,f5,f6,f7,f8,f9,
                          f10,f11,f12,Instring);
      }

      if(inkey(-55)) {system("*fx15,0"); break;  }


/****************************************************/
/*                                                  */
/*           Right Arrow Selection Key.             */
/*                                                  */
/****************************************************/

      if((inkey(-115))&&(f12==1))
      {
        flg=1;  f1=1;  f2=2;
        label();
        if(f12==1) icons1(f1,f,f3,f4,f5,f6,f7,f87,f9,
                          f10,f11,f12,Instring);
        else       icons2(f1,f2,f3,f4,f5,f6,f7,f8,f9,
                          f10,f11,f12,Instring);
      }

/****************************************************/
/*                                                  */
/*           Right Arrow Control Keys.              */
/*                                                  */
/****************************************************/

      if(inkey(-58)&&flg==2&&f12==1)
      {
        aheight2+=3;
```

```
        if((aheight2+alength2)>980) aheight2=980-alength2;
        arrow2(alength2,aheight2);
      }

      if(inkey(-42)&&flg==2&&f12==1)
      {
        aheight2-=3;
        if(aheight2<136) aheight=136;
        arrow2(alength2,aheight2);
      }

      if(inkey(-122)&&flg==2&&f12==1)
      {
        alengh2+=3;
        if(alength2>830) alength2=830;
        if((alength2+alenght2)>980) aheight2=980-alength2;
        arrow2(alength2,aheight2);
      }

      if(inkey(-74)&&flg==2&&f12==1)
      {
        x=(((aheight2+alenght2-136)/832.0)*52.0+1);
        top2=(int)x;
        x=(((aheight2-136)/832.0)*52.0+1);
        bottom2=(int)x;
        if(multdisp==2)
        {
          for(i=1;i<=fcount;i++)
          {
           for(f=1;f<=indm[1];f++)
            for(g=1;g<=indm[1];g++) c[f][g]=d[i][f][g]);
           ind=indm[1];
           display(c,top1,bottom1,top2,bottom2,ind,step,
                   bfg,blur,fcount,sharp);
          }
        }
        else
        {
          if(invert==1)    display(c,top1,bottom1,top2,
             bottom2,ind,step,bfg,blur,fcount,sharp);
          if(invert==2) invdisplay(c,top1,bottom1,top2,
             bottom2,ind,step,bfg,blur,fcount,sharp);
        }
      }


/**********************************************************/
/*                                                        */
/*            Left Arrow Control Keys.                    */
/*                                                        */
/**********************************************************/

      if(inkey(-58)&&flg==1&&f12==1)
      {
        aheight1+=3;

        if((aheight1+alength1)>980) aheight1=980-alength1;
        arrow1(alength1,aheight1);
```

```
      }

      if(inkey(-42)&&flg==1&&f12==1)
      {
        aheight1-=3;
        if(aheight1<136) aheight1=136;
        arrow1(alength1,aheight1);
      }

      if(inkey(-122)&&flg==1&&f12==1)
      {
        alength1+=3;
        if(alength1>830) alength1=830;
        if((alength1+alenght1)>980) aheight1=980-alength1;
        arrow1(alength1,aheight1);
      }

      if(inkey(-74)&&flg==1&&f12==1)
      {
        x=(((aheight1+alenght1-136)/832.0)*52.0+1);
        top1=(int)x;
        x=(((aheight1-136)/832.0)*52.0+1);
        bottom1=(int)x;
        if(multdisp==2)
        {
           for(i=1;i<=fcount;i++)
           {
            for(f=1;f<=indm[1];f++)
             for(g=1;g<=indm[1];g++) c[f][g]=d[i][f][g]);
            ind=indm[1];
            display(c,top1,bottom1,top2,bottom2,ind,step,
                    bfg,blur,fcount,sharp);
           }
        }
        else
        {
           if(invert==1)    display(c,top1,bottom1,top2,
             bottom2,ind,step,bfg,blur,fcount,sharp);
           if(invert==2) invdisplay(c,top1,bottom1,top2,
             bottom2,ind,step,bfg,blur,fcount,sharp);
        }
      }

/*********************************************************/
/*                                                       */
/*             Left Arrow Normal Key.                    */
/*                                                       */
/*********************************************************/

      if(inkey(-86)&&flg==1&&f12==1)
      {
        alength1=850;
        aheight1=136;
        gcol(0,63);
        rectanglefill(960-13,100,35,aheight2+alenght2+30);
        arrow1(alength1,aheight1);
      }
```

18

```
/*****************************************************/
/*                                                 */
/*            Right Arrow Normal Key.              */
/*                                                 */
/*****************************************************/

      if(inkey(-86)&&flg==2&&f12==1)
      {
        alength2=850;
        aheight2=136;
        gcol(0,63);
        rectanglefill(960-13,100,35,aheight1+alenght1+30);
        arrow2(alength2,aheight2);
      }

/*****************************************************/
/*                                                 */
/*            Convert Display to Colour.           */
/*                                                 */
/*****************************************************/

      if(inkey(-116)&&f12==1)
      {
        f3=2;
        bfg=1;
        if(f12==1) icons1(f1,f2,f3,f4,f5,f6,f7,f8,f9,
                          f10,f11,f12,Instring);
        else       icons2(f1,f2,f3,f4,f5,f6,f7,f8,f9,
                          f10,f11,f12,Instring);
        if(multdisp==2)
        {
           for(i=0;i<=fcount;i++)
           {
             for(f=1;f<=indm[1];f++)
              for(g=1;g<=indm[1];g++) c[f][g]=d[i][f][g];
             ind=indm[1];
             display(c,top1,bottom1,top2,bottom2,ind,step,
                     bfg,blur,fcount,sharp);
           }
        }
        else
        {
           if(invert==1)    display(c,top1,bottom1,top2,
               bottom2,ind,step,bfg,blur,fcount,sharp);
           else             invdisplay(c,top1,bottom1,top2,
               bottom2,ind,step,bfg,blur,fcount,sharp);
        }
           f3=1;
           if(f12==1) icons1(f1,f2,f3,f4,f5,f6,f7,f8,f9,
                             f10,f11,f12,Instring);
           else       icons2(f1,f2,f3,f4,f5,f6,f7,f8,f9,
                             f10,f11,f12,Instring);
      }
```

```
/******************************************************/
/*                                                    */
/*          Convert Display to Black/White.           */
/*                                                    */
/******************************************************/

    if(inkey(-21)&&f12==1)

    {
      f4=2;
      bfg=2;
      if(f12==1) icons1(f1,f2,f3,f4,f5,f6,f7,f8,f9,
                        f10,f11,f12,Instring);
      else       icons2(f1,f2,f3,f4,f5,f6,f7,f8,f9,
                        f10,f11,f12,Instring);
      if(multdisp==2)
      {
          for(i=0;i<=fcount;i++)
          {
            for(f=1;f<=indm[1];f++)
             for(g=1;g<=indm[1];g++) c[f][g]=d[i][f][g];
            ind=indm[1];
            display(c,top1,bottom1,top2,bottom2,ind,step,
                    bfg,blur,fcount,sharp);
          }
      }
      else
      {
          if(invert==1)    display(c,top1,bottom1,top2,
              bottom2,ind,step,bfg,blur,fcount,sharp);
          else             invdisplay(c,top1,bottom1,top2,
              bottom2,ind,step,bfg,blur,fcount,sharp);
      }
          f4=1;
          if(f12==1) icons1(f1,f2,f3,f4,f5,f6,f7,f8,f9,
                            f10,f11,f12,Instring);
          else       icons2(f1,f2,f3,f4,f5,f6,f7,f8,f9,
                            f10,f11,f12,Instring);
    }

/******************************************************/
/*                                                    */
/*              Blur the Display.                     */
/*                                                    */
/******************************************************/

    if)inkey(-117)&&(blur==1)&&f12==1)
    {
      f5=2;
      if(f12==1) icons1(f1,f2,f3,f4,f5,f6,f7,f8,f9,
                        f10,f11,f12,Instring);
      else       icons2(f1,f2,f3,f4,f5,f6,f7,f8,f9,
                        f10,f11,f12,Instring);
      blur=2;
      for(f=1;f<=(ind*3);f++)
       for(g=1;g<=(ind*3);g++)
        c[f][g]=a[(int)((f+2)/3.0)][(int)((g+2)/3.0)]*x;
      for(g=1;g<=(ind*3)-2;g++)
      {
```

20

```
        dmy[1][g]=c[1][g];
        dmy[2][g]=c[2][g];
        dmy[3][g]=c[3][g];
    }
    for(f=4;f<=(ind*3);f++)
    {
        for(g=1;g<=(ind*3);g++)
        {
        c[f-2][g+1]=(dmy[1][g]*.25 + dmy[2][g]*0.5 +
                     dmy[3][g]*.25 + dmy[1][g+1]*0.5 +
                     dmy[2][g+1]  + dmy[3][g+1]*0.5 +
                     dmy[1][g+2]*.25 + dmy[2][g+2]*.5 +
                     dmy[3][g+2]*.25)/4.0;
        if(c[f-2][g+1]<0)
        {
            if((c[f-2][g+1]*-1.0)>mins) mins=c[f-2][g+1];
            else if(c[f-2][g+1]>maxs) maxs=c[f-2][g+1];
        }
        for(g=1;g<+(ind*3);g++)
        {
            dmy[1][g]=dmy[2][g];
            dmy[2][g]=dmy[3][g];
            dmy[3][g]=c[f][g];
        }
    }
    maxs+=mins;
    for(f=1;f<=(ind*3)-2;f++)
    {
     for(g=1;g<=(ind*3)-2;g++)
     {
        c[f][g]+=mins;
        c[f][g]*=(53.0/maxs);
     }
    }

    f5=1;
    system("*fx112,1");
    cls();
    if(invert==1)      display(c,top1,bottom1,top2,
             bottom2,ind,step,bfg,blur,fcount,sharp);
    if(invert==2) invdisplay(c,top1,bottom1,top2,
             bottom2,ind,step,bfg,blur,fcount,sharp);
    arrow1(alength1,aheight1);
    arrow2(alength2,aheight2);
    if(f12==1) icons1(f1,f2,f3,f4,f5,f6,f7,f8,f9,
                      f10,f11,f12,Instring);
    else       icons2(f1,f2,f3,f4,f5,f6,f7,f8,f9,
                      f10,f11,f12,Instring);
    system("*fx113,1");
    system("*fx112,2");
    if(f12==1) icons1(f1,f2,f3,f4,f5,f6,f7,f8,f9,
                      f10,f11,f12,Instring);
    else       icons2(f1,f2,f3,f4,f5,f6,f7,f8,f9,
                      f10,f11,f12,Instring);
    system("*fx112,1");
    toglescreen=1;
}
```

```
/*********************************************************/
/*                                                       */
/*        Detect the Edges of the Image.                 */
/*                                                       */
/*********************************************************/

        if(inkey(-118)&&blur==1&&f12==2)
        {
          f6=2;
          if(f12==1) icons1(f1,f2,f3,f4,f5,f6,f7,f8,f9,
                            f10,f11,f12,Instring);
          else       icons2(f1,f2,f3,f4,f5,f6,f7,f8,f9,
                            f10,f11,f12,Instring);
          blur=1;
          system("*fx112,1");
          cls();
          system("*fx113,1");
          mode(0);
          colour(63);
          cls();
          tab(10,5);
          printf("Update Original or Last screen (L/O): ");
          while(1)
          {
             scanf("%c",&onelet);
             if((onelet=='o')||(onelet=='O'))
               { choice=1; break; }
             if((onelet=='l')||(onelet=='L'))
               { choice=2; break; }
          }
          gcol(60,255);
          move(200,200);  draw(800,200);
          move(200,200);  draw(200,800);
          move(200,400);  draw(800,400);
          move(200,600);  draw(800,600);
          move(200,800);  draw(800,800);
          move(400,200);  draw(400,800);
          move(600,200);  draw(600,800);
          move(800,200);  draw(800,800);

          tab(17,8);  printf("(1,1)");
          tab(29,8);  printf("(2,1)");
          tab(40,8);  printf("(3,1)");
          tab(17,14); printf("(1,2)");
          tab(29,14); printf("(2,2)");
          tab(40,14); printf("(3,2)");
          tab(17,20); printf("(1,3)");
          tab(29,20); printf("(2,3)");
          tab(40,20); printf("(3,3)");

          tab(17,11); printf("> "); scanf("%f",&grid[1][1]);
          tab(29,11); printf("> "); scanf("%f",&grid[2][1]);
          tab(40,11); printf("> "); scanf("%f",&grid[3][1]);
          tab(17,17); printf("> "); scanf("%f",&grid[1][2]);
          tab(29,17); printf("> "); scanf("%f",&grid[2][2]);
          tab(40,17); printf("> "); scanf("%f",&grid[3][2]);
          tab(17,23); printf("> "); scanf("%f",&grid[1][3]);
          tab(29,23); printf("> "); scanf("%f",&grid[2][3]);
          tab(40,23); printf("> "); scanf("%f",&grid[3][3]);
```

```c
if(choice==1)
{
   for(f=1;f<=ind;f++)
    for(g=1;g<=ind;g++) c[f][g]=a[f][g];
}
else
{
   for(f=1;f<=ind;f++)
    for(g=1;g<=ind;g++) c[f][g]=e[f][g];
}

for(f=4;f<=ind;f++)
{
   for(g=1;g<=ind;g++)
    e[f-2][g+1]=(dmy[1][g]*grid[1][1] + dmy[2][g]*
                 grid[1][2] + dmy[3][g]*grid[1][3]
                 + dmy[1][g+2]*grid[3][1] +
                 dmy[2][g+2] * grid[3][2] +
                 dmy[3][g+2] * grid[3][3] +
                 dmy[1][g+1] * grid[2][1] +
                 dmy[3][g+1] * grid[2][3] +
                 dmy[2][g+1] * grid[2][2];
   for(g=1;g<=ind;g++)
   {
        dmy[1][g]=dmy[2][g];
        dmy[2][g]=dmy[3][g];
        dmy[3][g]=c[f][g];
   }
}
maxs=-1.0e10;
mins=1.0e10;
for(f=1;f<=ind;f++)
{
  for(g=1;g<=ind;g++)
  {
    mins=(mins<e[f][g])?mins:e[f][g];
    maxs=(maxs>e[f][g])?maxs:e[f][g];
  }
}
if((mins==0.0)&&(maxs==0.0)) break;
maxs+=fabs(mins);
for(f=1;f<=ind;f++)
{
  for(g=1;g<=ind;g++)
  {
    e[f][g]+=fabs(mins);
    c[f][g]=e[f][g]*(53.0/maxs);
  }
}

cls();
f6=1;
mode(15);
system("*fx112,1");
colour(128+63);
cls();
if(invert==1)    display(c,top1,bottom1,top2,
        bottom2,ind,step,bfg,blur,fcount,sharp);
if(invert==2) invdisplay(c,top1,bottom1,top2,
```

```
                bottom2,ind,step,bfg,blur,fcount,sharp);
        arrow1(alength1,aheight1);
        arrow2(alength2,aheight2);
        if(f12==1)  icons1(f1,f2,f3,f4,f5,f6,f7,f8,f9,
                             f10,f11,f12,Instring);
        else        icons2(f1,f2,f3,f4,f5,f6,f7,f8,f9,
                             f10,f11,f12,Instring);
        system("*fx113,1");
        system("*fx112,2");
        if(f12==1)  icons1(f1,f2,f3,f4,f5,f6,f7,f8,f9,
                             f10,f11,f12,Instring);
        else        icons2(f1,f2,f3,f4,f5,f6,f7,f8,f9,
                             f10,f11,f12,Instring);
        system("*fx112,1");
        toglescreen=1;


      }


/*********************************************************/
/*                                                       */
/*      Sharpen the Image on the display.                */
/*                                                       */
/*********************************************************/

        if(inkey(-117)&&sharp==1&&f12==2&&blur==1)
        {
          f5=2;
          if(f12==1)  icons1(f1,f2,f3,f4,f5,f6,f7,f8,f9,
                               f10,f11,f12,Instring);
          else        icons2(f1,f2,f3,f4,f5,f6,f7,f8,f9,
                               f10,f11,f12,Instring);
          sharp=2;
          for(f=1;f<=(ind*3);f++)
           for(g=1;g<=(ind*3);g++)
            c[f][g]=a[(int)((f+2)/3.0)][(int)((g+2)/3.0)]*x;
          system("*fx112,1");
          colour(128+63);
          cls();

          sharpenimage(c,top1,bottom1,top2,bottom2,
                  ind,step,bfg,blur,fcount,sharp,invert);
          f5=1;
          arrow1(alength1,aheight1);
          arrow2(alength2,aheight2);
          if(f12==1)  icons1(f1,f2,f3,f4,f5,f6,f7,f8,f9,
                               f10,f11,f12,Instring);
          else        icons2(f1,f2,f3,f4,f5,f6,f7,f8,f9,
                               f10,f11,f12,Instring);
          system("*fx113,1");
          system("*fx112,2");
          if(f12==1)  icons1(f1,f2,f3,f4,f5,f6,f7,f8,f9,
                               f10,f11,f12,Instring);
          else        icons2(f1,f2,f3,f4,f5,f6,f7,f8,f9,
                               f10,f11,f12,Instring);
          system("*fx112,1");
          toglescreen=1;
        }

        if(inkey(-117)&&f12==2&&blur==2)
        {
```

```
            system("*fx112,2");
            sharpenimage(c,top1,bottom1,top2,bottom2,ind,
                        step,bfg,blur,fcount,sharp,invert);
            f5=1;
            arrow1(alength1,aheight1);
            arrow2(alength2,aheight2);
            if(f12==1)  icons1(f1,f2,f3,f4,f5,f6,f7,f8,f9,
                              f10,f11,f12,Instring);
            else        icons2(f1,f2,f3,f4,f5,f6,f7,f8,f9,
                              f10,f11,f12,Instring);
            system("*fx113,2");
            system("*fx112,1");
            if(f12==1)  icons1(f1,f2,f3,f4,f5,f6,f7,f8,f9,
                              f10,f11,f12,Instring);
            else        icons2(f1,f2,f3,f4,f5,f6,f7,f8,f9,
                              f10,f11,f12,Instring);
            system("*fx112,2");
            toglescreen=2;
        }




/****************************************************/
/*                                                  */
/*        Select other Fuction Key sequences.       */
/*                                                  */
/****************************************************/

        if(inkey(-30)
        {
          if(f12==1) f12=2; else f12=1;
          if(f12==1) icons1(f1,f2,f3,f4,f5,f6,f7,f8,f9,
                            f10,f11,f12,Instring);
          else       icons2(f1,f2,f3,f4,f5,f6,f7,f8,f9,
                            f10,f11,f12,Instring);
          while(inkey(-30));
        }


/****************************************************/
/*                                                  */
/*        Toggle Screen Display and Writing.        */
/*                                                  */
/****************************************************/

        if(inkey(-118)) toglescreen=1;
        if(inkey(-23))  toglescreen=2;
        if(toglescreen==1)
        {
          system("*fx113,1");
          system("*fx112,1");
        }
        else
        {
          system("*fx113,2");
          system("*fx112,2");
        }
```

25

```
/**********************************************************/
/*                                                        */
/*          Invert the Screen Display.                    */
/*                                                        */
/**********************************************************/

      if(inkey(-119)&&f12==2)
      {
        if(invert==1) invert=2;
        f8=2;
        if(f12==1) icons1(f1,f2,f3,f4,f5,f6,f7,f8,f9,
                          f10,f11,f12,Instring);
        else       icons2(f1,f2,f3,f4,f5,f6,f7,f8,f9,
                          f10,f11,f12,Instring);
        if(multdisp==2)
        {
          for(i=0;i<=fcount;f++)
          {
           for(f=1;f<=indm[1];f++)
            for(g=1;g<=indm[1];g++)
             c[f][g]=d[i][f][g];
           ind=indm[1];
           if(invert==1)    display(c,top1,bottom1,top2,
                    bottom2,ind,step,bfg,blur,i,sharp);
            if(invert==2) invdisplay(c,top1,bottom1,top2,
                    bottom2,ind,step,bfg,blur,i,sharp);
          }
        }
        else
        {
        if(invert==1)    display(c,top1,bottom1,top2,bottom2
                          ind,step,bfg,blur,fcount,sharp);
        if(invert==2)invdisplay(c,top1,bottom1,top2,bottom2,
                          ind,step,bfg,blur,fcount,sharp);

        }
        f8=1;
        if(f12==1) icons1(f1,f2,f3,f4,f5,f6,f7,f8,f9,
                          f10,f11,f12,Instring);
        else       icons2(f1,f2,f3,f4,f5,f6,f7,f8,f9,
                          f10,f11,f12,Instring);

      }

/**********************************************************/
/*                                                        */
/*       Read Normalized CT numbers on grid.              */
/*                                                        */
/**********************************************************/

      if(inkey(-120)&&f12==2)
      {
        if(f12==1) icons1(f1,f2,f3,f4,f5,f6,f7,f8,f9,
                          f10,f11,f12,Instring);
        else       icons2(f1,f2,f3,f4,f5,f6,f7,f8,f9,
                          f10,f11,f12,Instring);
        procmouse(a,step,ind);
        f9=1;
        if(f12==1) icons1(f1,f2,f3,f4,f5,f6,f7,f8,f9,
                          f10,f11,f12,Instring);
```

```
           else        icons2(f1,f2,f3,f4,f5,f6,f7,f8,f9,
                              f10,f11,f12,Instring);

      }

/*****************************************************/
/*                                                   */
/*         Convert to Exponential Display.           */
/*                                                   */
/*****************************************************/

      if(inkey(-31)&&f12==2)
      {
        f10=2;
        if(f12==1) icons1(f1,f2,f3,f4,f5,f6,f7,f8,f9,
                          f10,f11,f12,Instring);
        else        icons2(f1,f2,f3,f4,f5,f6,f7,f8,f9,
                          f10,f11,f12,Instring);
        x=53.0/(exp(maxx[1]));
        for(f=1;f<=ind;f++)
         for(g=1;g<=ind;g++)
          c[f][g]=exp(a[f][g])*x;
        if(multdisp==2)
        {
           for(i=0;i<=fcount;i++)
           {
             printf("****** %f *******",maxx[i]);
             x=53.0/(exp(maxx[i]));
             for(f=1;f<=indm[1];f++)
              for(g=1;g<=indm[1];g++)
               c[f][g]=exp(d[i][f][g])*x;
             ind=indm[1];
             display(c,top1,bottom1,top2,bottom2,ind,step
                     bfg,blur,i,sharp);
           }
        }
        else
        {
           if(invert==1)   display(c,top1,bottom1,top2,
                 bottom2,ind,step,bfg,blur,fcount,sharp);
           if(invert==2)invdisplay(c,top1,bottom1,top2,
                 bottom2,ind,step,bfg,blur,fcount,sharp);
        }
        f10=1;
        if(f12==1) icons1(f1,f2,f3,f4,f5,f6,f7,f8,f9,
                          f10,f11,f12,Instring);
        else        icons2(f1,f2,f3,f4,f5,f6,f7,f8,f9,
                          f10,f11,f12,Instring);
      }


/*****************************************************/
/*                                                   */
/*         Convert to Logorithimic Diaplsy.          */
/*                                                   */
/*****************************************************/

      if(inkey(-29)&&f12==2)
      {
```

```
            f11=2;
            if(f12==1) icons1(f1,f2,f3,f4,f5,f6,f7,f8,f9,
                              f10,f11,f12,Instring);
            else        icons2(f1,f2,f3,f4,f5,f6,f7,f8,f9,
                              f10,f11,f12,Instring);
            x=53.0/(log(maxx[1]));
            for(f=1;f<=ind;f++)
             for(g=1;g<=ind;g++)
              c[f][g]=exp(a[f][g])*x;
            if(multdisp==2)
            {
                for(i=0;i<=fcount;i++)
                {
                  printf("****** %f *******",maxx[i]);
                  x=53.0/(log(maxx[i]));
                  for(f=1;f<=indm[1];f++)
                   for(g=1;g<=indm[1];g++)
                    c[f][g]=log(d[i][f][g])*x;
                  ind=indm[1];
                  display(c,top1,bottom1,top2,bottom2,ind,step
                          bfg,blur,i,sharp);
                }
            }
            else
            {
                if(invert==1)    display(c,top1,bottom1,top2,
                      bottom2,ind,step,bfg,blur,fcount,sharp);
                if(invert==2)invdisplay(c,top1,bottom1,top2,
                      bottom2,ind,step,bfg,blur,fcount,sharp);
            }
            f11=1;
            if(f12==1) icons1(f1,f2,f3,f4,f5,f6,f7,f8,f9,
                              f10,f11,f12,Instring);
            else        icons2(f1,f2,f3,f4,f5,f6,f7,f8,f9,
                              f10,f11,f12,Instring);
        }


/*******************************************************/
/*                                                     */
/*          Restore the Original Image.                */
/*                                                     */
/*******************************************************/

        if(inkey(-52)&&f12==2)
        {
          for(f=1;f<=ind;f++)
           for(g=1;g<=ind;g++)
             c[f][g]=a[f][g]*53.0/maxx[1];
          if(multdisp==2)
           {
            for(i=0;i<=fcount;i++)
             {
              for(f=1;f<=indm[1];f++)
               for(g=1;g<=indm[1];g++)
                c[f][g]=d[i][f][g];
              ind=indm[1];
              display(c,top1,bottom1,top2,bottom2,
                      ind,step,bfg,blur,i,sharp);
             }
```

```
        }
        else
        {
         if(invert==1)       display(c,top1,bottom1,top2,
                 bottom2,ind,step,bfg,blur,fcount,sharp);
          if(invert==2) invdisplay(c,top1,bottom1,top2,
                 bottom2,ind,step,bfg,blur,fcount,sharp);
        }
      }

/******************************************************/
/*                                                    */
/*         Exit from the program.                     */
/*                                                    */
/******************************************************/

      if(inkey(-29)&&f12==1)

      {
      fclose(fp);
      cls();
      exit(0);
      }

/******************************************************/
/*                                                    */
/*         Display Image on Full screen size.         */
/*                                                    */
/******************************************************/

      if(inkey(-120)&&f12==1)
      {
        stp=(int)1023/ind);
        cls();
        fulldisplay(c,top1,bottom1,top2,bottom2,ind,step,
                    bfg,blur,fcount,sharp);
      }

/******************************************************/
/*                                                    */
/*         Multi-File Display Routine.                */
/*                                                    */
/******************************************************/

      if(inkey(-114)&&f12==2)
      {
        system("*fx15,1");
        vdu(6);
        cls();
        colour(128+63);
        cls();
        colour(1);
        vduq(23,,1,0,0,0,0,0,0,0);
        fcount=0;
        while(1)
        {
           cls();
           system("*.");
           printf("\n\n\n\tInput file name: ");
```

29

```
        fgets(Instring,STRINGLEN,stdin);
        if((fp=fopen(Instring,"r"))==NULL)
        {
          cls();
          printf("ERROR - cannot open file");
          system("*run p.testdisp");
        }
        ch=fgetc(fp);
        if(ch==128) cc=2; else c=1;
        rewind(fp):
        fclose(fp);
        if(cc==2)
        {
          free(a); free(b); free(c); free(d);
          system("*run p.convertbbc");
        }
        else
        {
          if((fp=fopen(Instring,"rb"))==NULL)
          {
           cls();
           printf("ERROR - cannot open file");
           system("*run p.testdisp");
          }
          i=0;
          fscanf(fp,"%g",&maxx[fcount]);
          while(fscanf(fp,"%g",&b[i++]))!=EOF);
          fclose(fp);
        }

        ii=i*1.0;
        x=sqrt(ii);
        indm[fcount]=(int)x;
        step=(int)(400.0/x);
        i=0;
        for(f=1;f<=indm[fcount];f++)
         for(g=1;g<=indm[fcount];g++)
          d[fcount][f][g]=b[i++];
        if(maxx[fcount]==0.0) break;
        x=53.0/maxx[fcount];
        for(f=1;f<=indm[fcount];f++)
        {
         for(g=1;g<=indm[fcount];g++)
         {
          d[fcount][f][g]*=x;
          if(d[fcount][f][g]>53.0) d[fcount][f][g]=53.0;
         }
        }
        if(inkey(-35)) break;
        if(fcount==3) break;
        fcount++;
}
cls();
vduq(23,1,0,0,0,0,0,0,0,0);
for(i=0;i<=fcount;i++)
{
  for(f=1;f<=indm[1];f++)
   for(g=1;g<=indm[1];g++)
    c[f][g]=d[i][f][g];
```

```c
                ind=indm[1];
                display(c,top1,bottom1,top2,bottom2,ind,step,bfg,
                        blur,i,sharp);
                if(f12==1)  icons1(f1,f2,f3,f4,f5,f6,f7,f8,f9,
                                   f10,f11,f12,Instring);
                else        icons2(f1,f2,f3,f4,f5,f6,f7,f8,f9,
                                   f10,f11,f12,Instring);
            }
            multdisp=2;
            arrow1(alength1,aheight1);
            arrow2(alength2,aheight2);
        }


        if(inkey(-115)&&f12==2) break;




/*********************************************************/
/*                                                       */
/*           Save Screen to Disk.                        */
/*                                                       */
/*********************************************************/

        if(inkey(-119)&&f12==1)
        {
           system("*load 4:.!paint.!sprites");
           system("savescreen image");
        }

/*********************************************************/
/*                                                       */
/*         Subtract two images and save the result.      */
/*                                                       */
/*********************************************************/

        if(inkey(-116)&&f12==2)
        {
           system("*fx15");
           mode(0);
           cls();
           fcount=0;
           f3=2;
           while(1)
           {
              mode(0);
              cls();
              system("*.");
              printf("\n\n\n\n\tInput the file name: ");
              fgets(Instring,STRINGLEN,stdin);
              if((fp=fopen(Instring,"rb"))==NULL)
              {
                 cls();
                 printf("ERROR - cannot open file");
                 system("*run p.testdisp");
              }
              ch=fgetc(fp);
              if(ch==128) cc=2; else cc=1;
              fclose(fp);
```

31

```c
    if(cc==2)
    {
      free(a);free(b);free(c);free(d);
      system("*run p.convertbbc");
    }
    else
    {
      if((fp=fopen(Instring,"rb"))==NULL)
      {
        cls();
        printf("ERROR - cannot open file");
        system("*run p.testdisp");
      }
      i=0;
      fscanf(fp,"%g",&maxx[fcount]);
      while((fscanf(fp,"%g",&b[i++]))!=EOF);
      fclose(fp);
    }
    ii=i*1.0;
    x=sqrt(ii);
    indm[fcount]=(int)x;
    step=(int)(400.0/x);
    i=0;
    for(f=1;f<=indm[fcount];f++)
     for(g=1;g<=indm[fcount];g++)
      d[fcount][f][g]=b[i++];


    /* to find the mean inside the cylinder  */

    for(f=1;f<=48;f++)
     for(g=1;g<=48;g++) xx[f][g]=0;
    pixel=0;
    outside[fcount]=0.0;
    for(i=14;i<20;i++)
    {
      for(angle=0;angle<=2.0*PI;angle+=PI/40.0)
      {
       g=(int)(23.5+(i*cos(angle)));
       f=(int)(23.5+(i*sin(angle)));
       if(xx[f][g]!=1)
       {
          outside[fcount]+=d[fcount][f][g];
          xx[f][g]=1;
          pixel++;
       }
      }
    }
    mmm[fcount]=outside[fcount]/(pixel*1.0);
    if(fcount==1) break;
    fcount++;
}

mode(15);
cls();
vduq(23,1,0,0,0,0,0,0,0,0);
for(i=0;i<=fcount;i++)
{
  for(f=1;f<=indm[1];f++)
```

32

```c
        for(g=1;g<=indm[1];g++)
          c[f][g]=d[i][f][g]*(53.0/maxx[i]);
      ind=indm[1];
      display(c,top1,bottom1,top2,bottom2,ind,step,bfg,
              blur,i,sharp);
      if(f12==1) icons1(f1,f2,f3,f4,f5,f6,f7,f8,f9,
                        f10,f11,f12,Instring);
      else       icons2(f1,f2,f3,f4,f5,f6,f7,f8,f9,
                        f10,f11,f12,Instring);
    }
    dist=1;
    tab(69,5); printf("E - End");
    while(1)
    {
     maxx[2]=0.0;
     diff=mmm[0]-mmm[1];
     for(f=1;f<=indm[0];f++)
     {
        for(g=1;g<=indm[0];g++)
        {
         d[1][f][g]+=diff;
         d[2][f][g]=d[0][f][g]-d[1][f][g];
        maxx[2]=(maxx[2]?d[2][f][g])?maxx[2]:d[2][f][g];
        }
     }
     fp=fopen("Subtract","w");
     fprintf(fp,"%10.6f\n",maxx[2]);
     x=53.0/maxx[2];
     for(f=1;f<=indm[fcount];f++)
     {
      for(g=1;g<=indm[fcount];g++)
      {
       fprintf(fp,"%10.6f\n",d[2][f][g]);
       d[2][f][g]*=x;
      }
     }
     fclose(fp);
     i=2;
     for(f=1;f<=indm[fcount];f++)
      for(g=1;g<=indm[fcount];g++)
       c[f][g]=d[i][f][g];
     ind=ndm[fcount];
     display(c,top1,bottom1,top2,bottom2,ind,step,bfg,
             blur,i,sharp);
     if(f12==1) icons1(f1,f2,f3,f4,f5,f6,f7,f8,f9,
                       f10,f11,f12,Instring);
     else       icons2(f1,f2,f3,f4,f5,f6,f7,f8,f9,
                       f10,f11,f12,Instring);
     dist=2;
    }

/* Moving the image during subtraction   */

    if(inkey(-21)&&f12==2)
    {
     for(f=1;f<=indm[fcount];f++)
      for(g=1;g<=indm[fcount];g++)
       a[f][g]=d[0][f][g];
     moveno=0;
```

33

```c
moved=0;
f4=2;
if(f12==1) icons1(f1,f2,f3,f4,f5,f6,f7,f8,f9,
                  f10,f11,f12,Instring);
else        icons2(f1,f2,f3,f4,f5,f6,f7,f8,f9,
                  f10,f11,f12,Instring);
while(1)
{
  tab(70,9);  printf("<== ==>");
  tab(69,12); printf("No. = %d ",moveno);
  tab(70,15); printf("%c  v",94);
  tab(69,18); printf("No. = %d ",moved);
  if(inkey(-122))
  {
   moveno++;
   for(f=1;f<=ind;f++)
    {
     for(g=1;g<=ind-1;g++)
      d[0][f][g+1]=a[f][g];
     d[0][f][1]=a[f][ind];
    }
    for(f=1;f<=ind;f++)
     for(g=1;g<=ind;g++)
      a[f][g]=d[0][f][g];
  }
  if(inkey(-26))
  {
   moveno--;
   for(f=1;f<=ind;f++)
    {
     for(g=2;g<=ind;g++)
      d[0][f][g-1]=a[f][g];
     d[0][f][ind]=a[f][1];
    }
    for(f=1;f<=ind;f++)
     for(g=1;g<=ind;g++)
      a[f][g]=d[0][f][g];
  }
  if(inkey(-42))
  {
   moved++:
   for(g=1;g<=ind;g++)
    {
     for(f=1;f<=ind-1;f++)
      d[0][f+1][g]=a[f][g];
     d[0][1][g]=a[ind][g];
    }
    for(f=1;f<=in;f++)
     for(g=1;g<=ind;g++)
      a[f][g]=d[0][f][g];
  }
  if(inkey(-58))
  {
   moved--;
   for(g=1;g<=ind;g++)
    {
     for(f=2;f<=ind;f++)
      d[0][f-1][g]=a[f][g];
    }
```

```
                for(f=1;f<=ind;f++)
                  for(g=1;g<=ind;g++)
                    a[f][g]=d[0][f][g];
                }
                for(i=1;i<=1e4;i++);
                if(inkey(-74) {dist=1; break;}
              }
              for(f=1;f<=ind;f++)
               for(g=1;g<=ind;g++)
                d[0][f][g]=a[f][g];
              f3=1;
              if(f12==1) icons1(f1,f2,f3,f4,f5,f6,f7,f8,f9,
                               f10,f11,f12,Instring);
              else       icons2(f1,f2,f3,f4,f5,f6,f7,f8,f9,
                               f10,f11,f12,Instring);
            }
            if(inkey(-35)) break;
          }
          colour(128+63);
          tab(70,9);  printf("                    ");
          tab(70,15); printf("                    ");
          tab(69,12); printf("                    ");
          tab(69,18); printf("                    ");
          tab(69,5);  printf("                    ");
          f3=1;
          if(f12==1) icons1(f1,f2,f3,f4,f5,f6,f7,f8,f9,
                           f10,f11,f12,Instring);
          else       icons2(f1,f2,f3,f4,f5,f6,f7,f8,f9,
                           f10,f11,f12,Instring);
        }
      }
    }
}          /* end of main program   */



/****************************************************/
/*                                                  */
/* Left window function. Display colours full  range. */
/*                                                  */
/****************************************************/
void        arrow2(alength2,aheight2)
int         alength2,aheight2;
{
      void        draw(int,int);
      void        move(int,int);
      void        gcol(int,int);
      void        vduq(int,int,int,int);

      vduq(23,17,2,0x00);
      gcol(0,63);
      rectanglefill(1050-13,100,30,aheight2-80);
      recatnglefill(1050-13,aheight2+alength2-10,30,1100);
      gcol(0,3);
      move(1050-13,aheight2);
      draw(1050+13,aheight2);
      move(1050-13,aheight2+alength2);
      draw(1050-13,aheight2+alenght2);
```

```c
        move(1050-2,aheight2+alength2);
        draw(1050-2,aheight2);
        move(1050+2,aheight2+alength2);
        draw(1050+2,aheight2);
}


/*****************************************************/
/*                                                   */
/* Right window function. Displays colours indicated. */
/*                                                   */
/*****************************************************/

void        arrow1(alength1,aheight1)
int         alength1,aheight1;
{
        void        draw(int,int);
        void        move(int,int);
        void        gcol(int,int);
        void        vduq(int,int,int,int);

        vduq(23,17,2,0x00);
        gcol(0,63);
        rectanglefill(970-13,100,30,aheight1-80);
        recatnglefill(970-13,aheight1+alength1-10,30,1100);
        gcol(0,3);
        move(970-13,aheight1);
        draw(970+13,aheight1);
        move(970-13,aheight1+alength1);
        draw(970-13,aheight1+alenght1);

        move(970-2,aheight1+alength1);
        draw(970-2,aheight1);
        move(970+2,aheight1+alength1);
        draw(970+2,aheight1);
}


/*****************************************************/
/*                                                   */
/*              Window Level Names.                  */
/*                                                   */
/*****************************************************/

void        label()
{
        void colour(int);
        void tab(int,int);
        colour(128+63);
        if(flg==1) colour(48);
        else colour(0);
        tab(58,5);  printf("S");
        tab(58,6);  printf("e");
        tab(58,7);  printf("l");
        tab(58,8);  printf("e");
        tab(58,9);  printf("c");
        tab(58,10); printf("t");
        tab(58,11); printf("i");
        tab(58,12); printf("o");
```

```
            tab(58,13); printf("n");
            tab(58,16); printf("W");
            tab(58,17); printf("i");
            tab(58,18); printf("n");
            tab(58,19); printf("d");
            tab(58,20); printf("o");
            tab(58,21); printf("w");

            if(flg==2) colour(48);
            else colour(0);
            tab(67,5); printf("E");
            tab(67,6); printf("x");
            tab(67,7); printf("p");
            tab(67,8); printf("a");
            tab(67,9); printf("n");
            tab(67,10); printf("c");
            tab(67,11); printf("i");
            tab(67,12); printf("o");
            tab(67,13); printf("n");
            tab(67,16); printf("W");
            tab(67,17); printf("i");
            tab(67,18); printf("n");
            tab(67,19); printf("d");
            tab(67,20); printf("o");
            tab(67,21); printf("w");
            colour(3);
}

/********************************************************/
/*                                                      */
/*                Display Routine.                      */
/*                                                      */
/********************************************************/

int  display(c,top1,bottom1,top2,bottom2,ind,step,bfg,
             blur,fno,sharp);
float     c[693][693];
int       top1,top2,bottom1,bottom2,ind,step;
int       bfg,blur,fno,sharp;
{

     int  t,g,f,tt[54],cc[54],in,stp,xx,y;
     float x;
     void      rectanglefill(int,int,int,int);
     void      gcol(int,int);
     void      vduq(int,int,int,int,int);

     static int ttc[]={1,1,1,1,1,1,65,180,250,1,65,1,65,
                       180,1,65,180,250,180,250,65,1,1,
                       180,65,1,65,1,1,65,180,1,65,180,
                       250,180,250,250,180,65,250,180,65,
                       250,180,65,1,250,180,65,1,250,65,1};

     static int ccc[]={0,0,0,0,0,16,16,16,16,32,32,48,48,
                       48,52,52,52,52,56,56,60,60,61,40,
                       40,40,24,24,25,25,25,14,14,14,14,
                       15,15,31,31,31,11,11,11,7,7,7,7,
                       2,2,2,2,1,1,1};
```

37

```
}
if(blur==2||sharp==2)
{
stp=(int)(step/3.0);
in=ind*3;
}
else
{
in=ind;
stp=step;
}
for(f=1;f<=inf++)
{
for(g=1;g<=in;g++)
{
t=(int)c[f][g];
if(t>top2) t=0;
if(t<bottom2) t=0;
t-=bottom2;
if(t<0)   t=0
x=t*1.0;
t=(int)((53.0*t)/(top2-bottom2));
if(top1>53.0) top1=53.0;
if(t>top1)  t=0;
if(t<bottom1)  t=0;
if(tt[t]==1)    vdug(23,17,2,0x00);
if(tt[t]==65)   vdug(23,17,2,0x40);
```

```
static int ttm[]={1,1,1,1,1,1,65,65,180,180,180,
                  250,250,250,1,1,65,65,65,180,180,
                  180,250,250,250,1,1,65,65,65,180,180,
                  180,180,250,250,250,1,1,65,65,65,180,
                  180,180,180,250,250,250,250,250,
                  250,250};

static int ccm[]={0,0,0,0,0,0,0,0,0,0,0,0,0,21,
                  21,21,21,21,21,21,21,21,21,21,21,
                  42,42,42,42,42,42,42,42,42,42,21,21,
                  42,63,63,63,63,63,63,63,42,42,42,42,
                  63,63,63,63,63,63,63};

if(fno==0)   {xx=0;    y=0;}
if(fno==1)   {xx=440;  y=0;}
if(fno==2)   {xx=0;    y=440;}
if(fno==3)   {xx=440;  y=440;}
if(bfg==1)
{
for(f=0;f<=53;f++)
    {
    cc[f]=ccc[f];
    tt[f]=ttc[f];
    }
}
else
{
for(f=0;f<=53;f++)
    {
    cc[f]=ccm[f];
    tt[f]=ttm[f];
    }
}
```

```c
          if(tt[t]==180) vduq(23,17,2,0x80);
          if(tt[t]==250) vduq(23,17,2,0xc0);
          gcol(0,cc[t]);
          rectanglefill(25+xx+((g-1)*stp),1000-y-(f*stp),
                        stp-2,stp-2);
          if(inkey(-35)) break;
        }
        if(inkey(-35)) break;
      }
      for(t=0;t<=53;t++)
      {
        if(tt[t]==1)   vduq(23,17,2,0x00);
        if(tt[t]==65)  vduq(23,17,2,0x40);
        if(tt[t]==180) vduq(23,17,2,0x80);
        if(tt[t]==250) vduq(23,17,2,0xc0);
        gcol(0,cc[t]);
        rectaglefill(1000,120+(t*16),20,20);
      }
      label();
}


/****************************************************/
/*                                                  */
/*          Inverted Display Routine.               */
/*                                                  */
/****************************************************/

int   invdisplay(c,top1,bottom1,top2,bottom2,ind,step,bfg,
                 blur,fno,sharp);
float       c[693][693];
int         top1,top2,bottom1,bottom2,ind,step;
int         bfg,blur,fno,sharp;
{

      int   t,g,f,tt[54],cc[54],in,stp,xx,y;
      float x;
      void        rectanglefill(int,int,int,int);
      void        gcol(int,int);
      void        vduq(int,int,int,int,int);

      static int ttc[]={1,65,250,1,65,180,250,,1,65,180,
                        250,65,180,250,65,180,250,250,180,
                        250,180,65,1,180,65,1,1,65,1,65,
                        180,1,1,65,250,180,250,180,65,1,
                        180,65,1,65,1,250,180,65,1,1,1,1,
                        1,1};

      static int ccc[]={1,1,1,2,2,2,2,7,7,7,7,11,11,11,
                        31,31,31,15,15,14,14,14,14,25,25,
                        25,24,24,40,40,40,61,60,60,56,56,
                        52,52,52,52,48,48,48,32,32,16,16,
                        16,16,0,0,0,0,0};


      static int ttm[]={250,250,250,250,250,250,180,180,
                        180,65,65,65,1,1,1,250,250,250,180
```

39

```
                      180,180,65,65,65,1,1,1,250,250,250
                      180,180,180,65,65,65,1,1,1,250,250
                      250,180,180,180,65,65,65,1,1,1,1,1
                      ,1,1};

         static int ccm[]={63,63,63,63,63,63,63,63,63,63,63,
                      63,63,63,63,42,42,42,42,42,42,42,
                      42,42,42,42,42,21,21,21,21,21,21,
                      21,21,21,21,21,21,0,0,0,0,0,0,0,0
                      0,0,0,0,0,0,0};

         if(fno==0) {xx=0;    y=0;}
         if(fno==1) {xx=440; y=0;}
         if(fno==2) {xx=0;    y=440;}
         if(fno==3) {xx=440; y=440;}
         if(bfg==1)
         {
          for(f=0;f<=53;f++)
          {
           cc[f]=ccc[f];
           tt[f]=ttc[f];
          }
         }
         else
         {
          for(f=0;f<=53;f++)
          {
           cc[f]=ccm[f];
           tt[f]=ttm[f];
          }
         }
         if(blur==2||sharp==2)
         {
          stp=(int)(step/3.0);
          in=ind*3;
         }
         else
         {
          in=ind;
          stp=step;
         }
         for(f=1;f<=in;f++)
         {
          for(g=1;g<=in;g++)
          {
           t=(int)c[f][g];
           if(t>top2) t=top2;
           if(t<bottom2) t=0;
           t-=bottom2;
           if(t<0) t=0
           x=t*1.0;
           t=(int)((53.0*t)/(top2-bottom2));
           if(top1>53.0) top1=53.0;
           if(t>top1) t=53;
           if(t<bottom1) t=53;
           if(tt[t]==1)   vduq(23,17,2,0x00);
           if(tt[t]==65)  vduq(23,17,2,0x40);
           if(tt[t]==180) vduq(23,17,2,0x80);
           if(tt[t]==250) vduq(23,17,2,0xc0);
           gcol(0,cc[t]);
```

```
            rectanglefill(25+xx+((g-1)*stp),1000-y-(f*stp),
                           stp-2,stp-2);
            if(inkey(-35)) break;
           }
           if(inkey(-35)) break;
          }
          for(t=0;t<=53;t++)
          {
           if(tt[t]==1)    vduq(23,17,2,0x00);
           if(tt[t]==65)   vduq(23,17,2,0x40);
           if(tt[t]==180)  vduq(23,17,2,0x80);
           if(tt[t]==250)  vduq(23,17,2,0xc0);
           gcol(0,cc[t]);
           rectaglefill(1000,120+(t*16),20,20);
          }
          label();
}


/*****************************************************/
/*                                                   */
/*           Declaration of Function Keys.           */
/*                                                   */
/*****************************************************/

void icons1(f1,f2,f3,f4,f5,f6,f7,f8,f9,f10,
            f11,f12,Instring)
int  f1,f2,f3,f4,f5,f6,f7,f8,f9,f10,f11,f12;
char Instring[20];
{

        void      tab(int,int);
        void      colour(int);

        if(f1==2)
        {
         colour(128+1);
         tab(1,29); printf(" F1   ");
         tab(1,30); printf("Left ");
        }
        else
        {
         colour(128+63);
         tab(1,29); printf(" F1   ");
         tab(1,30); printf("Left ");
        }
        if(f2==2)
        {
         colour(128+1);
         tab(7,29); printf(" F2   ");
         tab(7,30); printf("Right");
        }
        else
        {
         colour(128+63);
         tab(7,29); printf(" F2   ");
         tab(7,30); printf("Right");
        }
```

```
if(f3==2)
{
 colour(128+1);
 tab(14,29); printf(" F3   ");
 tab(14,30); printf("Colr ");
}
else
{
 colour(128+63);
 tab(14,29); printf(" F3   ");
 tab(14,30); printf("Colr ");
}
if(f4==2)
{
 colour(128+1);
 tab(21,29); printf(" F4   ");
 tab(21,30); printf(" B/W ");
}
else
{
 colour(128+63);
 tab(21,29); printf(" F4   ");
 tab(21,30); printf(" B/W ");
}
if(f5==2)
{
 colour(128+1);
 tab(27,29); printf(" F5   ");
 tab(27,30); printf("Blur ");
}
else
{
 colour(128+63);
 tab(27,29); printf(" F5   ");
 tab(27,30); printf("Blur ");
}
if(f6==2)
{
 colour(128+1);
 tab(33,29); printf(" F6 ");
 tab(33,30); printf("Sc.1");
}
else
{
 colour(128+63);
 tab(33,29); printf(" F6 ");
 tab(33,30); printf("Sc.1");
}
if(f7==2)
{
 colour(128+1);
 tab(40,29); printf(" F7   ");
 tab(40,30); printf("Sc.2 ");
}
else
{
 colour(128+63);
 tab(40,29); printf(" F7   ");
 tab(40,30); printf("Sc.2 ");
```

```
}
if(f8==2)
{
 colour(128+1);
 tab(46,29); printf(" F8   ");
 tab(46,30); printf("Hcopy");
}
else
{
 colour(128+63);
 tab(46,29); printf(" F8   ");
 tab(46,30); printf("Hcopy");
}
if(f9==2)
{
 colour(128+1);
 tab(53,29); printf(" F9   ");
 tab(53,30); printf("F/Scr");
}
else
{
 colour(128+63);
 tab(53,29); printf(" F9   ");
 tab(53,30); printf("F/Scr");
}
if(f10==2)
{
 colour(128+1);
 tab(60,29); printf(" F10 ");
 tab(60,30); printf("      ");
}
else
{
 colour(128+63);
 tab(60,29); printf(" F10 ");
 tab(60,30); printf("      ");
}
if(f11==2)
{
 colour(128+1);
 tab(67,29); printf(" F11 ");
 tab(67,30); printf("Exit ");
}
else
{
 colour(128+63);
 tab(67,29); printf(" F11 ");
 tab(67,30); printf("Exit ");
}
if(f12==2)
{
 colour(128+1);
 tab(74,29); printf(" F12 ");
 tab(74,30); printf("More ");
}
else
{
 colour(128+63);
 tab(74,29); printf(" F12 ");
```

```
         tab(74,30); printf("More ");
         }
         tab(21,27);
         printf("File: %s",Instring);
}




/*****************************************************/
/*                                                   */
/*          Declaration o Function Keys.             */
/*                                                   */
/*****************************************************/

void icons1(f1,f2,f3,f4,f5,f6,f7,f8,f9,f10,
            f11,f12,Instring)
int  f1,f2,f3,f4,f5,f6,f7,f8,f9,f10,f11,f12;
char Instring[20];
{

     void       tab(int,int);
     void       colour(int);

     if(f1==2)
     {
      colour(128+1);
      tab(1,29); printf(" F1  ");
      tab(1,30); printf("Multi");
     }
     else
     {
      colour(128+63);
      tab(1,29); printf(" F1  ");
      tab(1,30); printf("Multi");
     }
     if(f2==2)
     {
      colour(128+1);
      tab(7,29); printf(" F2  ");
      tab(7,30); printf("Singl");
     }
     else
     {
      colour(128+63);
      tab(7,29); printf(" F2  ");
      tab(7,30); printf("Singl");
     }



     if(f3==2)
     {
      colour(128+1);
      tab(14,29); printf(" F3  ");
      tab(14,30); printf("Subtr");
     }
     else
     {
```

44

```c
  colour(128+63);
  tab(14,29); printf(" F3   ");
  tab(14,30); printf("Subtr");
}
if(f4==2)
{
  colour(128+1);
  tab(21,29); printf(" F4   ");
  tab(21,30); printf("Move ");
}
else
{
  colour(128+63);
  tab(21,29); printf(" F4   ");
  tab(21,30); printf("Move");
}
if(f5==2)
{
  colour(128+1);
  tab(27,29); printf(" F5   ");
  tab(27,30); printf("Sharp");
}
else
{
  colour(128+63);
  tab(27,29); printf(" F5   ");
  tab(27,30); printf("Sharp");
}
if(f6==2)
{
  colour(128+1);
  tab(33,29); printf(" F6 ");
  tab(33,30); printf("Edge");
}
else
{
  colour(128+63);
  tab(33,29); printf(" F6 ");
  tab(33,30); printf("Edge");
}
if(f7==2)
{
  colour(128+1);
  tab(40,29); printf(" F7   ");
  tab(40,30); printf("      ");
}
else
{
  colour(128+63);
  tab(40,29); printf(" F7   ");
  tab(40,30); printf("      ");

}
if(f8==2)
{
  colour(128+1);
  tab(46,29); printf(" F8   ");
  tab(46,30); printf("Invt.");
}
```

```c
else
{
 colour(128+63);
 tab(46,29); printf(" F8   ");
 tab(46,30); printf("Invt.");
}
if(f9==2)
{
 colour(128+1);
 tab(53,29); printf(" F9   ");
 tab(53,30); printf("CT No");
}
else
{
 colour(128+63);
 tab(53,29); printf(" F9   ");
 tab(53,30); printf("CT No");
}
if(f10==2)
{
 colour(128+1);
 tab(60,29); printf(" F10 ");
 tab(60,30); printf("Edisp");
}
else
{
 colour(128+63);
 tab(60,29); printf(" F10 ");
 tab(60,30); printf("Edisp");
}
if(f11==2)
{
 colour(128+1);
 tab(67,29); printf(" F11 ");
 tab(67,30); printf("Ldisp");
}
else
{
 colour(128+63);
 tab(67,29); printf(" F11 ");
 tab(67,30); printf("Ldisp");
}
if(f12==2)
{
 colour(128+1);
 tab(74,29); printf(" F12 ");
 tab(74,30); printf("More ");
}
else
{
 colour(128+63);
 tab(74,29); printf(" F12 ");
 tab(74,30); printf("More ");
}
tab(21,27);
printf("File: %s",Instring);
}
```

```c
/**************************************************/
/*                                                */
/*          Read CT number with mouse.            */
/*                                                */
/**************************************************/

int   procmouse(a,step,ind)
int   step,ind;
float     a[150][150];
{

     int   xm,ym,bm,bmf=1;
     float ct,setval;
     int   mouseX(void);
     int   mouseY(void);
     int   mouseB(void);
     void tab(in,int);
     void vduq(int,int,int,int,int,int,int,int,int,int);

     system("*pointer");
     tab(70,9); printf("CT Number");
     tab(69,12); printf("X Cord:");
     tab(69,14); printf("Y Cord:");
     tab(71,25); printf("E - End");
     while(1)
     {
      xm=mouseX();
      ym=mouseY();
      bm=mouseB();
      xm-=25;
      ym-=(1000-(ind*step));
      xm=(int)(xm/step);
      ym=(int)(ym/step);
      xm++;
      ym++;
      if(xm>ind) xm=ind;
      if(ym>ind) ym=ind;
      if(xm<1) xm=1;
      if(ym<1) ym=1;
      ct=a[xm][ym];

      if(bm==4) { bmf=2; setval=0.017/ct; }
      if(bmf==2) ct=(((ct*setval)-0.017)*(500/0.017));
      if(bmf==2) {tab(70,10); printf("%5d",(int)ct);}
      tab(75,12);
      printf(" %2d ",xm);
      tab(75,14);
      printf(" %2d ",ym);
      if(inkey(-35)) break;
     }
     colour(128+63)
     tab(69,10); printf("                 ");
     tab(69,9);  printf("                 ");
     tab(69,12); printf("                 ");
     tab(69,14); printf("                 ");
     tab(71,25); printf("                 ");
     system("*pointer 0");
}
```

47

```
/******************************************************/
/*                                                    */
/*        Routine for sharpening Images.              */
/*                                                    */
/******************************************************/

int   sharpenimage(c,top1,bottom1,top2,bottom2,ind,step,
                   bfg,blur,fcount,sharp,invert)
float      c[693][693];
int   top1,top2,bottom1,bottom2,ind,step,bfg,blur;
int   fcount,sharp,invert;
{
     float      mins,maxs,dmy[6][693];
     int        f,g
     mins=0.0;
     maxs=0.0;
     for(g=1;g<=(ind*3);g++)
     {
      dmy[1][g]=c[1][g];
      dmy[2][g]=c[2][g];
      dmy[3][g]=c[3][g];
      dmy[4][g]=c[4][g];
      dmy[5][g]=c[5][g];
     }
     for(f=6;f<=(ind*3);f++)
     {
      for(g=1;g=(ind*3);g++)
      {
       c[f-3][g+2]=0 - dmy[1][g+1*2 - dmy[1][g+2]*4 -
                  dmy[1][g+3]*2 - dmy[2][g]*2 +
                  dmy[2][g+1]*2 + dmy[2][g+2]*4 +
                  dmy[2][g+3]*2 - dmy[2][g+4]*2 -
                  dmy[3][g]*4 + dmy[3][g+1]*4 +
                  dmy[3][g+2]*12 + dmy[3][g+3]*4 -
                  dmy[3][g+4]*4 - dmy[4][g]*2 +
                  dmy[4][g+1]*2 + dmy[4][g+2]*4 +
                  dmy[4][g+3]*2 - dmy[4][g+4]*2 -
                  dmy[5][g+1]*2 - dmy[5][g+2]*4 -
                  dmy[5][g+3]*2;
      if(c[f-3][g+2]<0)
      {
       if((c[f-3][g+2]*-1.0)>mins) mins=c[f-3][g+2];
      }
      else
      {
       if(c[f-3][g+2]>maxs) maxs=c[f-3][g+2];
      }
      for(g=1;g<=(ind*3);g++)
      {
       dmy[1][g]=dmy[2][g];
       dmy[2][g]=dmy[3][g];
       dmy[3][g]=dmy[4][g];
       dmy[4][g]=dmy[5][g];
       dmy[5][g]=c[f][g];
      }
     }
     maxs+=mins;
```

```
          for(f=1;f<=(ind*3);f++)
          {
           for(g=1;g<=(ind*3);g++)
           {
            c[f][g]+=mins;
            c[f][g]*=(53.0/maxs);
           }
          }
          if(invert==1) display(c,top1,bottom1,top2,bottom2,
                      ind,step,bfg,blur,fcount,sharp);
          if(invert==2) invdisplay(c,top1,bottom1,top2,
                  bottom2,ind,step,bfg,blur,fcount,sharp);
}


/****************************************************/
/*                                                  */
/*           Full Screen Display.                   */
/*                                                  */
/****************************************************/


int fulldisplay(c,top1,bottom1,top2,bottom2,ind,step,bfg,
           blur,fno,sharp);
float      c[693][693];
int        top1,top2,bottom1,bottom2,ind,step;
int        bfg,blur,fno,sharp;
{
     int   t,g,f,tt[54],cc[54],in,stp,xx,y;
     float x;
     void        rectanglefill(int,int,int,int);
     void        gcol(int,int);
     void        vduq(int,int,int,int,int);

     static int ttc[]={1,1,1,1,1,1,65,180,250,1,65,1,65,
                       180,1,65,180,250,180,250,65,1,1,
                       180,65,1,65,1,1,65,180,1,65,180,
                       250,180,250,250,180,65,250,180,65,
                       250,180,65,1,250,180,65,1,250,65,1};

     static int ccc[]={0,0,0,0,0,16,16,16,16,32,32,48,48,
                       48,52,52,52,52,56,56,60,60,61,40,
                       40,40,24,24,25,25,25,14,14,14,14,
                       15,15,31,31,31,11,11,11,7,7,7,7,
                       2,2,2,2,1,1,1};


     static int ttm[]={1,1,1,1,1,1,65,65,65,180,180,180,
                       250,250,250,1,1,1,65,65,65,180,180
                       180,250,250,250,1,1,1,65,65,65,180,
                       180,180,250,250,250,1,1,1,65,65,65,
                       180,180,180,250,250,250,250,
                       250,250};

     static int ccm[]={0,0,0,0,0,0,0,0,0,0,0,0,0,0,0,21,
                       21,21,21,21,21,21,21,21,21,21,21,
                       42,42,42,42,42,42,42,42,42,42,42,
```

49

```
                        42,63,63,63,63,63,63,63,63,63,63,
                        63,63,63,63,63};

        if(fno==0)  {xx=0;    y=0;}
        if(fno==1)  {xx=440;  y=0;}
        if(fno==2)  {xx=0;    y=440;}
        if(fno==3)  {xx=440;  y=440;}
        if(bfg==1)
        {
          for(f=0;f<=53;f++)
          {
            cc[f]=ccc[f];
            tt[f]=ttc[f];
          }
        }
        else
        {
          for(f=0;f<=53;f++)
          {
            cc[f]=ccm[f];
            tt[f]=ttm[f];
          }
        }
        if(blur==2||sharp==2)
        {
          stp=(int)(step/3.0);
          in=ind*3;
        }
        else
        {
          in=ind;
          stp=step;
        }
        for(f=1;f<=inf++)
        {
          for(g=1;g<=in;g++)
          {
            t=(int)c[f][g];
            if(t>top2)  t=0;
            if(t<bottom2)  t=0;
            t-=bottom2;
            if(t<0)  t=0
            x=t*1.0;
            t=(int)((53.0*t)/(top2-bottom2));
            if(top1>53.0)  top1=53.0;
            if(t>top1)  t=53;
            if(t<bottom1)  t=53;
            if(tt[t]==1)    vduq(23,17,2,0x00);
            if(tt[t]==65)   vduq(23,17,2,0x40);
            if(tt[t]==180)  vduq(23,17,2,0x80);
            if(tt[t]==250)  vduq(23,17,2,0xc0);
            gcol(0,cc[t]);
            rectanglefill(150+xx+((g-1)*stp),1023-y-(f*stp),
                          stp-2,stp-2);
            if(inkey(-35))  break;
          }
          if(inkey(-35))  break;
        }
        for(t=0;t<=53;t++)
        {
```

```
      if(tt[t]==1)   vduq(23,17,2,0x00);
      if(tt[t]==65)  vduq(23,17,2,0x40);
      if(tt[t]==180) vduq(23,17,2,0x80);
      if(tt[t]==250) vduq(23,17,2,0xc0);
      gcol(0,cc[t]);
      rectaglefill(1000,120+(t*16),20,20);
      }
      label();
   }
```

The following program will drive the stepper motors
and take the data in a 24 X 24 CT scan. It runs on
the BBC computer.

```
1       CLOSE#0
10      CLEAR:CLS
11      LAST=999
15      XX=OPENOUT("DATA")
20      PROCLOADDATA
30      DIM COUNT(8,2,NUMSTEPS):REF=-1
40      PROCVARIABLES
50      PROCASSEMB
60      PROCsetup
70      PROCSETPHA
80      PROCSETIO
90      VDU3
100     PROCSCAN
110     PROCRETURN
115     CLOSE#0
120     END
130     DEF PROCLOADDATA
150      NUMSTEPS=24:NUMROTS=24:SIZESTEP=2
160      EMAX=24:TT%=10
180      ENDPROC
190     DEF PROCSCAN
195      GH=0
200      FOR stp%=0 TO NUMSTEPS-1
204      CLS
205      PRINT"STEP No. ";stp%
210      D=124:R=108
220      dir=0
235      FOR ROTAT=0 TO NUMROTS-1]
240      S=600/NUMROTS
250      PROCCOUNT
253      IF LAST<>ROTAT GOTO 250
254      PROCROTATE
256      NEXT ROTAT
260      S=(SIZESTEP*48)+11:D=124:R=108
270      PROCSTEP(S)
280      PROCROTATEBACK
370      NEXT stp%
280     ENDPROC
390     DEF PROCSTEP(S)
400      B=&FE60
410      &(B+2)=255
420      FOR X=1 TO S
430      &B=D
440      Q=TIME+5
450      REPEAT
460      UNTIL TIME>=Q
470      &B=R
480      Q=TIME+5
490      REPEAT
500      UNTIL TIME>=Q
510      NEXT X
520     ENDPROC
530     DEF PROCROTATE
540      D=14:R=12
550      PROCSTEP(S)
```

```
560   ENDPROC
570   DEF PROCRETURN
580    S=600+(600/NUMROTS)
590    PROCSTEP(S)
600    CLS:PRINT TAB(2,12)"SCAN FINISHED"
610   ENDPROC
620   DEF PROCCCOUT
630    PROCsetup
640    PROCclear
650    PROCstartpha
660    VDU3
670    TIME=0
680    REPEAT
690    UNTIL TIME=9500
700    PROCTRANSFER
710    PROCINTERPRET
720   ENDPROC
730   DEF PROCTRANSFER
740    PROCsetup
750    PROCrunio
760    CALL INIT
770    IF ?(DELAYL)= AND ?(DELAYH)=0 THEN VDU3:PRINT"***":
      VDU2:GOTO 740
780    ?MEMLOC=00:?(MEMLOC+1)=&48:?114=255
790    VDU3
800   ENDPROC
810   DEF PROCsetup
820    *FX5,2
830    *FX8,6
840    *FX7,6
850    VDU2
860    VDU1,7
870   ENDPROC
880   DEF PROCSETPHA
890    VDU1,67:FOR TT=1 TO 1000:NEXT TT
900    VDU1,83:FOR TT=1 TO 1000:NEXT TT
910    VDU1,80:FOR TT=1 TO 1000:NEXT TT
920    VDU1,78:FOR TT=1 TO 1000:NEXT TT
930    VDU1,64:FOR TT=1 TO 1000:NEXT TT
940    VDU1,43:FOR TT=1 TO 1000:NEXT TT
950    VDU1,78:FOR TT=1 TO 1000:NEXT TT
960    VDU1,65:FOR TT=1 TO 1000:NEXT TT
970    VDU1,78:FOR TT=1 TO 1000:NEXT TT
980    VDU1,90:FOR TT=1 TO 1000:NEXT TT
990    VDU1,57:FOR TT=1 TO 1000:NEXT TT
1000   VDU1,48:FOR TT=1 TO 1000:NEXT TT
1010   VDU1,78:FOR TT=1 TO 1000:NEXT TT
1020  ENDPROC
1030  DEF PROCSETIO
1040   VDU1,67:FOR TT=1 TO 1000:NEXT TT
1050   VDU1,83:FOR TT=1 TO 1000:NEXT TT
1060   VDU1,73:FOR TT=1 TO 1000:NEXT TT
1070   VDU1,78:FOR TT=1 TO 1000:NEXT TT
1080   VDU1,64:FOR TT=1 TO 1000:NEXT TT
1090   VDU1,88:FOR TT=1 TO 1000:NEXT TT
1100   VDU1,78:FOR TT=1 TO 1000:NEXT TT
1110   VDU1,64:FOR TT=1 TO 1000:NEXT TT
1120   VDU1,49:FOR TT=1 TO 1000:NEXT TT
1130   VDU1,78:FOR TT=1 TO 1000:NEXT TT
```

```
1140   VDU1,64:FOR TT=1 TO 1000:NEXT TT
1150   VDU1,85:FOR TT=1 TO 1000:NEXT TT
1160   VDU1,78:FOR TT=1 TO 1000:NEXT TT
1170   VDU1,64:FOR TT=1 TO 1000:NEXT TT
1180   VDU1,71:FOR TT=1 TO 1000:NEXT TT
1190   VDU1,78:FOR TT=1 TO 1000:NEXT TT
1200 ENDPROC
1210 DEF PROCCLEAR
1220   VDU1,67:FOR TT=1 TO 1000:NEXT TT
1230   VDU1,48:FOR TT=1 TO 1000:NEXT TT
1240   VDU1,62:FOR TT=1 TO 1000:NEXT TT
1250   VDU1,65:FOR TT=1 TO 1000:NEXT TT
1260 ENDPROC
1270 DEF PROCstartpha
1280   VDU1,67:FOR TT=1 TO 1000:NEXT TT
1290   VDU1,82:FOR TT=1 TO 1000:NEXT TT
1300   VDU1,80:FOR TT=1 TO 1000:NEXT TT
1310 ENDPROC
1320 DEF PROCrunio
1330   VDU1,67:FOR TT=1 TO 1000:NEXT TT
1340   VDU1,82:FOR TT=1 TO 1000:NEXT TT
1350   VDU1,73:FOR TT=1 TO 1000:NEXT TT
1360   VDU3
1370 ENDPROC
1380 DEF PROCINTERPRET
1390   A$=""
1400   MEM=18705
1410   FOR mem=MEM TO MEM+12
1420    IF ?(mem)>=48 AND ?(mem)<=57 OR ?(mem)=32 THEN GOTO
       1440
1430   A$=A$+CHR$(?(mem))
1440   NEXT mem
1450   IF A$=" " GOTO 1500
1460   COUNT1(1,dir,stp%)=VAL(A$)
1470   PRINT#XX,COUNT1(1,dir,stp%)
1480   PRINT COUNT1(1,dir,stp%),ROTAT,stp%:LAST=ROTAT
1490   GOTO 1510
1500   IF A$=" " THEN PROCclearMEM:PROCTRANSFER:GOTO 1400
1510   A$=" "
1520   PROCclearMEM
1530 ENDPROC
1540 DEF PROCclearMEM
1550   MEM=18600
1560   REPEAT
1570   ?MEM=0
1580   MEM=MEM+1
1590   UNTIL MEM=19000
1600 ENDPROC
1610 DEF PROCVARIABLES
1620   CONREG=&FE08:STATREG=&FE08:RECREG=&FE09
1630   MEMLOC=&70:STORE=&72:NUMCHR=&73:COMPARE1=&74:
       COMPARE2=&75:DELAYL=&76:DELAYH=&77
1640   ?MEMLOC=00:?(MEMLOC+1)=&48:?STORE=255:?COMPARE1=&49
       :?COMPARE2=&F7
1650 ENDPROC
1660 DEF PROCASSEMB
1670 FOR N=0 TO 2 STEP 2
1680 P%=30000
1690 [OPT N
1700 .INIT      LDA #03
```

```
1710            STA  CONREG
1720            LDA  #&12
1730            STA  CONREG
1740            LDA  #255
1750            STA  DELAYH
1760            LDA  #255
1770            STA  DELAYL
1780  .LOOP     LDY  #00
1790            DEC  DELAYL
1800            LDA  #00
1810            CMP  DELAYL
1820            BEQ  SKP
1830            LDA  #01
1840            BIT  STATREG
1850            BEQ  LOOP
1860            LDA  RECREG
1870            CMP  #22
1880            BEQ  LOOP
1890            CMP  #23
1900            BEQ  LOOP
1910            CMP  #13
1920            BEQ  LOOP
1930            CMP  #0
1940            BEQ  LOOP
1950            CMP  #10
1960            BEQ  LOOP
1970            CMP  #25
1980            BEQ  LOOP
1990            LDY  STORE
2000            STA  (MEMLOC),Y
2010            CMP  #04
2020            BEQ  QUIT
2030            INY
2040            STY  STORE
2050            CPY  NUMCHR
2060            BEQ  LOOP2
2070            JMP  COMP
2080            JMP  INIT
2090  .LOOP2    INC  (MEMLOC+1)
2100            JMP  INIT
2110  .COMP     LDX  (MEMLOC+1)
2120            CPX  COMPARE1
2130            BEQ  CONP
2140            JMP  INIT
2150  .CONP     LDX  STORE
2160            CPX  COMPARE2
2170            BEQ  QUIT
2180            JMP  INIT
2190  .SKP      DEC  DELAYH
2200            LDA  #00
2210            CMP  DELAYH
2220            BEQ  QUIT
2230            LDA  #255
2240            STA  DELAYL
2250            JMP  LOOP
2260  .QUIT     RTS
2270  ]
2280  NEXT N
2290  ENDPROC
```

```
2300 DEF PROCROTATEBACK
2310  S=615
2320  D=14:R=12
2330  PROCSTEP(S)
2340 ENDPROC
```

```c
/********************************************************/
/*                                                      */
/* Program to add Poisson Noise to the projection data. */
/*                                                      */
/*              Written By:   Neil O'Hare               */
/*                                                      */
/********************************************************/

#include <stdio.h>
#include <math.h>
#include <float.h>
#include <stdlib.h>
#include <arthur.h>

#define PI 3.14159

int noise1(float);
int rand();
int time();


int main(void)
{
      int i,j;
      int x,cc[50],sec;
      float a[50][50];
      FILE *fp;

      time(&sec);
      srand(sec);
      fp=fopen("JONIE","r");
      for(i=1;i<=45;i++)
      {
            fscanf(fp,"%d",&cc[i]);
      }
      fclose(fp);
      fp=fopen("Noisedat","w");
      for(i=1;i<=45;i++)
      {
        for(j=1;j<=45;j++)
        {
           a[i][j]=(float)noise1((float)cc[i])*1.0;
           printf("%f      %d       %d",a[i][j],i,j);
        }
      }
      for(i=1;i<=45;i++)
      {
       for(j=1;j<=45;j++)
       {
        fprintf(fp,"%f",a[j][i]);
        printf("%f",a[j][i]);
       }
      }
      fclose(fp);
      return(1);
}
```

57

```c
/*********************************************************/
/*                                                     */
/*         Adding   poisson noise   to   the   data.   */
/*                                                     */
/*********************************************************/
int  noise1(float  n)
{
     float  x,r,rn,i,d,t,p,q,z;
     r=sqrt(n);
     rn=(float)rand()/33000.0;
     i=t=0.0;
     d=(6.0*r)/100.0;
     for(x=(-3.0*r);t<=rn;x+=d)
     {
      p=(1.0/ (float) sqrt( (double)2*PI*n) ) * (float)
        exp((double)-0.5*((x*x)/n));
      i+=p;
      z=x-(3.0*r);
       q=(1.0/(float)sqrt( (double)2*PI*n) ) * (float)
        exp((double)-0.5*((z*z)/n));
      t=(i-(p+q)/2.0)*d;
      d=(6.0*r)/100.0;
     }
     return((int)n+x);
}
```

```
/*******************************************************/
/*                                                     */
/*     Program to generate simulated data, subtract    */
/*       images, add poisson noise and reconstruct.    */
/*                                                     */
/*              Written By: Neil O'Hare                */
/*                                                     */
/*******************************************************/


#include <stdio.h>
#include <math.h>
#include <stdlib.h>
#include <arthur.h>


#define   PI    3.14159
#define   steps 100.
#define   theta PI/steps
#define   step  0.042/steps

float a[(int)(steps*steps)+5];
float f[(int)(steps*2)+10][(int)(steps*2)+10]=0.0;

int time();

void main()
{
      int         i,r,t,k,s,j,p,rb,rc,sec;
      int         pixel=0,pixeli=0;
      int         gg,ff;
      int         xx[(int)(steps*2)+1][(int)(steps*2)+1];

      float       mo=0.0,mi=0.0,angle;
      float       maxx,minn1,minn2,phi;
      float       cosphi,tanphi,x,y,jc,menn;
      float       xl[(int)(steps*steps)+5];
      float       stp[(int)(steps*steps)+(int)(steps*15)];
      float       lambda[(int)steps+15][(int)steps+15];
      float       atten[(int)steps+1],fact,mw,mr;
      float       cept,range,xb,xc,b,c;

      char        Instring[15],buffer[6];

      float       noise1(float);
      float       cos(float),tan(float);

      FILE *fp;


/*******************************************************/
/*                                                     */
/*         Reading the data from chosen file.          */
/*                                                     */
/*******************************************************/

      mr=42.0;
      fp=fopen("0analy","r");
      for(i=1;i<=(steps*steps);i++)
```

```c
    fscanf(fp,"%f",&a[i]);
fclose(fp);
maxx=0.0;
rc=(steps/2.0)-2;
for(rb=(int)((steps/2.0)*0.7);
     rb<=(int)((steps/2.0)*0.7);rb+=2)
{
 menn=0.0;
 while(menn>.165||menn<.16)
 for(mw=44.0;mw<=47.;mw+=0.5)
 {
   for(j=1;j<=(steps+15);j++)
   for(k=1;k<=(steps+15);k++)
      lambda[k][j]=0.0;
   for(i=1;i<=((steps*steps)+5);xl[i++]=0.0);
   for(i=1;i<=((steps*steps)+(steps*15));
        stp[i++]=0.0);
   for(s=1;s<=(int)(steps/2.0)+1;atten[s++]=1.0);
   for(s=1;s<=rb;s++)
   {
      fact=((s-0.5)*(s-0.5));
      xb=sqrt((rb*rb)-fact);
      xc=sqrt((rc*rc)-fact);
      b=(xb)*2;
      c=(xc-xb)*2;
      atten[s]=exp(-(mw*b+mr*c)*step);
   }
   time(&sec);
   srand(sec);
   for(s=rb+1;s<=rc;s++)
   {
    fact=((s-0.5)*(s-0.5));
    xc=sqrt((rc*rc)-fact);
    c=(xc)*2;
    atten[s]=exp(-(mr*c)*step);
   }
   i=1;
   for(j=0;j<=steps-1;j++)
   {
    for(s=1;s<=steps;s++)
     {
      if(s<(int)((steps/2.0)+1))
          xl[i++]=atten[(int)((steps/2.0)+1)-s];
      if(s>(int)(steps/2.0))
          xl[i++]=atten[s-(int)(steps/2.0)]*3000;
     }
   }
   for(i=1;i<=(steps*steps);i++)
   {
    if (xl[i]==0) xl[i]=4;
    xl[i]=noise1(xl[i]);
   }

/*

   fp=fopen("0analy","w");
   for(i=1;i<=(steps*steps);i++)
    fprintf(fp,"%f",xl[i]);
   fclose(fp);
   exit(0);
*/
```

60

```
                    maxx=3300.0;
                    for (i=1;i<=(steps*steps);i++)
                    {
                     jc=(float)log((double)a[i]/xl[i]);
                     xl[i]=jc;
                    }

        /*****************************************************/
        /*                                                   */
        /*          The Backprojection Algorithim            */
        /*                                                   */
        /*****************************************************/

                    i=1;
                    for(r=0;r<=(steps-1);r++)
                    {
                     for(t=((r*(steps+10))+1);t<=((r*(steps+10))+5);t++)
                     stp[t]=0.0;
                     for (t=((r*(steps+10))+(steps+6));
                          t<=((r*(steps+10))+(steps+10));t++)
                       stp[t]=0.0;
                     for (t=((r*(steps+10))+6);
                          t<=((r*(steps+10))+(steps+5));t++)
                       stp[t]=xl[i++];
                    }
                    for(r=0;r<=(steps-1);r++)
                    {
                     for(k=((r*(steps+10))+6);
                          k<=((r*(steps+10))+(steps+5));k++)
                      {
                       lambda[(int)(k-(r*(steps+10))-5)][r]
                        =(stp[k]*0.25)-((stp[k-1]*0.101)+
                        (stp[k+1]*0.101))-((stp[k-3]*0.0112)
                        +(stp[k+3]*0.0112))-((stp[k-5]*0.004)+
                        (stp[k+5]*0.004));
                      }
                    }
                    for(j=1;j<=(steps*2);j++)
                     for(k=1;k<=(steps*2);k++) f[k][j]=0.0;
                    for(r=0;r<=(steps-1);r++)
                    {
                     phi=r*theta;
                     cosphi=cos(phi);
                     tanphi=tan(phi);
                     if(r==(int)(steps/2.0))
                      {
                       for(s=1;s<=(steps*2);s++)
                        {
                         p=((s+1.0)/2.0);
                         for(j=1;j<=(steps*2);j++)
                          f[s][j]+=(lambda[p][r]/(steps*2.0));
                        }
                      continue;
                      }
                     range=fabs(0.5/cosphi);
                     if(range>steps) range=steps;
                     for(s=1;s<=(steps*2);s++)
                      {
                       cept=((steps+0.5)-s)/cosphi;
                       for(x=-(steps-0.5);x<=(steps-0.5);x++)
```

61

```c
          {
           y=(x*tanphi)+cept;
           k=(int)(steps+1)+x;
           jc=(steps+1.0)-y;
           if((jc>(steps*2+7.0))||(jc<-7.0)) continue;
           for(j=(jc-range);j<=(jc+range);j++)
            {
             if((j<=0)||(j>(steps*2))) continue;
             p=((s+1.0)/2.0);
             f[k][j]+=(lambda[p][r]/(steps*2.0));
            }
          }
        }
      }

/*****************************************************/
/*                                                   */
/*         Saving the backprojected image.           */
/*                                                   */
/*****************************************************/

        sprintf(Instring,"fsub");
        sprintf(buffer,"%d",(int)((mw-mr)*10));
        strcat(Instring,buffer);
        minn1=10000.0;
        for(j=1;j<=(steps*2);j++)
        {
          for(k=1;k<=(steps*2);k++)
          {
           f[k][j]+=10.0;
           minn1=(minn1>f[k][j])?f[k][j]:minn1;
           xx[k][j]=0;
          }
        }
        maxx=0.0;
        for(j=1;j<=(steps*2);j++)
        {
          for(k=1;k<=(steps*2);k++)
          {
           f[k][j]-=minn1;
           maxx=(maxx<f[k][j])?f[k][j]:maxx;
          }
        }
        for(j=1;j<=(steps*2);j++)
          for(k=1;k<=(steps*2);k++)
            f[k][j]/=maxx;
        fp=fopen(Instring,"w");
        fprintf(fp,"1.00");
        for(j=1;j<=(steps*2);j++)
        {
          for(k=1;k<=(steps*2);k++)
          {
           fprintf(fp,"%f",f[k][j]);
          }
        }
        fclose(fp);
        pixeli=pixel=0;
        mi=0.0;
        for(j=1;j<=(rb*2);j++)
        {
```

62

```
      for(angle=0.0;angle<=2.0*PI;
         angle+=(PI/(steps*2.0)))
     {
       gg=(int)(steps-0.5+(j*cos(angle)));
       ff=(int)(steps-0.5+(j*sin(angle)));
       if(xx[ff][gg]!=1)
       {
        mi+=f[ff][gg];
        xx[ff][gg]=1;
        pixeli++;
       }
     }
    }
    mi/=pixeli;
    mo=0.0;
    for(j=(rb*2)+1;j<=(rb*2)+4;j++)
    {
     for(angle=0.0;angle<=2.0*PI;
         angle+=(PI/(steps*2.0)))
     {
       gg=(int)(steps-0.5+(j*cos(angle)));
       ff=(int)(steps-0.5+(j*sin(angle)));
       if(xx[ff][gg]!=1)
       {
        mo+=f[ff][gg];
        xx[ff][gg]=1;
        pixel++;
       }
     }
    }
    mo/=pixel;

    menn=(mi-mo);
    printf("mean = %5.3fdu = %5.3f    rb =
             %d",menn,mw-mr,rb);
    if(menn>.165) mw-=0.1;
    if(menn<.16) mw+=0.1;
    if(menn<.14) mw+=1.0;
   }
   printf("mean = %5.3f  du = %5.3f     rb =
             %d",menn,mw-mr,rb);
  }

}

/*******************************************************/
/*                                                     */
/*       Adding Poisson Noise to the Data.             */
/*                                                     */
/*******************************************************/

int noise1(float  n)
{

     float      x,r,rn,i,d,t,p,q,z;

     r=sqrt(n);
     rn=(float)rand()/33000.0;
     i=t=0.0;
     d=(6.0*r)/100.0;
```

63

```c
for(x=(-3.0*r);t<=rn;x+=d)
{
 p=(1.0/(float)sqrt((double)2*PI*n))
   (float)exp((double)-0.5*((x*x)/n));
 i+=p;
 z=x-(3.0*r);
 q=(1.0/(float)sqrt((double)2*PI*n)) *
   (float)exp((double)-0.5*((z*z)/n));
 t=(i-(p+q)/2.0)*d;
 d=(6.0*r)/100.0;
}
return((int)n+x);

}
```

C.Backart

```c
/**********************************************************/
/*                                                        */
/*    The following program yields an image in a 40x40    */
/*    matrix. It uses the backprojection algorithm        */
/*    first and uses the image obtained as the starting   */
/*    point for the ART algorithm.                        */
/*                                                        */
/*          Written By:    Neil O'Hare                    */
/*                                                        */
/**********************************************************/

#include    <stdio.h>
#include    <auther.h>
#include    <math.h>
#include    <float.h>
#include    <stdlib.h>
#include    <time.h>

#define     STRINGLEN1      10

void main()
{

/**********************************************************/
/*                                                        */
/*     Declaration & Initialisation of variables.         */
/*                                                        */
/**********************************************************/

        int         j,cc,dsa,t,n,p,i,k,r,s;
        int         s1,r1,a,z,ff,rotate,step;
        int         tim,jj[600],kk[600];

        float       fx[40][40],sum2,vb,ill,ii,mean;
        float       ffr,minutes,minn1,minn2,maxx,maxx1;
        float       xl[1601],xx[41][41],l[1601],yy[41][41];
        float       f[81][81],corrct[2200],lambda[50][50];
        float       stp[2200],diff,vv[600],standev,oldstd;
        float       theta,phi,cosphi,tanphi,range,cept;
        float       x1,v,correct,correct1,x,y,jc,sum1;

        double      cos(double),tan(double),fabs(float);
        double      log(double);

        FILE        *fp,*fopen();

        char        Instring[STRINGLEN];

        j=cc=dsa=t=n=p=i=k=r=s=s1=r1=0;
        a=z=ff=rotate=step=tim=0;
        sum2=vb=ill=ii=mean=ffr=minutes=minn1=0.0;
        minn2=maxx=diff=standev=oldstd=theta=phi=0.0;
        cosphi=tanphi=range=cept=x1=v=x=y=jc=sum1=0.0;
        correct=correct1=0.0;
        for(i=1;i<=600;i++){ jj[i]=kk[i]=0; vv[i]=0.0; }
        for(i=1;i<=2200;i++) corrct[i]=stp[i]=0.0;
        for(k=1;k<=40;k++)
```

65

```c
            {
             for(j=1;j<=40;j++) fx[j][k]=xx[j][k]=yy[j][k]=0.0;
            }
            for(k=1;k<=1601;k++) l[k]=0.0;
            for(k=1;k<=50;k++)
            {
             for(j=1;j<=50;j++) lambda[j][k]=0.0;
            }
            for(k=1;k<=81;k++)
             for(j=1;j<=81;j++) f[j][k]=0.0;
```

```c
/******************************************************/
/*                                                    */
/*        Reading the data from a chosen file.        */
/*                                                    */
/******************************************************/

            cls();
            system("*.");
            printf("\n\n\n\t Input the file name:   ");
            fgets(Instring,STRINGLEN,stdin);
            fp=fopen(Instring,"r");
            cls();
            for(i=1;i<=1600;i++) fscanf(fp,"%e",&xl[i]);
            printf("\t---- File now closed. ----\n\n\n");
            fclose(fp);
            maxx=0;
            for(i=1;i<=1600;i++) maxx=(xl[i]>maxx)?xl[i]:maxx;
            for(i=1;i<=1600;i++) l[i]=log((double)maxx/xl[i]);
            cc=1;
            for(j=1;j<=40;j++)
             for(k=1;k<=40;k++) xx[j][k]=l[c++];
```

```c
/******************************************************/
/*                                                    */
/*      Shifting the data by a chosen amount.         */
/*                                                    */
/******************************************************/

            printf("Input the shifting factor: - ");
            scanf("%f",&xl);
            correct=xl;
            if(correct>0.0) dsa=-1; else dsa=1;
            correct=(correct<0.0)?(correct*-1.0):correct;
            correct1=1.0-correct;
            i=1;
            for(j=1;j<=40;j++)
            {
             for(k=1;k<=40;k++)
             {
              if((k+dsa)>40) yy[j][k]=0.0;
              yy[j][k]=(correct1*xx[j][k])+
                       (correct*xx[j][(k+dsa)]);
             }
            }
            steps=40;
            theta=3.14159/40;
```

```
/*****************************************************/
/*                                                   */
/*         The backprojection algorithm.             */
/*                                                   */
/*****************************************************/


        i=1;
        for(r=0;r<=(steps-1);r++)
        {
         for(t=((r*(steps+10))+1);t<=((r*(steps+10))+5);t++)
         stp[t]=0.0;
         for (t=((r*(steps+10))+(steps+6));
              t<=((r*(steps+10))+(steps+10));t++)
             stp[t]=0.0;
         for (t=((r*(steps+10))+6);
              t<=((r*(steps+10))+(steps+5));t++)
             stp[t]=xl[i++];
        }
        for(r=0;r<=(steps-1);r++)
        {
         for(k=((r*(steps+10))+6);
             k<=((r*(steps+10))+(steps+5));k++)
         {
            lambda[(int)(k-(r*(steps+10))-5)][r]
             =(stp[k]*0.25)-((stp[k-1]*0.101)+
              (stp[k+1]*0.101))-((stp[k-3]*0.0112)
              +(stp[k+3]*0.0112))-((stp[k-5]*0.004)+
              (stp[k+5]*0.004));
         }
        }
        for(j=1;j<=(steps*2);j++)
         for(k=1;k<=(steps*2);k++) f[k][j]=0.0;
        for(r=0;r<=(steps-1);r++)
        {
         phi=r*theta;
         cosphi=cos(phi);
         tanphi=tan(phi);
         if(r==(int)(steps/2.0))
         {
            for(s=1;s<=(steps*2);s++)
            {
             p=((s+1.0)/2.0);
             for(j=1;j<=(steps*2);j++)
              f[s][j]+=(lambda[p][r]/(steps*2.0));
            }
         continue;
         }
         range=fabs(0.5/cosphi);
         if(range>steps) range=steps;
         for(s=1;s<=(steps*2);s++)
         {
          cept=((steps+0.5)-s)/cosphi;
          for(x=-(steps-0.5);x<=(steps-0.5);x++)
            {
             y=(x*tanphi)+cept;
             k=(int)(steps+1)+x;
             jc=(steps+1.0)-y;
             if((jc>(steps*2+7.0))||(jc<-7.0)) continue;
             for(j=(jc-range);j<=(jc+range);j++)
```

67

```c
            {
             if((j<=0)||(j>(steps*2))) continue;
             p=((s+1.0)/2.0);
             f[k][j]+=(lambda[p][r]/(steps*2.0));
            }
          }
        }
      }
```

```
/******************************************************/
/*                                                    */
/*        Saving the backprojected image.             */
/*                                                    */
/******************************************************/
```

```c
      printf("\n\n\n\n");
      fp=fopen("artrecon","w");
      i=1;minn1=minn2=1.0e20;
      for(j=1;j<=80;j++)
      {
       for(k=1;k<=80;k++)
       {
        fprintf(fp,"%f\n",f[k][j]);
        minn1=(sum1<minn1)?sum1:minn1;
       }
      }
      fclose(fp);
      cls();
      printf("\n\n\nFinished Backprojection\n\n");
```

```
/******************************************************/
/*                                                    */
/*      Reading the data for the ART section.         */
/*                                                    */
/******************************************************/
```

```c
      fp=fopen(Instring,"r");
      i=1;
      minn2=1.0E20;
      maxx=0.0;
      for(j=0;j<=39;j++)
      {
       for(k=0;k<=39;k++)
       {
        fscanf(fp,"%e",&f[k][j]);
        minn2=(f[k][j]<minn2)?f[k][j]:minn2;
       }
      }
      fclose(fp);
      for(j=0;j<=39;j++)
      {
       for(k=0;k<=39;k++)
       {
        f[k][j]/=minn2;;
        maxx=(f[k][j]>maxx)?f[k][j]:maxx;
       }
      }
      a=j=k=r=s=z=tim=i=0;
      ill=vb=ii=sum1=sum2=v=diff=0.0;
      standev=oldstd=0.0;
```

```c
        fp=fopen("artrecon","r");
        for(j=0;j<=39;j++)
         for(k=0;k<=39;k++)
           fscanf(fp,"%f",&fx[k][j]);
        fclose(fp);

/*********************************************************/
/*                                                       */
/*                The ART Algorithm.                     */
/*                                                       */
/*********************************************************/

        for(tim=1;tim<=20;tim++)
        {
                r1=0;
                s1=1;
                fp=fopen("farea40","r");
                rewind(fp);
input:          fscanf(fp,"%f,%d,%d,%d,%d\n",&v,&k,&j,&s,&r);
                s-=1;
                j-=1;
                k-=1;
                if((s==s1)&&(r==r1))
                {
                 if(v<100.0)
                  {
                   sum1+=(v*fx[k][j]);
                   sum2+=(v*v);
                  }
                 vv[a]=v;
                 jj[a]=j;
                 kk[a]=k;
                 a++;
                }
                else
                {
                 ill=f[s1][r1];
                 vb=log(maxx/ill);
                 for(z=0;z<=(a-1);z++)
                  {
                   fx[kk[z]][jj[z]]+=(0.2*vv[z]*(vb-sum1)/sum2);
                  }
                 vb=ill=0.0;
                 for(z=0;z<=160;++z)
                  {
                   vv[z]=0.0;
                   jj[z]=kk[z]=0;
                  }
                 if(v>=100.0) goto ohno;
                 s1=s;
                 r1=r;
                 a=0;
                 sum1=sum2=0.0;
                 sum1+=(v*fx[k][j]);
                 sum2+=(v*v);
                 vv[a]=v;
                 kk[a]=k;
                 jj[a]=j;
                 a++;
                 if(a>=160) a=160;
```

```c
            }

ohno:       if(v>=100.0)
            {
             fclose(fp);
             mean=0.0;
             for(j=0;j<=39;j++)
               for(k=0;k<=39;k++)
                 mean+=fx[k][j];
             mean/=1600.0;
             diff=0.0;
             for(j=0;j<=39;j++)
               for(k=0;k<=39;k++)
                 diff+=((fx[k][j]-mean)*(fx[k][j]-mean));
             ii=standev=0.0;
             standev=(sqrt(diff))/40.0;
             ii=oldstd-standev;
             if(ii<0.0 ii*=-1.0;

/************************************************************/
/*                                                          */
/*   Saving the image and checking for convergence.         */
/*                                                          */
/************************************************************/

             maxx=0.0;
             fp=fopen("fartrecon","w");
             ff=clock();
             ffr=ff;
             minutes=ffr/6000.0;
             printf("Time taken so far = %7.2lf\n",minutes);
             for(j=0;j<=39;j++)
               for(k=0;k<=39;k++)
                 maxx1=(fx[k][j]>maxx1)?fx[k][j]:maxx1;
             fprintf(fp,"%f\n",maxx1);
             for(j=0;j<=39;j++)
               for(k=0;k<=39;k++)
                 fprintf(fp,"%10.6lf\n",fx[k][j]);
             fclose(fp);
             if(ii<(oldstd/70.0)) goto end;
             oldstd=standev;
            }
            else
            {
             goto input;
            }

end:        printf("\n\n\nFinished\n\n");

}
```

70

```c
/*****************************************************/
/*                                                 */
/*   The following program calculates the overlapareas */
/*   between each pixel in the grid and each beam that */
/*   passes through the grid. These are necessary for */
/*   the implementation of ART.                     */
/*                                                 */
/*            Written By: Neil O'Hare              */
/*                                                 */
/*****************************************************/

#include <stdio.h>
#include <float.h>
#include <math.h>

#define    pi    3.1415926

void main()
{

    int       w,r,s,xp,yp,j,k;

    float     theta,cepta,ceptb,slope,area;
    float     cortop,corbot,ya,yb,slicearea,x;

    FILE      *fp,*fopen();

/*****************************************************/
/*                                                 */
/*   Find the slope and intercept points of each beam. */
/*                                                 */
/*****************************************************/

    fp=fopen("farea40","w");
    for(w=0;w<=1;++w)
     {
      for(r=0;r<=19;++r)
       {
        printf("%3d\n","r");
        theta=pi*(r/40.0);
        for(s=1;s<=40;++s)
         {
          slope=tan(theta);
          if(slope<0.0) slope*=-1.0;
          cepta=(21-s)/(cos(theta));
          if(cos(theta)<0.0) cepta*=-1.0;
          ceptb=(20-s)/(cos(theta));
          if(cos(theta)<0.0) ceptb*=-1.0;

/*****************************************************/
/*                                                 */
/*      Calculate the overlaparea and save result.   */
/*                                                 */
/*****************************************************/

          for(k=1;k<=40;k++)
           {
            for(j=1;j<=40;j++)
             {
```

71

```
            xp=k-21;
            yp=20-j;
            if((yp>((slope*xp)+cepta))&&(yp>((slope*(xp+1))+
             cepta))) continue;
            if(((yp+1)<((slope*xp)+ceptb))&&((yp+1)<((slope*
             (xp+1))+ceptb))) continue;
            area=0.0;
            for(x=(xp+0.01);x<=(xp+0.99);x+=0.02)
            {
             cortop=corbot=0.0;
             ya=(slope*x)+cepta;
             yb=(slope*x)+ceptb;
             if((ya>(yp+1))&&(yb<(yp+1))) cortop=0.0;
             if((ya<=(yp+1))&&(ya>=yp))
              cortop=(yp+1-ya)*0.02;
             if((yb>=yp)&&(yb<=(yp+1))) corbot=(yb-yp)*0.02;
             if(yb<yp)&&(ya>yp) corbot=0.0;
             clisearea=0.02-cortop-corbot;
             if(ya<yp) slicearea=0.0;
             area+=slicearea;
            }

            if(area==0.0) continue;
            if(w==0) fprintf(fp,"%10.6lf,%3d,%3d,%3d,%3d\n",
                              area,j,k,s,r);
            if(w==1) fprintf(fp,"%10.6lf,%3d,%3d,%3d,%3d\n",
                              area,j,(41-k),s,(r+20));
         }
        }
       }
      }
     }
    fprintf(fp,"100.0,1,1,1,1");
    fclose(fp);

  }
```

```c
/**********************************************************/
/*                                                        */
/*      Program to calculate the minimum concentration    */
/*       of an analyte as a function of X and f for       */
/*                  the K-edge case.                      */
/*                                                        */
/*              Written By: Neil O'Hare                   */
/*                                                        */
/**********************************************************/


#include <stdio.h>
#include <stdlib.h>
#include <math.h>

main()
{

        float   s,x,rho,um,Ca,ual;
        float   f,S,G,B,p,Not,r,Q,uah;
        float   h,j,bit1,bit2,bit3,bit4;

        FILE    *fp;

        S=100.0;
        Not=1.0E6;
        ual=0.624;
        uah=3.829;
        Ca=0.1;
        um=0.034;
        rho=1000.0;
        Q=6.0;
        G=3.0;

        fp=fopen("eqn.dat","w");

        for(x=0.5;x<=5.0;x+=0.2)
        {
        for(f=0.1;f<=1.0;f+=0.1)
        {

            do
            {

                bit1=0.0;
                for(s=1;s<=(f*S/2.0);s++)
                {
                 h=(4.0*(s-0.5)*(s-0.5)/(S*S));
                 j=(f*f)-h;
                 h=1.0-h;
                 j=sqrt((double)j);
                 h=sqrt((double)h);
                 bit1+=exp(-x*h + (x*Ca*ual*j/(rho*um)));
                }
                bit1*=(2.0/S);

                bit4=0.0;
                for(s=1;s<=(f*S/2.0);s++)
                {
```

73

```c
            h=(4.0*(s-0.5)*(s-0.5)/(S*S));
            j=(f*f)-h;
            h=1.0-h;
            j=sqrt((double)j);
            h=sqrt((double)h);
            bit4+=exp(-x*h + (x*Ca*uah*j/(rho*um)));
            }
            bit4*=(2.0/S);

            bit1=(bit1-bit4);
            if(bit1<0.0)  bit1*=-1.0;

            bit2=0.0;
            for(s=1;s<=(f*S/2.0);s++)
            {
             h=(4.0*(s-0.5)*(s-0.5)/(S*S));
             j=(f*f)-h;
             h=1.0-h;
             j=sqrt((double)j);
             h=sqrt((double)h);
             bit2+=exp(-x*h + (x*Ca*ual*j/(rho*um)));
            }
            bit2*=(2.0/S);

            bit3=0.0;
            for(s=(f*S/2.0)+1.0;s<=(S/2.0);s++)
            {
             h=(4.0*(s-0.5)*(s-0.5)/(S*S));
             h=1.0-h;
             h=sqrt((double)h);
             bit3+=exp(-x*h);
            }
            bit3*=(2.0/S);
            bit2=bit2+bit3;

            bit3=0.0;
            bit3=G*f*Q*sqrt((double)S);
            bit3/=sqrt((double)Not);
            bit3=bit2*bit3;

            Ca+=0.1;

        }while(bit1<bit3);
        fprintf(fp,"%f   %f   %f\n",f,x,Ca);
        printf("f = %f    X = %f Ca = %f \n",f,x,Ca);
        Ca=0.1;


    }
    }
    fclose(fp);


}
```

```
/*****************************************************/
/*                                                   */
/*    Program to calculate the minimum detectable    */
/*     fractional differance in mass attenuation     */
/*      coefficient as a function of X and F for     */
/*              the monochromatic case.              */
/*                                                   */
/*            Written By: Neil O'Hare                */
/*                                                   */
/*****************************************************/

#include <stdio.h>
#include <math.h>
#include <stdlib.h>

main()
{

        double   N,x,s,S,f,u;
        double   bit1,bit2,du;
        double   i,h,j,k,Not;
        double   bit3;

        FILE     *fp;


        u=42.0;
        S=50.;
        Not=1.E6;
        N=Not/(S*S);
        x=(0.045*u);
        printf("\n\n\n");


        fp=fopen("eqn.dat","w");
        f=0.5;
        du=33.1;

    for(x=0.1;x<=5.0;x+=0.1)
    {
    for(f=0.1;f<=1.0;f+=0.5)
    {

      N=Not/(S*S);
      du=0.01;
      s=(float)floor((double)(f*S/2.));

      bit3=0.0;
      for(i=1.0;i<=(S/2.0);i++)
      {
       h=0.0;
       h=(i-0.5)*(i-0.5)*4.0/(S*S);
       h=1.0-h;
       h=(float)sqrt((double)h);
       bit3+=(2.*S*N*exp(-x*h));
      }
      bit3=sqrt((double)bit3/S);
```

```c
          bit3*=9.0;
          bit1=0.0;


          do
          {

          bit1=0.0;
          for(i=1.0;i<=s;i++)
          {
           h=0.0;
           h=(i-0.5)*(i-0.5)*4.0/(S*S);
           h=1.0-h;
           h=(float)sqrt((double)h);
           bit1+=(2.*S*N*exp(-x*h));
          }

          bit2=0.0;
          for(i=1.0;i<=s;i++)
          {
           h=0.0;
           h=(i-0.5)*(i-0.5)*4.0/(S*S);
           j=sqrt((double)((f*f)-h));
           k=sqrt((double)(1.0-h));
           bit2+=(2.*S*N*exp(-x*k-((x*du/u)*j)));
          }

          bit1-=bit2;
          bit1/=(f*S);

          if(bit3>bit1) du+=0.1;

          }while(bit3>=bit1);

          fprintf(fp,"%f   %f   %f\n",x,f,du/u);

}
}
fclose(fp);

}
```

Appendix 2
Glossary of Medical Terms

Glossary of Medical and Anatomical Terms.

Abscopal Effect – Refers to secondary effects of irradiation outside treated volumes due to hormonal effects.

Acromegaly – Enlargement of head, and other symptoms associated with pituitary gland tumors.

Acute Dose Response – A response occurring either during or shortly after completion of treatment.

Adrenal Venogram – Visualisation of suspected masses in the adrenal glands. A catheter is inserted into the femoral vein, then through the vena cava up to the adrenal vein. This method has largely been surpassed by CT.

Alopecia – Loss of hair.

Amniography – Under fluoroscopic or ultrasonic guidance, a slender needle is placed in the amniotic sac and contrast material is injected. The subsequent ingestion of the contrast material by the fetus is helpful in determining certain abnormalities of he fetal gut.

Aneurysm – A sac formed by abnormal dilation of the weakened wall of a blood vessel.

Angioma – A tumor made up of blood or lymph vessels.

Angioplasty – A balloon tipped catheter is inserted into an area of narrowing, inflated under fluoroscpoic visualisation so as to dilate the area of narrowing.

Anorexia – Loss of appetite.

Arthrography – This is the study of joints and usually involves the administration of a water-soluble contrast material and air to distend the interior of the joint.

Asthenia – Lack or loss of strength and energy: weakness.

Ataxia – Loss of muscular coordination.

Atelectasis – Collapse of lung tissue caused by pressure from without, as from exudates, tumors, and the like; the density approaches that of muscle tissue.

Barium Enema – Barium is administered through a rectal tube to outline the interior of the colon.

Barium Enema (air contrast) – In this examination the colon or large bowel is half filled with barium and subsequently distended with large volumes of air. This allows excellent coating of the mucosal surface an is particularly helpful in looking for small erosive or ulcerative abnormalities, and also early cancers.

Barium Swallow – Barium is administered orally an the swallowing mechanism is examined both fluoroscopically and radiographically.

Benign – Non-malignant tumor.

Bronchrography - Local anesthetic is applied to the mucosa of the trachea and bronchial tree and an iodized oily contrast material is introduced into the trachea and bronchial tree through a small opaque catheter to the area of lung under investigation.

Buccal Mucosa - Inner lining of the cheek.

Cachexia - General ill health and malnutrition.

Cancer - A malignant new growth anywhere in the body which tends to spread, ulcerate, and destroy healthy tissue.

Carcinoma - Any of several kinds of epithelial cancer.

Carditis - Inflammation of the heart.

Cerebral Angiography - A direct puncture of the carotid arteries or puncture of a femoral artery and subsequent insertion of a catheter are the most common methods used to study the vascular circulation of the brain.

Cervical Spine - The cervical spine is the most flexible portion of the entire spinal column. As a results of this extreme degree of modality it is extremely common to have degenerative changes particularly in the region of the fifth, sixth and seventh cervical vertebral bodies.

Cervix - The lower and narrow end of the uterus.

Chemotherapy - Treatment of malignancies with drugs which act on the entire system of the body; consequently these drugs are called systemic treatment.

Cholangiography - An iodine containing contrast agent which is water soluble is injected through a peripheral vein, excreted by the liver, collects in the gallbladder, and is ultimately routed into the intestinal tract for excretion. The i.v. examination is not dependent on the small bowel for absorption, but is again dependent on normal liver function.

Cholecystography - An organic compound containing iodine in tablet form is administered the evening prior to the examination. The material is absorbed through the mucosa of the small bowel, passed through to the liver where it is excreted into the biliary system, and concentrated in the gallbladder. This examination is aimed at the evaluation of the gallbladder but is inherently dependent on normal liver function.

Clinical Staging - A method for describing the extent of a primary tumor, the condition of the regional lymph nodes, and the absence or presence of distant metastases determined by history, clinical examination, radiography, scans, lab reports, and initial biopsy report.

Colposcopy - Examination of the vagina and cervix by means of the colposcope.

Colpostat - A device for retaining something, such as a radium applicator in the vagina.

Coronary Angiography - Selective examination of the right and left coronary arteries supplying the heart, by means of contrast agent imaging.

Cystitis - Inflammation of the bladder.

Dacryocystogram - Dacrystrography is the evaluation of the tear duct that connects the eye with the nose and which is responsible for drainage of tears from the eye. The examination itself involves localisation of the opening of the duct and subsequent injection of 1cc of oily contrast material to determine whether the duct is open or

2

obstructed.

Diplopia - Double vision.

Discography - This procedure involves the injection of an oily contrast material directly into the intervertebal disc space. The purpose of this examination is to confirm the presence of a ruptured disc.

Dysphagia - Difficulty in swallowing.

Dysphonia - Difficulty in speaking.

Dysplasia - Abnormal tissue development.

Dyspnea - Difficulty in breathing.

Dysuria - Pain upon urination.

Ectasia - Dilation, expansion or distension.

Edema - Swelling.

Emphysema - Presence of air in the interstitial tissue of the lung.

Epidural Venogram - Selective catheterisation and injection of the veins around the spinal column. Used to assist in the evaluation of suspected herniated discs.

Epithelium - The covering of the internal and external surfaces of the body, including the lining of vessels and other small cavities.

Erythema - Redness of skin inflammation.

Esophagitis - Inflammation of the esophagus.

Etiology - The science or theory of the causes or origins of diseases.

Exenteration - Surgical removal of the organs, commonly used to indicate radical excision of the contents of the pelvis.

Exophthalmos - Protrusion of the eyeballs.

Exophytic - A cauliflower-like growth on the surface of an organ or structure in which the growth originated.

Fibroma - A tumor composed mainly of fibrous tissue.

Fibrosis - An abnormal increase in the amount of fibrous tissue in an organ or the skin; the narrowing or closing of minute arteries and capillaries by inflammatory internal fibrosis.

Fistula - An abnormal opening or passageway generally caused by disease or radiation necrosis between one hollow organ and another or to the skin.

Foramen - A natural opening or passage.

Fossa - A trench or channel a general term used to denote a hollow or depressed area.

Friable - Easily pulverized or crumbled.

Fungating - A large exophytic mass which has become necrotic.

Glioblastoma - Inoperable tumor of a cerebral hemisphere.

Gravida - Pregnancy.

Gynecomastia - Overdevelopment of male mammary glands.

Hemangioma - A benign tumor made up of newly formed blood vessels.

Hematemesis - Vomiting of blood.

Hematoma - A local swelling or tumor filled with effused blood.

Hematuria - Blood in the urine.

Hemianopisa - Loss of one half of the visual field.

Hemiparesis - Partial paralysis of one side of the body.

3

Hemoptysis - The coughing up of blood, usually caused by bleeding of the lungs or bronchi.
Histology - The tissue structure of an organism or of a part of the body.
Hyperplasia - The abnormal multiplication or increase in the number of normal cells in the normal arrangement of the tissue.

Indurated - Firm, hard.
Infarction - The death of part or the whole of an organ that occurs when the artery carrying its blood supply is obstructed.
Interstitial - Situated in the interspaces of a tissue.
Intrathecal - Within a sheath.
Ischemia - Deficiency of blood in a part, due to functional constriction or obstruction of a blood vessel.

Keloid - A new growth or tumor of the skin, these growths tend to recur after removal and are sometimes tender or painful.

Lacteals - The lymphatic vessels of the small intestine which contain a milk white fluid during the process of digestion and convey it into the blood through the thoracic duct.
Laporatomy - Surgical incision through the flank.
Laryngogram - Laryngography involves the application of a topical anesthetic to the surface lining of the larynx and vocal chords. Direct application of an oily contrast material is then performed.
Late effects - Effects of radiation which do not become evident until a period of many months or even years following completion of irradiation.
Lateral - Toward the outer margins of the body.
Leukoplakia - A disease marked by development on the tongue of white, thickened patches; it sometimes becomes malignant.
Lymphangiogram - A roentgenogram of the lymphatic vessels.
Lymphatics - A system of vessels with very thin transparent walls which collect fluid from the tissues and return it to the circulatory system.
Lysis - Decomposition and removal, as of killed tumor cells, resulting in regression of a mass.

Macroscopic - Visible to the naked eye.
Malignant - Life threatening.
Mastoids - The mastoids cells are air-containing pockets in the lateral portion of the temporal bones. The mastoid cells are the direct continuation of the middle ear an are frequently involve with infection and inflammation.
Medial - Toward the the center line of the body.
Metastasis - The shifting of disease from one part or organ of the body to another unrelated to it, as by the transfer of pathogenic organisms or of a malignant tumor.
Mucosa - A mucous membrane generally lining internal passages of the body opening to the exterior.
Mucositis - Inflammation of the mucosal membrane, sometimes caused by radiation.
Mycosis Fungoides - A rare chronic skin disease marked by the development on the face, scalp and chest of firm,

reddish tumors that are painful and have a tendency to spread and ulcerate.

Myelography - This is the general term describing a radiographic procedure in which contrast material is introduced into the spinal subarachnoid space by means of a spinal tap in order to evaluate the spinal cord and its appendages and their relationship to the bony spinal canal.

Myocardium - The middle layer of the three layers forming the wall of the heart, the others being the endocardium and epicardium. The myocardium forms the greater part of this wall.

Necropsy - Examination of a body after death.
Necrosis - Death of tissue in small localised areas.
Necrotic - Characterised by necrosis.
Neoplasm - Any abnormal growth of tissue, tumor, etc.
Nephrotomography - This involves taking thin slices at several levels through the kidneys by the normal tomography method.
Nocturia - Excessive urination at night.

Oncology - The study of tumors.
Orchiectomy - Excision of one or both testes.
Orchitis - Inflammation of testes.
Orthopnea - Inability to breath except in the upright position.
Otits - Inflammation of the ear.
Otits Media - Inflammation of the middle ear.

Palliative Treatment - Limited treatment designed in general to improve the quality of the rest of the patient's life.
Panotitis - Inflammation of all the parts of the ear.
Pansinusitis - Inflammation of all the parts of the paranasal sinus.
Papilloma - A branching or lobuated benign tumor derived from epithelium.
Paracentesis - Surgical puncture of a cavity for the aspiration of fluid.
Paranasal Sinuses - These are air-containing bony cavities on either side of the nose, between the eyebrows, and also posterior to the soft tissues of the interior of the nose.
Parenchyma - The essential elements of an organ relating to its function.
Paresthesia - An abnormal spontaneous sensation, such as burning or prickling.
Parotid - Situated or occurring near the ear, such as the parotid gland.
Patholgy - The branch of medicine dealing with the nature of disease, especially cells.
Perfusion - Artificial passage of fluid through blood vessels.
Pericarditis - Inflammation of the pericardium.
Pericardium - A membrane surrounding the heart.
Petechiae - Small pinpoints of red hemorrhagic spots in the skin.
Pleura - The serous membrane investing the lungs and the lining of the thoracic cavity.
Pneomoencephalogram - A spinal tap is performed, some

spinal fluid removed and replaced with a small volume of air which rises cranially to fill and outline the normally fluid-filled ventricular system of the brain. This examination is somewhat dangerous and uncomfortable for the patient. It has largely been replaced by cranial computed tomography.

Pneumonitis -A condition of localised acute inflammation of the lung without gross toxemia.

Pneumothorax - An accumulation of air or gas in the plural cavity.

Polyp - A protruding growth from the mucous membrane.

Primary - The initial site of a malignancy.

Proctitus - Inflammation of the mucous membrane of the rectum.

Prophylactic - Preventing the spread of disease not yet detectable.

Prosthesis - The replacement of an absent part by an artificial substitute.

Pulmonary Angiography - Selective examination of the right and left pulmonary arteries is occasionally used to document or further clarify suspected pulmonary embolism.

Pyelogram - An X-ray of the kidney and ureter, especially showing the pelvis of the kidney.

Radiation Potentiator - Any agent such as a drug which incenses the sensitivity of the cells or tissues to the radiation.

Radical Treatment - Treatment designed with the aim of removing or destroying all the malignancy present.

Remote Sequelae - Effects which occur after an expended period of time and are very slow in occurrence.

Retroperitoneal - Behind the peritoneum.

Sanguinous - Containing blood.

Sarcoma - A tumor made up of substance like the embryonic connective tissue, ie. composed of closely packed cells. Sarcomas are often highly malignant.

Scoliosis - Abnormal curvature of the spine.

Serous - Pertaining to or resembling serum.

Sialogram - Sialography involves the introduction of oily contrast material into the ducts of the major salivary glands. Evaluation for the presence of small stones is the primary indications for this examination.

Sigmoid - The sigmoid flexure is the S-shaped portion of the colon extending from the anus upward and curving to the left side of the body.

Sinusitis - Inflammation of the sinus.

Speculum - An appliance for opening to view a passage or cavity of the body.

Spinal Angiography - This examination is dangerous, difficult and time consuming. Its chief indication is in the evaluation of vascular malformations or tumors involving the spinal cord.

Squamous Cells - Plate-like cells composing the outer layer of the skin or lining of a body cavity.

Stenosis - Narrowing or stricture of a duct or canal; vaginal stenosis often follows radiation treatment.

Sternum - A longitudinal plate of bone forming the middle of the anterior wall of the thorax.

Stroma - The structure elements of an organ.

Sulcus - A grove, trench or furrow.
Synergism - A characteristic exhibited when two separate
agents in combination produce an effect greater than that
produced by each agent separately.
Systole - Contraction of the heart, during which blood is
pumped into the aorta and the arteries.

Telangiectasia - Chronic dilation of capillaries and small
arterial branches producing small, reddish tumors in the
skin, as of the face.
Thoracic Angiography - An arterial catheter is placed into
the ascending aorta above the aortic valve. Contrast
material is the injected to evaluate the origins of the
vessels supplying the cerebral circulation or to look for
evidence of abnormality of the aortic wall.
Thoracotomy - Surgical incision of the wall of the chest.
Thorax - The chest, the part of the body cavity between
the neck and the diaphragm.
Threshold Dose - The dose below which no effect occurs.
Tolerance Dose - That dose above which damage to healthy
tissues is unacceptable.
Tracheotomy - Incision of the trachea through the skin and
muscles o the neck.
Tumor - A mass of new tissue growth independent of its
surrounding structures, having no physiological function.
Tumoricidal Dose - That dose at which local tumor control
is obtained.
Tumor Staging - The practice of dividing malignancies into
groups according to the extent or spread of the disease.
Staging is useful both in prognosis and in planning of
treatment.

Urography (intravenous IVP) - This commonly used procedure
involves the i.v. administration of a water-soluble iodine
containing material which is primarily concentrated and
excreted by the kidneys. It also allows visualisation of
the ureters and the bladder.
Urography (hypertensive IVP) - Rapid i.v. administration
of contrast material over a timed interval is followed by
radiographs at 1,2,3,4 and 5 mins. In some patients with
sustained hypertension of renal origin, a significant
delay in the appearance of the contrast material may be
seen in the affected kidney.

Venocavagraphy - Evaluation of the inferior (lower half of
the body) or superior (upper half of the body) vena cava
is frequently done by administration of i.v. contrast
material through a peripheral vein.
Viscera - Large interior organs in the body cavities.

Appendix 3
Altered equations to account for object extent.

If E is the extent of the object in terms of the number steps, then the following are the final equations for the monochromatic and K-edge cases that take this into account.

Monochromatic Case:

$$\sum_{s=1}^{r} \frac{2}{S} \exp\left[-X_1\left(1 - \frac{(s-0.5)^2 \cdot 4}{(S-E)^2}\right)^{1/2}\right] \quad -$$

$$\sum_{s=1}^{r} \frac{2}{S} \exp\left[-X_1\left(1 - \frac{(s-0.5)^2 \cdot 4}{(S-E)^2}\right)^{1/2} - \frac{\Delta U X_1}{U_1}\left(f^2 - \frac{(s-0.5)^2 \cdot 4}{(S-E)^2}\right)^{1/2}\right]$$

$$\geq P.\left\{\sum_{s=1}^{\frac{S-E}{2}} \frac{2}{S} \exp\left[-X_1\left(1 - \frac{(s-0.5)^2 \cdot 4}{(S-E)^2}\right)^{1/2}\right] + S.E\right\}^{1/2}$$

where,

$$P = \frac{Q.F.S}{(2.N_ot)^{1/2}} \quad \text{and} \quad Q = \rho.B$$

K-Edge Case:

$$\sum_{s=1}^{r} \frac{2}{S} \exp\left[-X_{m1}\left(1 - \frac{4.(s-0.5)}{(S-E)^2}\right)^{2 \; 1/2} -$$

$$\left(\frac{X_{m1}.C_a.\mu_{a1}}{\rho_m.\mu_{m1}}\right)\left(f^2 - \frac{4.(s-0.5)^2}{(S-E)^2}\right)^{1/2}\right]$$

$$- \sum_{s=1}^{r} \frac{2}{S} \exp\left[- X_{mh}\left(1 - \frac{4.(s-0.5)^2}{(S-E)^2}\right)^{1/2} - \left(\frac{X_{mh}.C_a.\mu_{ah}}{\rho_m.\mu_{mh}}\right)\left(f^2 - \frac{4.(s-0.5)^2}{(S-E)^2}\right)^{1/2} \right]$$

$$= \frac{G.f.B.\rho.S}{(2.N_{ot})^{1/2}} . \left\{ \sum_{s=1}^{r} \frac{2}{S} \exp\left[- X_{ml}\left(1 - \frac{4.(s-0.5)^2}{(S-E)^2}\right)^{1/2} \right. \right.$$

$$\left. - \left(\frac{X_{ml}.C_a.\mu_{al}}{\rho_m.\mu_{ml}}\right)\left(f^2 - \frac{4.(s-0.5)^2}{(S-E)^2}\right)^{1/2} \right]$$

$$\sum_{s>r}^{\frac{S-E}{2}} \frac{2}{S} \exp\left[- X_{ml}\left(1 - \frac{4.(s-0.5)^2}{(S-E)^2}\right)^{1/2}\right]$$

$$\left. S.E \right\}^{1/2}$$

2

Appendix 4
MRI imaging methods.

Spin - Lattice Relaxation Times: When a static magnetic field is applied to a material containing randomly oriented nuclei, more will orient themselves in the direction of the field, so that a net magnetisation will result. When they are now perturbed from this state, either by changes in the magnetic field or the application of a radio-frequency field, and the perturbation ceases, the nuclear magnets return to equilibrium by an exponential relaxation process which has a characteristic time constant T_1.

To measure T_1, the strength of the magnetisation is measured after various short intervals of the order of milliseconds by applying a 90 deg pulse to enable the measurement to be made in a receiving coil set up at right angles to the static field.

Spin - Spin Relaxation Time: Each nuclear magnet is not only subject to the static magnetizing field and the applied rf field, but also to the magnetic field arising from other spinning nuclei in the vicinity. The degree of interaction which it experiences will be subject to statistical variations, so that the individual nuclei will be subject to slightly different magnetic fields, and thus their Larmor precession frequencies will differ from one to another. Thus, when the nuclei are perturbed initially, they will precess in phase, however, this spin-spin interaction between the nuclei will lead to some speeding up and others slowing down. Thus the spinning nuclei return to an equilibrium distribution which is characterised by a random phase distribution, before they return to the lowest energy state, ie. when they become

aligned with the magnetic field.

The measurement of the spin-spin relaxation time T_2 is performed using a similar technique to that used to measure T_1. In this case however, the 90° pulse is followed by a series of 180° pulses. Due to the increasing degree of dephasing due to neighboring nuclei, a series of echoes is set up made up of several free induction decay signals, the amplitude of which gradually reduce with a time constant T_2. T_1 is always greater than T_2, however, in liquids they approach equality.

Nuclear Density: T_1 and T_2 are time constants which characterise the spin-lattice and spin-spin decay processes, however the nuclear density ρ is measured by the intensity of the free induction decay signal measured at different points in the volume being scanned. It can be used, along with the other parameters, to image proton distributions in patients or samples.

Chemical Shift: Shift in the Larmor frequency arises from the partial screening of the nucleus by the electrons attached to that particular atom. This screening differs between different chemical compounds, and can be used to obtain structural information. Chemical shift cannot be used for imaging purposes but analysis of the shifts can give information as to the organ metabolism, diseased tissue, extent of ischemia in the heart, etc.

Fourier Transform Reconstruction

The method of Fourier reconstruction was originally derived by Bracewell [01] in 1956 for use in radioastromony and was further developed by DeRosier and Kulg [02] for electron microscopy, by Rowley [03] in optical holography and by several authors in the area of radiography / CT [04,05].

Direct reconstruction methods are based on the central section theorem which states that a one-dimensional fourier transform of a projection is equal to a particular section of the two-dimensional fourier transform of the object itself. With reference to figure AP5.01, a single projection is taken in the x direction yielding a projection given by

$$\mathbb{G}(y) = \int f(x,y) \ dx \qquad (A5.01)$$

This projection represents an array of line integrals in the x direction. To demonstrate the central section theorem, the two-dimensional fourier transform of $f(x,y)$ is used. This is given by

$$\mathbb{F}(u,v) = \iint f(x,y).\exp\left[-i2\pi(ux + vy)\right]dx.dy \qquad (A5.02)$$

where u and v are the coordinates in fourier space. When u = 0, this transformation becomes

$$\mathbb{F}(0,v) = \iint f(x,y).\exp\left[-i2\pi vy\right]dx.dy \qquad (A5.03)$$

$$= \int \left[\int f(x,y) \ dx\right].\exp\left[-i2\pi vy\right]dy \qquad (A5.04)$$

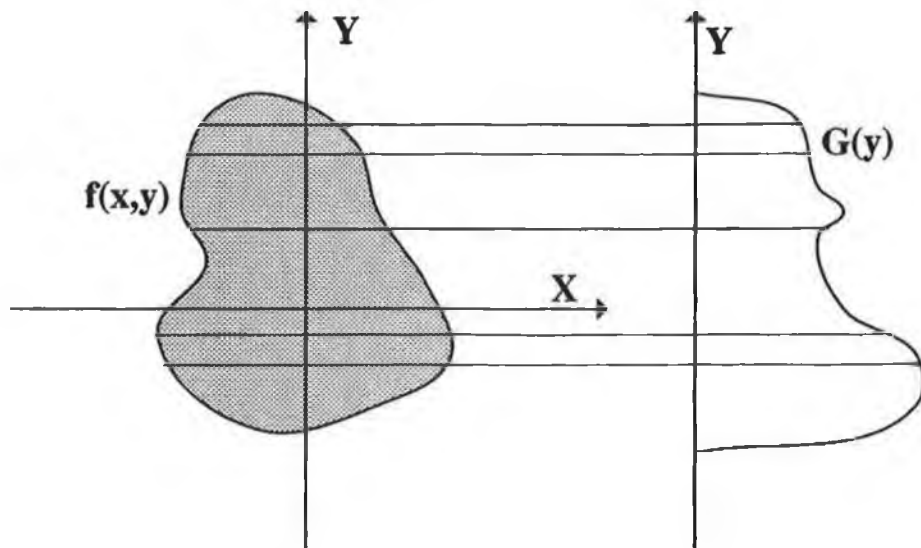$$= \mathscr{F}\left[\mathbb{G}(y)\right] \qquad (A5.05)$$

Figure AP5.01
An illustration of the central section theorem showing the linear attenuation coefficient distribution f(x,y) and the projection G(y).
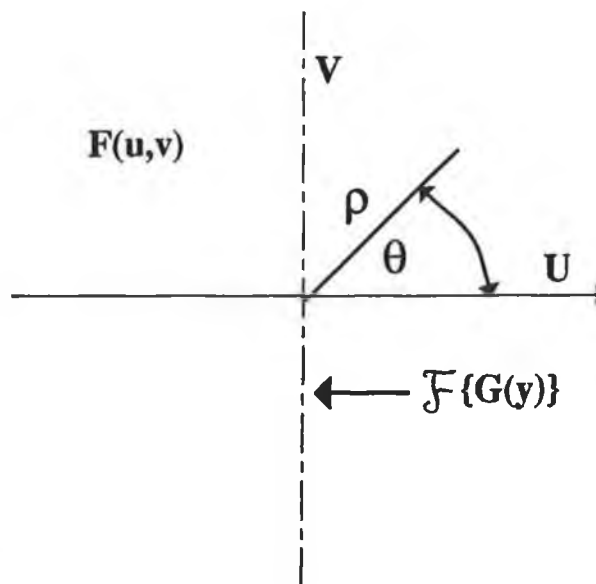

Figure AP5.02
Fourier domain illustration of the central section theorem.

where $\mathcal{F}$ is the one-dimensional fourier transform.

With u = 0, this fourier transform gives a line on the $\mathbb{F}(u,v)$ plane, as shown by the dashed line in figure AP5.02. Obviously, if the fourier transform is taken at various projection angles then this plane will be filled. The inverse transform of $\mathbb{F}(u,v)$ will now give the required f(x,y) distribution. Converting equation A5.02 into polar coordinates, the two dimensional fourier transform of a projection, along the line P, a perpendicular distance R from the origin, is given by

$$\mathbb{F}(\rho,\theta) = \mathcal{F}\left\{\mathbb{G}(R,\theta)\right\} \qquad (A5.06)$$

where $u = \rho.\cos(\theta)$, $v = \rho.\sin(\theta)$ and $R = x.\cos(\theta) + y.\sin(\theta)$.

Thus, the fourier transform of a projection at angle θ forms a line in the two-dimensional plane at this angle. After filling the entire $\mathbb{F}(\rho,\theta)$ plane with these transforms at all angles, f(x,y) can be obtained using a two-dimensional inverse fourier transform given by

$$f(x,y) = \iint \mathbb{F}(u,v).\exp\left[i2\pi(ux + vy)\right]du.dv \qquad (A5.07)$$

which in polar form is given by

$$= \int_0^{2\pi}\int_0^{\infty} \rho.\mathbb{F}(\rho,\theta)\exp\left[i2\pi\rho(x\cos\theta + y\sin\theta)\right]d\rho d\theta \qquad (A5.08)$$

In summary, the above equations can be used for image reconstruction as follows:

1) Take the one-dimensional fourier transform of the projections.

2) Interpolate this data to provide a two-dimensional matrix of fourier coefficients.

3) Take an inverse two-dimensional fourier transform to give the linear attenuation coefficient.

Interpolation is needed because the fourier coefficients obtained from step 1 do not form a rectangular matrix needed by the two-dimensional inverse fourier transform. This interpolation requires a large amount of computational time and thus other methods have been developed.

Iterative Methods:

The most straightforward solution to reconstructing a two-dimensional distribution from its projections involves linear algebra. The 2-D image is reconstructed using a matrix inversion of the projection data.

$$P(r,\Phi) = \int_{r,\Phi} F(x,y) \, ds$$

$$ds = \text{Pixel width}$$
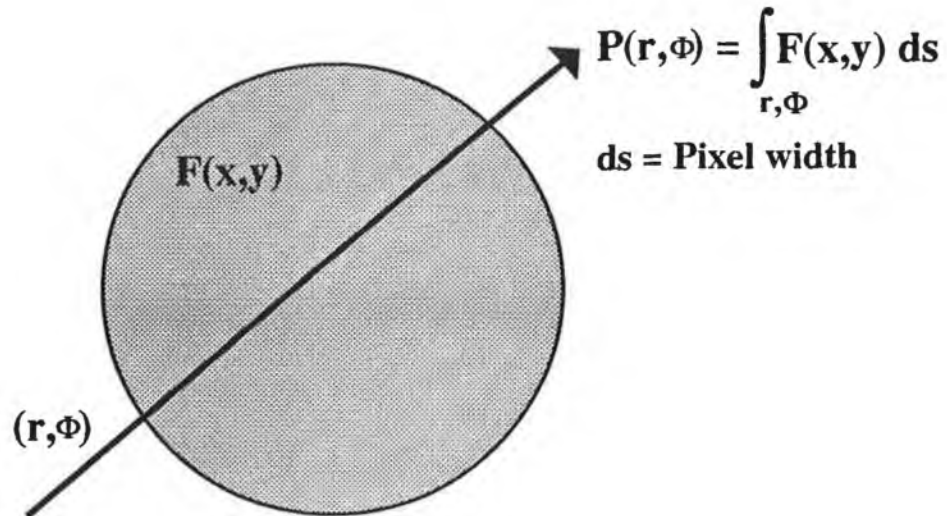
Figure AP5.03
Diagram showing the line integral of an object.

The integral of F(x,y) (density function of an object or the linear attenuation coefficient in the case of X-Ray tomography) along a ray (r,ϕ) is called the ray-sum or the ray-projection P, see figure AP5.03.

$$P(r,\phi) = \int_{r,\phi} F(x,y) \, ds \qquad (A5.09)$$

We can replace the above equation with the following set of algebraic equations,

$$P_j = \sum_{i=1}^{N} W_{ij} \, F_i \qquad (A5.10)$$

where W_{ij} is the weighting factor that represents the contribution of the i-th cell/pixel to the j-th ray-sum, P_j. Note that most of the weighting factors are zero, since only a small number of cells contribute to a given ray.

The above equation represents an array of M equations in N unknowns which, in principle, can be solved by

4

inverting the matrix W_{ij}, that is,

$$F_i = \sum_{j=1}^{M} \left(W^{-1} \right)_{ij} P_j \qquad (A5.11)$$

where W^{-1} is the inverse matrix of W.

For images of reasonable complexity, this is quite formidable. There are several reasons for this:

1) If there are not enough projections to provide N independent equations (ie. M < N), there will be many possible solutions.

2) Due to noise and other artifacts, the projection data will be inconsistent in which case there is no possible solution.

3) The size of the matrix can be very large, eg. 720 X 720.

One general class of solutions involves an iterative procedure. This is an attempt to find a two-dimensional distribution that matches all the projections. An initial distribution is assumed and it is compared with the measured projections. Using one of a variety of iterative algorithms, the initial distribution is successively modified. This method is generally known as the Algebraic Reconstruction Technique, or ART. [18].

Algebraic Reconstruction Techniques (ART):

The ART system, illustrated in fig AP5.04, is based on the very general premise that the resultant reconstruction should match the measured projections. The iterative process is started with all reconstruction elements F_i set to a constant such as the mean $\bar{F}$ or zero. In each iteration the difference between the measured data for a projection ray and the sum of the reconstructed elements along that ray is calculated. A correction factor is calculated and applied to the projection data. This process is repeated until some convergence condition is reached. This original idea, developed by Gordon et al., in 1970 [06], has been modified into many different variations.

The variation originally devised by Herman et al. in 1973 [07],a given set of ray-projections are calculated and corresponding corrections applied to all points. These updated density values are then used for calculating the

5
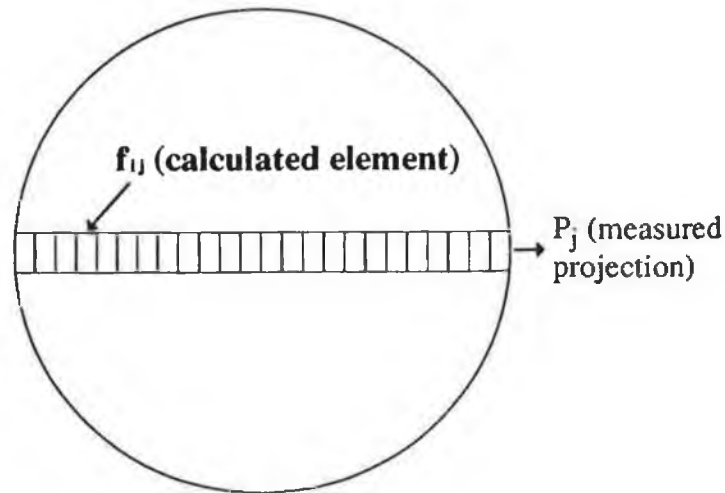
Figure AP5.04
**The ART system showing one projection with the elements
of the reconstruction matrix along this ray shown.**

next projection. This variation is the most efficient as a
large amount of updating is incorporated during each
iteration without any increase in computational time.
However a penalty is paid in that the method is less able
to handle noisy data. There are two common methods of
applying this correction to the beam, *additive* and
multiplicative correction.

Additive Correction: Each cell receives a correction
in proportion to its weighting factor W_{ij},

$$\Delta f^1_{ij} \quad = \quad \frac{W_{ij} \ \Delta p_j}{\sum\limits_{i=1}^{N} W^2_{ij}} \qquad (A5.12)$$

The denominator is a normalizing factor to ensure that the
total change in a ray-sum, if all the cells are corrected,
is Δp_j. Here W_{ij} are the overlap areas for each pixel on
the ij grid, with each beam. The calculation of these
values are discussed later.

$$\Delta p_j = p_j - p^c_j \qquad (A5.13)$$

where p_j = measured ray-sum value, and p^c_j = calculated
ray-sum value.

$$\Rightarrow \quad f^c_{ij} = f^a_{ij} + \Delta f^1_{ij} \qquad (A5.14)$$

where f^c_{ij} is the corrected density value of cell i,j and
f^a_{ij} is the pre corrected value. Δf^1_{ij} are the corrections

6

which are to be calculated so that, if applied to all the cells constituting the j-th ray, the calculated ray-sum will be increased by Δp_j.

Multiplicative Correction: Each cell receives a correction in proportion to its assigned density f_i^a.

$$\Delta f_{ij}^1 = \frac{f_i^a \, \Delta p_j}{p_j^c} \qquad (A5.15)$$

Again the normalization is such that the total ray correction is Δp_j. Using equation A5.14 and rearranging we get

$$f_i^a + \Delta f_{ij}^1 = \frac{f_i^a \, p_j}{p_j^1} \qquad (A5.16)$$

which shows that the corrected density is equal to the former density multiplied by the ratio of the measured and calculated ray-sums.

Therefore, in multiplicative ART, each reconstructed element is changed in proportion to its magnitude, whereas in additive ART each element is changed by a fixed amount, independent of its magnitude.

The weighting factors W_{ij}, are just the overlap areas, shown in figure AP5.05. In order to increase the speed and accuracy of these iterative methods, constraints can be placed on the densities. Some of the more common are:

1)   No density can be less than zero.

2)   No density can be greater than a given maximum.

3)   Cells contained within rays whose ray-sum is zero are assigned a density value of zero.

Iterative methods can also be classified according to the sequence in which corrections are made and incorporated during an iteration, as this choice has a significant effect on the performance of the method. Three such variations have been proposed, as follows:

Simultaneous Correction (ILST). In the simplest approach, all projections are calculated at the beginning of the iteration and corrections are applied simultaneously to all cells; that is, no updates are

7
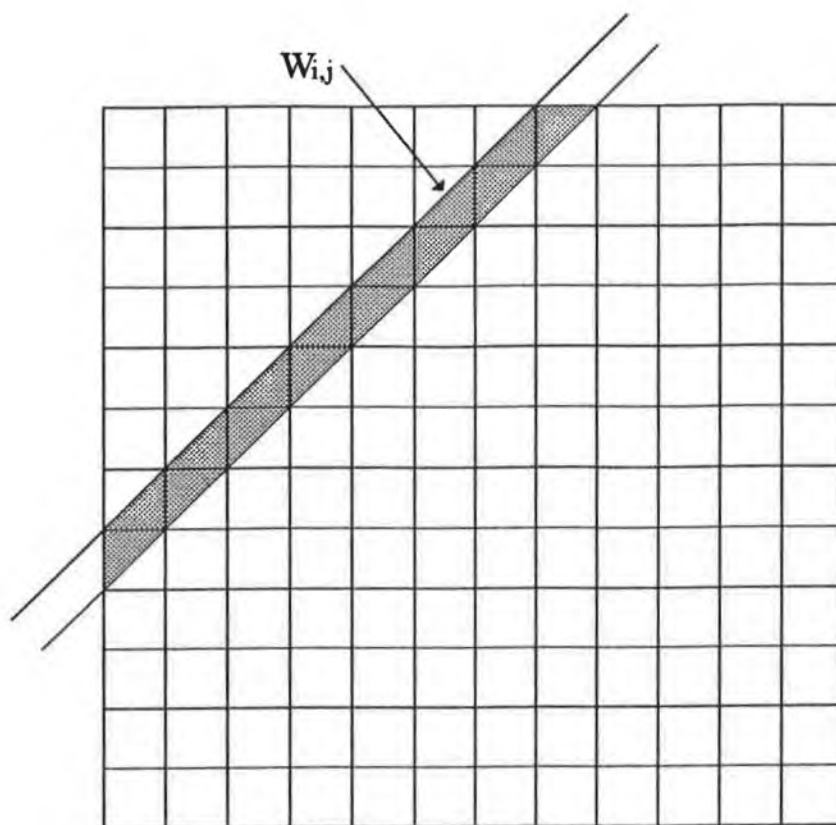
Figure AP5.05
**Diagram showing the overlap areas ($W_{i,j}$'s) of one beam
with the pixels in the i*j reconstruction grid.**

incorporated until the end of the iteration. This approach
was first tried by Bracewell [01] who found that, as it
stands, the method does not converge. The reason is that
each cell is corrected many times over for each ray
passing through it, resulting in a vast overcorrection.
This can be overcome by using a dampening factor.
Bracewell's original dampening factor was chosen so that a
best least-squares fit to the data was produced after each
iteration, and therefore the method has sometimes been
referred to as the Iterative Least-Squares Technique.

Point by Point Correction (SIRT). In this sequence,
each point is corrected simultaneously for all rays
passing through it, and these corrections are incorporated
before moving to other points. The technique was
introduced in electron microscopy by Gilbert (1972) who
named it Simultaneous Iterative Reconstruction Technique.
The number of multiplications is larger than for ILST

because each ray-sum is recalculated many times during the iteration.

Although ART is the most efficient, points are corrected first for one ray, then for another, so that a true averaging is never performed and the values at the end of the iteration reflect the last projection more than ones used early in the iteration. The two other variations, ILST and SIRT, do not converge as rapidly as ART, but do a better job averaging out noisy data. Of these two, ILST is faster. An optimum iterative procedure may be one that uses ART for the first one or two iterations and then switches to ILST.

We now discuss a range of techniques that have been proposed and used to improve the performance of the iterative methods discussed above. Some of these are based on *a priori* knowledge of the image that is expected, while others, based on mathematical or practical experience, are aimed at faster convergence of the image or a reduction in the effect of errors. Some of these procedures will now be described.

Initialisation: Most iterative algorithms have a high tolerance in regard to the initial choice of the value of f_{ij}. An initial value for each cell which is similar to the desired f_{ij} would be the most desirable. This is not always available and in such cases the f_{ij}'s are usually set to some arbitrary value. Some work has been done on a new method for choosing this initial value which will be discussed later.

Constraints: If *a priori* knowledge is available about the range in which the values of the linear attenuation coefficient of the image must lie, then this can be used to improve convergence accuracy and speed. A very common constraint is that no value may take on negative values (linear attenuation coefficients are always positive). Another example is that of knowing what is the maximum linear attenuation coefficient within the body to be scanned. Constraints may then be placed on the values which the various pixels can be assigned to.

Selective Smoothing: In many applications, images are

composed of regions of general uniformity. In such cases, application of a general smoothing function on these regions, but not across them, during the iterative procedure gives improved results. Such a selective smoothing operation has been described by Herman et al., [18].

Dampening Factor: The introduction of a dampening factor r into equations A5.14 and A5.15 yielding

$$f^c_{ij} = f^a_{ij} + r.\Delta f_{ij} \tag{A5.17}$$

$$f^c_{ij} = \frac{r.f^a_{ij}.\Delta p_i}{p^a_j} \tag{A5.18}$$

leads to only a partial correction to the pixel values if $0 < r < 1$. Sweeney and Vest [08] found that $r < 0.5$ improved the reconstruction. Also, Herman and Lent [09] found that a low value (0.025 - 0.25) resulted in excellent reconstructions in terms of the standard deviations of the pixels between iterations. For values of r in the range $0.5 - 1.0$, the standard deviation of the pixels oscillates about the correct value as the iterations proceed [10]. However, as r is decreased and thus the oscillations decrease, the number of iterations necessary to achieve the convergence criteria increases.

Convergence Criteria: Various methods for deciding when to stop the iterations have been proposed. One of these gives a measure of the entropy S given by

$$S = -\frac{1}{\ln(K)} \sum_{k=1}^{K} \frac{f^l_k}{\bar{f}}.\ln\left(\frac{f^l_k}{\bar{f}}\right) \tag{A5.19}$$

where K is the number of pixels in a projection line, f^l_k is the image pixel value and $\bar{f}$ is the mean pixel value [09]. This may be used to stop the iterations according to the outcome of a test such as

$$|S^{l+1} - S^l| < \alpha.S^l \tag{A5.20}$$

where α is some control parameter.

The above are just some of the devices that are used to improve the performance of iterative algorithms. However, these methods which received large popularity in the initial stages of development of CT, have been superseded by filtered backprojection techniques already

10

discussed. This is predominantly due to the computational time taken for reconstruction of an image.

Backprojection - ART Combination Reconstruction Program.

The iterative reconstruction techniques discussed produces an image by comparing calculated results with actual measurements for each beam position. It calculates a correction factor such that the calculated equals the actual result. This process is repeated several times for every beam position. Initially, an image size and form are assumed and the values taken for each pixel are usually uniform over the whole image. This leads to several iterations being necessary to form a correct image. A new approach at forming the initial image was developed. This consisted of forming an image by the method of backprojection and using this image as the initial image for the ART routine. This had the effect of decreasing the number of iterations necessary for convergence and thus reducing the reconstruction time while still maintaining the benefit of the results produced by ART.

Dummy projection data was produced for four rods, each 5 pixels wide in a 40 x 40 pixel image. This data was first reconstructed by the ART program only. The program took 12 iterations and 67.87 minutes to produce an image. Using the backprojection-ART combination program, the image was produced after only 2 iterations and 18.75 minutes. The backprojection-ART program listing is shown on pages 65 to 70 of appendix 1 with the program to calculate the overlap areas, needed by the ART section of the program, shown on pages 71 to 72.

The Dirac Delta Function.

If $f(X)$ is any continuous function at the point X_0, then the delta function is defined by the integral

$$\int_a^b f(X)\delta(X - X_0) \, dx = \begin{cases} f(X_0) & \text{if } a < X_0 < b \\ 0 & \text{otherwise.} \end{cases} \qquad (A5.21)$$

For the above integral to be finite, the delta function must have the property;

$$\int_{-\infty}^{\infty} \delta(X - X_0) \, dx = 1 \qquad (A5.22)$$

Sometimes, the argument of a delta function is some other function $g(X)$. If $g(X)$ has only one root in the range of integration then it may be expanded into a Taylor series yielding

$$\delta(\,g(X)\,) = \delta\left(\,g(X_0) + (X - X_0)\,\frac{dy}{dx}\,\bigg|_{X_0}\,\right) \qquad (A5.23)$$

Higher terms in the expansion are not needed since the neighborhood around the root (X_0) is arbitrarily small. Since $g(X_0) = 0$,

$$\delta\left(\,g(X)\,\right) = \frac{\delta(X - X_0)}{dy/dx|_{X_0}} \quad , \text{ ie. } \delta(aX) = a^{-1}.\,\delta(X)$$

$$(A5.24)$$

If $g(X)$ has N roots in the range of integration, then

$$\delta\left(\,g(X)\,\right) = \sum_{n=1}^{N} \frac{\delta(X - X_n)}{|dg/dx|_{X_n}} \qquad (A5.25)$$

where $g(X_n) = 0$ and $dg/dx|_{X_n} \neq 0$.

Polar geometry used in discussion on the backprojection method of reconstruction (chapter 2).

$$\text{Cos}(\Phi) = \frac{x}{R} \qquad\qquad \text{Sin}(\Phi) = \frac{y}{R}$$

$$x = R\ \text{Cos}(\Phi) \qquad \text{and} \qquad y = R\ \text{Sin}(\Phi)$$

$$x^2 = R\ x\ \text{Cos}(\Phi) \qquad \text{and} \qquad y^2 = R\ y\ \text{Sin}(\Phi)$$

$$x^2 + y^2 = R\left(x\ \text{Cos}(\Phi) + y\ \text{Sin}(\Phi)\right)$$

$$x^2 + y^2 = R^2$$

$$R = x\ \text{Cos}(\Phi) + y\ \text{Sin}(\Phi)$$
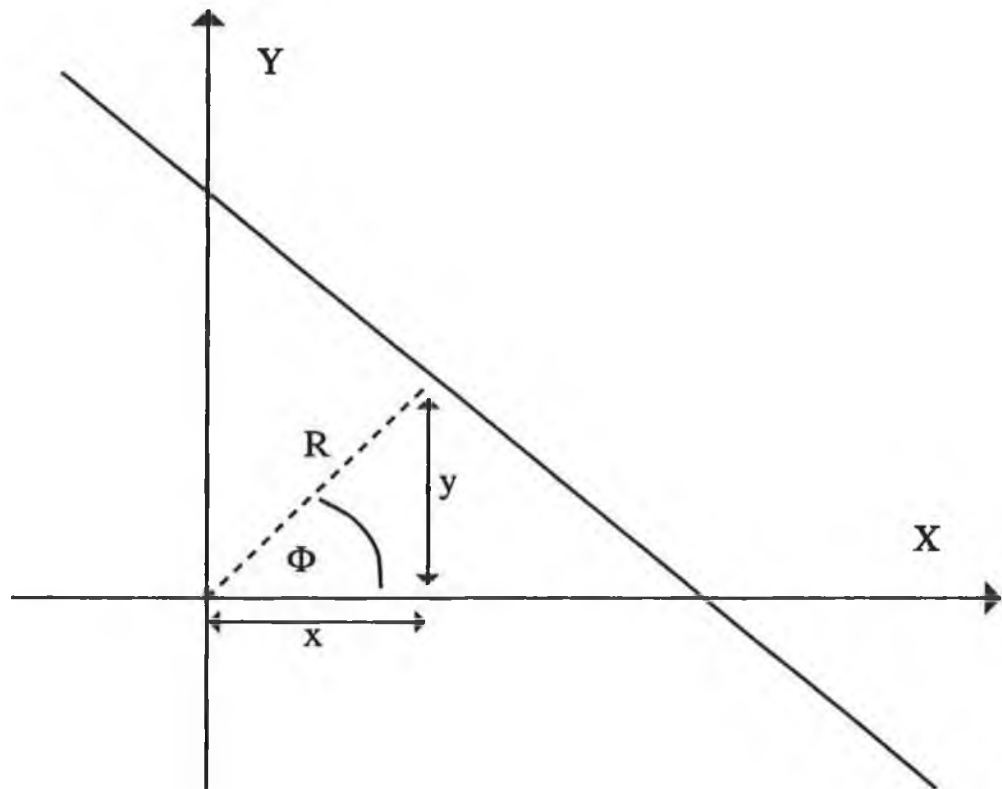
[01] Bracewell, R.N.
"Strip integration in radio astronomy",
Aust. Jour. Physics, No. 9, pp.198-217, 1956

[02] DeRosier, D.J., and Klug, A.
"Reconstruction of three-dimensional structures from electron micrographs",
Nature, No. 217, pp.130-134, 1968.

[03] Rowley, P.D.
Jour. Opt. Soc. Am., No. 59, pp.1496-1498, 1969

[04] Bates, R.H., Lewitt, R.M., Peters, T., Smith, P.R.
Image Processing for 2-D and 3-D Reconstruction from Projections, Stanford, Aug. 4-7, pp WA2-1, 1975.

[05] Herman, G.T., Lakshminarayanan, A.V., Rowland, S.W.,
"The reconstruction of objects from shadowgraphs with high contrasts."
Pattern Recognition, No.7, pp.157-165, 1976.

[06] Gordon, R., Bender, R., Herman, G.T.,
"Algebraic Reconstruction Techniques for three-dimensional electron microscopy and x-ray photography."
Jour. Theor. Biolog., Vol. 29, pp.471-481, 1970.

[07] Herman, G.T.,
"Reconstruction of binary patterns from a few projections."
Internation Computing Symposium 1973, pp.371-379, North-Holland Publ. Assoc.

[08] Sweeney, D.H., Vest, C.M.
"Reconstruction of 3-D refractive index fields from multidirectional interferometric data."
Applied Optics, No.12, pp.2649-2664, 1973.

[09] Herman, G.T., Lent, A., Lutz, P.H.
"Relaxation methods for image reconstruction."
Comm. A.C.M., Vol. 21, pp.152-158, 1978

[10] Webb, S.
"Reconstruction of cross sections from transmission projections - A short simplified review and comparison of performance of reconstruction algorithms."
Physical Aspects of Medical Imaging, Wiley & Sons, 1981.

Appendix 6
Radiation detectors.

Gas-Filled Detectors: The essential features of the gas-filled detector are shown in figure AP6.01. Ionising radiation passing through the gas, dissipates part or all of its energy by generating electron-ion pairs. These move under the influence of the electric field producing a current on the electrodes. For a constant intensity source incident on the detector, if the potential between the electrodes is steadily increased, then the charge collected per unit time changes as shown in figure AP6.02. Also shown is the relative effect three different particles have on the signal detected. No counter operates in region I as a slight change in tube voltage will change the signal considerably. *Ionisation chambers* operate in region II. No charge multiplication takes place and the output signal is proportional to the energy of the particle, therefore, measurement of the particle's energy is possible. *Proportional counters* operate in region III. Charge multiplication takes place, but the output signal is proportional to the particle energy. *Geiger-Muller (GM) counters* work in region IV. They provide a very strong signal requiring no preamplification. However, the signal is independent of particle type or energy. Therefore, it is only used as a particle counter. In region V, a single ionising event starts a continuous discharge in the gas and the device fails to operate as a counter.

Scintillation Detectors: Scintillators are materials that produce bursts or scintillations of light when ionising radiation is incident upon them. The amount of light produced is small and therefore needs amplification by a photomultiplier tube. Amplifications of the order of 10^6 are common for many commercial tubes. Figure Ap6.03
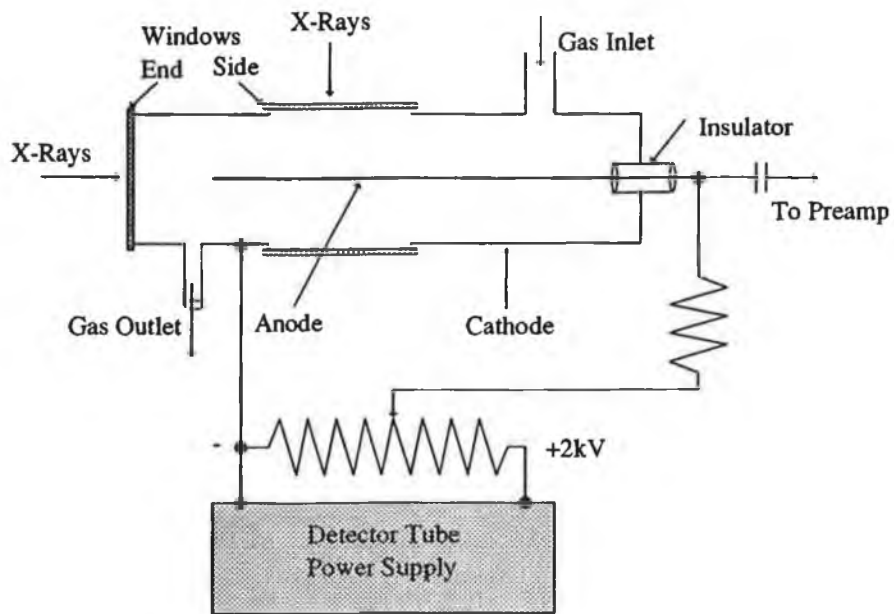
Figure AP6.01
Structure of the gas-filled x-ray detector. The tube is shown to have both end and side widows for illustration only.
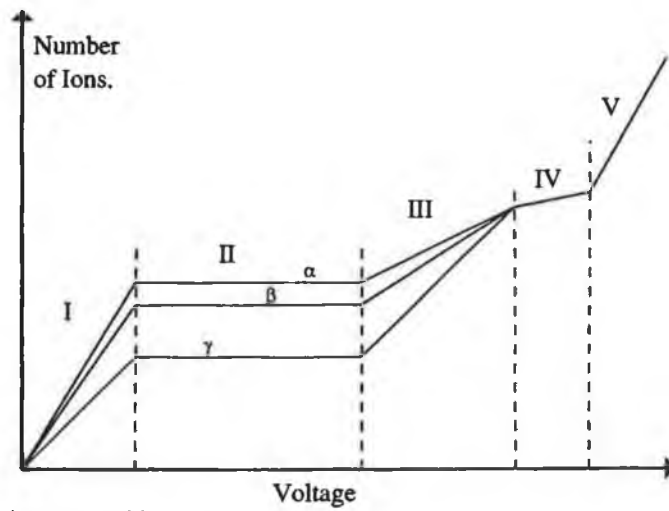
Figure AP6.02
The relationship between charge collected and applied voltage for three different particles.
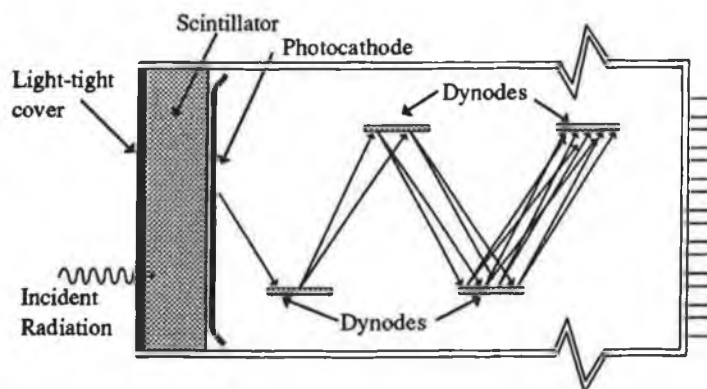
Figure AP6.03
Schematic diagram of a scintillation detector.

shows a diagram of a scintillation detector. There are various forms of scintillators including *inorganic, organic/liquid, plastic and gaseous* scintillators. The most common of these in terms of medical imaging are the inorganic ones which include CsI(Tl), NaI(Tl), CaI(Na) and CaF_2(Eu). The element in parentheses is an activator and is the agent responsible for the luminescence of the crystal. It is present in relatively small concentrations, eg. thallium in NaI(Tl) is 10^{-3} on a per mole basis [06].

Appendix 7
Mass attenuation coefficients and periodic table of elements.

Mass Attenuation Coefficients (m²/kg) vs. Energy for various elements.

Energy	Water	Copper	Alumin	Iodine	Tungst	Cerium	Tin	Gold	Lead	Uraniu	Gadolin	Air
20	0.0796	3.350	0.340	2.490	6.570	3.310	2.102	7.882	8.636	7.106	4.300	0.0764
30	0.0372	1.080	0.112	0.840	2.270	1.120	4.095	2.752	3.032	4.128	1.450	0.0350
40	0.0267	0.483	0.056	2.190	1.070	0.522	1.931	1.298	1.436	1.983	0.900	0.0247
50	0.0226	0.259	0.037	1.23	0.595	1.520	1.064	0.726	0.804	1.121	1.900	0.0207
60	0.0206	0.158	0.028	0.750	0.371	0.945	0.653	0.453	0.502	0.703	1.200	0.0187
70	0.0190	0.115	0.024	0.530	1.100	0.600	0.420	0.300	0.325	0.500	0.800	0.0175
80	0.0184	0.076	0.020	0.350	0.781	0.441	0.301	0.900	0.242	0.339	0.550	0.0166
90	0.0177	0.05	0.018	0.250	0.575	0.300	0.230	0.680	0.640	0.250	0.400	0.0160
100	0.0171	0.046	0.017	0.193	0.440	0.245	0.167	0.516	0.555	0.195	0.300	0.0154
110	0.0166	0.040	0.0165	0.163	0.375	0.200	0.150	0.360	0.480	0.150	0.230	0.015
120	0.0162	0.035	0.0155	0.125	0.325	0.175	0.120	0.300	0.410	0.450	0.180	0.0145
130	—	—	—	—	0.175	—	0.1	0.250	0.340	0.350	—	—
140	—	—	—	—	—	—	0.08	0.200	0.270	0.255	—	—
150	0.0150	—	—	0.069	—	0.087	0.061	0.186	0.201	0.259	—	0.0135

Period · Ia

Legend: 1.0079 = atomic mass, H, 1 = atomic number

Inert Gases

Period	Ia	IIa	IIIa	IVa	Va	VIa	VIIa	VIII			Ib	IIb	IIIb	IVb	Vb	VIb	VIIb	Inert Gases
1	1.00797 H 1																	4.00260 He 2
2	6.941 Li 3	9.01218 Be 4											10.81 B 5	12.0112 C 6	14.0067 N 7	15.9994 O 8	18.9984 F 9	20.179 Ne 10
3	22.9898 Na 11	24.305 Mg 12											26.9815 Al 13	28.086 Si 14	30.9738 P 15	32.06 S 16	35.453 Cl 17	39.948 Ar 18
4	39.098 K 19	40.08 Ca 20	44.9559 Sc 21	47.90 Ti 22	50.9414 V 23	51.996 Cr 24	54.9380 Mn 25	55.847 Fe 26	58.9332 Co 27	58.71 Ni 28	63.546 Cu 29	65.38 Zn 30	69.72 Ga 31	72.59 Ge 32	74.9216 As 33	78.96 Se 34	79.904 Br 35	83.80 Kr 36
5	85.4678 Rb 37	87.62 Sr 38	88.9059 Y 39	91.22 Zr 40	92.9064 Nb 41	95.94 Mo 42	98.9062 Tc 43	101.07 Ru 44	102.906 Rh 45	106.4 Pd 46	107.868 Ag 47	112.40 Cd 48	114.82 In 49	118.69 Sn 50	121.75 Sb 51	127.60 Te 52	126.905 I 53	131.30 Xe 54
6	132.905 Cs 55	137.34 Ba 56	138.906 ☆La 57	178.49 Hf 72	180.948 Ta 73	183.85 W 74	186.2 Re 75	190.2 Os 76	192.22 Ir 77	195.09 Pt 78	196.967 Au 79	200.59 Hg 80	204.37 Tl 81	207.19 Pb 82	208.980 Bi 83	(210) Po 84	(210) At 85	(222) Rn 86
7	(223) Fr 87	226.025 Ra 88	(227) ✝Ac 89	(261) 104	(260) 105	(263) 106												

☆ Lanthanides (rare earths)

140.12 Ce 58	140.908 Pr 59	144.24 Nd 60	(147) Pm 61	150.4 Sm 62	151.96 Eu 63	157.25 Gd 64	158.925 Tb 65	162.50 Dy 66	164.930 Ho 67	167.26 Er 68	168.934 Tm 69	173.04 Yb 70	174.97 Lu 71

✝ Actinides

232.038 Th 90	231.036 Pa 91	238.029 U 92	237.048 Np 93	(244) Pu 94	(243) Am 95	(247) Cm 96	(247) Bk 97	(251) Cf 98	(254) Es 99	(257) Fm 100	(258) Md 101	(255) No 102	(256) Lr 103